Simultaneous Determination of Trace Elements using Multi-Element Graphite Furnace Atomic Absorption Spectrometry

dem Fachbereich Chemie (IAC)

der Universität Duisburg-Essen

Zur Erlangung des akademischen Grades eines

Dr. rer. nat.

genehmigte Dissertation

von

Khaled Elsherif

aus Benghazi / Libyen

Referent: Prof. Dr. Heinz-Martin Kuss

Korreferent: Priv. Doz. Dr. Ursula Telgheder

Datum der Einreichung 11.12.2008

Datum der mündlichen Prüfung 24.03.2009

Acknowledgements

I am indebted to many people for their long-lasting support and encouragement which was invaluable for the successful completion of this research work. In the following lines some of them are gratefully acknowledged. However, I am aware of the fact that there are many more and these words cannot express the gratitude and respect I feel for all of those.

Firstly, I like to take this opportunity to thank the people who provided scientific and financial support to make this work possible. I must thank ***Prof. Dr. Heinz-Martin Kuss*** who initiated the thesis projects, offered me a warm welcome in his group and gave me the unique opportunity to use the research facilities in his lab.

My sincere thanks go to many friends and colleagues for scientific discussion, advice and continuous support always so greatly appreciated, among them ***Dr. Abdelsalam Asweisi*** and ***Dr. Bülend Bayraktar*** who introduced me to the secrets of Graphite Furnace Atomic Absorption spectroscopy and for many valuable ideas and suggestions. I like to express further greatest thanks for help and encouragement to my friends ***Dr. Roman Rodreguez***, ***Rajab El-kailany***, ***Nabil Bader*** and others.

Last but by no means least, I like to thank my ***family*** and close relatives for general education and the opportunity to start and pursue a career in science. I am particularly indebted to my ***parents*** for their never-ending encouragement and ongoing support. Very special thanks go to my ***wife*** for her patience during my work and finding supporting words of deep sense, not always related to science but to life in general.

Abstract

Simultaneous Multi-Element Atomic Absorption Spectrometer (SIMAA 6000) has been used to determine groups of elements (up to four) simultaneously, by using 2-operating and 4-operating modes. A direct, simple, fast and accurate methodology for the simultaneous multi-element determination have developed. Compromised conditions (e.g. temperature program and use of universal modifier) for the multi-element mode have been determined. The temperature program has been carefully optimized for the multi-element mode taking into account all analytes to be determined. The optimization depends on the elements to be determined simultaneously and the matrix. Also, a universal powerful matrix modifier has been used in order to increase the stability of the elements (especially the volatile elements). This has permitted the use of a common temperature program including volatile and less volatile elements. The Pd+Mg mixture modifier has stabilized the high and mid volatile elements. For less volatile elements, the modifier had no stabilization effect on these elements. But the modifier in this case has prevented the formation of refractory compounds which increase the volatilization process of these elements. Ir coating of the tube or platform has extended significantly the tube lifetime. The sensitivity values for the multi-element determination were comparable to those of the single-element. The decreasing in sensitivity values is a result of using higher atomization temperature in the multi-element mode and/or decreasing the lamp intensities. The detection limits values of the multi-element determination were higher than those of the single-element which is mainly as a result of decreasing the lamp intensities in the multi-element mode compared to the single-element mode. Another effect which could cause the higher detection limits is the use of higher atomization temperature. The operational conditions (the temperatures, use of modifier, and the operating mode) have affected the absorption signals of the elements. This effect has appeared in terms of increasing or decreasing the appearance time, peak height, and peak width. The accuracy of the methods was tested by analyzing number of certified materials and the concentrations obtained were in good agreement with certified values

I. Table of Contents

II. List of Figures 7

III. List of Tables 13

1 Introduction to Multi-Element Graphite Furnace Atomic Absorption Spectrometry 19

1.1 Review 19

1.2 Basic Features of the GFAAS 20

1.2.1 System Design 20

1.2.2 Temperature Program 21

1.2.2.1 Drying Step 21

1.2.2.2 Pyrolysis Step 22

1.2.2.3 Atomization Step 22

1.2.2.4 Cleaning Step 23

1.2.3 Background Correction 24

1.2.3.1 Continuum Source 24

1.2.3.2 Self-Reversal Methods 24

1.2.3.3 Zeeman-Effect 25

1.2.4 Atomization Mechanism & Stabilization in Graphite Furnace 27

1.3 Simultaneous Multi-Element Graphite Furnace AAS Systems 29

1.3.1 Line Source Multi-Element Systems 30

1.3.1.1 Model Z-9000 from Hitachi 30

1.3.1.2 AA Scan 4 from Thermo-Jarrell Ash 30

1.3.1.3 Analyte 5 (Leeman Labs) 31

1.3.1.4 SIMAA 6000 from Perkin-Elmer 31

1.3.2 Continuum Source Multi-Element Systems 31

1.3.3 Summary 32

2 SIMAA 6000 Design and the Multi-Element Compromised Conditions 33

2.1 Overview 33
2.2 Basic Features of SIMAA 6000 System 33
2.2.1 Furnace Design (Transversely Heated Graphite Atomizer THGA) 35
2.2.1.1 The Stabilized Temperature Platform Furnace (STPF) 36
2.2.2 The Tetrahedral Echelle Polychromator Optical System (TEP) 38
2.2.3 Solid-State Detector 40
2.3 Compromised Conditions for Simultaneous Multi-Element Determinations 41
2.3.1 Pyrolysis and Atomization Temperatures 42
2.3.2 Chemical Modification 43
2.4 Important Terms 46
2.4.1 Sensitivity and Characteristic 46
2.4.2 The Detection Limits 47
3 Aims 49
4 Experimental Section 50
4.1 Instrumentation 50
4.2 Reagents and Standard Solutions 50
4.3 Sample Preparation 52
4.3.1 Trace Elements Urine Sample (Seronorm 0511545) 52
4.3.2 Lyphocheck Urine Metals Control-Level 1 (69061) 53
4.3.3 Pork Liver (GBW 08551), Pig Kidney (BCR-CRM 186), and Bovine Liver (NIST-SRM 1577b) 53
4.3.4 Tea Sample (GBW 08505) 53
4.4 Contamination Control 53
5 Results and Discussions 54
5.1 Overview 54
5.2 Single-Element Determinations without Modifier 54
5.3 Single-Element Determination with Modifier 62

5.3.1 With $Pd(NO_3)_2 + Mg(NO_3)_2$ Modifier 63
5.3.2 With Magnesium Nitrate ($Mg(NO_3)_2$) Modifier 67
5.3.3 With Ir-permanent Modifier 69
5.4 Multi-Element Determinations with 2-Operating Mode 72
5.4.1 Multi-Element Determination of Be, Cr, and Cu 72
5.4.2 Multi-Element Determination of Bi, Sb, Cu, and Mn 75
5.4.3 Multi-Element Determination of Cu, Mn, and Se 77
5.4.4 Multi-Element Determination of Pb and Se 79
5.4.4.1 With Pd+Mg Modifier 80
5.4.4.2 With Ir Permanent Modifier 81
5.4.5 Multi-Element Determination of Bi, Sb, and Cd 83
5.4.5.1 With Pd+Mg Modifier 83
5.4.5.2 With Ir Permanent Modifier 85
5.5 Multi-Element Determinations with 4-Operating Mode 88
5.5.1 Multi-Element determination of Al, Be, Cr, and V 88
5.5.2 Multi-Element Determination of Be, Cr, Cu, and Mn 91
5.5.3 Multi-Element Determination of Bi, Sb, Cu, Mn, and Se 93
5.5.4 Multi-Element Determination of Bi, Pb, Sb, and Se 96
5.6 The Effect of the Operating mode and the Use of Modifier on Absorption Signals and Sensitivity 98
5.6.1 Aluminium (Al) 98
5.6.2 Beryllium (Be) 99
5.6.3 Bismuth (Bi) 101
5.6.4 Cadmium (Cd) 102
5.6.5 Chromium (Cr) 104
5.6.6 Copper (Cu) 105
5.6.7 Manganese (Mn) 106

5.6.8 Lead (Pb) 108
5.6.9 Antimony (Sb) 109
5.6.10 Selenium (Se) 111
5.6.11 Vanadium (V) 112
5.7 Summary of Multi-Element Determination 113
5.8 The Effect of the Urine Matrix on the Multi-Element Determination 115
5.8.1 Multi-Element Determination of Al, Be, Cr, and V 116
5.8.2 Multi-Element Determination of Be, Cr, Cu 118
5.8.3 Multi-Element Determination of Bi, Sb, Cu, and Mn 119
5.8.4 Multi-Element Determination of Cu, Mn, and Se 121
5.8.5 Multi-Element Determination of Pb and Se 123
5.8.5.1 With 5µg Pd + 3µg Mg Modifier 124
5.8.5.2 With Ir Permanent Modifier 125
5.8.6 Multi-Element Determination of Bi, Sb, and Cd 127
5.8.6.1 With 5µg Pd + 3µg Mg modifier 127
5.8.6.2 With Ir Permanent Modifier 128
5.9 Analysis of Certified Reference Materials 130
5.9.1 Multi-Element Determination of Al, Be, Cr, and V 131
5.9.1.1 Trace Element Urine Sample from Seronorm (0511545) 131
5.9.1.2 Lyphochek Urine Metals Control Level 1 from BIO-RAD (69061) 134
5.9.1.3 Bovine Liver from National Institute of Standards and Technology (NIST-SRM 1577b) 136
5.9.1.4 Pork Liver from National Research Centre for Certified Reference Materials (GBW 08551) 138
5.9.1.5 Comparison of the results of Different Samples 140
5.9.2 Multi-Element Determination of Be, Cr, and Cu 141
5.9.2.1 Trace Element Urine Sample from Seronorm (0511545) 141

5.9.2.2 Lyphochek Urine Metals Control–Level 1 from BIO-RAD (69061) 143

5.9.2.3 Tea sample from National Research Centre for Certified Reference Materials (GBW 08505) 145

5.9.2.4 Bovine Liver from National Institute of Standards and Technology (NIST-SRM 1577b) 147

5.9.2.5 Comparison of the Results of Different Samples 149

5.9.3 Multi-Element Determination of Bi, Cu, Mn, and Sb 150

5.9.3.1 Trace Element Urine Sample from Seronorm (0511545) 150

5.9.3.2 Lyphochek Urine Metals Control–Level 1 from BIO-RAD (69061) 152

5.9.3.3 Pig Kidney from Institute for Reference Materials and Measurements (BCR-CRM 186) 155

5.9.3.4 Bovine Liver from National Institute of Standards and Technology (NIST-SRM 1577b) 157

5.9.3.5 Comparison of the results of Different Samples 159

5.9.4 Multi-Element Determination of Cu, Mn, and Se 160

5.9.4.1 Trace Element Urine Sample from Seronorm (0511545) 160

5.9.4.2 Lyphocheck Urine Metals Control–Level 1 from BIO-RAD (69061) 162

5.9.4.3 Pig Kidney from Institute for Reference Materials and Measurements (BCR-CRM 186) 164

5.9.4.4 Comparison of the results of Different Samples 166

5.9.5 Multi-Element Determination of Pb and Se 166

5.9.5.1 Trace Element Urine Sample from Seronorm (0511545) 166

5.9.5.1.1 With Pd+Mg modifier 167

5.9.5.1.2 With Ir permanent Modifier 168

5.9.5.2 Lyphocheck Urine Metals Control–Level 1 from BIO-RAD (69061) 169

5.9.5.3 Pork Liver from National Research Centre for Certified Reference Materials (GBW 08551) 171

5.9.5.4 Tea Sample from National Research Centre for Certified Reference Materials (GBW 08505) 173
5.9.5.5 Comparison of the results of Different Samples 174
5.9.6 Multi-Element Determination of Bi, Cd, and Sb 175
5.9.6.1 Trace Element Urine Sample from Seronorm (0511545) 175
5.9.6.1.1 With Pd+Mg modifier 175
5.9.6.1.2 With Ir permanent modifier 177
5.9.6.2 Lyphocheck Urine Metals Control–Level 1 from BIO-RAD (69061) 179
5.9.6.3 Bovine Liver from National Institute of Standards and Technology (NIST-SRM 1577b) 181
5.9.6.4 Pig Kidney from Institute for Reference Materials and Measurements (BCR-CRM 186) 183
5.9.6.5 Pork Liver from National Research Centre for Certified Reference Materials (GBW 08551) 185
5.9.6.6 Tea Sample from National Research Centre for Certified Reference Materials (GBW 08505) 187
5.9.6.7 Comparison of the results of Different Samples 189
5.9.7 Summary 190
5.10 Conclusion 190
6 References: 192

II. List of Figures

Figure 1.1 Diagram of the basic components of a GFAAS 21

Figure 1.2 Pyrolysis and atomization curves 23

Figure 1.3 Effect of the atomization temperature [(a) 1800^{o}C, (b) 2000^{o}C, (c) 2200^{o}C and (d) 2400^{o}C] on the absorbance profiles of tellurium[42] 23

Figure 1.4 Self-reversal background correction 27

Figure 1.5 Normal Zeeman-effect splitting 27

Figure 2.1 Schematic diagram of the basic components of SIMAA 6000 35

Figure 2.2 Temperature distribution in a Massmann-type furnace 37

Figure 2.3 Temperature distribution in a transverse heated furnace 37

Figure 2.4 Schematic diagram of a THGA with integrated platform 38

Figure 2.5 Solid-state detector for simultaneous multi-element determinations 41

Figure 5.1 Pyrolysis and atomization curves with and without modifier in the single-element mode 58

Figure 5.2 Calibration curves of the elements with Pd+Mg modifier in the single-element mode 64

Figure 5.3 Calibration curves of the elements with Mg modifier in the single-element mode 68

Figure 5.4 Calibration curves of the elements with Ir-permanent modifier in the single-element mode 70

Figure 5.5 Pyrolysis and atomization curves for multi-element mode in aqueous solution of Be, Cr, and Cu using Pd+$Mg(NO_3)_2$ as a modifier 73

Figure 5.6 Calibration curves of the multi-element mode in aqueous solution of Be, Cr, and Cu with Pd+Mg modifier 74

Figure 5.7 Pyrolysis and atomization curves for multi-element mode in aqueous solution of Bi, Sb, Cu, and Mn using Pd+$Mg(NO_3)_2$ as a modifier 75

Figure 5.8 Calibration curves of the multi-element mode in aqueous solution of Bi, Sb, Cu, and Mn with Pd+Mg modifier 76

Figure 5.9 Pyrolysis and atomization curves for multi-element mode in aqueous solution of Cu, Mn, and Se using Pd+$Mg(NO_3)_2$ as a modifier 78

Figure 5.10 Calibration curves of the multi-element mode in aqueous solution of Cu, Mn, and Se with Pd+Mg modifier 78

Figure 5.11 Pyrolysis and atomization curves for multi-element mode in aqueous solution of Pb and Se using Pd+$Mg(NO_3)_2$ as a modifier 80

Figure 5.12 Calibration curves of the multi-element mode in aqueous solution of Pb and Se with Pd+Mg modifier 81

Figure 5.13 Pyrolysis and atomization curves for multi-element mode in aqueous solution of Pb and Se using Ir permanent modifier 82

Figure 5.14 Calibration curves of the multi-element mode in aqueous solution of Pb and Se with Ir permanent modifier 82

Figure 5.15 Pyrolysis and atomization curves for multi-element mode in aqueous solution of Bi, Sb, and Cd using Pd+Mg modifier 84

Figure 5.16 Calibration curves of the multi-element mode in aqueous solution of Bi, Sb, and Cd with Pd+Mg modifier 84

Figure 5.17 Pyrolysis and atomization curves for multi-element mode in aqueous solution of Bi, Sb, and Cd using Ir modifier 86

Figure 5.18 Calibration curves of the multi-element mode in aqueous solution of Bi, Sb, and Cd with Ir modifier 87

Figure 5.19 Pyrolysis and atomization curves for multi-element mode in aqueous solutions of Al, Be, Cr, and V using $Mg(NO_3)_2$ as a modifier 89

Figure 5.20 Calibration curves of the multi-element mode in aqueous solution of Al, Be, Cr, and V with Mg modifier 90

Figure 5.21 Calibration curves of the multi-element mode in aqueous solution of Be, Cr, Cu, and Mn with Pd+Mg modifier 92

Figure 5.22 Calibration curves of the multi-element mode in aqueous solution of Bi, Cu, Mn, Sb, and Se with Pd+Mg modifier 94

Figure 5.23 Calibration curves of the multi-element mode in aqueous solution of Bi, Cu, Mn, Sb, and Se with Pd+Mg modifier 97

Figure 5.24 Absorption signals of aluminium 98

Figure 5.25 Absorption signals of beryllium 99

Figure 5.26 Absorption signals of bismuth 101

Figure 5.27 Absorption signals of cadmium 102

Figure 5.28 Absorption signals of chromium..... 104

Figure 5.29 Absorption signals of copper 105

Figure 5.30 Absorption signals of manganese 106

Figure 5.31 Absorption signals of lead 108

Figure 5.32 Absorption signals of antimony 109

Figure 5.33 Absorption signals of selenium..... 111

Figure 5.34 Absorption signals of vanadium 113

Figure 5.35 Pyrolysis and atomization curves for multi-element determinations of Al, Be, Cr, and V using 5µg Mg modifier in diluted (1:4) urine sample spiked with 10, 2, 6, 80 ppb Al, Be, Cr, and V, respectively 117

Figure 5.36 Absorbance signals of diluted (1:4) spiked urine sample at 1500^{o}C pyrolysis and 2500^{o}C atomization with 5µg Mg modifier in the multi-element determinations of Al, Be, Cr, and V 118

Figure 5.37 Pyrolysis and atomization curves for multi-element determinations of Be, Cr, and Cu using 5µg Pd + 3µg Mg modifier in diluted (1:4) urine sample spiked with 2, 6, 10 ppb Be, Cr, and Cu, respectively 119

Figure 5.38 Absorbance signals of diluted (1:4) spiked urine sample at 1200^{o}C pyrolysis and 2300^{o}C atomization with 5µg Pd + 3µg Mg modifier in the multi-element determinations of Be, Cr, and Cu 119

Figure 5.39 Pyrolysis and atomization curves for multi-element determinations of Bi, Cu, Mn, and Sb using 5µg Pd + 3µg Mg modifier in diluted (1:4) urine sample spiked with 80, 10, 6, 80 ppb Bi, Cu, Mn, and Sb, respectively..... 121

Figure 5.40 Absorbance signals of diluted (1:4) spiked urine sample at 1000^{o}C pyrolysis and 2000^{o}C atomization with 5µg Pd + 3µg Mg modifier in the multi-element determinations of Bi, Cu, Mn, and Sb 121

Figure 5.41 Pyrolysis and atomization curves for multi-element determinations of Cu, Mn, and Se using 5µg Pd + 3µg Mg modifier in diluted (1:4) urine sample spiked with 10, 6, 80 ppb Cu, Mn, and Se, respectively..... 123

Figure 5.42 Absorbance signals of diluted (1:4) spiked urine sample at 900°C pyrolysis and 2000°C atomization with 5µg Pd + 3µg Mg modifier in the multi-element determinations of Cu, Mn, and Se 123

Figure 5.43 Pyrolysis and atomization curves for multi-element determinations of Pb and Se using 5µg Pd + 3µg Mg modifier in diluted (1:4) urine sample spiked with 40, 80 ppb Pb and Se, respectively 125

Figure 5.44 Absorbance signals of diluted (1:4) spiked urine sample at 1000°C pyrolysis and 1900°C atomization with 5µg Pd + 3µg Mg modifier in the multi-element determinations of Pb and Se 125

Figure 5.45 Pyrolysis and atomization curves for multi-element determinations of Pb and Se using 500µg Ir permanent modifier in diluted (1:4) urine sample spiked with 40, 80 ppb Pb and Se, respectively 126

Figure 5.46 Absorbance signals of diluted (1:4) spiked urine sample at 800°C pyrolysis and 2000°C atomization with 500µg Ir permanent modifier in the multi-element determinations of Pb and Se 126

Figure 5.47 Pyrolysis and atomization curves for multi-element determinations of Bi, Sb, and Cd using 5µg Pd + 3µg Mg modifier in diluted (1:4) urine sample spiked with 80, 80, and 2 ppb Bi, Sb, and Cd, respectively 128

Figure 5.48 Absorbance signals of diluted (1:4) spiked urine sample at 600°C pyrolysis and 1900°C atomization with 5µg Pd + 3µg Mg modifier in the multi-element determinations of Bi, Sb, and Cd 128

Figure 5.49 Pyrolysis and atomization curves for multi-element determinations of Bi, Sb, and Cd using 500µg Ir permanent modifier in diluted (1:4) urine sample spiked with 80, 80, and 2 ppb Bi, Sb, and Cd, respectively 130

Figure 5.50 Absorbance signals of diluted (1:4) spiked urine sample at 550°C pyrolysis and 1900°C atomization with 500µg Ir permanent modifier in the multi-element determinations of Bi, Sb, and Cd 130

Figure 5.51 The standard addition curves in the multi-element determination of Al, Be, Cr, and V in urine reference sample from Seronorm 132

Figure 5.52 The standard addition curves in the multi-element determination of Al, Be, Cr, and V in urine reference sample from BIO-RAD 134

Figure 5.53 The standard addition curves in the multi-element determination of Al, Be, Cr, and V in Bovine Liver sample 137

Figure 5.54 The standard addition curves in the multi-element determination of Al, Be, Cr, and V in Pork Liver sample 139

Figure 5.55 The standard addition curves in the multi-element determination of Be, Cr, and Cu in urine reference sample from Seronorm 142

Figure 5.56 The standard addition curves in the multi-element determination of Be, Cr, and Cu in urine reference sample from BIO-RAD 144

Figure 5.57 The standard addition curves in the multi-element determination of Be, Cr, and Cu in Tea sample 146

Figure 5.58 The standard addition curves in the multi-element determination of Be, Cr, and Cu in Bovine Liver sample 148

Figure 5.59 The standard addition curves in the multi-element determination of Bi, Cu, Mn, and Sb in urine reference sample from Seronorm 151

Figure 5.60 The standard addition curves in the multi-element determination of Bi, Cu, Mn and Sb in urine reference sample from BIO-RAD 153

Figure 5.61 The standard addition curves in the multi-element determination of Bi, Cu, Mn and Sb in Pig Kidney sample 155

Figure 5.62 The standard addition curves in the multi-element determination of Bi, Cu, Mn and Sb in Bivine Liver sample 158

Figure 5.63 The standard addition curves in the multi-element determination of Cu, Mn, and Se in urine reference sample from Seronorm 161

Figure 5.64 The standard addition curves in the multi-element determination of Cu, Mn, and Se in urine reference sample from BIO-RAD 163

Figure 5.65 The standard addition curves in the multi-element determination of Cu, Mn, and Se in Pig Kidney sample 165

Figure 5.66 The standard addition curves in the multi-element determination of Pb and Se with Pd+Mg modifier in Urine reference sample from Seronorm 167

Figure 5.67 The standard addition curves in the multi-element determination of Pb and Se with Ir permanent modifier in Urine reference sample from Seronorm 169

Figure 5.68 The standard addition curves in the multi-element determination of Pb and Se in Urine reference sample from BIO-RAD 170

Figure 5.69 The standard addition curves in the multi-element determination of Pb and Se in Pork Liver sample 172

Figure 5.70 The standard addition curves in the multi-element determination of Pb and Se in Tea sample..... 173

Figure 5.71 The standard addition curves in the multi-element determination of Bi, Cd, and Sb with Pd+Mg modifier in Urine reference sample from Seronorm 176

Figure 5.72 The standard addition curves in the multi-element determination of Bi, Cd, and Sb with Ir permanent modifier in Urine reference sample from Seronorm 178

Figure 5.73 The standard addition curves in the multi-element determination of Bi, Cd, and Sb in Urine reference sample from BIO-RAD 180

Figure 5.74 The standard addition curves in the multi-element determination of Bi, Cd, and Sb in Bovine Liver sample 182

Figure 5.75 The standard addition curves in the multi-element determination of Bi, Cd, and Sb in Pig Kidney sample 184

Figure 5.76 The standard addition curves in the multi-element determination of Bi, Cd, and Sb in Pork Liver sample 186

Figure 5.77 The standard addition curves in the multi-element determination of Bi, Cd, and Sb in Tea sample 188

III.List of Tables

Table 1.1 Normal furnace program for SIMAA 6000 instrument 21

Table 2.1 Multi-Element analytical procedures developed by SIMAA 6000 34

Table 2.2 Comparison between the single-element and multi-element detection limits ($\mu g.l^{-1}$) 42

Table 4.1 The lamp types and setting parameters for each lamp 50

Table 4.2 Standard reference solutions 51

Table 4.3 Temperature program for SIMAA 6000 system 52

Table 4.4 Temperature program for the metal coating 52

Table 4.5 Certified reference materials 52

Table 5.1 The pyrolysis and atomization temperatures without modifier in the single-element mode 61

Table 5.2 Comparing the single-element determinations with the multi-element mode of Be, Cr, and Cu (pyrolysis=1200^{o}C, atomization=2300^{o}C) 73

Table 5.3 Comparing the single-element mode with the multi-element determination of Bi, Sb, Cu, and Mn (pyrolysis=1100^{o}C, atomization=2000^{o}C) 77

Table 5.4 Comparing the single-element mode with the multi-element mode of Cu, Mn, and Se (pyrolysis=1200^{o}C, atomization=2000^{o}C) 79

Table 5.5 Comparing the single-element mode with the multi-element mode of Pb and Se using Pd+Mg modifier (pyrolysis=1000^{o}C, atomization=1900^{o}C) 81

Table 5.6 Comparing the single-element mode with the multi-element mode of Pb and Se using Ir permanent modifier (pyrolysis=1200^{o}C, atomization=2000^{o}C) 83

Table 5.7 Comparing the single-element mode with the multi-element mode of Bi, Sb, and Cd using Pd+Mg modifier (pyrolysis=700^{o}C, atomization=1900^{o}C) 85

Table 5.8 Comparing the single-element mode with the multi-element determination of Bi, Sb, and Cd using Ir modifier (pyrolysis=700^{o}C, atomization=2100^{o}C) 88

Table 5.9 Comparing the single-element mode with the multi-element mode of Al, Be, Cr, and V (pyrolysis=1500^{o}C, atomization=2500^{o}C) 89

Table 5.10 Comparing the single-element mode with the multi-element determination of Be, Cr, Cu, and Mn using Pd+Mg modifier (pyrolysis=1200^{o}C, atomization=2300^{o}C)..... 92

Table 5.11 Comparing the single-element mode with the multi-element determination of Bi, Cu, Mn, Sb, and Se using Pd+Mg modifier (pyrolysis=1100^{o}C, atomization=2000^{o}C) 94

Table 5.12 Comparing the single-element mode with the multi-element determination of Bi, Pb, Sb, and Se using Pd+Mg modifier (pyrolysis=1000^{o}C, atomization=1900^{o}C) 96

Table 5.13 The effect of operating mode on detection limits and characteristic mass values115

Table 5.14 The analytical values of Seronorm Trace Elements Urine..... 116

Table 5.15 Optimum Temperature Program for Simultaneous Determination of Al, Be, Cr, and V in Urine reference sample from Seronorm 131

Table 5.16 The results of simultaneous determination of Al, Be, Cr, and V in urine reference sample from Seronorm 133

Table 5.17 Detection limits, characteristic mass, and relative standard deviations for simultaneous determination of Al, Be, Cr, and V in urine reference material from Seronorm 133

Table 5.18 The results of simultaneous determination of Al, Be, Cr, and V in urine reference sample from BIO-RAD 136

Table 5.19 Detection limits, characteristic mass, and relative standard deviations for simultaneous determination of Al, Be, Cr, and V in urine reference material from BIO-RAD 136

Table 5.20 The results of simultaneous determination of Al, Be, Cr, and V in Bovine Liver sample..... 138

Table 5.21 Detection limits, characteristic mass, and relative standard deviations for simultaneous determination of Al, Be, Cr, and V in Bovine Liver sample 138

Table 5.22 The results of simultaneous determination of Al, Be, Cr, and V in Pork Liver sample..... 140

Table 5.23 Detection limits, characteristic mass, and relative standard deviations for simultaneous determination of Al, Be, Cr, and V in Pork Liver sample 140

Table 5.24 Optimum Temperature Program for Simultaneous Determination of Be, Cr, and Cu in Urine reference sample from Seronorm 141

Table 5.25 The results of simultaneous determination of Be, Cr, and Cu in urine reference sample from Seronorm 143

Table 5.26 Detection limits, characteristic mass, and relative standard deviations for simultaneous determination of Be, Cr, and Cu in urine reference material from Seronorm . 143

Table 5.27 The results of simultaneous determination of Be, Cr, and Cu in urine reference sample from BIO-RAD 145

Table 5.28 Detection limits, characteristic mass, and relative standard deviations for simultaneous determination of Be, Cr, and Cu in urine reference material from BIO-RAD. 145

Table 5.29 The results of simultaneous determination of Be, Cr, and Cu in Tea sample..... 147

Table 5.30 Detection limits, characteristic mass, and relative standard deviations for simultaneous determination of Be, Cr, and Cu in Tea sample 147

Table 5.31 The results of simultaneous determination of Be, Cr, and Cu in Bovine Liver... 149

Table 5.32 Detection limits, characteristic mass, and relative standard deviations for simultaneous determination of Be, Cr, and Cu in Bovine Liver 149

Table 5.33 Optimum Temperature Program for Simultaneous Determination of Bi, Sb, Cu, and Mn in Urine reference sample from Seronorm..... 150

Table 5.34 The results of simultaneous determination of Bi, Cu, Mn, and Sb in urine reference sample from Seronorm 152

Table 5.35 Detection limits, characteristic mass, and relative standard deviations for simultaneous determination of Bi, Cu, Mn, and Sb in urine reference material from Seronorm 152

Table 5.36 The results of simultaneous determination of Bi, Cu, Mn, and Sb in urine reference sample from BIO-RAD 154

Table 5.37 Detection limits, characteristic mass, and relative standard deviations for simultaneous determination of Bi, Cu, Mn, and Sb in urine reference material from BIO-RAD 154

Table 5.38 The results of simultaneous determination of Bi, Cu, Mn, and Sb in Pig Kidney sample..... 156

Table 5.39 Detection limits, characteristic mass, and relative standard deviations for simultaneous determination of Bi, Cu, Mn, and Sb in Pig Kidney 157

Table 5.40 The results of simultaneous determination of Bi, Cu, Mn, and Sb in Bovine Liver sample 159

Table 5.41 Detection limits, characteristic mass, and relative standard deviations for simultaneous determination of Bi, Cu, Mn, and Sb in Bovine Liver 159

Table 5.42 Optimum Temperature Program for Simultaneous Determination of Cu, Mn, and Se in Urine reference sample from Seronorm 160

Table 5.43 The results of simultaneous determination of Cu, Mn, and Se in urine reference sample from Seronorm 162

Table 5.44 Detection limits, characteristic mass, and relative standard deviations for simultaneous determination of Cu, Mn, and Se in urine reference material from Seronorm 162

Table 5.45 The results of simultaneous determination of Cu, Mn, and Se in urine reference sample from BIO-RAD 164

Table 5.46 Detection limits, characteristic mass, and relative standard deviations for simultaneous determination of Cu, Mn, and Se in urine reference material from BIO-RAD 164

Table 5.47 The results of simultaneous determination of Cu, Mn, and Se in Pig Kidney 165

Table 5.48 Detection limits, characteristic mass, and relative standard deviations for simultaneous determination of Cu, Mn, and Se in Pig Kidney 166

Table 5.49 Optimum Temperature Program for Simultaneous Determination of Pb and Se with Pd+Mg modifier in Urine reference sample from Seronorm 167

Table 5.50 The results of simultaneous determination of Pb and Se with Pd+Mg modifier in urine reference sample from Seronorm 168

Table 5.51 Detection limits, characteristic mass, and relative standard deviations for simultaneous determination of Pb and Se with Pd+Mg modifier in urine reference material from Seronorm 168

Table 5.52 The results of simultaneous determination of Pb and Se with Ir permanent modifier in urine reference sample from Seronorm 169

Table 5.53 Detection limits, characteristic mass, and relative standard deviations for simultaneous determination of Pb and Se with Ir permanent modifier in urine reference material from Seronorm 169

Table 5.54 The results of simultaneous determination of Pb and Se in urine reference sample from BIO-RAD 171

Table 5.55 Detection limits, characteristic mass, and relative standard deviations for simultaneous determination of Pb and Se in urine reference material from BIO-RAD..... 171

Table 5.56 The results of simultaneous determination of Pb and Se in Pork Liver sample .. 172

Table 5.57 Detection limits, characteristic mass, and relative standard deviations for simultaneous determination of Pb and Se in Pork Liver 172

Table 5.58 The results of simultaneous determination of Pb and Se in Tea sample..... 174

Table 5.59 Detection limits, characteristic mass, and relative standard deviations for simultaneous determination of Pb and Se in Tea sample 174

Table 5.60 Optimum Temperature Program for Simultaneous Determination of Bi, Cd, and Sb in Urine reference sample from Seronorm 175

Table 5.61 The results of simultaneous determination of Bi, Cd, and Sb with Pd+Mg modifier in urine reference sample from Seronorm 177

Table 5.62 Detection limits, characteristic mass, and relative standard deviations for simultaneous determination of Bi, Cd, and Sb with Pd+Mg modifier in urine reference material from Seronorm 177

Table 5.63 The results of simultaneous determination of Bi, Cd, and Sb with Ir permanent modifier in urine reference sample from Seronorm 179

Table 5.64 Detection limits, characteristic mass, and relative standard deviations for simultaneous determination of Bi, Cd, and Sb with Ir permanent modifier in urine reference material from Seronorm 179

Table 5.65 The results of simultaneous determination of Bi, Cd, and Sb in urine reference sample from BIO-RAD 181

Table 5.66 Detection limits, characteristic mass, and relative standard deviations for simultaneous determination of Bi, Cd, and Sb in urine reference material from BIO-RAD . 181

Table 5.67 The results of simultaneous determination of Bi, Cd, and Sb in Bovine Liver sample..... 183

Table 5.68 Detection limits, characteristic mass, and relative standard deviations for simultaneous determination of Bi, Cd, and Sb in Bovine Liver sample 183

Table 5.69 The results of simultaneous determination of Bi, Cd, and Sb in Pig Kidney sample 185

Table 5.70 Detection limits, characteristic mass, and relative standard deviations for simultaneous determination of Bi, Cd, and Sb in Pig Kidney sample 185

Table 5.71 The results of simultaneous determination of Bi, Cd, and Sb in Pork Liver sample 187

Table 5.72 Detection limits, characteristic mass, and relative standard deviations for simultaneous determination of Bi, Cd, and Sb in Pork Liver sample 187

Table 5.73 The results of simultaneous determination of Bi, Cd, and Sb in Tea sample 189

Table 5.74 Detection limits, characteristic mass, and relative standard deviations for simultaneous determination of Bi, Cd, and Sb in Pork Liver sample 189

1 Introduction to Multi-Element Graphite Furnace Atomic Absorption Spectrometry

1.1 Review

Atomic Absorption Spectrometry (AAS) was developed for rapid element determination and it is now widely used for the determination of trace elements in many various materials. Different atomization techniques as flame, graphite furnace, hydride, and cold vapour have been developed and studied. This technique has become a very powerful one, especially for routine works, in hundreds of laboratories around the world[1].

In the last decades, additional demands on the spectroscopic element determination have become more and more important. These demands include high sample throughput, short total analysis time, and reduction of consumption of reagents and consumables[1]. Graphite furnace atomic absorption spectrometry (GFAAS), also known as electrothermal atomic absorption spectroscopy (ETAAS), is a suitable and widely used technique to determine elements at trace levels[2, 3]. For many elements, GFAAS offers detection limits superior to those of inductively coupled plasma atomic emission spectroscopy (ICP-AES). Moreover, sample consumption in GFAAS is much lower than of ICP-AES meaning that experiments can be conducted on a microscale level, consuming lower quantities of expensive standards and generally less amounts of waste[4]. GFAAS is particularly advantageous in the analysis of complex samples. Removal of solvent, pyrolysis, and atomization can be carried out in discrete steps permitting, particularly with the aid of chemical modification, selective removal of matrix components. Thus freedom from interferences can be attained in many cases. The analytical performance of GFAAS with respect to complex matrices has been demonstrated by a wealth of practical investigations[5-8]. In addition, GFAAS offers high selectivity and sensitivity, capability for direct analysis with minimal sample preparation, solid sampling and easily operating or handling[2].

Compared with atomic emission spectroscopic technique, GFAAS suffers from the very beginning from the fact that it has been developed as a single-element technique. The multi-element determination is possible in sequential manner only. Thus, due to the usual length of the electrothermal programs (sometimes several minutes), its main drawback is a time-consuming analysis. Another main disadvantage of GFAAS over emission methods is the poor dynamic range of about two orders of magnitude only (up to 10 in some ICP-AES

realizations). This calls often for frequent dilution of the sample, operations which lower sample throughput and consequently the global productivity of the analysis[9].

Many different multi-element instruments have been used for the simultaneous multi-element determination of trace metals, such as Inductively Coupled Plasma incorporating Atomic Emission Spectrometry (ICP-AES)[10], or Mass Spectrometry (ICP-MS)[11], X-ray Fluorescence Spectrometry[12], Cathodic Stripping Voltammetry (CSV)[13], and Multi-Element Graphite Furnace Atomic Absorption Spectrometry (GFAAS)[14-19]. The most important commercially available multi-element instruments for trace elemental determination are ICP-based. The applicability of ICP-based instruments has been limited by difficulties in dealing with high salt concentrations and the need for relatively large sample volumes. Consequently, separation or preconcentration of analyte from matrix prior to the measurement is necessary. Although ICP-MS has been emerged as a method with a power of detection which is at least comparable to that of GFAAS, the MS detector is rather complex and expensive[20].

Since 1960s a variety of multi-element AAS techniques have been developed and performed. Both line and continuous sources have been used, various optical dispersion systems, and several types of detectors have been tested[5, 21-36]. In recent years, owing to the availability of several commercial multi-element GFAAS instruments (four types at least), the analytical potential of GFAAS has increased[37].

At present, the most updated commercial instrumentation is a line source simultaneous spectrometer[38], equipped with Transversely Heated Graphite Atomizer (THGA) with integrated platform, Zeeman-effect background corrector, and solid-state detector, making possible the operation under Stabilized Temperature Platform Furnace (STPF) conditions[39]. This instrument allows simultaneous determination up to six elements[40].

1.2 Basic Features of the GFAAS

1.2.1 System Design

The general construction of a GFAAS system is shown schematically in Figure 1.1. The most important components are a radiation source (line source) which emits the spectrum of the analyte element; an electrothermal atomizer, in which the atoms of the element to be analyzed are formed; a monochromator for the spectral dispersion of the radiation with an exit slit for selection of the resonance line; a detector permitting measurement of radiation intensity, followed by an amplifier and a readout device that presents a reading. In addition, modern instruments are equipped with a background correction method.

Figure 1.1 Diagram of the basic components of a GFAAS

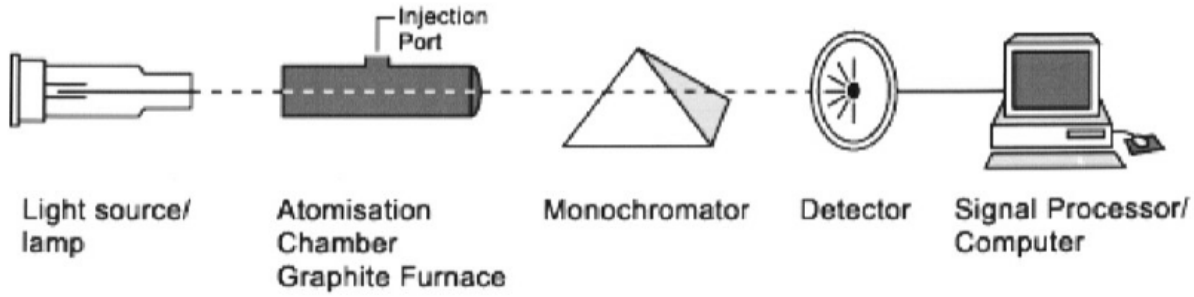

1.2.2 Temperature Program

An analysis of an aqueous sample is begin by either injecting or spraying 10-100 µl of the sample through the dosing hole into the graphite tube. The tube is then heated through a series of steps under a particular purge gas. A sample furnace program is presented in Table 1.1. These steps are as follows: drying, pyrolysis, atomization, and cleaning.

Table 1.1 Normal furnace program for SIMAA 6000 instrument

Step	Temperature (^{o}C)	Ramp Time (s)	Hold Time (s)	Gas Flow (ml.min^{-1})
Dry 1	110	1	30	250
Dry 2	130	15	30	250
Pyrolysis	Variable*	10	20	250
Atomization	Variable*	0	5	0
Clean-out	2450	1	3	250

*depend on the element.

1.2.2.1 Drying Step

The purpose of the drying step is to remove any solvent from the sample. The sample must be dried slowly. If the tube is heated too rapidly, the solvent may boil and splatter through the dosing hole, resulting in analyte loss. With the transversely heated graphite atomizer (THGA), which is used in this work, a two step drying procedure has been used. 110^{o}C with a ramp of 1s and a hold time of 30s, followed by 130^{o}C with a 5s ramp and 30s hold initially heats the platform and solvent, then removes the solvent vapour from the system and ensures even and smooth drying.

1.2.2.2 Pyrolysis Step

After drying, the sample is subjected to one or more thermal pre-treatment steps to reduce matrix constituents prior to atomization. This decreases the possibility of chemical interferences and reduces the magnitude of the background signal. For many elements, the use of a matrix modifier improves the analysis. The modifier salt is added to the sample in high concentration, transforming the analyte into a more well-defined compound. The matrix modifier can either stabilize the analyte element in order to permit a higher pyrolysis temperature or make the matrix more volatile for more effective pyrolysis[41]. The optimal pyrolysis temperature should be empirically determined by plotting the integrated absorbance versus temperature (pyrolysis curve). The optimal pyrolysis temperature is as high as possible without loss of the integrated absorbance signal. A typical pyrolysis curve is shown in Figure 1.2.

1.2.2.3 Atomization Step

During the atomization step, the tube is rapidly heated to the atomization temperature. This rapid heating atomizes the chemical compounds, creating an atomic vapour inside the furnace. Elements in the atomic vapour then absorb light from the line source. The change in light intensity can then be measured using a photomultiplier tube or other types of photodetectors. During the atomization step the internal gas flow is switched off. The temperature selected for atomization should be high enough to guarantee complete volatilization of the analyte element. The optimal temperature depends upon the properties of the compound in which the element resides. A plot of integrated absorbance versus atomization temperature (atomization curve) should reveal a point where maximum absorbance occurs at minimum temperature. The typical atomization curve is shown in Figure 1.2. The shape of the peak can also indicate whether the atomization temperature should be raised or lowered. Increasing the temperature will cause the analyte to vaporize more quickly, improving a broad, tailing peak, as in Figure 1.3

Figure 1.2 Pyrolysis and atomization curves

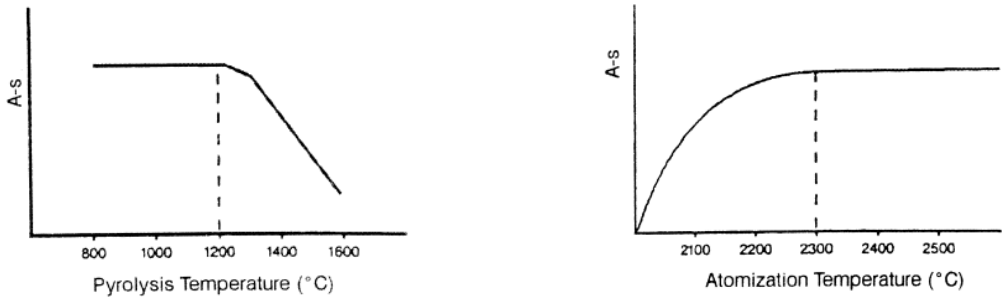

Figure 1.3 Effect of the atomization temperature [(a) 1800°C, (b) 2000°C, (c) 2200°C and (d) 2400°C] on the absorbance profiles of tellurium[42]

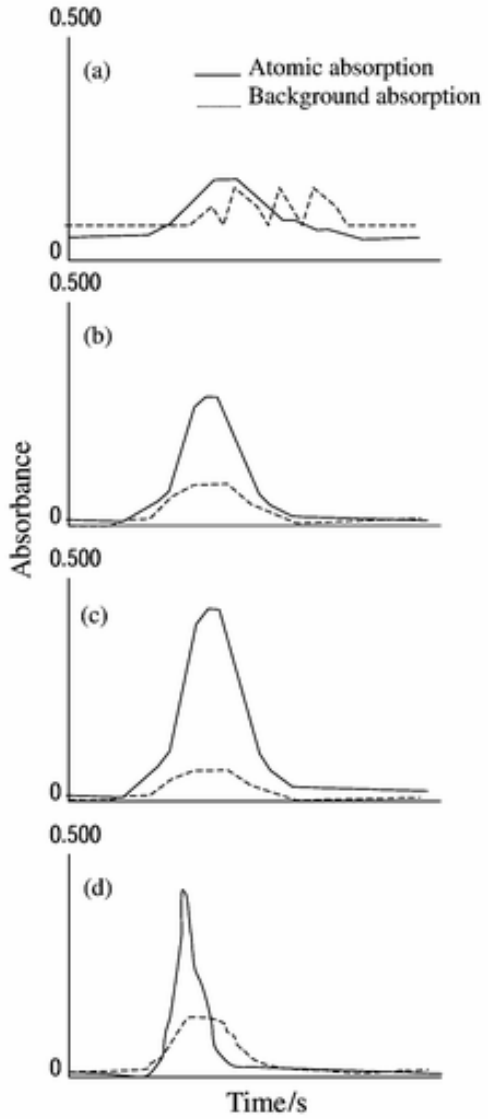

1.2.2.4 Cleaning Step

Before running the next sample introduction, the tube is heated to a high temperature for 3s with internal gas flow to ensure complete removing of analyte atoms. Residual sample

remaining in the tube interfere the subsequent atomization. In the THGA furnace, a clean-out step of 2400^{o}C to 2500^{o}C is used. A clean-out step higher than 2500^{o}C for long periods (>5s) may decrease tube lifetime.

1.2.3 Background Correction

Often, in the course of atomization, broad band light absorbing or light scattering species are generated. To generate an absorbance curve that truly reflects absorbance from analyte atoms, a background correction method needs to be employed. The three most common methods are the use of a continuum source (Deuterium Lamp), self-absorption, and the Zeeman-effect.

1.2.3.1 Continuum Source

To correct for background absorbance using a continuum source such as deuterium lamp, a rotating chopper is employed to alternately pass light from the deuterium lamp and the line source through the sample. If the slit width of the monochromator is wide enough, absorbance of continuum light by the atomic vapour will be minimal, and a change in signal from the deuterium source will reflect a change in background absorbance. Therefore, a background subtracted absorbance signal can be determined[43]. The background absorption (BG) – determined with the deuterium arc lamp – is subtracted from total absorption (AA+BG) determined with the HCL or EDL. The result of this calculation is the correct analyte absorption (AA), if:

- The optical beams for the two sources have the same spatial intensity distributions in the furnace

- The background attenuation is homogeneous over the optical bandwidth of the monochromator. This is usually the case for background originating from scattering but not always for background by molecular absorption and never for atomic absorption.

- The intensities of the two light sources are similar enough that can be handled by the instrument electronics.

1.2.3.2 Self-Reversal Methods

A background correction method that does not employ a second light source is the self-reversal method. When a high current is applied to a hollow cathode lamp, the energy of the excited species becomes high enough to form a cloud of atoms that are not excited. These unexcited atoms absorb the light emitted from the excited atoms, resulting in the effect known

as self-reversal, illustrated in Figure 1.4. At high current, the output peak is considerably broadened and the intensity at peak centre is reduced. To use this method to correct for background effects, the light source is alternately held at high and low current. When the light source is at low, the total absorbance is acquired. When the light source is at high current, the absorbance due to the background is obtained. Using this information, a background corrected absorbance signal can be calculated[43]. In comparison with two sources method, the determination of background absorbance is performed with much more similar spectral resolution in the two measurement phases. There are significant disadvantages, however:

- The lifetime of any HCL is reduced when currents much higher than the standard operating current are used.

- Line profiles for moderately refractory and refractory elements show only a minor dip; the remaining absorbance is much smaller than AA and the detection limits may deteriorate when the background corrector is used.

- The significantly higher stray light level results in curvature of the calibration function even at relatively low absorbance values.

- The background must not be structured to such an extent that it can not be considered constant over the spectral width of the broadened emission profile.

Instruments with a background corrector based on the line-reversal or Smith-Hieftje Principle are therefore used only for some analyte elements and are always equipped with additional continuum source background corrector.

1.2.3.3 Zeeman-Effect

Another commonly used method of background correction employs the Zeeman Effect. Although, there are several methods of employing Zeeman background correction, a simple example will be provided here. When a source of atomic absorption or emission lines is placed in a magnetic field, these lines are split to energies slightly higher and lower than the absorption or emission wavelength. The lines are also split into differing polarities, depending on how the magnetic field is applied. An example of normal Zeeman splitting is shown in Figure 1.5. In the simplest case the ground state is split into two levels. The excited state is split as well. During electron excitation, 4 transitions should theoretically be possible: low-low, low-high, high-low, and high-high. In the first and in the fourth case the transition energies are the same as those without the magnetic field, in the other cases the energies are higher or lower. The wavelength difference between the transitions is small, but in the case of

a 1 T field, large enough to shift the so called σ-profiles far enough that the overlap of these components with the emission profile is minimized. The absorbance of the central profile (the so called π component) is still half of the absorbance without the magnetic field but due to the magnetic field it can only absorb light of a certain direction of polarization. This depends on the direction of the magnetic field. If the field is parallel to the propagation direction of the light beam, the resonance wavelength can not be absorbed at all, if the field is perpendicular to the light beam, only the light polarised parallel to the magnetic field can be absorbed by the π component. This phenomenon named the Zeeman Effect. It is used in the longitudinal version (magnetic field parallel to the light beam) as well as in a transverse version (magnetic field perpendicular to the light beam). The Zeeman Effect can be used to correct for background absorbance by chopping the line source with a polarizing chopper and applying a magnetic field to the graphite furnace. With this configuration, the line source alternates at polarity σ and π, whereas the central absorbance line is fixed by the magnetic field at polarity π. Light from the source can only be absorbed by the analyte when it is in the correct polarity. Therefore, I_o is obtained when the source is emitting at polarity σ, and I is obtained when the source is emitting at polarity π. Because I and I_o are being measured closely in time, any broad band absorption or scattering species present in the furnace will affect the signal of both I and I_o[43]. The function of the Zeeman background corrector is neither limited to a wavelength range nor by the properties of the lamp. It will even rapidly correct for fluctuations in source intensity as the same source is measured with and without the analyte absorption.

The Zeeman Effect principle works only if the background absorption is unaffected by the magnetic field. This is probably true for light scattering in general and it is true for molecules as well. It is true for metals only if the split of the matrix atomic line profiles in the magnetic field does not result in an overlap with the analyte emission profile.

However, for the Zeeman Effect correction, as with each of the common background correction methods, although background is measured closely in time with analyte absorbance signal, none of the listed methods provide truly simultaneous background correction.

Figure 1.4 Self-reversal background correction

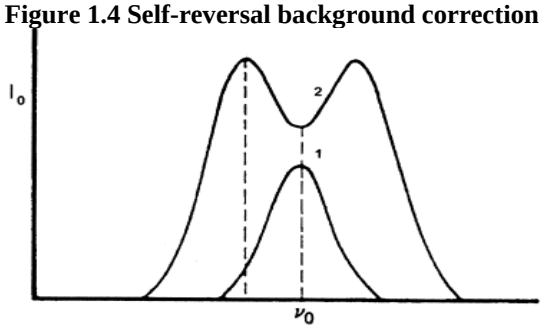

Figure 1.5 Normal Zeeman-effect splitting

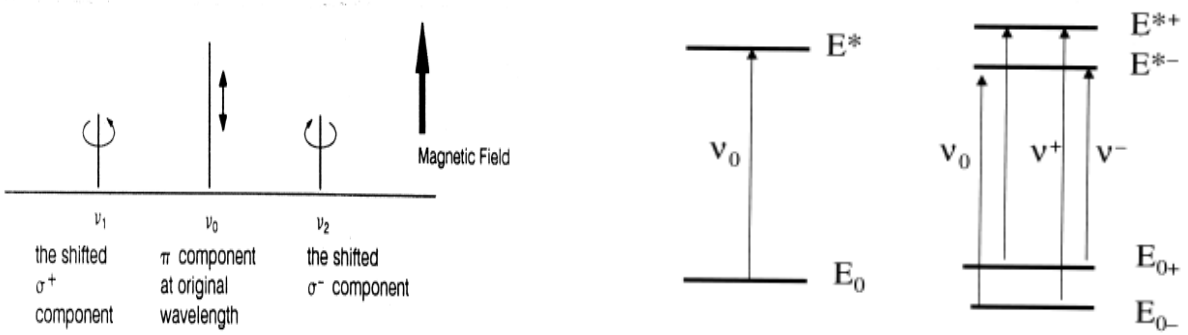

1.2.4 Atomization Mechanism & Stabilization in Graphite Furnace

The atomization can emanate from either molecules or atoms, according to the nature of the sample and the behaviour of the analyte element. If it emanates from molecules, atomization can be either a simple thermal decomposition (dissociation) of a compound, or the reduction of an oxide on the glowing graphite surface. If atomization emanates from the elemental form, it can be either desorption or volatilization. Because of the small quantity and wide distribution of the sample, boiling as the atomization mechanism can be excluded by deduction.[44].

Sturgeon et al.[45] investigated atomization mechanisms on the basis of a thermodynamic/kinetic approach. They identified three possible pathways by which gas phase atoms may be formed: carbon reduction of the analyte oxide with subsequent sublimation of the metal, thermal dissociation of the metal oxide, and thermal dissociation of the metal chloride. In later work, Sturgeon and Chakrabarti[46, 47] refined their procedure and proposed four mechanisms:

(1) Reduction of the solid oxide on the graphite surface according to:

$MO_{(s)} \rightarrow M_{(l)} \leftrightarrow \frac{1}{2} M_{2(g)} \rightarrow M_{(g)}$

where M: Co, Cr, Cu, Fe, Mo, Ni, Pb, Sn, and V.

(2) Thermal decomposition of solid oxide according to:

$MO_{(s)} \rightarrow M_{(g)} + \frac{1}{2} O_{2(g)}$

where M: Al, Cd, and Zn.

(3) Dissociation of oxide molecules in the vapour phase according to:

$MO_{(s)} \leftrightarrow MO_{(g)} \rightarrow M_{(g)} + \frac{1}{2} O_{2(g)}$

where M: Cd, Mg, Mn, and Zn.

(4) Dissociation of halide molecules in the vapour phase according to:

$MX_{(s)} \rightarrow MX_{(l)} \rightarrow MX_{(g)} + X_{(g)}$

$MX_{(g)} \rightarrow M_{(g)}$ and $MX_{(g)} \rightarrow X_{(g)}$

where M: Cd, Fe, Zn and X: Cl.

Reactions (1) and (2) requiring intimate contact with the graphite surface depend strongly on the rate of heating used for atomization. Reactions (3) and (4), in contrast, are via dissociation in the vapour phase and should therefore depend strongly on the temperature of the inert gas and whether the graphite surface is in thermal equilibrium with the gas phase[44]. When the sample is in the form of nitrate or sulphate, the metal oxide usually results on heating; even when the sample is in the form of halide, this may still be true, because hydrolysis to oxygen-containing species frequently occurs in this case[45].

During the investigation on the formation and transport of atoms in graphite furnace, Smets[48] found two groups of elements for each. For the formation of atoms, the rate-determining step is either the reduction of the oxide on carbon, volatilization of the metal released by reduction of the oxide on carbon. He found that the only exception was aluminium, for which he assumed a vapour phase dissociation of AlO. For the transport of atoms from the furnace, Smets also proposed two mechanisms. Elements such as Ag, As, Au, Bi, Hg, Pb, Se, and Zn are transported by diffusion from the tube. The integrated absorbance is directly proportional to the integrated rate of formation of atoms. The gas stream through the tube has a considerable influence on the sensitivity for these elements. In contrast, elements such as Ba, Be, Ca, Cr, Cu, Fe, K, Li, Mn, Mo, Na, Ni, Sr, U, and V are not transported from the tube by diffusion. They are repeatedly volatilized and condensed in a type of short-range distillation resulting from the prevailing temperature gradient or specific "sticking probability". In this respect the formation of stable carbides or intercalation compounds with graphite can be considered. An alteration in the gas flow rate has no marked

influence on the sensitivity for these elements. Resulting from longer residence time of the atoms in the radiation beam, the peaks generated are clearly broader and consequently the integrated absorbance higher.

In graphite furnaces of the Massmann type, the furnace is not in equilibrium with respect to either volume or time at the moment of atomization. At the tube wall, the element is volatilized and atomized while the temperatures of the graphite tube and the inert gas continue to change. If the element is determined in a different matrix, it can be volatilized and atomized at another temperature. The peak shaped atomization signal will consequently be shifted on the time axis. This means that the absorption signals for both samples will be different, both in peak height and peak area, even when the concentration of the analyte element is the same[44]. Slavin et al.[39] combining a number of already recommended procedures into one package and thus improving the properties of Massmann type furnaces. First of all, it is important that the graphite tube is heated as quickly as possible to the required final temperature. At the same time, atomization of the analyte element is delayed by use of the platform proposed by L'vov et al.[49]. The graphite tube can attain the final temperature and the inert gas in the tube has time to reach this temperature before the platform reaches the atomization temperature and the analyte element is volatilized. It is naturally important that the inert gas stream through the tube is interrupted during or even better slightly before atomization. If the inert gas is in thermal equilibrium with the tube wall at the moment of atomization, no further expansion of the gas takes place, thus avoiding a further loss of atoms. Transport of atoms from the tube is then only via diffusion. A further important criterion for achieving thermal equilibrium in a Massmann furnace at the moment of volatilization is that the temperature step from the thermal pretreatment temperature to the atomization temperature should not be too large. Slavin[39] quotes a temperature of 1000°C, which should not be exceeded if possible. If matrix modification[41] is used in addition, it is often possible to raise the thermal pretreatment temperature, and it is possible to meet the requirement of a temperature step less than 1000°C for most elements.

1.3 Simultaneous Multi-Element Graphite Furnace AAS Systems

At the end of the 1980s, several commercial systems have become available[1]. Commercial multi-element AAS systems are available from Hitachi (Danburg, CT) since 1988, Thermo Jarrel Ash (Franklin, MA) since 1990, Leeman Labs (Chelmsford, MA) since 1993, and Perkin-Elmer (Norwalk, CT) since 1994[5, 35, 50-54]. A review on multi-element AAS in general is available[55]. Harnly[56] also reviewed multi-element AAS with a continuum source.

1.3.1 Line Source Multi-Element Systems

Hollow cathode lamps (HCLs) and electrodeless discharge lamps (EDLs), which are the most widely used line sources, commonly, require that one lamp be used for each element. The multi-element HCL and multi-element EDL were proposed and widely used beginning in the mid-1990s[57]. Although still available, multi-element lamps are not widely used. This is primarily due to the reduced sensitivity of the element in the multi-element lamp compared to the element in a single-element lamp[57]. Multi-element HCLs are mostly studied for elements with similar properties and are usually limited to between two and four elements[57]. Studies on the use of line sources for multi-element atomic absorption measurements[14-19, 27, 33, 58-60] have been reported where the superiority in sensitivity and detection limits were easily retained as against the continuum source[60]. Several systems have been developed. The following description lists several of these commercial systems.

1.3.1.1 Model Z-9000 from Hitachi

Since the late of 1980s, Hitachi has marked a simultaneous multi-element system, model Z-9000[51, 57]. The system utilized Zeeman background correction and used four HCLs focused simultaneously through the atomizer. Four photomultiplier tubes (PMTs) allowed for continuous monitoring of each element. The Z-9000 Hitachi system can analyze four elements in one furnace firing. The multi-element system offers the following advantages over the single-element or dual-element systems. These include: high sample throughput; shorter analysis time; saving on consumables; expansion of dynamic working range; internal standards; and smaller required working sample[51, 57]. Yasuda et al.[61] used the Z-9000 to investigate the expansion of the dynamic range using peak height measurement and a new data-processing method. The working range was extended between a factor of one to two orders of magnitude. Optimization of parameters for multi-element determinations Cd, Pb, and Zn indicated that higher heating rates and rapid atomization produced reliable results.

1.3.1.2 AA Scan 4 from Thermo-Jarrell Ash

Thermo-Jarrell Ash Corporation has developed an instrument, the AA Scan 4, capable for simultaneous determination of four elements in a graphite furnace[4, 57, 62]. The instrument employs multiple light sources but only a single monochromator and PMT. To analyze different lines, a mirror is placed on a galvanometer to sequentially transmit light from each line source into the instrument. In a similar fashion, the monochromator grating is also on a galvanometer to sequentially focus the analytical wavelengths from each source onto the PMT.

This instrument was capable of simultaneously determining four elements using self-reversal background correction[57]. The AA Scan 4 has been used to successfully determine Cd and Pb in certified blood samples[63].

1.3.1.3 Analyte 5 (Leeman Labs)

Leeman Labs have introduced Analyte 5 simultaneous graphite furnace AA system[50]. The Analyte 5 is capable of simultaneous determination of several elements using multiple light sources. The instrument employs a reverse polychromator to combine the source beams and notch filters to achieve wavelength discrimination for a single PMT detector. Background correction is performed by self-reversal[64]. This instrument is limited in flexibility because the elements to be studied must be specified when the instrument is manufactured[65].

1.3.1.4 SIMAA 6000 from Perkin-Elmer

The most recent simultaneous multi-element GFAAS system which appeared on the AA market is the SIMAA 6000 from Perkin-Elmer. This instrument presents several innovations: dedicated echelle polychromator optics in a tetrahedral configuration (TEP), solid-state (multi-channel) detector, and transversely heated graphite furnace atomizer (THGA) with longitudinal Zeeman background correction[9]. The SIMAA 6000 allows simultaneous determination of up to four elements (up to six using multi-element hollow cathode lamps). In the next chapter, we have described the basic features of this system in details.

1.3.2 Continuum Source Multi-Element Systems

The use of a continuum source as a light source was proposed and used to overcome the problems associated with multi-element lamps. The most common light source used in these systems is a xenon arc lamp[4]. Several systems have been designed. The most significant difference in these systems is the choice of spectrometer and detector. With the advent of fast, sensitive array detectors, much of the research in continuum source atomic absorption has focused on using array detectors to measure atomic signal[4]. A disadvantage of the continuum source is that the spectral bandpass is much greater than that of the hollow cathode lamp line profile widths and the intensity can be unstable[57]. This results in decreased sensitivity, higher detection limits, and a reduced linear range[57]. Harnly et al.[66] developed a multi-element system based on a xenon arc (300 W) continuum source and an echelle polychromator modified for wavelength modification, which has been named SIMAAC (Simultaneous Multi-element Atomic Absorption with continuum source). The system was capable of analysing up to 16 elements at one time, using double-beam operation and background correction.

Detection limits were found to be comparable to those of single-element systems (AAS) for many elements. A major drawback, however, was lack of sensitivity below 280 nm[57].

1.3.3 Summary

Several graphite furnace spectrometers capable of simultaneous multi-element determinations have been developed. Each of these multi-element systems has distinct advantages over conventional line source GFAAS (LS-GFAAS). Both the continuum and multiple line source systems demonstrate the ability to monitor multiple elements simultaneously with detection limits and sensitivities approaching those of conventional single-element systems. However, the drawbacks of each system and the lack of standard multi-element analytical methodology demonstrate the need for continual research in the field of simultaneous multi-element GFAAS.

2 SIMAA 6000 Design and the Multi-Element Compromised Conditions

2.1 Overview

In this chapter, the basic features of the SIMAA 6000 system have been described. These include Echelle Polychromator Optics with a Tetrahedral Configuration (TEP), Transversely Heated Graphite Atomizer (THGA) integrated platform, and Solid-State (Multi-channel) Detector. TEP optical system allows the instrument to determine up to six elements simultaneously, significantly reducing analysis time. The THGA integrated platform with longitudinal Zeeman-Effect background corrector and Solid-State detector allow the instrument to operate under Stabilized Temperature Platform Furnace (STPF)[39].

SIMAA 6000 has been used for various multi-element determinations with acceptable performance[9, 17, 20, 40, 67-84], keeping the main features of GFAAS: high sensitivity, low detection limits, reduced sample requirements, and the possibility to carry out in situ sample decomposition inside the graphite furnace. Table 2.1 presents a summary of these applications.

In the multi-element determination, numbers of compromised conditions have to be optimized. These compromised conditions do not follow the best conditions compared with the single element measurements because each element has its own optimized setting of parameters which are different from the other elements. In this chapter, we have described these parameters which can affect the output of the analysis compared with the single-element determination.

2.2 Basic Features of SIMAA 6000 System

The basic components of SIMAA 6000 system from Perkin-Elmer is diagrammed in Figure 2.1. Four HCLs or EDLs from Perkin-Elmer can be used as a radiation source to simultaneous determination of four elements (or six elements using multi-element HCLs or EDLs). A transversely heated graphite furnace with integrated platform is used for atomization. An echelle polychromator in a tetrahedral configuration (TEP) is used to separate wavelengths. The detector in this system is a solid-state detector.

Table 2.1 Multi-Element analytical procedures developed by SIMAA 6000

Element	Sample	Chemical Modifier	LD (mgl^{-1})	M_o (pg)	Ref.
Mn	Serum	Pd+Mg	0.65	6.0	67
Se			5.0	46	
Cu	Serum	-	4.0	26	68
Fe			2.2	16	
Zn			0.4	2.7	
As	Drinking water	Pd+Mg	0.7	39	69
Cu			0.2	17	
Mn			0.6	60	
Sb			0.3	43	
Se			0.9	45	
Al	Fuel ethanol	Pd+Mg	1.2	37	70
As			2.5	73	
Cu			0.2	31	
Fe			1.6	16	
Mn			0.2	45	
Ni			1.1	9.0	
Bi	Wine	Pd+Mg	-	-	71
Pb			0.9	45	
Cu	Sea water	Pd+Mg and 5% H_2	0.4	-	72
Mn			0.7	-	
Mo			1.2	-	
Cr	Urine	Mg	0.08	7.8	74
Mn			0.16	4.6	
Cd	Wine	Pd+Mg	0.03	0.6	75
Pb			0.8	33	
As	Atmospheric particulate matter	Pd+Mg	0.26	37	76
Cd			0.02	2.2	
Ni			0.97	28	
Pb			4.3	1400	
Al	Urine	Pd+ 5% H_2	0.06	-	77
Cr			0.05	-	
Cu			0.08	-	
Mn			0.06	-	
Cr	Bismuth tellurite optical crystals	-	1.1	7.5	78
Mo			4.9	20	
V			6.7	58	
Cd	Foodstuffs	$NH_4H_2PO_4$+Mg	0.04	1.5	79
Pb			0.93	37	
As	Water	Ir	0.82	177	80
Bi			0.04	91	
Sb			0.26	107	
Se			0.29	90	
Te			-	-	
Cd	Potable and surface water	Pd+Mg	0.1	-	81
Cr			1	-	
Cu			1	-	
Ni			1	-	
Pb			1	-	
Mo	Seawater	$NH_4H_2PO_4$+Mg	0.35	-	82
V			0.32	-	
Cr	Serum	-	0.05	-	83
Ni			0.2	-	
Cd	Blood	$NH_4H_2PO_4$	0.2	-	83
Pb			4.5	-	
Cd	Urine	$NH_4H_2PO_4$	0.06	-	83
Pb			2.6	-	
Cu	Seawater	Pd+Mg	0.07	1.5	20
Mn			0.10	37	
Cd	Soil and sediment	-	0.001	0.44	9
Pb			0.1	22	
Co			0.05	22	
Cu			0.02	35	
Cd	Whole blood	Pd+Mg	-	-	84
Pb			-	-	
Co	Urine	Mg	0.18	-	17
Mn			0.09	-	

Figure 2.1 Schematic diagram of the basic components of SIMAA 6000

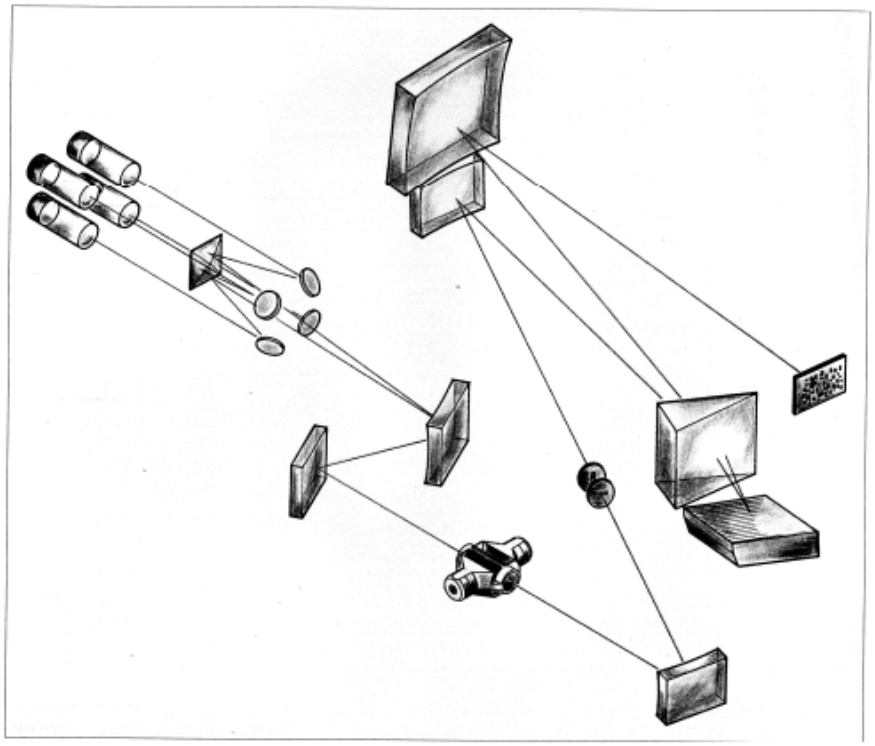

2.2.1 Furnace Design (Transversely Heated Graphite Atomizer THGA)

The HGA (Heated Graphite Atomizer) furnace was a development of the system originally described by Massmann[67, 85]. This design has been improved continually; however, it was known that three were several fundamental limitations to this design. The temperature distribution along the graphite tube in an HGA furnace is not uniform due to the contact of the tube ends with the water cooled contact cylinders. Although atomization from the L'vov platform and using a preatomization cool-down step can minimize or delay this temperature distribution, it is still present. This non-isothermal temperature distribution in the Massmann type furnaces leads to memory effects for refractory elements, gas phase interferences, and matrix condensation at the cooler tube ends[9, 86].

The THGA furnace, which is used with SIMAA 6000, evolved from the side-heated constant temperature graphite furnace described by Frech et al[87]. The transverse heated graphite tube design provides a uniform temperature distribution over the entire tube length. This means that the tube end reach the same temperature as the tube centre. Under these conditions, the formation of free atoms is optimum and recombination of atoms to molecules, the loss of atoms, and condensation on the cooler tube ends, which can produce memory effects, are affectively avoided.

The two types of graphite furnace and the temperature distribution are shown in Figure 2.2 and Figure 2.3, respectively. However, the sensitivity achieved with THGA is not so good as with longitudinally heated atomizer where characteristic masses achieved are two to three times lower[9, 88-91]. This is mainly due to reduced length of the observation volume[9].

The graphite furnace is heated by applying a known voltage across the tube and letting the resistance create the heat required. The temperature is raised to the specified atomization temperature as rapidly as possible (typically up to 2000^{o}C/s). Because the heat rate is faster than with conventional voltage controlled heating, the tube is closer to thermal equilibrium prior to sample atomization. Lower atomization temperatures may be feasible for many elements, which will help to increase tube life time. The THGA tube has an integrated L'vov platform, Figure 2.4, which is heated solely by radiation. The rapid heating of low mass integrated L'vov platform leads to maximum atomization efficiency and lower atomization temperatures[92].

2.2.1.1 The Stabilized Temperature Platform Furnace (STPF)

It was first proposed by W. Slavin, D. Manning, and G. Carnrick[39] and includes the following conditions:

1) Fast instrument electronics to follow the absorption profile

2) Signal integrations rather than peak height. Since the rate of vaporization of an analyte often depends upon the matrix, thus when the matrix of the standards and samples differ, the peak height absorbances can differ. The use of integrated absorbance helps to correct for differing rates of vaporization.

3) Accurate background correction, which is necessary to remove absorption signals that are not due to the analyte. Zeeman background correction has been of particular importance in achieving improved performance with the graphite furnace.

4) Rapid furnace heating to guarantee that the graphite tube is heated to the preselected temperature in the shortest time possible. The faster the heating rate the longer the period for thermal stabilization before the analyte is volatilized off the platform.

5) L'vov platforms and pyrolytically coated graphite tubes to delay the atomization of the analyte as long as possible. During that delay, the graphite tube and the inert gas are directly heated by conduction. The L'vov platform is primarily heated indirectly by radiation from the tube walls. This produces a time lag which allows the system to approach thermal equilibrium before the analyte is atomized.

6) Gas stop during atomization to give the highest sensitivity and thermal stabilization.

7) Use of matrix modifier to stabilize the analyte so that higher pyrolysis temperature can be used and remain on the platform until later in the atomization step.

All of these mutually dependent parameters should be used to take full advantage of the STPF concept, which leads to maximum analyte signal and minimum interferences[92].

Figure 2.2 Temperature distribution in a Massmann-type furnace

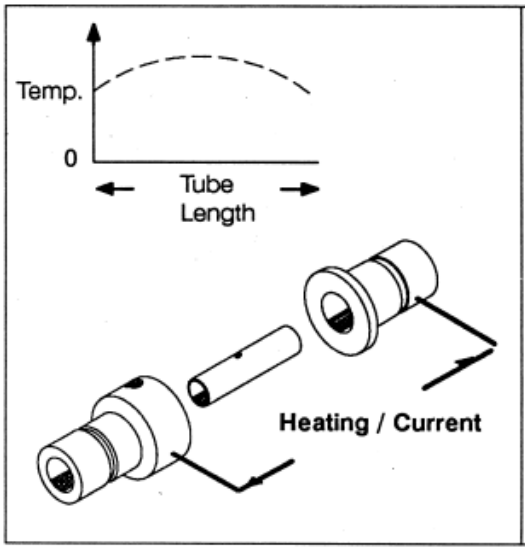

Figure 2.3 Temperature distribution in a transverse heated furnace

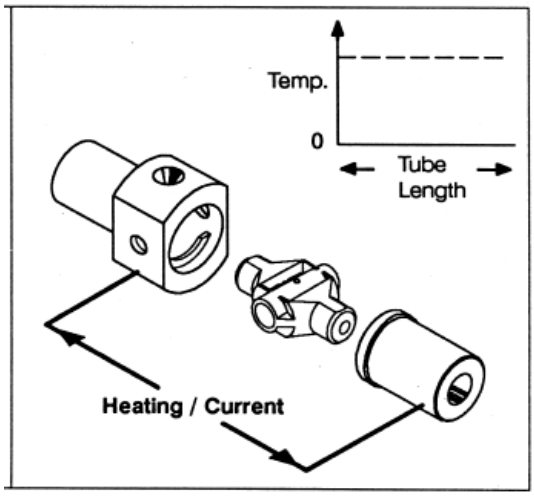

Figure 2.4 Schematic diagram of a THGA with integrated platform

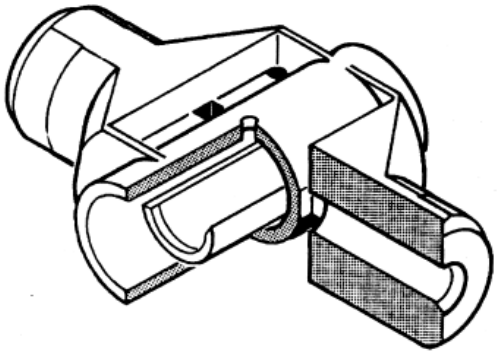

2.2.2 The Tetrahedral Echelle Polychromator Optical System (TEP)

The selectivity in GFAAS, defined as the ability to distinguish between two elements, is due to the fact that the measurement beam originates from sources which emit only a narrow line spectrum of the element (elements) of interest. If this light is transmitted through the atomizer by means of mirrors or lenses, and imaged a second time on a photosensitive cell, atom specific absorption can be detected. Generally, GFAAS is more complicated: the lamps in reality emit a spectrum of resonant and nonresonant lines, mixed with lines from other elements and from the fill gas of the lamp. In the atomizer a number of atoms, molecules, and particles are generated, the analyte atoms usually being only a small fraction – less than a thousandth – of the total absorbing species. Furthermore a lot of light is emitted in the atomizer which reaches the detector. Therefore, the line used for the measurement must be isolated by a monochromator or polychromator.

In a typical monochromator, the radiation which was imaged on the entrance slit is collimated onto a grating and separated into wavelengths (dispersed) depending on the angle of the grating relative to the incoming light only a specific part of the spectrum is transmitted through the exit slit onto the detector. The wider the exit slit of a given monochromator, the broader is the wavelength window reaching the detector. At the same time, the dimensions of the entrance and exit slits determine the amount of light reaching the detector. There are number of parameters that affect the resolution of monochromator: the number of lines per mm on the grating surface, focal length (the distance from the slits to the collimating mirror), and the blaze angle.

The detectors used (photomultiplier tubes) could be easily positioned behind the exit slit. Changing from line to next require a change of lamp and the setting of the new wavelength

with the help of a stepper motor driven grating and, in some cases, a change of the width of the entrance slit. Another way is to keep the grating fixed and to select the wavelength using one of a number of exit slits each positioned at the point at which a particular wavelength reaches the focal plane of the spectrometer. This will require a detector behind each of the slits and will be relatively complicated and expensive. It offers, however, the possibility of reading out a number of lines at the same time so that we speak of a polychromator rather than a monochromator.

Due to recent improvements in solid state detector technology, it has become feasible to combine a number of photosensitive spots on a one dimensional array or two dimensional surfaces. These can act both as wavelength selectors (comparable to an exit slit) and detectors. An echelle polychromator is designed to disperse light in two dimensions. An echelle polychromator system, shown in Figure 2.1, combines these features. Echelle polychromator contains two dispersive elements, in this case, a prism and a grating. The echelle grating is for the main dispersion and a quartz prism for the cross-dispersion. A grating is used under a very flat angle towards the incoming light with a relatively wide spacing of about 10 μm between grooves. Thus radiation is dispersed efficiently into very high orders resulting in very high resolution. However the spectra in many orders are superimposed. Therefore the orders must be separated by a second dispersive element in a direction perpendicular to that of the main dispersion. The resulting spectra are two-dimensional. The light from up to four HCLs or EDLs is combined via a beam combiner and then focused using toroidal mirrors through the THGA furnace. The light beam is then passed through the entrance slits into the TEP. From the lower collimating mirror the light is passed through the dispersion prism and onto the echelle grating. The light is passed back through the prism and upper camera mirror focuses the light onto the focal plane and the solid state detector. Rectangular photosensitive areas corresponding to the image of the entrance slit are positioned for – in this case – 60 wavelengths. In normal operation, the spectrum is generated and read out without any scanning within the optical system. If a wavelength for which no sensitive area has been positioned on the detector is required, the echelle can be shifted in two dimensions relative to the detector by tilting the camera by means of stepper motors. Thus light of any wavelength can be made to fall on a photosensitive area of the detector. The polychromator becomes a monochromator[93].

2.2.3 Solid-State Detector

The task of a detector is to transform radiation into an electric current. The most widely used tool for this purpose is a photomultiplier. The output current of a photomultiplier is converted to a voltage and amplified in conventional solid state circuitry yielding an electric signal. The combination of photomultiplier and amplifier should provide linear response of signal to light intensity over at least three orders of magnitude. This type of detectors seems to be the ideal photon capturing for optical spectroscopy. However, the device is relatively bulky and provides no wavelength selective reading. The wavelength must be limited by the monochromator exit slit. Thus light with wavelength within only one spectral window will be measured.

The trend in chemical analysis, however, is to obtain as much information per measurement as possible. The information content of a measurement can be increased if a solid state detector providing many photosensitive spots or areas on a semiconductor chip is used. The technology for solid state detection has progressed dramatically. A solid state detector for simultaneous multi-element AAS is shown in Figure 2.5.

The detector basically consists of a silicon wafer with photosensitive rectangular spots (photodiodes). The electrical charge is generated by impact of photons at the interface between a silicon dioxide (SiO_2) and a p+ layer doped with boron. The electric charges are transported rapidly in an electric field gradient to the PN junction of the photodiode. The individual diodes are connected to individual low noise, low power consumption charges amplifiers located at the chip. In this type of detector any group of eight diodes can be monitored simultaneously. As the quantum efficiency in the most important wavelength range between 200 nm and 500 nm is higher by a factor of between 2 and 5 than that of a typical photomultiplier, and AAS usually is shot noise limited, the use of a well-designed solid state detector results in significantly improved signal-to-noise performance. The main advantages solid state detectors, however, are the compact dimensions and great flexibility of application[93].

Figure 2.5 Solid-state detector for simultaneous multi-element determinations

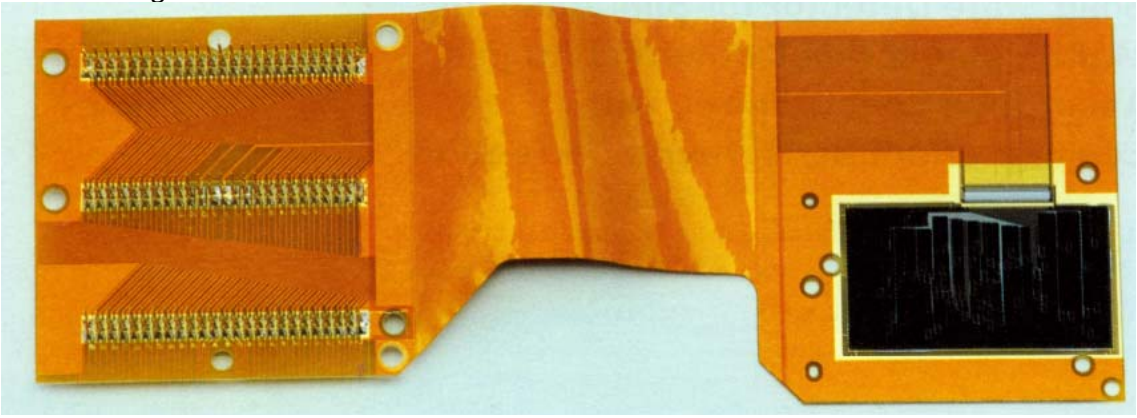

2.3 Compromised Conditions for Simultaneous Multi-Element Determinations

A potential hindrance to simultaneous multi-element determination by GFAAS is the necessity of using compromise furnace temperatures for multiple analytes. When GFAAS is used for single-element determinations, all experimental and instrumental parameters are optimized for one analyte. Consequently, the best optimized conditions, like the pyrolysis and atomization temperatures, are used. On the other hand, in the case of multi-element analysis other aspects are coming up. Because of the fact that the sample is heated only once in the atomization unit and all elements are atomized and hence measured under the same conditions, the adoption of compromised conditions for multi-element determinations are required. Depending on the suite of elements to be determined, the compromise parameters may be dramatically different than individually optimized single-element conditions. The questions of interest are:

- How severely will the sensitivity and the detection limit of the volatile elements be degraded using an atomization temperature suitable for the least volatile element?
- How severely will the chemical and spectroscopic interferences be increased using a pyrolysis temperature suitable for the most volatile element[94]?
- How severely will the sensitivity and the detection limit be affected using a combination radiation from a series of lamps (HCLs or EDLs) or multi-element lamps? Since multi-element lamps are problematic and combining the radiation from a series of lamps leads to reduced intensities and poorer signal-to-noise ratios (SNRs)[64].

Perkin-Elmer reports the detection limits for SIMAA 6000 in single-element and multi-element mode, Table 2.2, which are comparable to their previous single-element instrument, the 4100ZL[95, 96].

- Another criterion that may affect the multi-element determinations is the wide range concentration of the elements in a real sample which may recall dilution for some elements in the sample. This dilution can decrease the concentration of the other elements to or less than the detection limit which reduce the possibility of measuring these elements simultaneously.

Table 2.2 Comparison between the single-element and multi-element detection limits ($\mu g.l^{-1}$)

Element	Zeeman 4100ZL	SIMAA 6000	
		Single-element mode	Four element mode
As	10	0.16	0.2
Cd	0.4	0.003	0.006
Cr	2	0.01	0.02
Cu	5	0.1	0.17
Mn	2	0.01	0.03
Mo	4	0.03	0.06
Pb	3	0.1	0.2
Se	15	0.23	0.54
Tl	6	0.23	0.3
V	6	0.06	0.1

2.3.1 Pyrolysis and Atomization Temperatures

In the traditional, single-element mode of operation, the furnace temperatures for the drying, pyrolysis, and atomization steps are optimized for the element to be analyzed and the sample matrix. In the drying and pyrolysis steps, temperatures, gas type and flow, and chemical additives (matrix modifiers) are selected to provide reproducible drying and to remove or minimize the effect of matrix compounds which provide chemical and/or spectroscopic interferences. In the atomization step, the temperature and gas flow are selected which optimize the analytical sensitivity. Thus, selection of temperature is critical to the optimization of sensitivity and the minimization of interferences. In contrast, simultaneous multi-element determinations demand compromise furnace temperatures. The degree of compromise is a function of the suite of elements to be determined. The more extreme between the least and most volatile elements are, the less space there is for compromise. Thus, Cd and Pb dictate that the pyrolysis temperature to be less than 450^{o}C (without a modifier) and B and Ti dictate that the atomization temperature to be close to 2500^{o}C if these elements are to be included in the determination[94], and there is little space for change in these

temperatures. The limitation of a low pyrolysis temperature which is suitable for the most volatile element may restrict the ability to remove troublesome background which is a result from the chemical and spectroscopic interferences.

The first detailed investigation into the use of compromise multi-element furnace temperatures by Harnly and Kane[97], examined the variation of peak height and peak area (integrated) sensitivities as a function of the atomization temperature for a conventional, longitudinal-heated graphite furnace (model HGA-2100, Perkin-Elmer Corp., Norwalk, CT, USA). It was determined that, with or without a platform, a maximum pyrolysis temperature of 500^{o}C and a minimum atomization temperature of 2700^{o}C were necessary for a suite of nine elements (Co, Cr, Cu, Fe, Mn, Mo, Ni, V, and Zn). The maximum pyrolysis temperature (500^{o}C) was determined by Zn and the minimum atomization temperature (2700^{o}C) was determined by Mo and V. With these parameters, the peak area sensitivity of Zn was reduced by 50% (as compared to the maximum sensitivity at an atomization temperature of 1500^{o}C) for platform atomization and by less than 5% for atomization from the wall. Another investigation by Berglund[98] examined the use of a commercially available transversely heated graphite atomizer (THGA), with palladium as matrix modifier, for the simultaneous determination of 8 elements (Ag, Cd, Co, Cr, Mn, Mo, Pb, and V) using a single set of atomization parameters. The use of palladium allowed a pyrolysis temperature of 900^{0}C and the use of a transversely heated furnace made possible an atomization temperature of 2400^{o}C and dramatically reduced memory between atomizations (compared with a longitudinally heated furnace). Experimentally determined characteristic masses, for atomization at 2400^{o}C, were compared with calculated values for the same temperature and with calculated values for optimal, single-element temperatures. They showed that the loss in sensitivity ranged from 10%-20% for Cd, Co, Cr, Pb, and V and was negligible for Ag, Mn, and Mo. Then the biggest concern in the multi-element GFAAS is the loss in sensitivities and detection limits of volatile elements atomized at temperatures which are much higher than those used in the single-element mode[94]. The loss in sensitivity and detection limits of volatile elements can be explained as a result of analyte volatilizing before the final furnace temperature is reached and an increase in the absorption coefficient at higher temperatures[64, 94]. The high sensitivities at lower temperatures are also accompanied by broader peaks and longer integration times.

2.3.2 Chemical Modification

Matrix modification is the addition of a reagent (the modifier) in excess to the solution to be measured in GFAAS to convert the analyte element into a phase of higher

thermostability and/or to increase the volatility of interferences. The aim of analyte and matrix modification in GFAAS is to permit high enough pyrolysis temperatures to remove the bulk of interferences during thermal pretreatment of the sample without losing any analyte element prior to the atomization stage. To make the application of modifiers generally acceptable in GFAAS a number of requirements are expected to be met particularly for routine work. Among those are:

(i) The analyte element should be stabilized to as high a pyrolysis temperature as possible, hopefully at least 1000^{o}C, to allow volatilization of the bulk of interferences.

(ii) The modifier should be applicable to as many elements as possible for simplicity reasons.

(iii) The modifier should be available in high purity, and not contain the analyte element(s) in measurable concentrations.

(iv) The modifier should not contain an element at high concentration which has to be determined at trace levels in the furnace at later time.

(v) The modifier should not markedly reduce the life time of graphite tubes.

(vi) The modifier should not produce excessive background attenuation around the wavelength of the analyte element[99]. The use of modifiers became an essential part of ETAAS with the introduction of the stabilized temperature platform furnace concept (STPF)[39, 100].

The concept and the term matrix modification were introduced into GFAAS by Ediger[41]. Among the reagents, he proposed the addition of nickel to decrease the volatility of arsenic and selenium, and the addition of ammonium phosphate to stabilize cadmium. Ediger also proposed to add ammonium nitrate to sea water samples to allow removal of sodium chloride at lower pyrolysis temperatures at which the analyte element is not yet volatile. Other modifiers proposed in later years were molybdenum[101], lanthanum[102], phosphoric acid[103, 104], magnesium nitrate[105], potassium dichromate[106] and several others.

In 1992, Welz and co-workers proposed the mixture $Pd(NO_3)_2$ + $Mg(NO_3)_2$ as an universal modifier for 21 elements, including Al, Bi, Cd, Cu, Mn, Pb, Sb, and Se[100]. It was possible to increase pyrolysis and atomization temperatures without analyte loss, and similar furnace heating conditions could be used for all the elements[107].This modifier mixture was also used by Hinds et al.[108, 109] for the determination of lead in soil slurries. They found that the addition of magnesium avoided the low recoveries that occurred if palladium was used

alone[109], and this agreed with observations made by Schlemmer and Welz[99]. Shan and Ni[110] suggested that a thermally stable compound or alloy is formed between palladium and lead. Schlemmer and Welz[99] reported that most analytes are stabilized to about 1200^{o}C by palladium. This is very close to the appearance temperature of palladium (1250^{o}C), so they suggested that the analyte is embedded in the palladium matrix or forms an alloy. Further evidence for the formation of intermetallic species was presented by Wendl and Mueller-Vogi[111], who used X-ray diffraction spectrometry to study the use of palladium on modification of lead. They identified Pd_3Pb_2 and Pd_3Pb at a pyrolysis temperature of 820^{o}C, but only Pd_3Pb at 1127^{o}C. Shan and Wang[112] used X-ray photoelectron spectroscopy to obtain binding energies suggestive of Pd-Pb and Pd-Bi bonds. Scanning electron microscopy has shown selenium and palladium to physically associate with each other on the graphite furnace[113], and X-ray analysis revealed selenium: palladium ratio of 1. Styris et al.[114] used mass spectroscopy to confirm compound formation between selenium and palladium in a graphite furnace. They suggested that dissociation of the compound is followed by trapping of elemental selenium at high energy retention sites created by palladium. Retteberg and Beach[115] reported that near stoichiometric amounts of palladium had a signal delaying effect on tin, lead, and cadmium, which provided further evidence for compound formation. They suggested also that palladium must be in its free metallic form to act as a modifier and reducing agents enhance the decomposition of palladium oxide. H. Qiao and K. W. Jackson[107] have studied the effects of palladium and mixtures containing palladium on the absorbance characteristics of Pb, Tl, Cd, Se, Mn, and Co. They described a physical mechanism of palladium in the analyte modification and during the furnace heating; the analyte dissolves in molten palladium and may combine with it chemically. The addition of magnesium increases the speed of diffusion by causing palladium to form smaller droplets, and hence produces sharper absorbance peaks[107].

For simultaneous multi-element determinations, this mixture has been widely used[20, 67, 69-72, 75, 76, 81, 84]. Indeed, in simultaneous multi-element GFAAS the modifier and the heating program of the atomizer is common for all analytes. So, the optimum conditions should be selected as a compromise between required sensitivity and precision. With this modifier the compromise conditions for some groups of elements became more close to the optimum conditions for each element.

The normal modifier may be previously mixed with the sample (analytical solution) or separately injected into the graphite tube, either before or after the sample (analytical solution). Alternatively, the modifier can be present in the graphite tube as metal coating[116].

This type of modifier is called the permanent modifier. Permanent chemical modification usually consists in the introduction of a large amount of chemical modifier solution on the platform or on to the tube wall, followed by a stepwise drying-pyrolysis stage. This results in coating of the graphite surface with the thermally fixed modifier[117, 118]. Some advantages have been attributed to the use of permanent modifiers, such as simplicity, shorter time of determination, and fewer contamination problems[116]. However, the most emphasized property is that the modifier may remain in the tube for several hundred heating cycles, not needing to be introduced together with each aliquot of sample[119], which can significantly extend tube life time[120].

Tubes coated with Pd, Ir, and Rh were used in the determination by GFAAS of Cd, Mn, Pb, V, and Se[120] and also determination of As and Sb[121]. Good results were obtained for As, Se, and Pb using Ir-coated tubes in electrothermal vaporization-inductively coupled plasma mass spectrometry[122]. Platinum group elements (Ir, Pd, Pt, Rh, and Ru) as well as carbide-forming elements (Zr, Nb, Ta, and W) have been used to cover the graphite tube to collect gaseous hydrides and Hg vapour. Mixtures of elements of the platinum group were used as a permanent coating in the determination by hydride generation-atomic absorption spectrometry of Cd[123], Te[124], Sb, As, Bi, Cd, Pb, Tl, Sn, and Se[125] and As and Sb[126].

2.4 Important Terms

AAS is used as a relative analytical method. This means that the absorbance of an unknown sample is compared with the absorbances of so called blank solution – which represents the contamination level introduced by the laboratory environment and all reagents added to standards and samples – and with the absorbances of solutions containing known concentrations of the element(s) to be determined, the so-called reference solutions. The result of this instrument calibration is a blank absorbance value and a relation between analyte concentrations and absorbance values, the calibration curve. This relationship, the slope of the calibration curve, should be fairly constant within narrow boundaries for a given experimental setup.

2.4.1 Sensitivity and Characteristic

The slope of the analytical curve is termed the sensitivity S.

$$S = \Delta A / \Delta C$$

where: ΔA: change in absorbance and ΔC: change in concentration.

It is used to check the correct function of the instrument on the one hand, and/or to recognize erroneous standard solutions or chemical conditions. In order to be able to quickly check on the sensitivity without the necessity to establish a calibration curve and in order to define sensitivity in absolute terms, the normalized reciprocal sensitivity, the so-called characteristic mass m_o was defined. Characteristic mass is defined as the mass of analyte which gives an integrated absorbance of 0.0044. The characteristic mass can be calculated using the following equation:

$$m_o = (v / slope) \times 0.0044$$

where: v: the volume of injected volume in µl (which is 20 µl in this study). And it can be quantified in the linear range of the analytical curve by measuring the integrated absorbance of a reference solution and using the following equation:

$$m_o = (v \times C \times 0.0044) / A$$

where: C: the concentration of a reference solution in pg/µl and A: the integrated absorbance.

The characteristic mass is now a well established parameter used to validate the function of radiation source, spectrometer, sample introduction system, and graphite furnace including the graphite tube. If one of the components of the systems is not working properly, the characteristic mass will certainly be out of the range of about ±20% of the published value. The characteristic mass will depend on the experimental setup, the accuracy of the sample volume introduced, the linearity of the calibration function, the atomization efficiency, the atomization temperature, and the quality of the radiation source.

2.4.2 The Detection Limits

It should be noted that, while the magnitude of the absorbance signal can be predicted from the value given for characteristic concentration, no information is given on how small of an absorbance signal can be measured. Therefore, it is not possible to predict the maximum measurable concentration from a known characteristic concentration value. To determine this quantity, more information on the nature of the measured absorbance signal must be considered.

The smallest measurable concentration of an element will be determined by the magnitude of absorbance observed for the element (characteristic concentration) and the stability of the absorbance signal. An unstable or noisy signal makes it more difficult to distinguish small changes in observed absorbance which are due to small concentration differences, from those random variations due to baseline noise.

The term detection limit incorporates a consideration of both signal size and baseline noise to give an indication of the lowest concentration of an element which can be measured. The detection limit is defined by the IUPAC as the concentration which will give an absorbance signal three times the magnitude of the baseline noise. The baseline noise may be statistically quantitated typically by making 10 or more replicate measurements of the baseline absorbance signal observed for an analytical blank, and determining the standard deviation of the measurements. The detection limit is then defined as the concentration which will produce an absorbance signal three times the standard deviation of the blank. The detection limit can be calculated from the following equation:

$$DL = (3 \times \sigma) / \text{slope}$$

Where: σ is the standard deviation of 10 (or more) replicates of the blank.

Routine analytical measurements at the detection limit are difficult, due to the fact that, by definition, noise makes up a significant percentage of the total measurable signal. For good precision, it is necessary to limit routine analytical work to concentrations higher than the detection limit.

3 Aims

This work is aimed to develop and evaluate a fast, reliable, and comparable (in terms of detection limits and sensitivity) to the single-element analytical methodology for the simultaneous multi-element determination of trace and ultra trace elements in biological samples by multi-element atomic absorption system.

- Study the effects of the operational conditions (temperatures, modifiers, operating modes) on the absorption signals of the elements and the sensitivities of the calibration curves.
- Determination of detection limits and characteristic mass of a selected number of elements after optimization of experimental conditions of single-element determination.
- Study the influence of different matrix modifiers on the multi-element determinations comparing with the single-element determinations.
- Determination of best compromised conditions for the multi-element modes using two operating modes (2- and 4-element modes) and determination of detection limits and characteristic mass values. Comparison of results of single-element and multi-element mode.
- Minimizing matrix effects in multi-element modes for element determination of urine reference material.
- Application of simultaneous measurements for analysis of different biological samples using certified reference materials.

4 Experimental Section

4.1 Instrumentation

All simultaneous multi-element determinations were performed with a SIMAA 6000 system (Simultaneous Multi-element Atomic Absorption Spectrometer) equipped with a longitudinal Zeeman-effect background correction, an AS-72 autosampler, an Echelle optical arrangement, and a Solid-state detector (Perkin-Elmer GmbH, Bodenseewerk, D-88647 Überlingen). A transversely heated graphite atomizer (THGA) tubes (with and without end-capped) with an integrated platform were used throughout this work. A THGA with end-capped was used for the multi-element determination of Al, Be, Cr, and V. The whole system was controlled by means of AA Winlab^{TM} control software running under Microsoft Windows^{TM}. High-purity argon (99.998 %, Air Liquid Deutschland GmbH) was used as the purge gas. The rate of flow of the inert gas was 250 ml.min^{-1}. This flow was stopped during atomization. The lamps used were HCLs and EDLs from Perkin-Elmer. The lamp type of each element and the setting parameters for each lamp were summarized in Table 4.1. The integrated absorbance of the atomic absorption signal was used for the determination.

Table 4.1 The lamp types and setting parameters for each lamp

Element	Wavelength (nm)	Band pass (nm)	Lamp type	Lamp current (mA)
Al	309.3	0.7	HCL	25
Be	234.9	0.7	HCL	30
Cr	357.9	0.7	HCL	25
Cu	324.8	0.7	HCL	15
Bi	223.1	0.2	EDL	380
Cd	228.8	0.7	EDL	230
Mn	279.5	0.2	HCL	20
Pb	283.3	0.7	HCL	10
Sb	217.6	0.7	EDL	380
Se	196.0	2.0	EDL	290
Tl	276.8	0.7	HCL	6
V	318.4	0.7	HCL	40

4.2 Reagents and Standard Solutions

All solutions were prepared with high purity de-ionized water (18.2 MΩ) obtained from a Milli-Q water purification system (Millipore GmbH, Schwalbach, Deutschland).

Analytical reagent-grade HNO_3 65% (KMF Laborchemie Handels GmbH, Lohmer, Deutschland) was purified by sub-boiling distillation.

High purity standard reference solutions (1.000 $g.l^{-1}$) from Bernd Kraft GmbH, Duisburg-Deutschland, were used to prepare the analytical stock solutions which are kept in a refrigerator. A list of the standard reference solutions used is shown in Table 4.2.

Table 4.2 Standard reference solutions

Element	Concentration	Type	Source	Matrix
Al	1.000 $g.l^{-1}$	ICP/AAS Standard Solution	Bernd Kraft GmbH	0.5 $mol.l^{-1} HNO_3$
Cr	1000 ± 3 $\mu g.ml^{-1}$	High-Purity Standards	Charleston SC 29423	2% HNO_3
Mg	1.000 $g.l^{-1}$	AAS-Standard	Bernd Kraft GmbH	0.5 $mol.l^{-1} HNO_3$
Pd	1.000 $g.l^{-1}$	ICP-Standard	Bernd Kraft GmbH	As $Mn(NO_3)_2$ in 1 $mol.l^{-1} HNO_3$
Mn	1.000 $g.l^{-1}$	AAS-Standard	Bernd Kraft GmbH	0.5 $mol.l^{-1} HNO_3$
Be	1.000 $g.l^{-1}$	AAS-Standard	Bernd Kraft GmbH	0.5 $mol.l^{-1} HNO_3$
Se	1.000 $g.l^{-1}$	AAS-Standard	Bernd Kraft GmbH	SeO_2 in 0.5 $mol.l^{-1} HNO_3$
Pb	1.000 $g.l^{-1}$	AAS-Standard	Bernd Kraft GmbH	0.5 $mol.l^{-1} HNO_3$
Cu	1.000 $g.l^{-1}$	AAS-Standard	Bernd Kraft GmbH	As $Cu(NO_3)_2$ in 0.5 $mol.l^{-1} HNO_3$
Tl	1.000 $g.l^{-1}$	AAS-Standard	Bernd Kraft GmbH	As $TlNO_3$ in 0.5 $mol.l^{-1} HNO_3$
Sb	1.000 $g.l^{-1}$	AAS-Standard	Bernd Kraft GmbH	As $SbCl_3$ in 5 $mol.l^{-1}$ HCl
Bi	1.000 $g.l^{-1}$	AAS-Standard	Bernd Kraft GmbH	As $Bi(NO_3)_3$ in 1 $mol.l^{-1} HNO_3$
V	1.000 $g.l^{-1}$	AAS-Standard	Bernd Kraft GmbH	As NH_4VO_3 in 1 $mol.l^{-1} HNO_3$
Cd	1.000 $g.l^{-1}$	ICP/AAS Standard Solution	Bernd Kraft GmbH	0.5 $mol.l^{-1} HNO_3$
Ir	1.000 $g.l^{-1}$	ICP-Standard	Bernd Kraft GmbH	As $H_2(IrCl_6)$ in 1.0 $mol.l^{-1}$ HCl

The reference solutions for calibration and determination were prepared daily by appropriate dilution of the stock solution with 0.2% HNO_3.

The temperature program that has been used for the determination of the elements in single- and multi-element modes is shown in Table 4.3. Different pyrolysis, atomization, and cleaning temperatures depending on the elements, operating modes, matrix modifier, and sample have been used.

The chemical modifier solutions used were $Pd(NO_3)_2$, $Mg(NO_3)_2$, and Ir. In each measurement, 20 µl sample or standard solution, 5 µl 1.000 $g.l^{-1}$ Pd solution, and 3 µl 1.000 $g.l^{-1}$ $Mg(NO_3)_2$ solution were injected into the graphite tube at 20°C. In the simultaneous determination of Al, Be, Cr, and V, only 5 µl of 1.000 $g.l^{-1}$ $Mg(NO_3)_2$ was injected with the sample into the graphite tube. In the case of the multi-element determination by using a permanent modifier, the tubes were prepared by pipetting 20 µl of a 1.000 $g.l^{-1}$ of Ir, as chloride, and submitting the tube to the temperature program shown in Table 4.4[114]. The entire procedure, that is, the pipetting and heating, was repeated 25 times.

Table 4.3 Temperature program for SIMAA 6000 system

Step	Temperature (^oC)	Ramp Time (s)	Hold Time (s)	Gas Flow ($ml.min^{-1}$)
Dry 1	110	1	30	250
Dry 2	130	15	30	250
Pyrolysis	variable	10	20	250
Atomization	variable	0	5	0
Clean-out	variable	1	3	250

Table 4.4 Temperature program for the metal coating

Step	Temperature (^oC)	Ramp (s)	Hold (s)	Ar flow rate ($ml.min^{-1}$)
1	**90**	**5**	**30**	**250**
2	**140**	**5**	**30**	**250**
3	**1000**	**10**	**10**	**250**
4	**2000**	**0**	**5**	**0**
5	**20**	**1**	**10**	**250**

4.3 Sample Preparation

The accuracy of the methods was confirmed by analyzing different certified reference materials. The certified reference materials are shown in Table 4.5.

Table 4.5 Certified reference materials

Certified Material	LOT	Source
Trace Element Urine Sample	**0511545**	**Seronorm**
Lyphocheck Urine Metals Control- Level 1	**69061**	**BIO-RAD**
Bovine Liver	**NIST-SRM 1577b**	**National Institute of Standards and Technology**
Pig Kidney	**BCR-CRM 186**	**Institute for Reference Materials and Measurements**
Pork Liver	**GBW 08551**	**National Research Centre for Certified Reference Materials**
Tea	**GBW 08505**	**National Research Centre for Certified Reference Materials**

4.3.1 Trace Elements Urine Sample (Seronorm 0511545)

Exactly 5 ml de-ionized water was added to the sample and let it stand for 30 min, and then transfer it to a plastic tube. The sample was then kept in a refrigerator at -20^{o}C for later use. Before use, the sample was diluted 1:4 with 0.2% HNO_3.

4.3.2 Lyphocheck Urine Metals Control-Level 1 (69061)

The same procedure was applied as Seronorm sample except that, 25 ml de-ionized water was added and the sample was diluted 1:1 before use.

4.3.3 Pork Liver (GBW 08551), Pig Kidney (BCR-CRM 186), and Bovine Liver (NIST-SRM 1577b)

The samples were digested as described by Ronald Treble[127]. Firstly, the samples were dried at 80^{o}C for 4 h. and stored in desiccators before use. 0.5069 g (GBW 08551), 0.5218 g (BCR-CRM 186), and 0.5129 g (NIST-SRM 1577b) dried samples were allowed to digest in 5 ml concentrated distilled HNO_3 for a period of 72 h. at room temperature. The digested/acidified samples were transferred into 50 ml volumetric flask and diluted to the mark with de-ionized water. Before use, each sample was diluted as required.

4.3.4 Tea Sample (GBW 08505)

The sample was digested as described by Yin Ming[128]. The sample firstly was dried at 80^{o}C for 4 h. in a clean oven and stored in desiccators before use. A sample portion of 1.0217 g was weighed into a beaker and moistened with pure water. 10 ml HNO_3 and 2 ml $HClO_4$ were added in sequence. After standing overnight, the sample was evaporated to nearly dryness on a hotplate at 200^{o}C. The resulting residue was treated with 0.5 ml concentrated HNO_3 and some water, and then heated gently for 5 min till the solution turned clear. This solution was rinsed into a 50 ml volumetric flask and diluted to the mark with de-ionized water. The sample was diluted as required before use.

4.4 Contamination Control

All glassware, micropipette tips, autosampler cups, and polypropylene containers were acid washed with 10% (v/v) HNO_3 for 24 h. and thoroughly rinsed five times with distilled water before use. All solutions and samples were daily prepared in 0.2% (v/v) HNO_3.

5 Results and Discussions

5.1 Overview

In this chapter, we have firstly optimized the parameters for the single-element determinations. These conditions include the pyrolysis and atomization temperatures which have been determined with and without modifiers. Three types of modifiers have been used; $Mg(NO_3)_2$ modifier, the Pd+Mg mixture modifier and Ir-permanent modifier. From the optimized parameters, the sensitivities, the characteristic masses, and the detection limits have been determined.

Secondly, the compromised conditions for the multi-element determinations have been determined and then used to determine the sensitivities, the characteristic masses, and the detection limits.

To test the accuracy of our methods, the compromised conditions have been used to analyze number of certified reference materials. Also the effect of strong matrix on these compromised conditions has been studied by using urine reference material from Seronorm which has been diluted because of the high concentration of the elements.

5.2 Single-Element Determinations without Modifier

GFAAS is the most useful and powerful analytical techniques for the determination of trace elements because it offers fast analysis time, low sample consumption, low cost, and the most important high sensitivity and detection limits. These favourable features have to be retained if we use this technique for the simultaneous multi-element determinations. Some of these features, like analysis time, sample volume, and cost will be even improved with the multi-element mode. On the other hand, sensitivity and detection limits could be affected because multi-element determinations require the adoption of compromised conditions for instrumental and experimental parameters. These compromised conditions can cause loss of sensitivity and high detection limits depending upon the elements, to be simultaneously determined, and the matrix. In general, for simultaneous determinations, the more elements are selected, the more complicated it is to find the analytical compromised conditions adjustments, avoiding degradation of the sensitivity and repeatability[129]. In our research, we have selected the elements according to this basis. In the single-element determinations, we have started the study without a modifier and then we have made the study using different types of modifiers. All the optimizations have been made with the aqueous solutions.

Firstly, we can divide our elements into three groups of elements, according to the pyrolysis and atomization temperatures without any modifier:

i) Volatile elements: Cd, Bi, Pb, and Se

ii) Mid-volatile elements: Sb, Cu, and Mn

iii) Less-volatile elements: Cr, Al, Be, and V

From the pyrolysis and atomization curves for these elements, Figure 5.1, we will see that the highest pyrolysis temperatures which can be used for the first group; the volatile elements; were as follows: 200, 300, 450, and 550^{o}C for Se, Cd, Bi, and Pb respectively. In other words, the lowest atomization temperatures were: 1200, 1300, 1400, and 1500^{o}C for Cd, Bi, Pb, and Se respectively. The pyrolysis temperature for selenium was limited to 200^{o}C without modifier because of the formation of volatile selenium compounds as the oxides SeO and SeO_2, which are volatilized at temperatures higher than 130^{o}C, impairing the thermal treatment efficiency[114]. For Bi, bismuth oxide Bi_2O_3 (which is formed after the drying step) is reduced to a volatile suboxide at active sites on the graphite surface which is further reduced to metallic Bi upon colliding with the surface again. The volatile suboxide is responsible for metal losses during pyrolysis step[130]. Cadmium is a high volatile element[131] and as suggested by Sturgeon and Chakrabarti[46] the atomization of Cd in electrothermal atomizers takes place by the dissociation of the oxide CdO, the reduction of CdO by carbon being thermodynamically unfavourable. Thus the melting and sublimation temperatures of CdO are the most critical factors influencing Cd peak formation[131]. Lead is also a volatile element but less than cadmium. After the drying step, PbO is formed as a decomposition of the lead nitrate or hydrolysis of the chloride. Pb atoms are formed from the reduction of PbO which is favourable at 1040 K[45]. Double peak has been observed for Pb. Double peaks for Pb and other relatively volatile metals, such as Cd and Zn, have been reported for a variety of sample types and atomizer designs[132-139]. Several researchers have studied the Pb system and have offered some theoretical models for the production of double peaks. McLaren and Weeler[134] proposed that the two peaks observed for Pb result from the formation of the massicot and litharge dimorphic of PbO on the atomizer surface. It is assumed that these two dimorphic forms of PbO can be formed on the surface of the atomizer during the pyrolysis step and that this is the cause of the double peaks that occur for Pb. Both Fuller[140] and Regan and Warren[136] have reported that the condition of the graphite surface has an affect on the extent to which interferences are observed. The implication is that two distinct release mechanisms lead to the two peaks observed for Pb and that the condition of the graphite surface, i.e., whether the

furnace is new or old, determines the extent to which either mechanism occurs. Holcombe et al.[139] have concluded that the presence of O_2 in a graphite atomizer can have a profound effect on the atomizer surface, which in turn changes the release mechanism for Pb. It has been suggested that the formation of atomic vapour of the analyte is often preceded by the reduction of the metal oxide by the graphite surface. Two major types of active sites on graphite provide different mechanisms for PbO reduction and Pb vaporization. Deactivation of these sites by the chemisorptions of O_2 causes a shift to the secondary release mechanism. The two release mechanisms account for the double peaks and appearance temperature shifts which are observed for Pb.

For the second group, and from the pyrolysis and atomization curves, we will see that the highest pyrolysis temperatures which can be used were: 900, 1100, and 1200^{o}C for Sb, Cu, and Mn respectively. While the lowest atomization temperatures can be used were: 1600, 1700, 2000^{o}C for Mn, Sb, and Cu respectively. From the pyrolysis curve for Sb (Figure 5.1), we see that Sb is thermally stable up to 500^{o}C and above this temperature the absorption signal starts to decrease gradually with increasing temperature. L. Pszonicki[141] suggested that antimony is present in the solution in the form of antimonous acid and decomposed during the drying and early pyrolysis stages to oxide and successively reduced to elemental antimony that sublimes at temperatures above 500^{o}C. For manganese, Frech and Lundberg[142] suggested that the thermal dissociation of MnO as the mechanism of atom formation in ETAAS. The result obtained by Aggett and Sportt[143] was coincident with that of Frech and Lundberg. MnO is present on the graphite surface irrespective of whether it has been introduced as the chloride or the nitrate. For copper, upon heating, an aqueous solution of copper nitrate is converted into copper oxide (CuO) before the furnace attains the appearance temperature of 1450 K[45, 46]. Upon further heating, CuO is reduced by carbon to free Cu, which then sublime to gaseous atoms. Because the heat of desorption of copper from the graphite surface is approximately equal to that of sublimation of copper, the correlation between the experimentally observed enthalpy and the heat of sublimation is reasonable[144]. According to the thermodynamic calculations[144] the small amount of copper may vaporize totally at a temperature below the melting point of copper without passing through the liquid phase.

Finally the third group includes Al, Be, Cr, and V. These elements are less volatile than the others and they are usually called refractory elements because they formed very stable compounds with the carbon (carbides). From the pyrolysis curves, the maximum pyrolysis temperatures can be reached were as follows: 1000, 1400, 1500, and 1700^{o}C for Be, Cr, Al, and V respectively. The highest pyrolysis temperatures indicate the formation of carbides.

Wendl and Müller-Vogt[145], using X-ray results, have shown that both V and Cr form carbides, VC and Cr_3C_2 respectively. Firstly, V_2O_3 and Cr_2O_3 are formed. The oxides are reduced to carbides at temperatures higher than 1300 and 1500 K, respectively. These carbides start to decompose into the elements at temperatures higher than 2000 and 1700-1800 K, respectively[145]. The evaporation of V from VC was also described by Storms and McNeal[146], and the onset of the decomposition of Cr_3C_2 at temperatures higher than 1500 K by Lux and Eberle[147]. Therefore, the losses of atomizable V and Cr during the pyrolysis step are due to gas phase transport of the elements and VO and Cr_2O_3 could not be detected in the gas phase of the tube by molecular absorption in the temperature between 1700 and 2200 K[145]. In the case of beryllium, Majidi et al.[148] have suggested that atoms are formed from reduction of BeO by the furnace wall or thermal dissociation of a carbide. BeO has an extremely high boiling point, which means that the reduction of BeO by the furnace wall material, not thermal dissociation is the mechanism for beryllium atom formation[148]. Prell et al.[149] reported that carbides were detected mass-spectrometrically in the form of Be_2C, BeC_2, Be_2C_2, and Be_2C_4. Therefore, two mechanisms have been concluded for the atomization. For aluminium, Cathum[144] has suggested that the reduction of aluminium oxide is responsible for atoms formation. This oxide is produced from low-temperature thermal dissociation of the aluminium nitrate solution. Sturgeon et al.[45] interpreted the two energies that they obtained for aluminium atomization as an indication that $Al_2O_3(g)$ dissociate thermally, that the resulting AlO(g) also dissociate, and that both dissociations provide free aluminium. Another possible mechanism for the formation of gaseous aluminium atoms is by autocatalytic reduction of aluminium oxide by gaseous carbides, such as Al_4C_3 that may form during atomization[144]. The lowest atomization temperatures which can be used for these elements were as follows: 2300, 2300, 2300, and 2500^oC for Al, Be, Cr, and V respectively. In the case of V, the sensitivity increases with increasing the atomization temperature. But with SIMAA 6000, the maximum temperature be attained is 2600 and with this temperature the life time of the tube will decrease. For that reason we have decided to use 2500^oC as the atomization temperature for V.

The pyrolysis and atomization curves for all elements without modifier and the optimum pyrolysis and atomization temperatures for all elements without modifier are shown in Figure 5.1 and Table 5.1 respectively.

Figure 5.1 Pyrolysis and atomization curves with and without modifier in the single-element mode

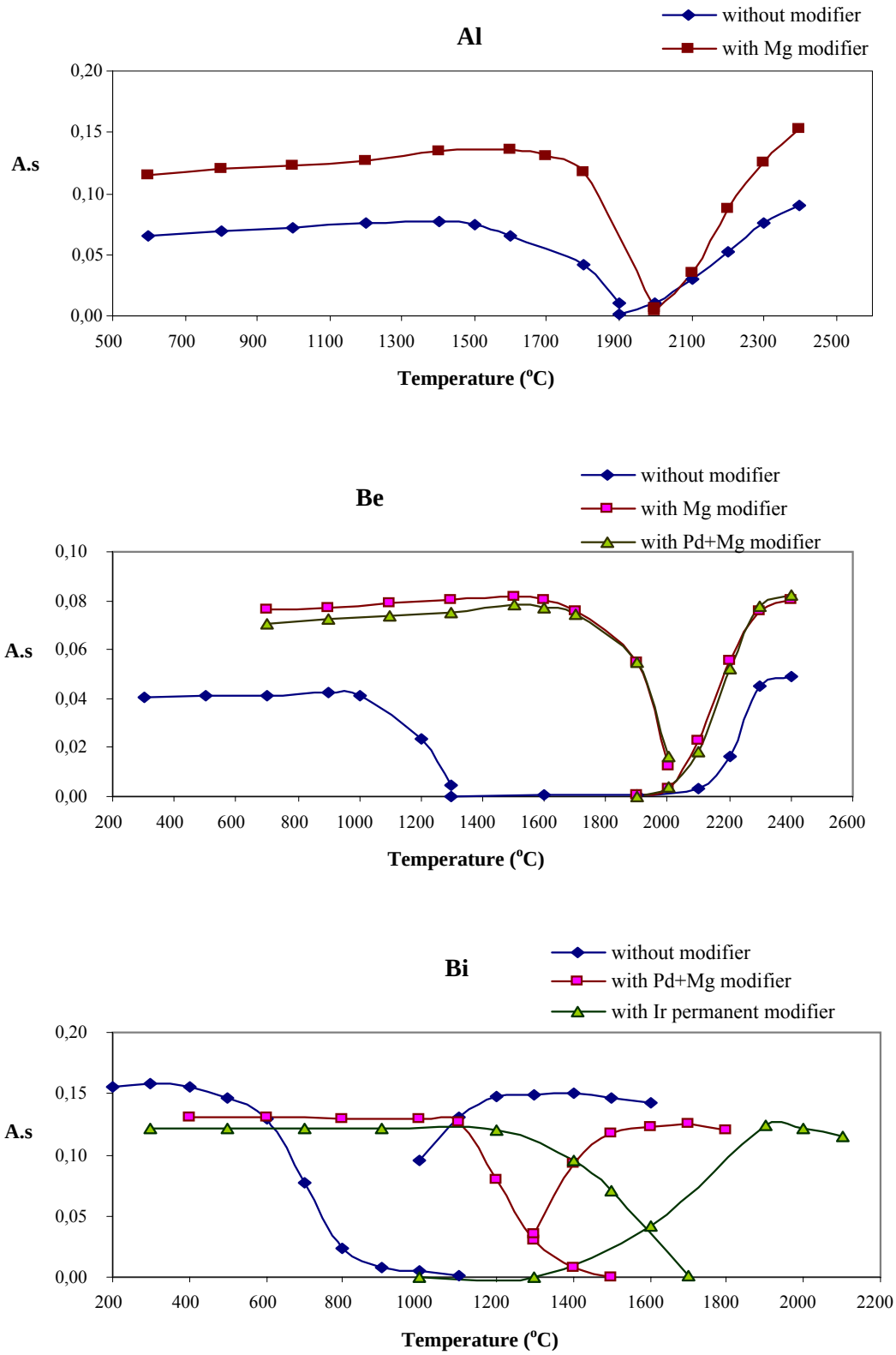

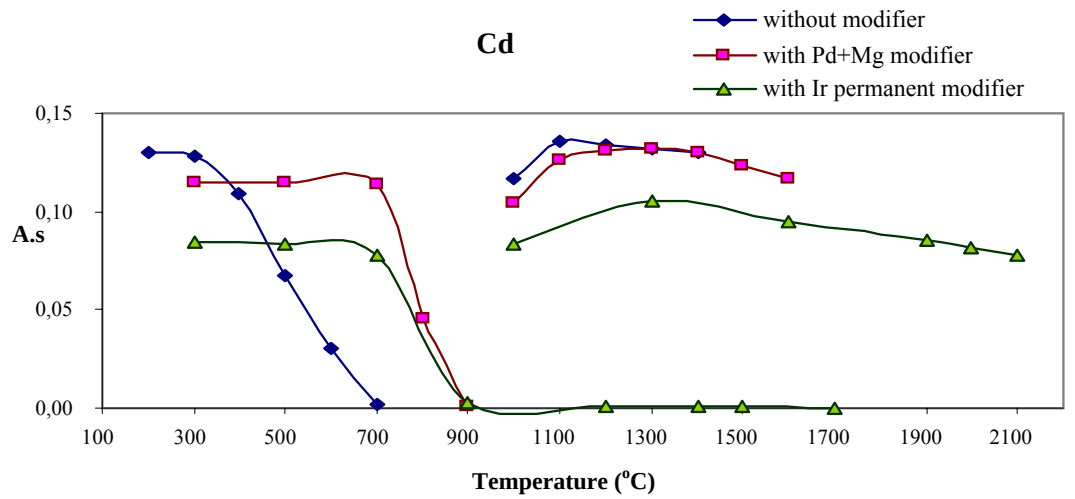
Cd
without modifier
with Pd+Mg modifier
with Ir permanent modifier
A.s
0,15
0,10
0,05
0,00
100
300
500
700
900
1100
1300
1500
1700
1900
2100
Temperature (°C)

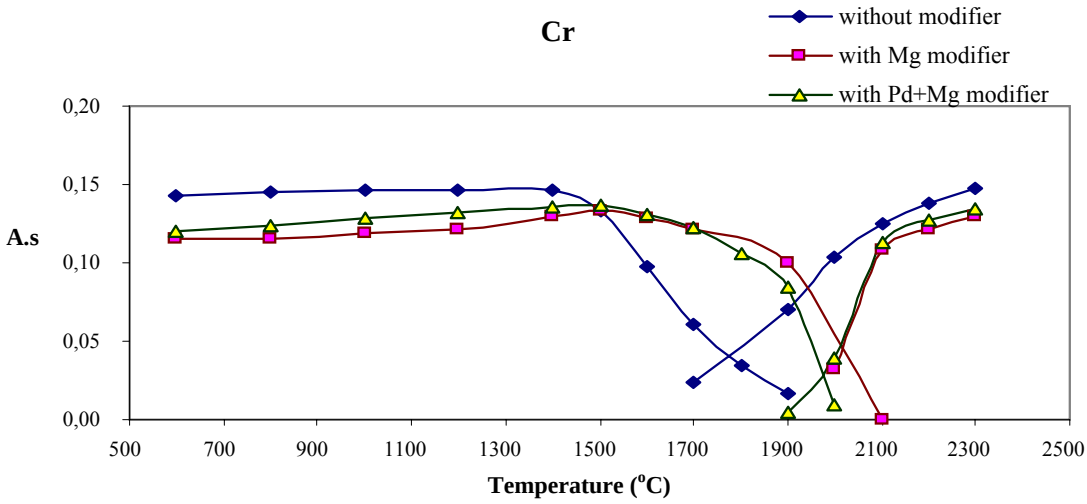
Cr
without modifier
with Mg modifier
with Pd+Mg modifier
A.s
0,20
0,15
0,10
0,05
0,00
500
700
900
1100
1300
1500
1700
1900
2100
2300
2500
Temperature (°C)

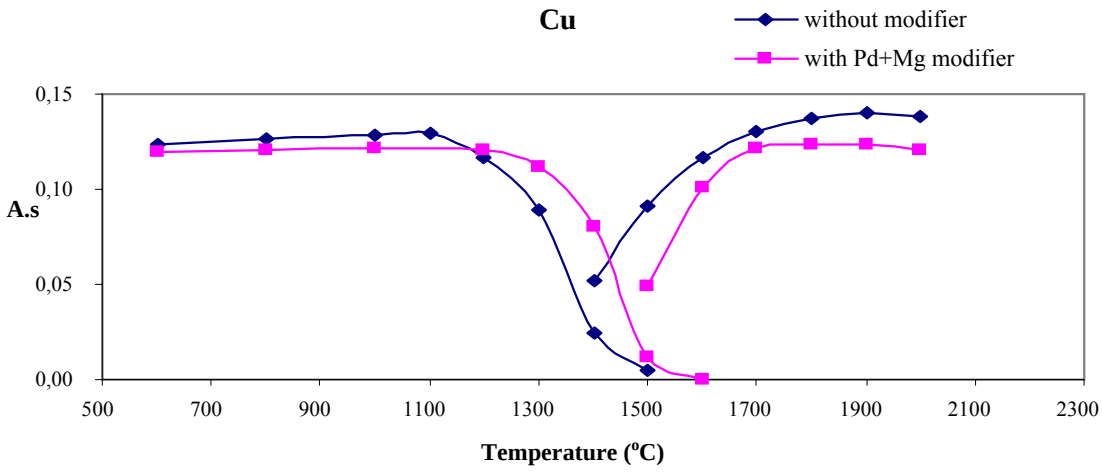
Cu
without modifier
with Pd+Mg modifier
A.s
0,15
0,10
0,05
0,00
500
700
900
1100
1300
1500
1700
1900
2100
2300
Temperature (°C)

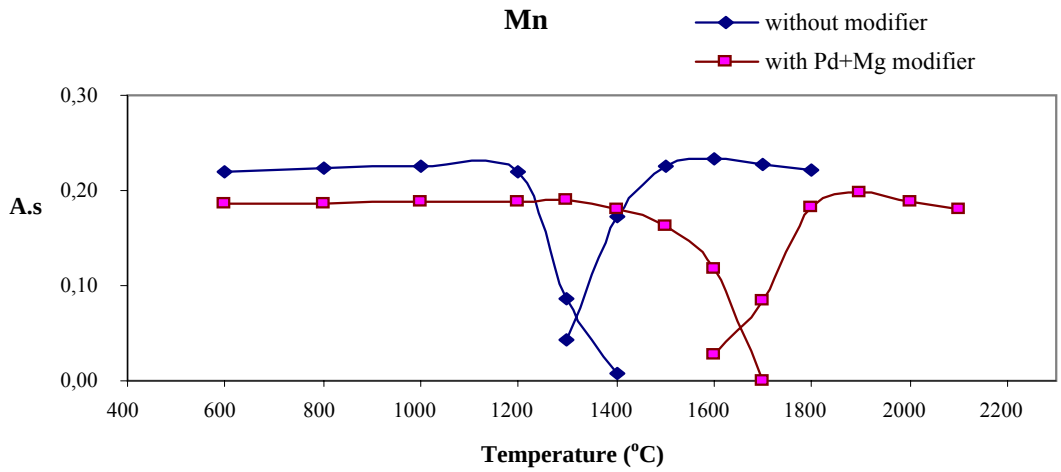
Mn
without modifier
with Pd+Mg modifier
A.s
0,30
0,20
0,10
0,00
400
600
800
1000
1200
1400
1600
1800
2000
2200
Temperature (°C)

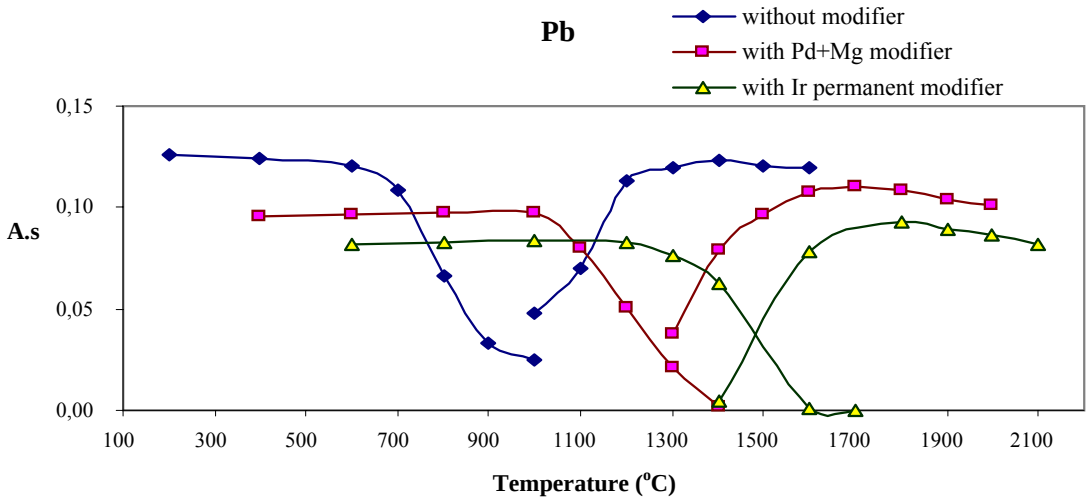
Pb
without modifier
with Pd+Mg modifier
with Ir permanent modifier
A.s
0,15
0,10
0,05
0,00
100
300
500
700
900
1100
1300
1500
1700
1900
2100
Temperature (°C)

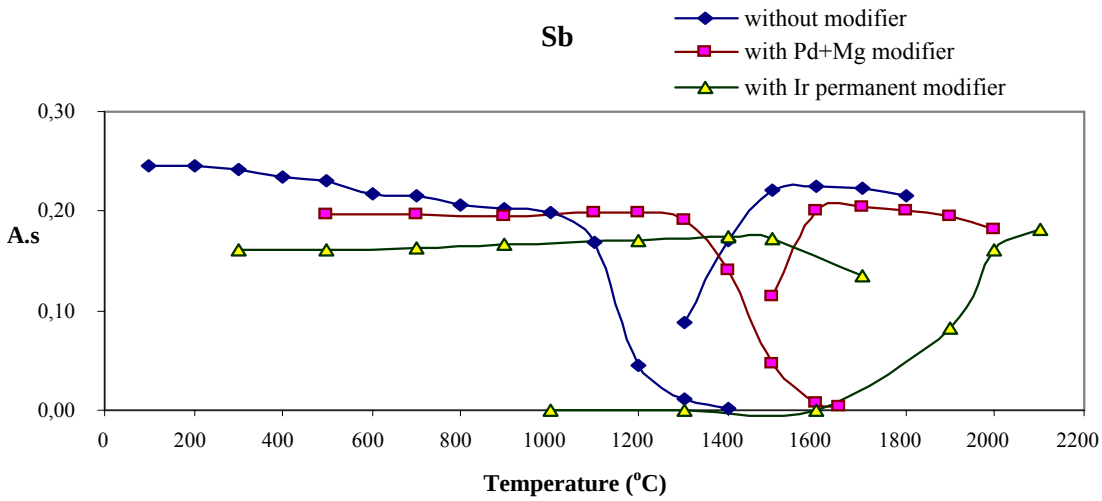
Sb
without modifier
with Pd+Mg modifier
with Ir permanent modifier
A.s
0,30
0,20
0,10
0,00
0
200
400
600
800
1000
1200
1400
1600
1800
2000
2200
Temperature (°C)

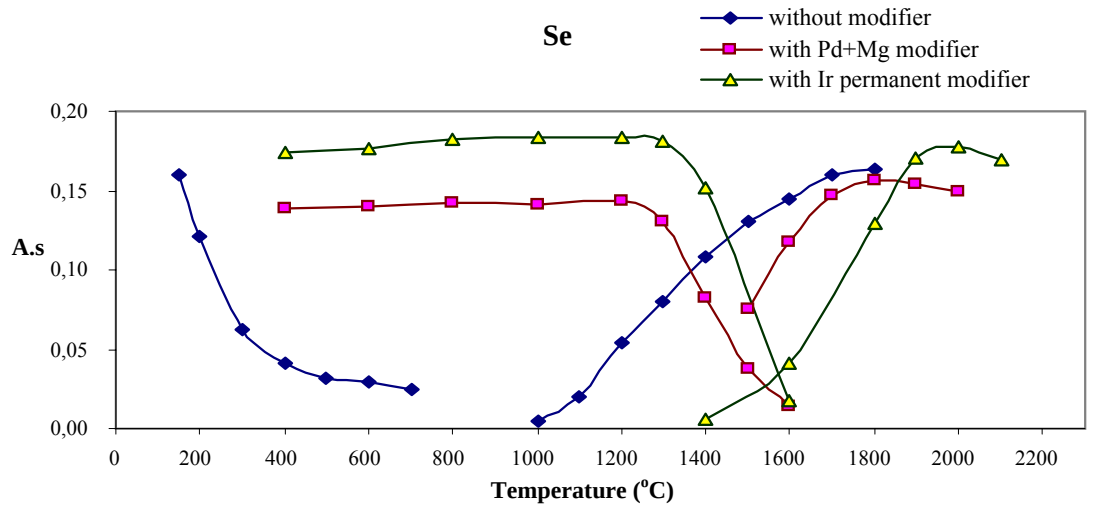

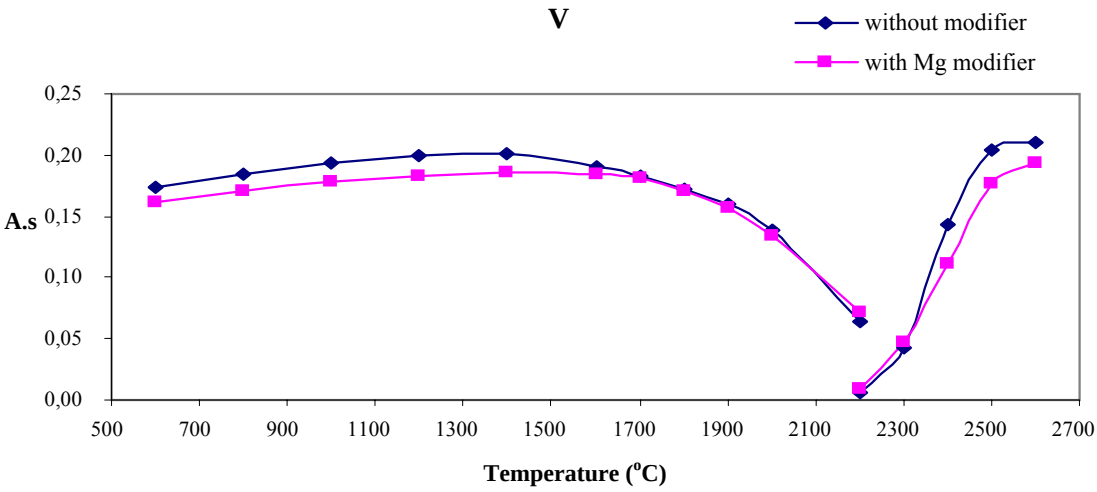

Table 5.1 The pyrolysis and atomization temperatures without modifier in the single-element mode

Element	Pyrolysis Temperature (°C)	Atomization Temperature (°C)
Al	1500	2300
Be	1000	2300
Bi	450	1300
Cd	300	1200
Cr	1400	2300
Cu	1100	2000
Mn	1200	1600
Pb	550	1400
Sb	900	1700
Se	200	1500
V	1700	2500

5.3 Single-Element Determination with Modifier

From the results above (previous section), addition of a matrix modifier is very important because of the high volatility of some elements (e.g. Se, Cd, Bi) and the large difference in thermal stability (in terms of pyrolysis and atomization temperatures) between the elements (the high volatile and the refractory elements) which plays a very important role for multi-element determinations. As the difference in the thermal stability is increased, the difficulty to find compromised conditions between these elements is increased. The use of matrix modification increases the stability of the volatile element which permits the use of higher pyrolysis and atomization temperatures. This will lead to a common temperature program for a wide variety of elements.

The mixture of palladium and magnesium nitrate has been widely used for simultaneous multi-element determinations by SIMAA 6000[40]. It is claimed as universal chemical modifier due to thermal stability improvement for 21 elements[100]. We have used this mixture as a modifier in our work. It has increased the pyrolysis temperature of the volatile elements compared with previously determined without modifier. Zhe-Ming[150] found that for the medium and low volatility elements (Mn and Mo), palladium has less stabilizing effect. For aluminium, magnesium nitrate has been recommended[151-153]. This matrix modifier facilitates the formation of stable aluminate and prevents the loss of aluminium as the volatile chloride[154]. The mechanism of the aluminium atomization in the presence of magnesium nitrate has been attributed to the embedment of aluminium in the magnesium oxide formed from the nitrate and the vaporization of aluminium is prevented[105]. The stabilization of both aluminium and beryllium by magnesium nitrate are similar and has been published[155-157]. $Pd(NO_3)_2$ and $Mg(NO_3)_2$ have been used as modifiers for the determination of chromium in urine[158-160]. Oliveira[74] has found that the best recovery and repeatability results were obtained for 3 μg magnesium nitrate. For that we have used magnesium nitrate in the simultaneous multi-element determination of Al, Be, Cr, and V. The optimizations with this modifier in the single-element mode for these elements have been carried out.

The use of permanent chemical modifiers allows increases the graphite tube lifetime, eliminates volatile impurities during the thermal coating process, decreases the detection limits, reduce the total heating cycle time, and minimize the high purity chemical consumption. The use of pre-reduced noble metal permanent modifiers such as Pd, Rh, Ru, Pt, and Ir[161-167], carbide forming elements (W, Zr, Nb, Ta)[168, 169], and mixed carbide forming elements (W, Zr) with Ir[125, 170, 171] have been applied successfully for trapping of hydride-

forming elements in ETAAS. In our study, we have used Ir as a permanent modifier for the simultaneous multi-element determinations which include: Cd, Bi, Pb, Se, and Sb. The optimizations using this modifier in the single-element mode for theses elements have been carried out.

Firstly, we have studied the effect of each modifier on the elements in single-element mode. According to the stabilization effect of the modifier we have selected our groups in the multi-element mode.

5.3.1 With $Pd(NO_3)_2$ + $Mg(NO_3)_2$ Modifier

The main purpose of using chemical modification in ETAAS is to stabilize the elements to a pyrolysis temperature as high as possible in order to remove the sample matrix efficiently in the thermal pre-treatment step hence less interferences are encountered in the final atomization process. However, chemical modification is more frequently applied to the stabilization of elements of high and medium volatility.

From the pyrolysis curves (Figure 5.1), the pyrolysis temperature of the volatile elements (Se, Cd, Bi, Pb), and Sb were 400-1000^{o}C higher in the presence of Pd+Mg modifier than those obtained with no modifier which are similar to those reported by Welz et al.[100]. The stabilizing effect of this modifier on these elements, which results from the formation of a chemical compound or of an inter-metallic phase and/or from an imbedding effect (as we have discussed in section 2.3.2), is not limited to the pyrolysis step but also increases the atomization temperature as in Figure 5.1. At higher atomization temperatures, the diffusion losses of these elements are higher so that lower integrated absorbances are obtained[100] (also see Figure 5.1). For mid-volatile elements (Cu and Mn) and less volatile elements (Cr), except Be, the differences were 100-200^{o}C. In the case of relatively low volatile elements, the appearance temperature of which are near to or even higher than that of Pd, the stabilizing effect of the later on the analytes will not be significant because palladium will vaporize at the same time with, or even earlier than the analyte[150]. These elements exhibit a high thermal stability by themselves. The important action of the modifier was not so much a further increase in the thermal stability of the analyte element but control of the chemical environment. This means that the modifier protected the analyte element from the formation of volatile compounds with matrix constituents. For beryllium, higher pyrolysis temperature (1600^{o}C) has been obtained with Pd+Mg modifier than without modifier (1000^{o}C). But the pyrolysis curve with this modifier is similar to that with magnesium nitrate modifier

indicating the same stabilization effects which are due to magnesium nitrate. There is no significant stabilization of palladium on beryllium for the same reason as Cu, Mn, and Cr.

The optimized pyrolysis and atomization temperatures in the presence of this modifier have been used to determine the characteristic masses and detection limits for the elements and the values have compared with those in multi-element mode. The detection limits were calculated as three times the standard deviation of ten replicate measurements of each blank. The calibration curve for each element in the presence of this modifier is shown in Figure 5.2.

Figure 5.2 Calibration curves of the elements with Pd+Mg modifier in the single-element mode

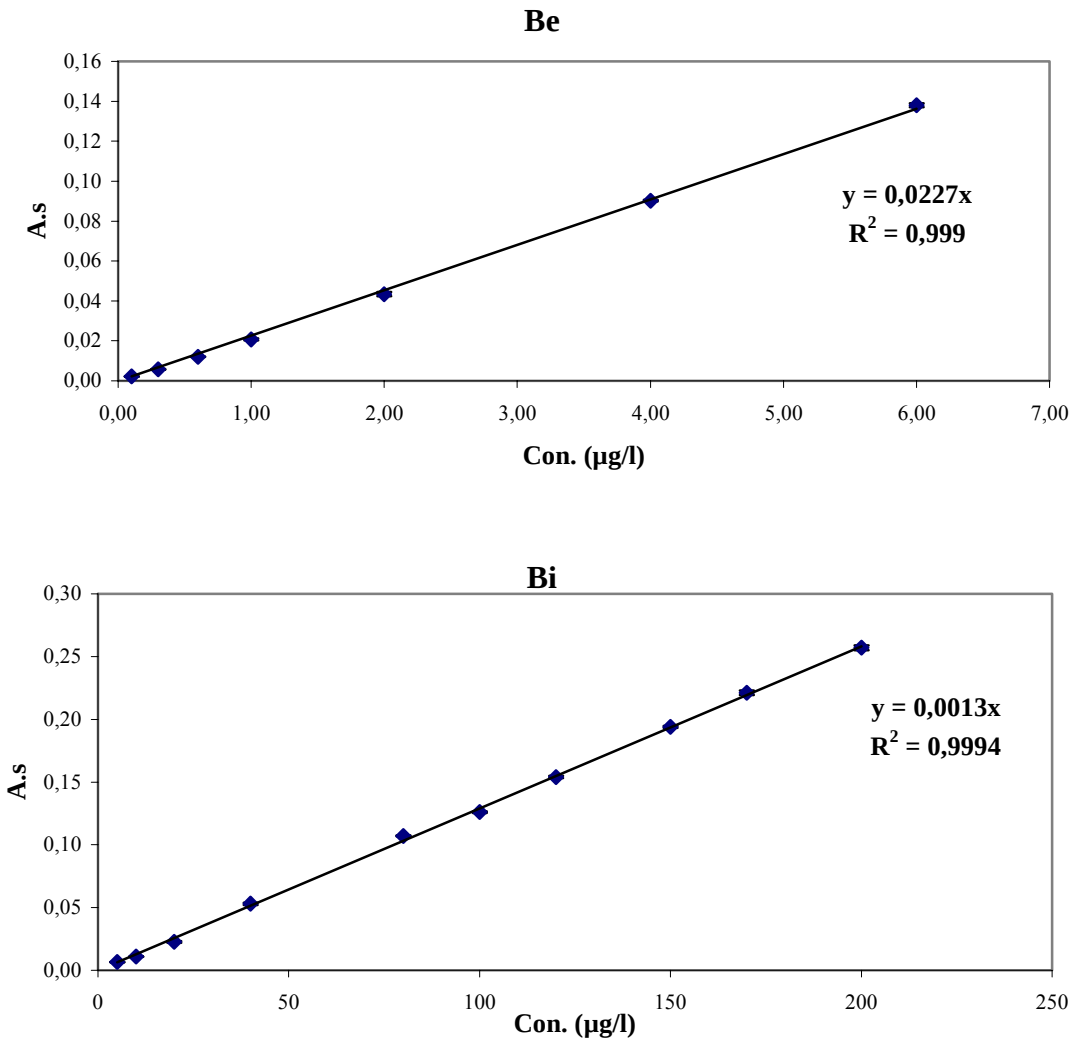

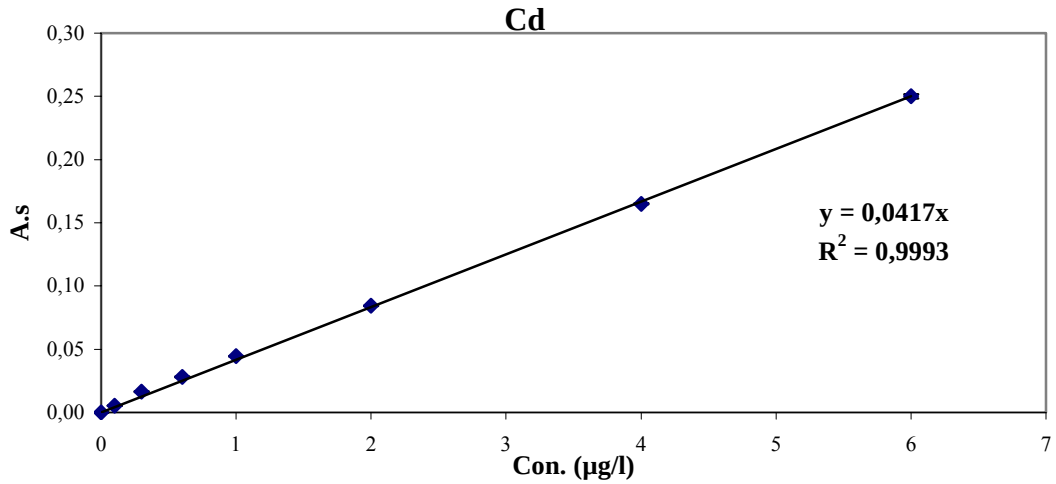
Cd
A.s
Con. (µg/l)
y = 0,0417x
R2 = 0,9993
0,30
0,25
0,20
0,15
0,10
0,05
0,00
0
1
2
3
4
5
6
7

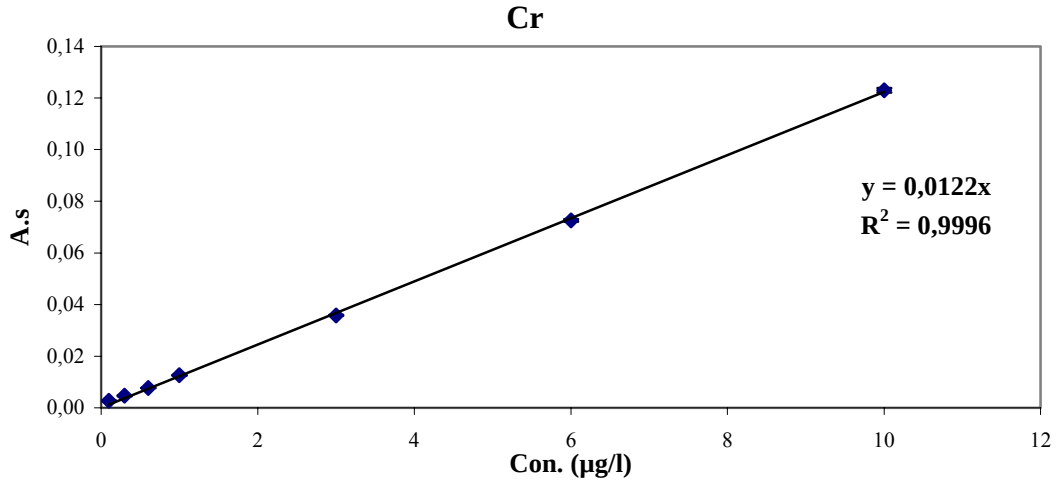
Cr
A.s
Con. (µg/l)
y = 0,0122x
R2 = 0,9996
0,14
0,12
0,10
0,08
0,06
0,04
0,02
0,00
0
2
4
6
8
10
12

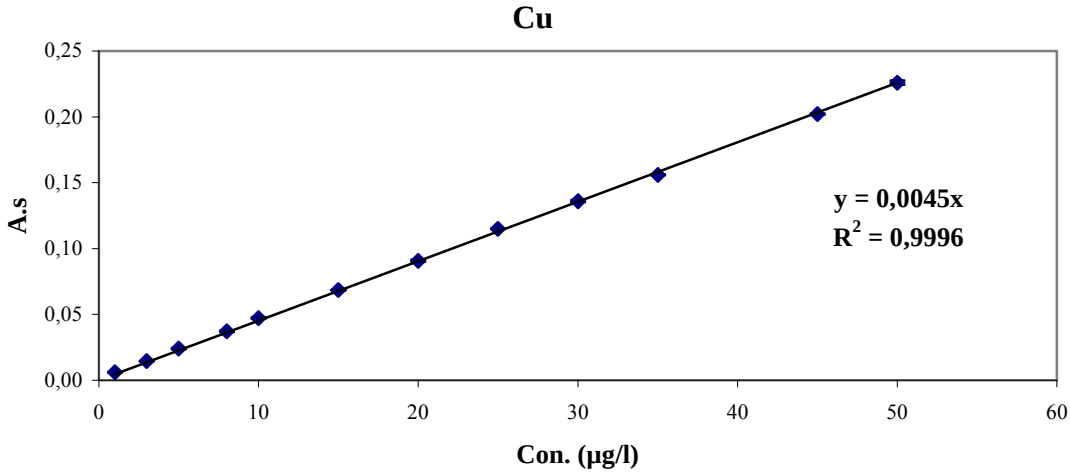
Cu
A.s
Con. (µg/l)
y = 0,0045x
R2 = 0,9996
0,25
0,20
0,15
0,10
0,05
0,00
0
10
20
30
40
50
60

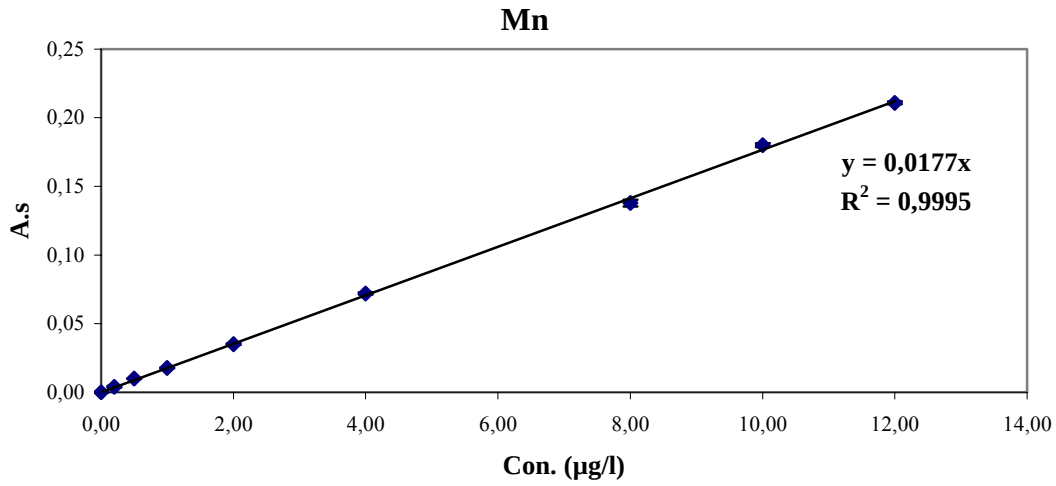
Mn
A.s
Con. (µg/l)
y = 0,0177x
R2 = 0,9995
0,25
0,20
0,15
0,10
0,05
0,00
0,00
2,00
4,00
6,00
8,00
10,00
12,00
14,00

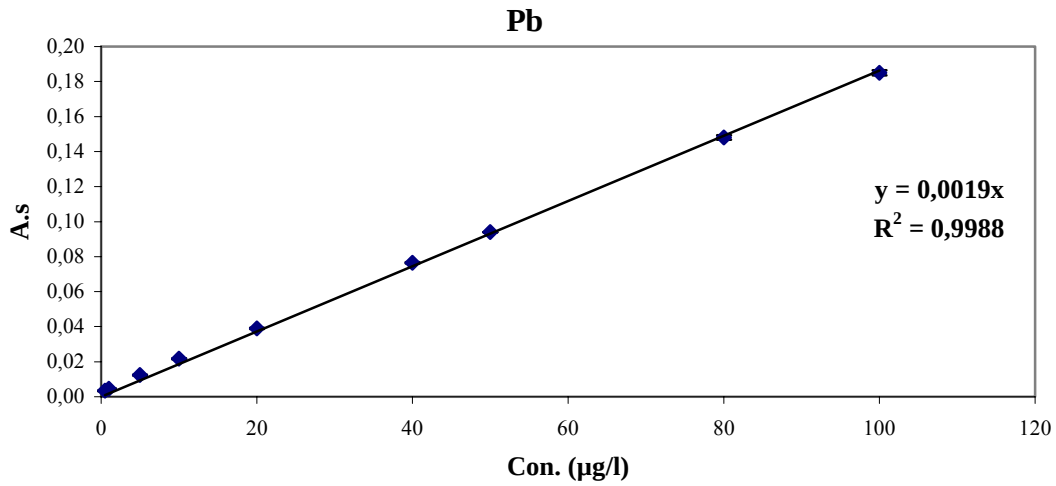
Pb
A.s
Con. (µg/l)
y = 0,0019x
R2 = 0,9988
0,20
0,18
0,16
0,14
0,12
0,10
0,08
0,06
0,04
0,02
0,00
0
20
40
60
80
100
120

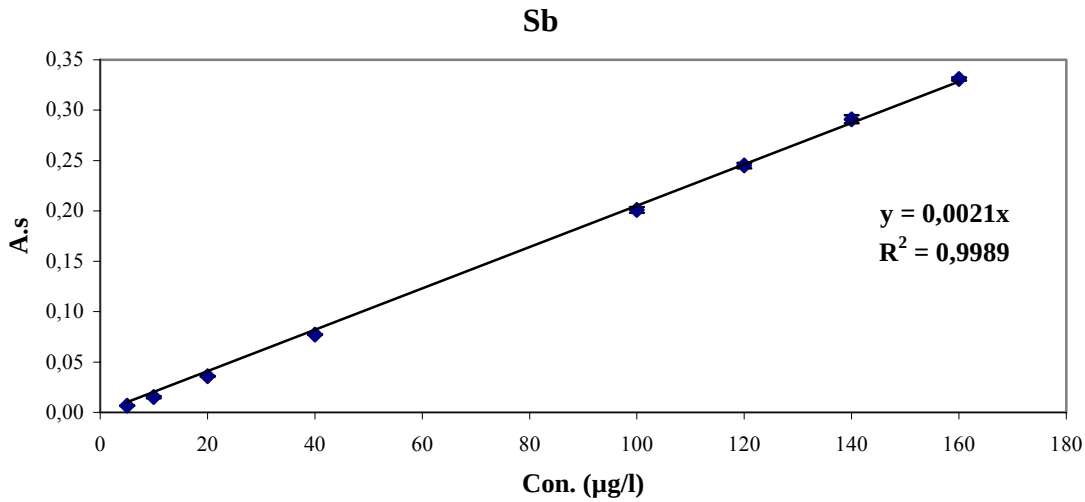
Sb
A.s
Con. (µg/l)
y = 0,0021x
R2 = 0,9989
0,35
0,30
0,25
0,20
0,15
0,10
0,05
0,00
0
20
40
60
80
100
120
140
160
180

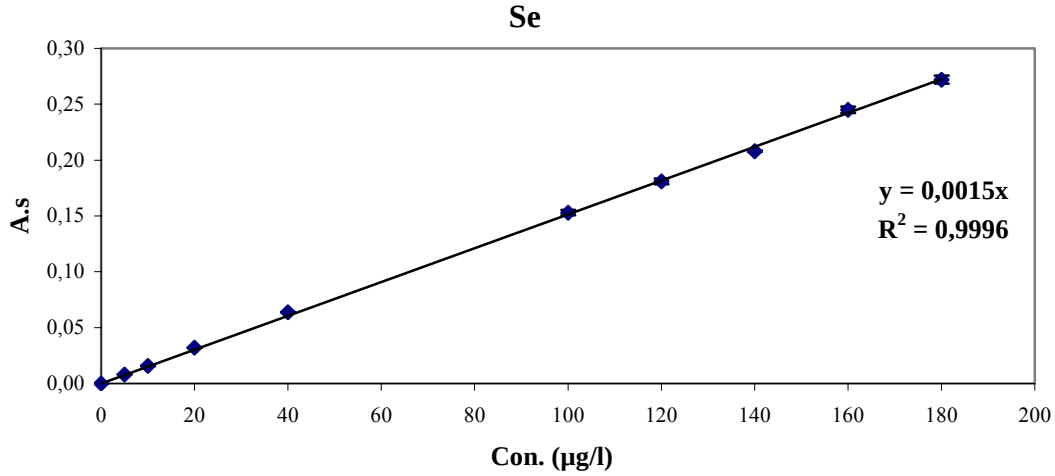

5.3.2 With Magnesium Nitrate ($Mg(NO_3)_2$) Modifier

We have used this modifier (5 µg $Mg(NO_3)_2$) in the simultaneous multi-element determination of Al, Be, Cr, and V using end-capped tubes. This modifier has been recommended for the stabilization of Al, Be[155-157], and Cr[158-160]. The most stabilizing effect has been observed for beryllium (about 600^{o}C). For aluminium and chromium, the stabilization effect was in the range 100-200^{o}C. However, for aluminium, the sensitivity was higher than that without modifier which has also been reported by Shan[154]. The increase in the sensitivity can also be attributed to the use of the end-capped tube. With this tube, the diffusional of the atomic vapour out of the tube are lowered and the sensitivity improved by a factor of 1.3-1.5 according to the element[9]. For vanadium, no stabilization effect has been observed (Figure 5.1). But generally; for all elements, the absorbance peaks have become sharper than without modifier and even with Pd+Mg modifier in the case of Al, Cr, and Be. Since we have used $Mg(NO_3)_2$ for the multi-element determination for this group of element, therefore, the optimum conditions (the pyrolysis and atomization temperatures) in the single-element mode have been determined. The optimum conditions with this modifier have been used to determine the characteristic mass and detection limit for these elements and the results are compared with those in multi-element mode. The calibration curves for these elements are shown in Figure 5.3.

Figure 5.3 Calibration curves of the elements with Mg modifier in the single-element mode

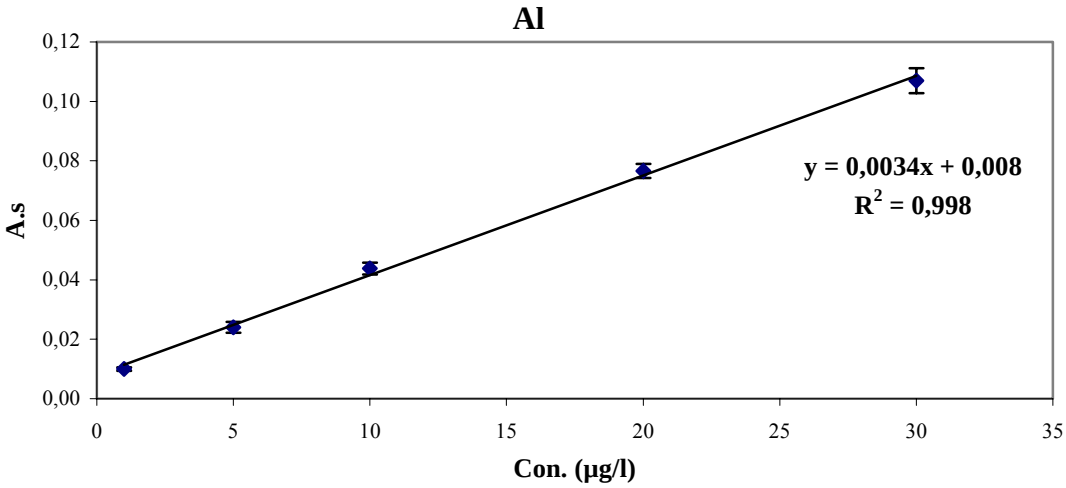

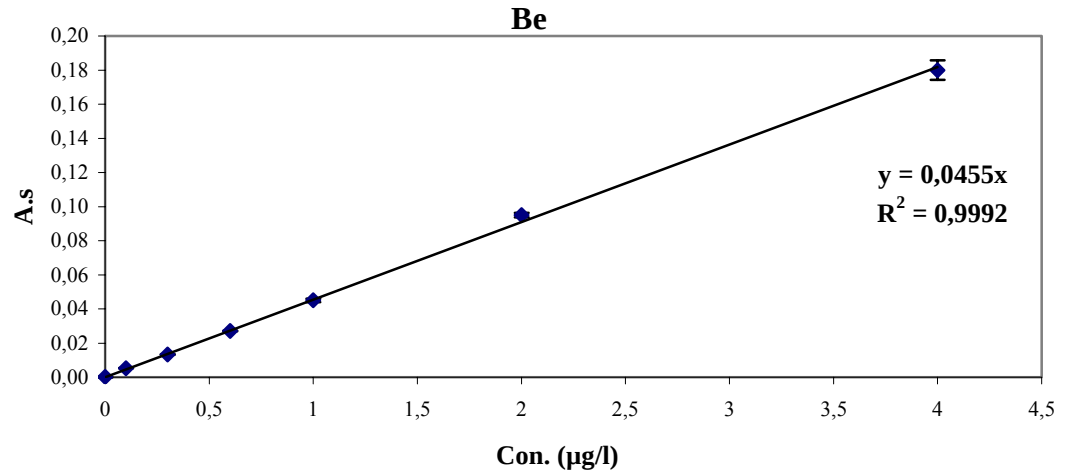

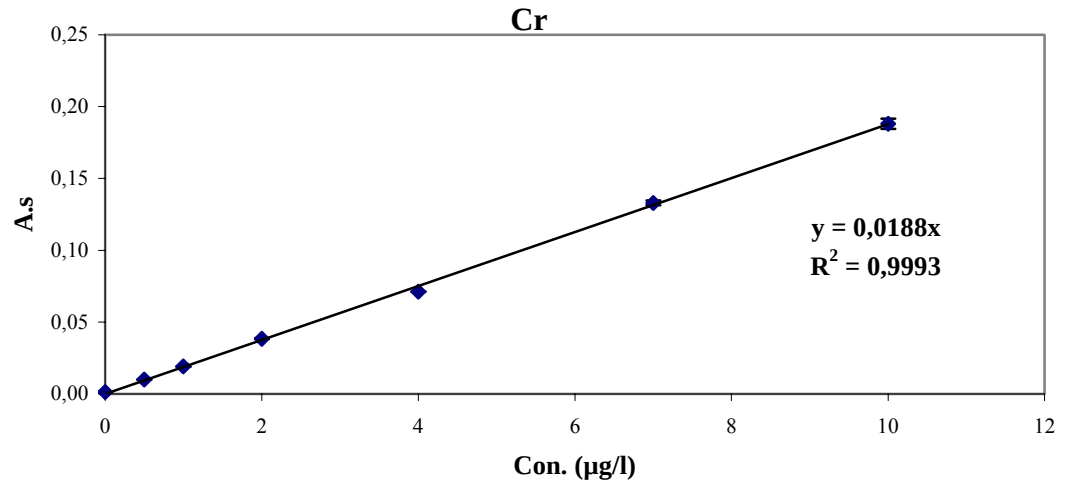

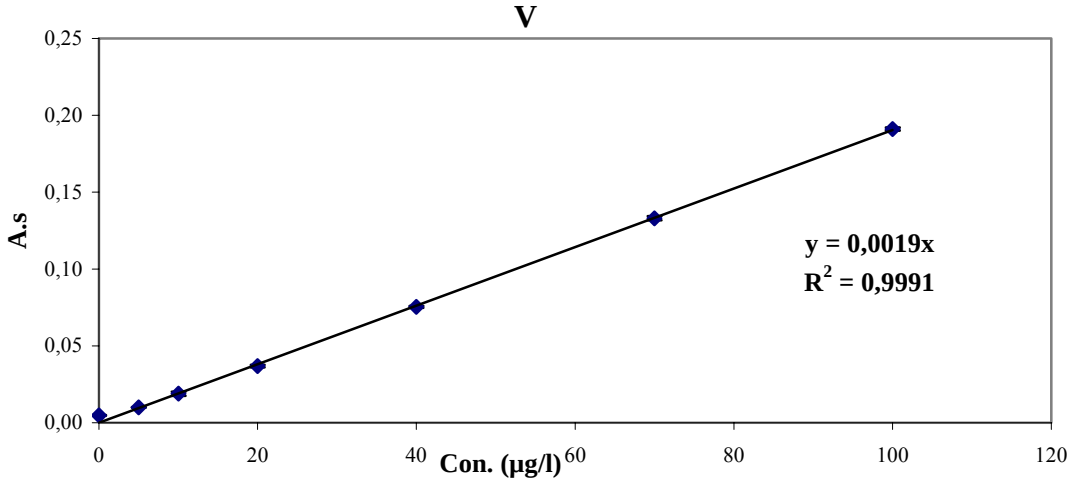

5.3.3 With Ir-permanent Modifier

Iridium is rather a refractory element with high melting (2410°C) and boiling (4527°C) points. These temperatures are significantly higher than the corresponding figures for palladium usually employed as universal chemical modifier (1552 and 2927°C)[118]. Tsalev et al.[125] have found that during a simulated clean-out step, Ir losses start at temperatures higher than 2200°C. Therefore, Ir absorbance signals were much more strongly depressed on pyrolytically coated platforms than those of Pd. This means that Ir is better retained on the graphite surface, making it a promising permanent modifier.

In this work, the tube was coated with 500 µg Ir by pipetting 20 µl of a 1.000 $g.l^{-1}$ solution of Ir, as chloride, and submitting the tube to the temperature program shown in Table 4.4. The entire procedure was repeated 25 times. We have tested this modifier with the volatile elements (Se, Cd, Bi, Pb, and Sb). The optimum pyrolysis and atomization temperatures obtained from pyrolysis and atomization curves for these elements are compared with the values of multi-element mode. The pyrolysis and atomization curves with this modifier are shown in Figure 5.1. For, Bi, Pb, Sb, and Se, higher pyrolysis temperatures; compared to that with Pd+Mg modifier, can be used. Also, higher atomization temperatures, especially for Sb, are required and this means more stabilization effect with this modifier will be obtained. For Cd, there was no change in the pyrolysis and atomization temperatures. But there was an increase in the appearance time. Broad absorbance, compared with Pd+Mg modifier, for Sb has been observed. At the same time, there are decrease in the sensitivity for these elements, except for Cd and Se, which can be a result from the higher atomization temperature that have been used with this modifier comparing with the other modifier (Pd+Mg modifier). At higher atomization temperatures, diffusion losses of elements are

higher so that lower integrated absorbances are obtained; hence, the m_o values are higher than those obtained with Pd+Mg modifier. The optimum pyrolysis and atomization temperatures have been used to determine the characteristic masses and detection limits and the results are compared with those in multi-element mode. The calibration curves are shown Figure 5.4.

Figure 5.4 Calibration curves of the elements with Ir-permanent modifier in the single-element mode

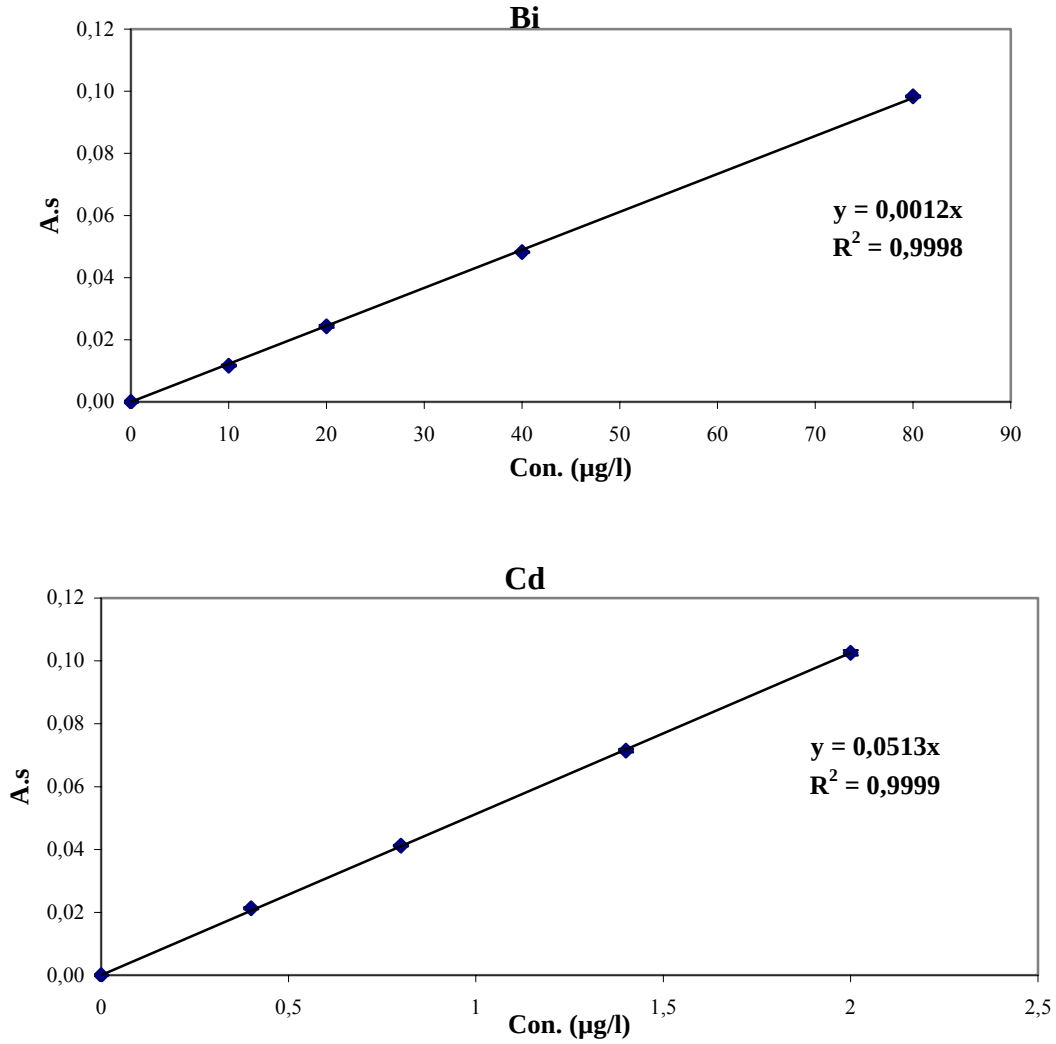

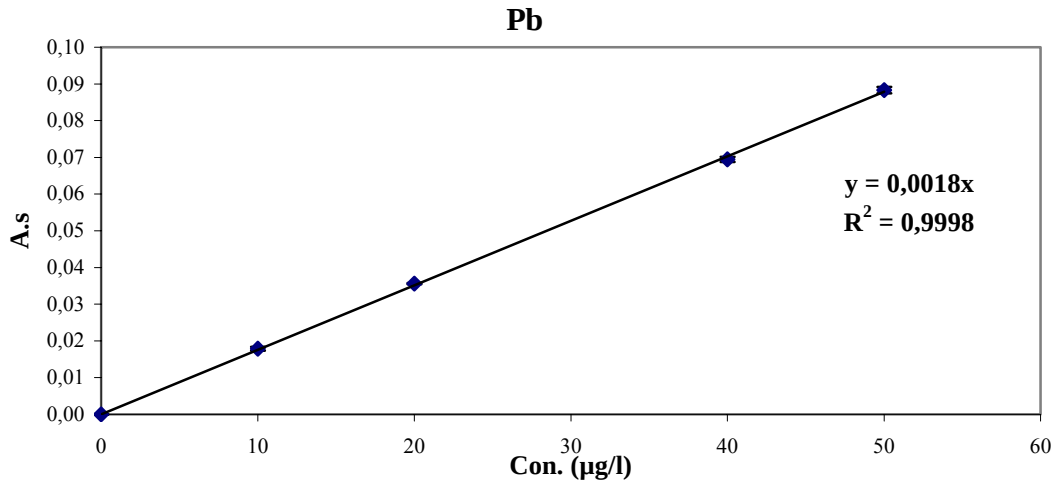
Pb
A.s
Con. (µg/l)
y = 0,0018x
R2 = 0,9998
0,00
0,01
0,02
0,03
0,04
0,05
0,06
0,07
0,08
0,09
0,10
0 10 20 30 40 50 60

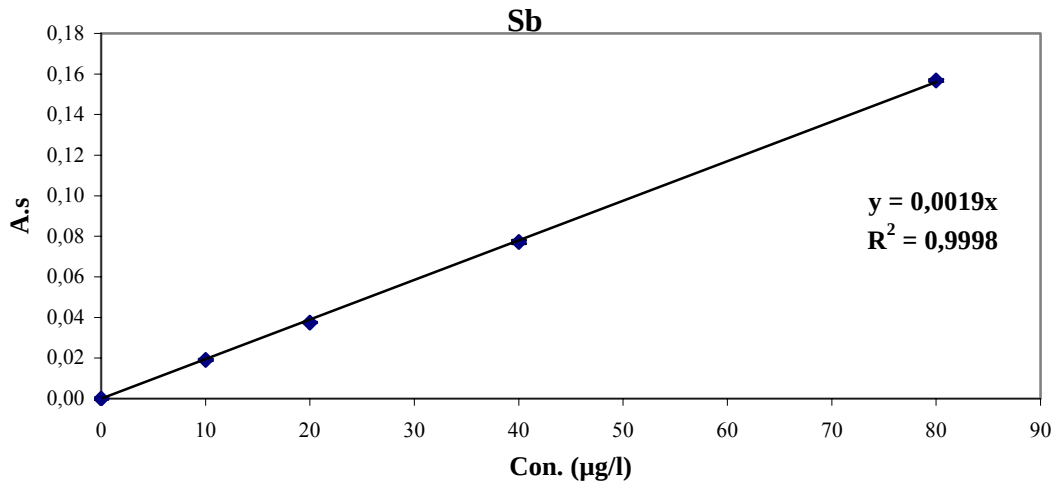
Sb
A.s
Con. (µg/l)
y = 0,0019x
R2 = 0,9998
0,00
0,02
0,04
0,06
0,08
0,10
0,12
0,14
0,16
0,18
0 10 20 30 40 50 60 70 80 90

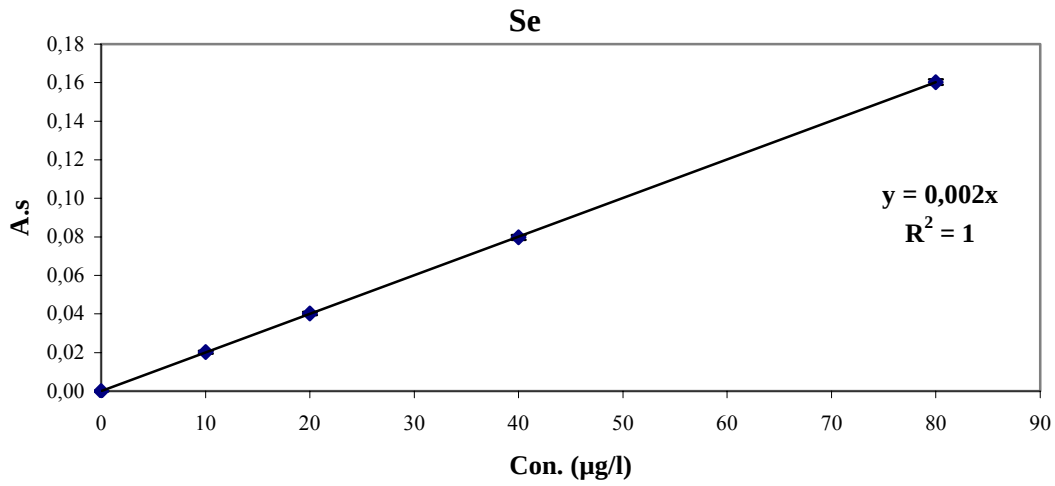
Se
A.s
Con. (µg/l)
y = 0,002x
R2 = 1
0,00
0,02
0,04
0,06
0,08
0,10
0,12
0,14
0,16
0,18
0 10 20 30 40 50 60 70 80 90

5.4 Multi-Element Determinations with 2-Operating Mode

As in any multi-element technique, SIMAAS requires compromised conditions, e.g., chemical modifier, pyrolysis and atomization temperatures, which can lead to significant sensitivity deterioration. In spite of instrumental advancements and the use of STPF conditions, the majority of the multi-element methods performed by SIMAAS are limited for few elements due to the difficulties to find out a more universal set of adjustments for the experimental and instrumental parameters. Even so, for 2-element operating mode, the time, reagent, and sample consumption are significantly reduced.

The 2-element operating mode has smaller effect on the sensitivity of the determination. The multi-element lamps; either HCLs or EDLs which can be for the determination of more than one element, have been used in this work to study the multi-element capability of the system. Among of them are Cr lamp which can be used for Cr and Cu, Mn lamp which can be used for Mn and Cu, and Sb lamp which can be used for Sb and Bi. The groups of elements for multi-element mode have been selected according to the stabilization effect of the modifier on these elements. Also, the effects of the operating mode on the sensitivity of the determination have been studied and the results were shown at the end of this section.

The compromised conditions for each group of element have been determined. The compromised procedures have been carried out using aqueous solutions and in the presence of different modifiers according to the group of elements selected. The compromised conditions, which are pyrolysis and atomization temperatures, have been used to determine the characteristic masses and detection limits for each element in the multi-element determinations and compared with those in the single-element determinations.

5.4.1 Multi-Element Determination of Be, Cr, and Cu

We have decided to determine the Cu with Be and Cr simultaneously because the Cr lamp can be used for Cr and Cu and that allow us to use the 2-lamp operating mode. For the multi-elemet determination of this group, we have used the mixture modifier (5 µg Pd + 3 µg Mg). The dependence of Be, Cr, and Cu absorbance on the pyrolysis and atomization temperatures was studied. The pyrolysis and atomization curves are shown in Figure 5.5. The optimum pyrolysis and atomization temperatures for the simultaneous determination were 1200 and 2300^{o}C, simultaneously. We have not increased the atomization temperature more than 2400^{o}C because the lifetime of the tube will decrease. The pyrolysis and atomization curves were made using the following concentrations: 4 ppb Be, 10 ppb Cr and 25 ppb Cu in 0.2% HNO_3. The optimized temperature program for the multi-element determination of Be,

Cr, and Cu is shown in Table 4.3. The cleanout temperature was 2500°C and the hold time was 4s. This optimized temperature program has been used to determine the characteristic masses and detection limits for these elements in the multi-element mode .These values are compared with those in the single-element mode and shown in Table 5.2. The values of detection limits were not so higher comparing with the single-element mode as for the simultaneous determination of Al, Be, Cr, and V. This is because the use of 2-operating mode comparing with 4-operating mode for first group. The values of characteristic mass were similar to those of the single-element mode especially for Be and Cr. The higher value in the case of Cu can be attributed to higher atomization temperature 2300°C for multi-element mode comparing to 2000°C for the single-element mode. The calibration curves which have been used to determine the characteristic masses and detection limits are shown in Figure 5.6.

Figure 5.5 Pyrolysis and atomization curves for multi-element mode in aqueous solution of Be, Cr, and Cu using Pd+Mg(NO$_3$)$_2$ as a modifier

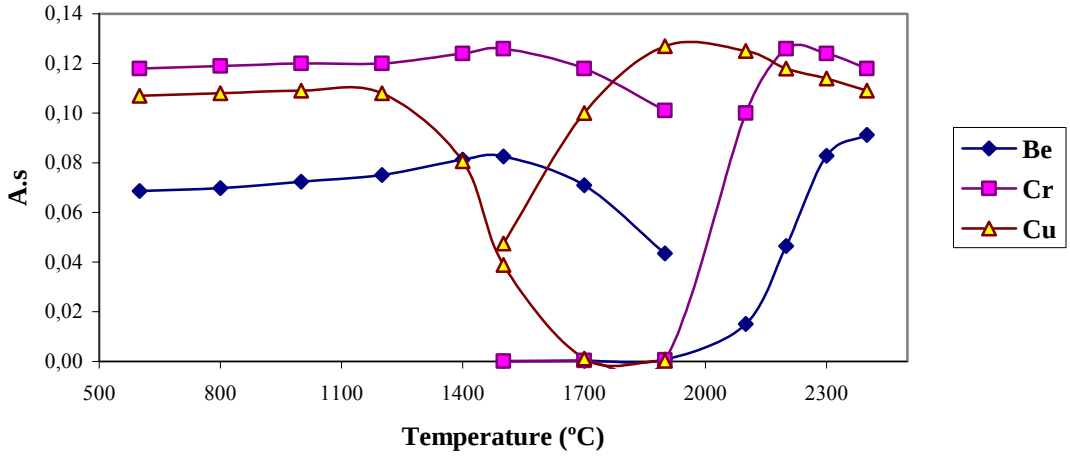

Table 5.2 Comparing the single-element determinations with the multi-element mode of Be, Cr, and Cu (pyrolysis=1200°C, atomization=2300°C)

Element	Pyrolysis (Single) (°C)	Atomization (Single) (°C)	LOD (ppb)		Characteristic mass (pg)	
			Single	Multi	Single	Multi
Be	1600	2300	0.026	0.030	3.9	4.4
Cr	1500	2300	0.049	0.054	7.2	7.9
Cu	1200	2000	0.13	0.14	19.6	21.0

Figure 5.6 Calibration curves of the multi-element mode in aqueous solution of Be, Cr, and Cu with Pd+Mg modifier

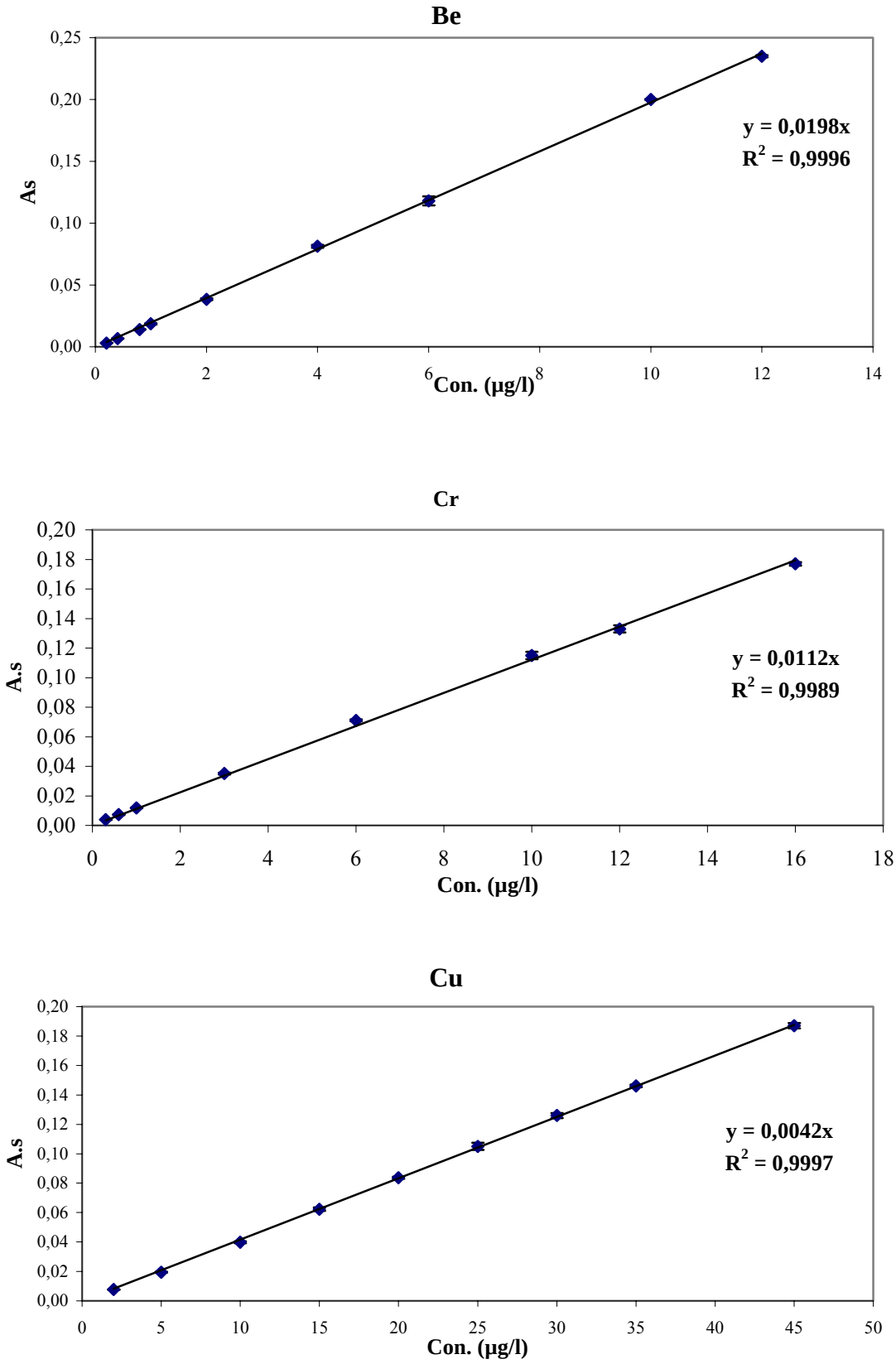

5.4.2 Multi-Element Determination of Bi, Sb, Cu, and Mn

The multi-element determination of this group has been carried out using 2-operating mode because the Sb and Mn lamps are multi-element lamps. Pyrolysis and atomization curves were carried out in order to define the compromise conditions for simultaneous determination of Bi, Sb, Cu, and Mn, since in simultaneous detection the heating program of the atomizer is the same for all analytes. Shown in Figure 5.7 are the pyrolysis and atomization temperature curves for 100 ppb Bi, 100 ppb Sb, 25 ppb Cu, and 10 ppb Mn in 0.2% HNO_3 in the presence of 5 µg Pd+ 3 µg Mg as a modifier. In order to determine all four elements simultaneously, 1100 and 2000^{o}C were chosen as an optimum pyrolysis and atomization temperatures, simultaneously. The optimum temperature program for the simultaneous determination of these elements is shown in Table 4.3. The cleanout temperature was 2500^{o}C and the hold time was 4s. Calibration curves constructed from the aqueous standards in 0.2% HNO_3; Figure 5.8, were used to determine the characteristic masses and detection limits of these elements in the multi-element mode and the values compared to those determined in the single-element mode are shown Table 5.3. The values of detection limits were higher for multi-element mode compared with those of single-element mode. For Bi and Sb were approximately three times higher and for Cu and Mn were about two times higher. This was because the lower light intensity produced form the lamps in multi-element mode comparing with single-element mode. The higher characteristic mass of Bi can be explained by the higher atomization temperature used in multi-element mode (2000^{o}C) compared with single-element mode (1800^{o}C). For Sb, it was not as higher as with Bi because the difference in the atomization temperatures was lower (100^{o}C).

Figure 5.7 Pyrolysis and atomization curves for multi-element mode in aqueous solution of Bi, Sb, Cu, and Mn using Pd+Mg$(NO_3)_2$ as a modifier

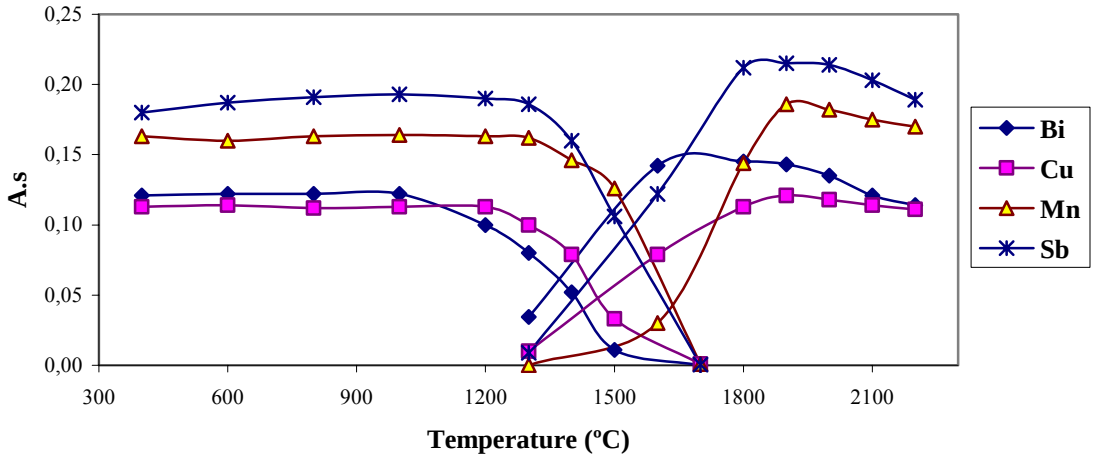

Figure 5.8 Calibration curves of the multi-element mode in aqueous solution of Bi, Sb, Cu, and Mn with Pd+Mg modifier

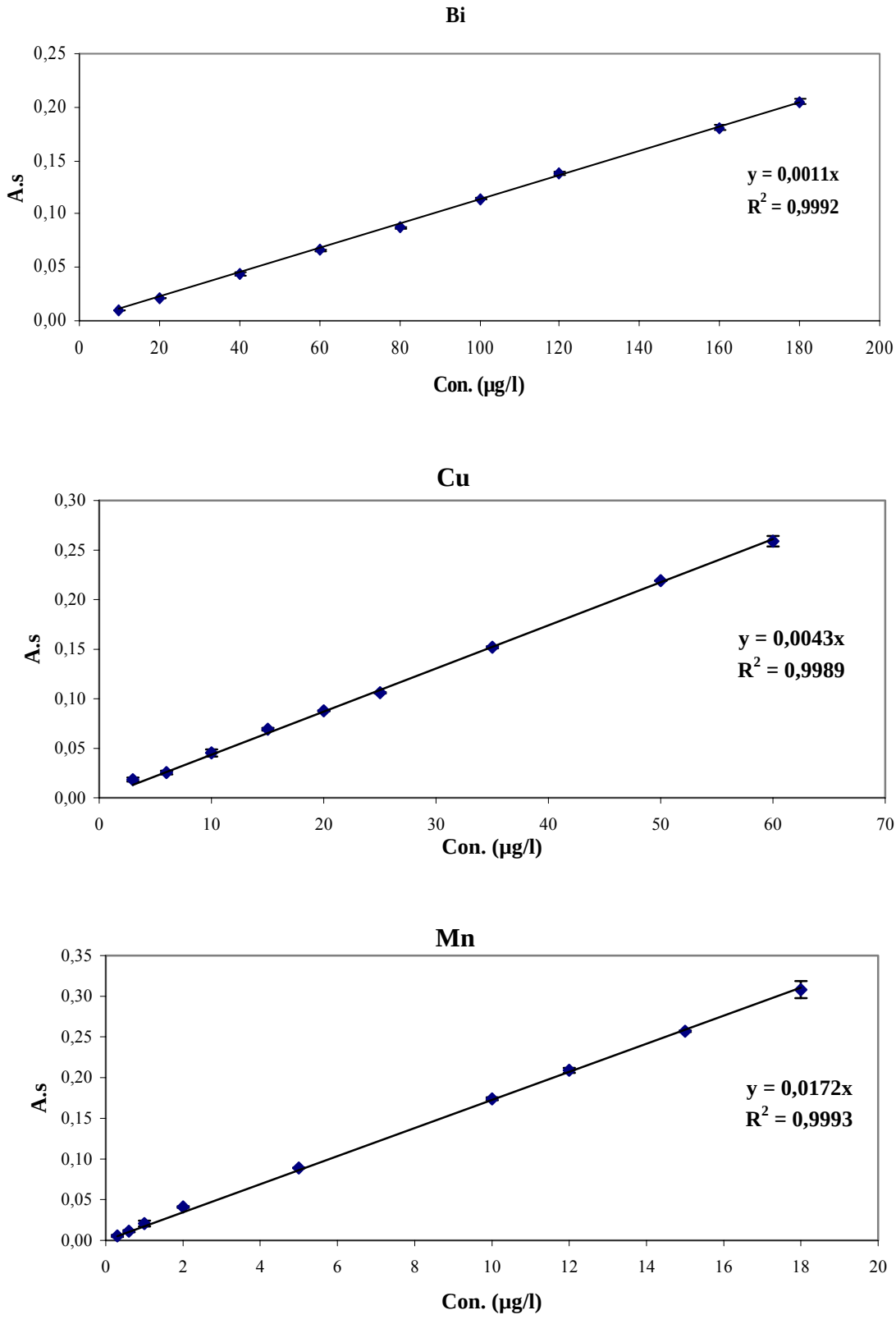

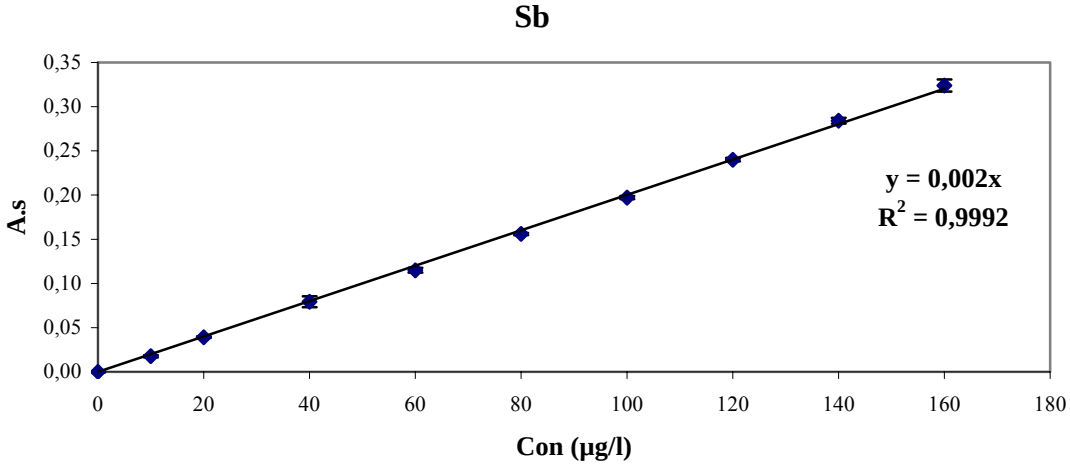

Table 5.3 Comparing the single-element mode with the multi-element determination of Bi, Sb, Cu, and Mn (pyrolysis=1100°C, atomization=2000°C)

Element	Pyrolysis (Single) (°C)	Atomization (Single) (°C)	LOD (ppb)		Characteristic mass (pg)	
			Single	Multi	Single	Multi
Bi	1100	1800	0.46	1.4	67.7	80
Cu	1200	2000	0.13	0.28	19.6	20.5
Mn	1400	2000	0.051	0.087	5.0	5.1
Sb	1300	1900	0.29	0.90	41.9	44

5.4.3 Multi-Element Determination of Cu, Mn, and Se

The multi-element determination of this group has been carried out using 2-operating mode because the Mn lamp is a multi-element lamp (for Mn and Cu). The pyrolysis and atomization curves have been constructed for 25 ppb Cu, 10 ppb Mn, and 100 ppb Se in 0.2% HNO_3 in the presence of 5 µg Pd + 3 µg Mg as a modifier and are shown in Figure 5.9. From the pyrolysis and atomization curves, a pyrolysis temperature of 1200°C and an atomization temperature of 2000°C were used as the optimum for the multi-element determination of these elements. The optimum temperature program for the simultaneous determination of Cu, Mn, and Se is shown in Table 4.3. The cleanout temperature was 2500°C and the hold time was 4s. We have used the optimum temperature program to construct the calibration curves of the elements in 0.2% HNO_3 (Figure 5.10) and from the calibration curves we have calculated the characteristic masses and the detection limits in the multi-element mode. The values of the characteristic masses and detection limits have been compares with those obtained in the

single-element mode (Table 5.4). The detection limits value of Se was high in the multi-element mode compared with single-element mode. This was as a result of decreased intensity of Se lamp that we have observed in multi-element mode compared with single-element mode. For Cu and Mn, they were comparable. However, the characteristic mass values were similar because the atomization temperatures of single-element mode and multi-element mode were similar (Cu and Mn) or the difference was not so high (Se).

Figure 5.9 Pyrolysis and atomization curves for multi-element mode in aqueous solution of Cu, Mn, and Se using Pd+Mg$(NO_3)_2$ as a modifier

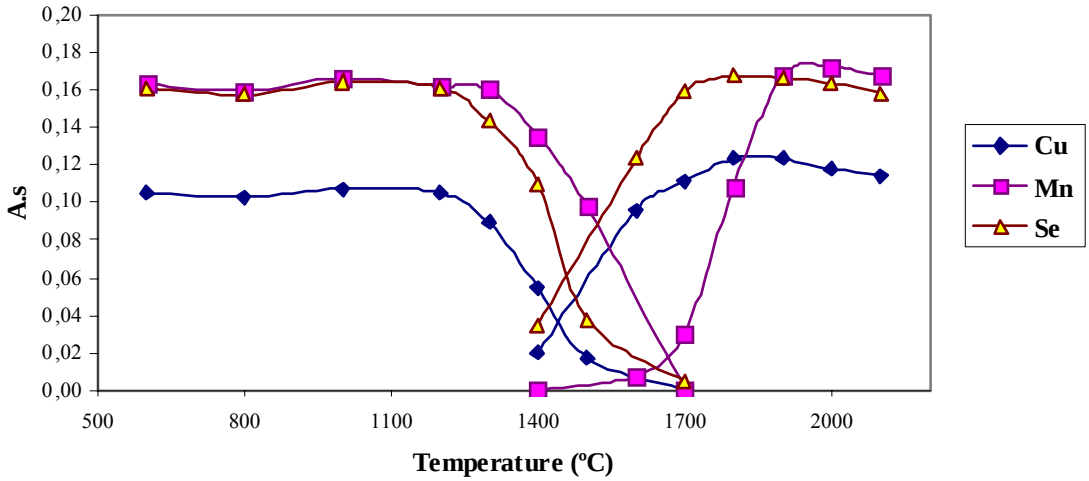

Figure 5.10 Calibration curves of the multi-element mode in aqueous solution of Cu, Mn, and Se with Pd+Mg modifier

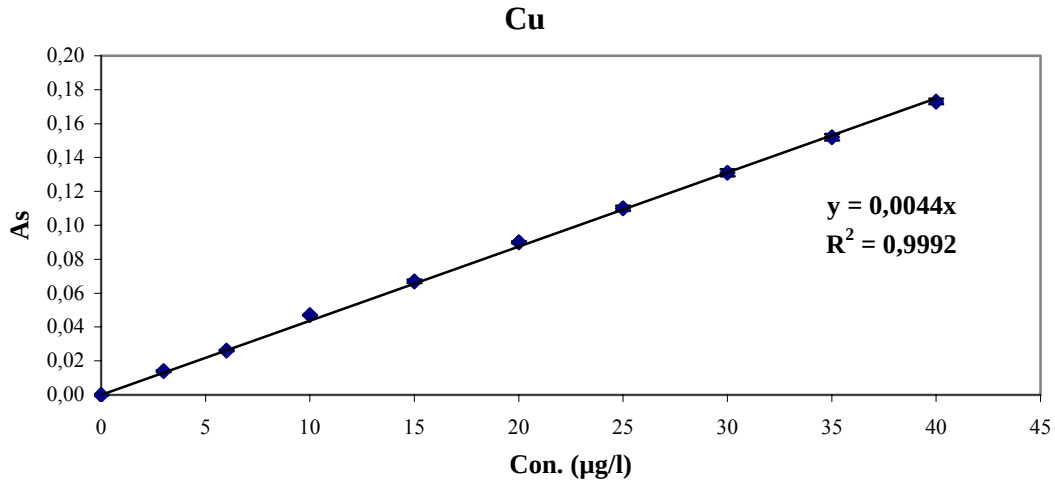

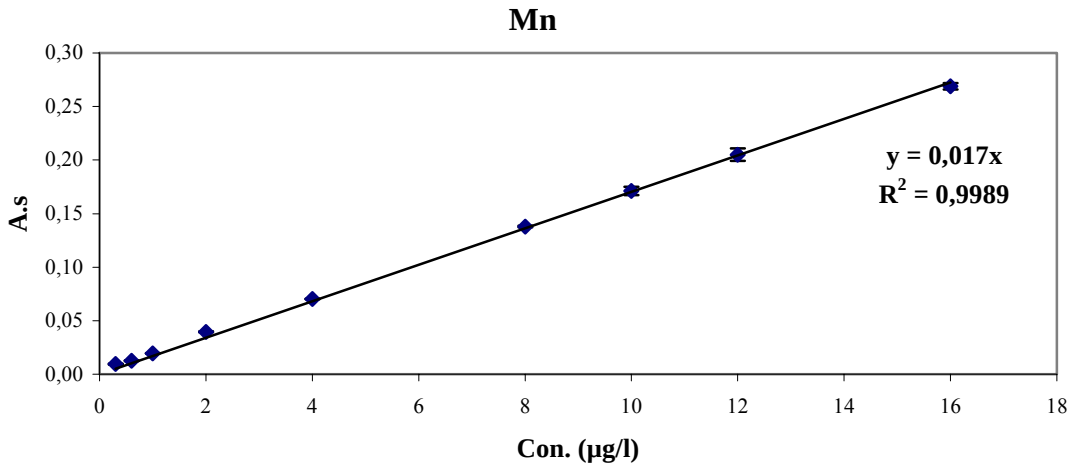

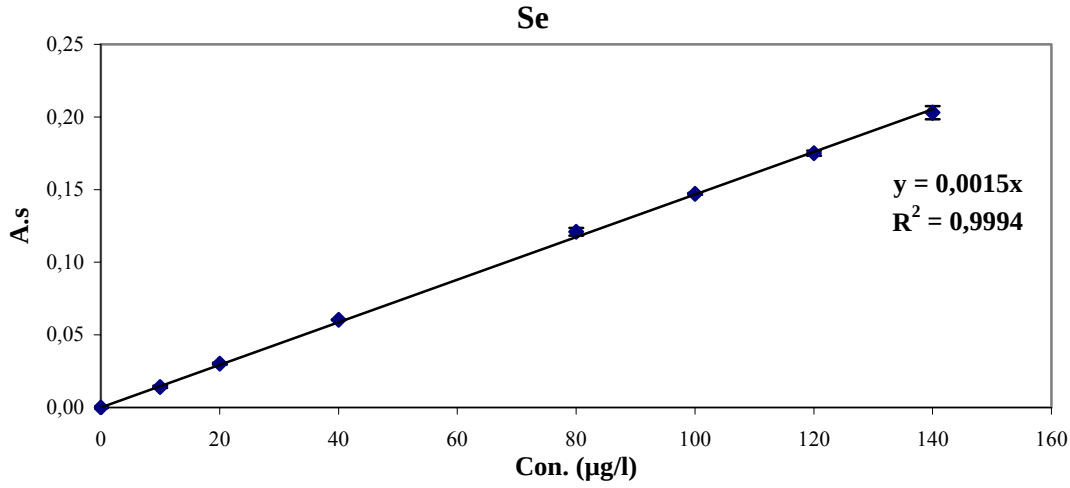

Table 5.4 Comparing the single-element mode with the multi-element mode of Cu, Mn, and Se (pyrolysis=1200°C, atomization=2000°C)

Element	Pyrolysis (Single) (°C)	Atomization (Single) (°C)	LOD (ppb)		Characteristic mass (pg)	
			Single	Multi	Single	Multi
Cu	1200	2000	0.13	0.20	19.6	20
Mn	1400	2000	0.051	0.070	5.0	5.2
Se	1200	1900	0.40	1.0	58.7	58.7

5.4.4 Multi-Element Determination of Pb and Se

Two types of modifiers have been used for the simultaneous determination of Pb and Se. The first one was the mixture of palladium nitrate and magnesium nitrate (5µg Pd + 3µg Mg). The second one was iridium as a permanent modifier.

5.4.4.1 With Pd+Mg Modifier

Pyrolysis and atomization curves were carried out in order to define the compromise conditions for simultaneous determination of Pb and Se. Shown in Figure 5.11 are the pyrolysis and atomization curves for 40 ppb Pb and 100 ppb Se in 0.2% HNO_3 and using 5 µg Pd + 3 µg Mg as a modifier. The effects of the pyrolysis and atomization temperatures are studied (shown in Figure 5.11). From pyrolysis and atomization curves and the absorption signals shapes, we have decided to use 1000 and 1900^{o}C as an optimum pyrolysis and atomization temperatures, respectively for the simultaneous determination of Pb and Se using Pd+Mg modifier. The optimum temperature program for the simultaneous determination of Pb and Se is shown in Table 4.3. The cleanout temperature was 2400^{o}C and the hold time was 3s. Calibration curves constructed from the aqueous standards in 0.2% HNO_3; Figure 5.12, were used to determine the characteristic masses and detection limits of these elements in the multi-element mode and the values compared to those determined in the single-element mode are shown Table 5.5. The detection limits values were comparable to those of single-element mode. Small differences can be attributed to the multi-operating mode. The differences in characteristic mass values were higher for Pb comparing with Se. This was a result of decreased sensitivity in multi-element mode (0.0016) compared with single-element mode sensitivity (0.0019).

Figure 5.11 Pyrolysis and atomization curves for multi-element mode in aqueous solution of Pb and Se using Pd+Mg$(NO_3)_2$ as a modifier

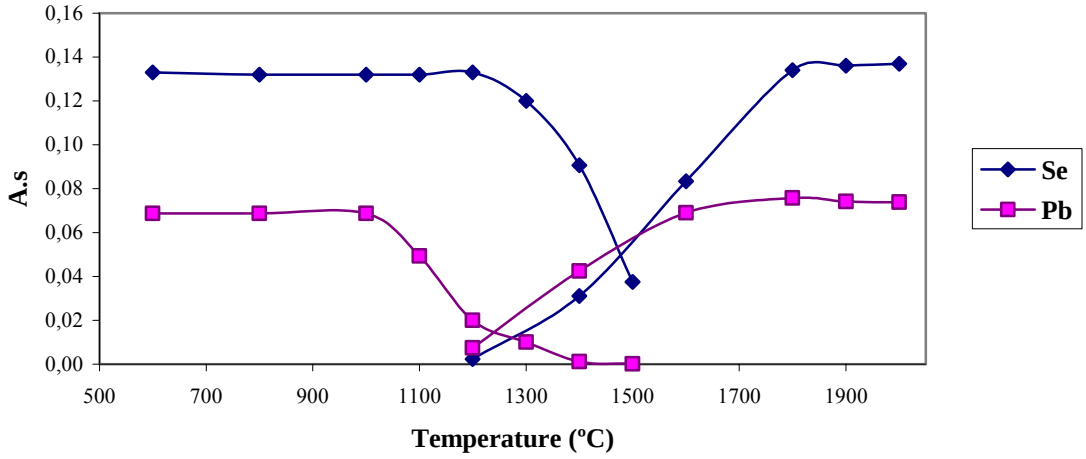

Figure 5.12 Calibration curves of the multi-element mode in aqueous solution of Pb and Se with Pd+Mg modifier

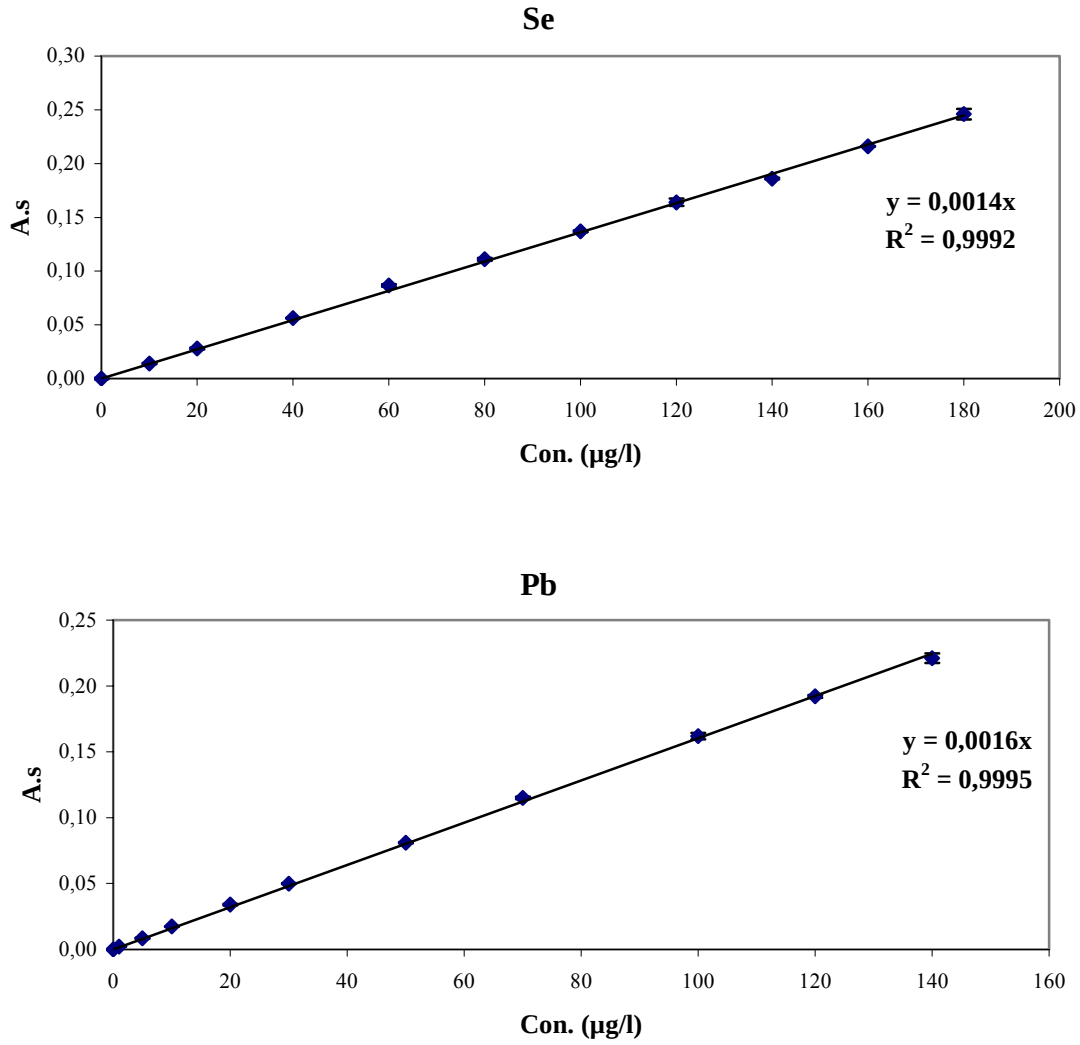

Table 5.5 Comparing the single-element mode with the multi-element mode of Pb and Se using Pd+Mg modifier (pyrolysis=1000°C, atomization=1900°C)

Element	Pyrolysis (Single) (°C)	Atomization (Single) (°C)	LOD (ppb)		Characteristic mass (pg)	
			Single	Multi	Single	Multi
Se	1200	1900	0.40	0.64	58.7	62.9
Pb	1000	1900	0.32	0.38	46.3	55

5.4.4.2 With Ir Permanent Modifier

The 500 µg iridium was thermally deposited on the graphite tube platform and used as permanent modifier. The concentrations of the elements that have been used to study the effects of the modifier on the pyrolysis and atomization curves were 40 ppb and 100 ppb in 0.2% HNO_3 for Pb and Se, respectively. From the pyrolysis and atomization curves; Figure

5.13, 1200 and 2000°C were used as an optimum pyrolysis and atomization temperatures. The optimum temperature program is summarized in Table 4.3. The cleanout temperature was 2400°C and the hold time 3s. Calibration curves constructed from the aqueous standards in 0.2% HNO_3; Figure 5.14, were used to determine the characteristic masses and detection limits of these elements in the multi-element mode and the values compared to those determined in the single-element mode are shown Table 5.6. The detection limits values for multi-element mode were comparable to those of single-element mode. The difference can be attributed to the use of multi-operating mode. The values of characteristic mass were same as of single-element mode.

Figure 5.13 Pyrolysis and atomization curves for multi-element mode in aqueous solution of Pb and Se using Ir permanent modifier

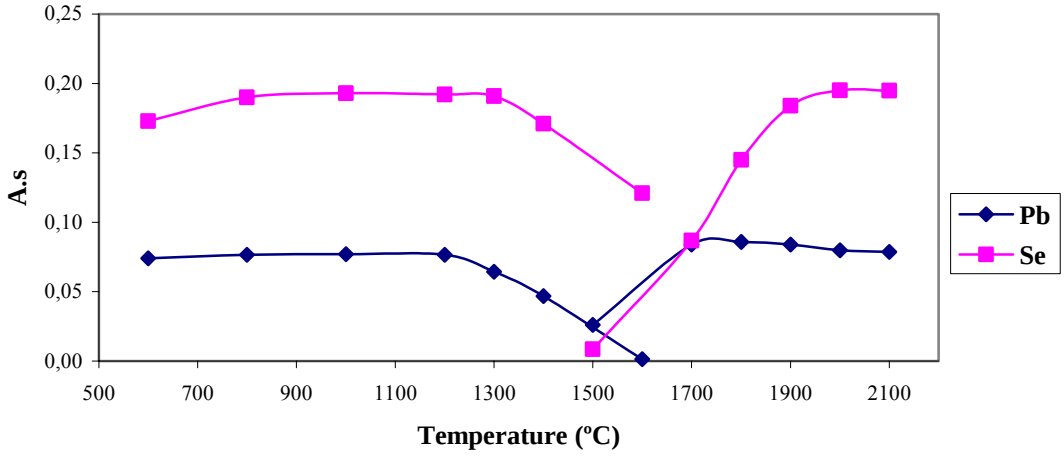

Figure 5.14 Calibration curves of the multi-element mode in aqueous solution of Pb and Se with Ir permanent modifier

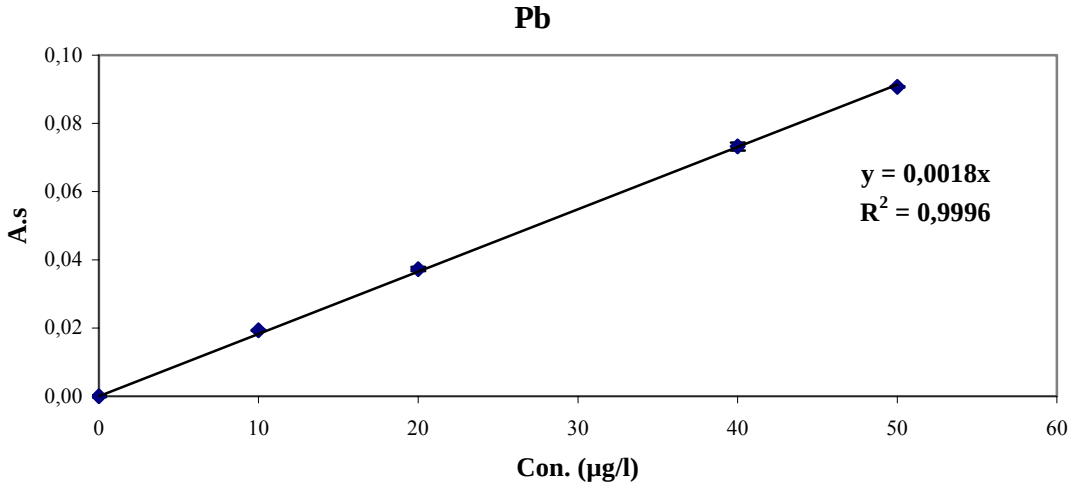

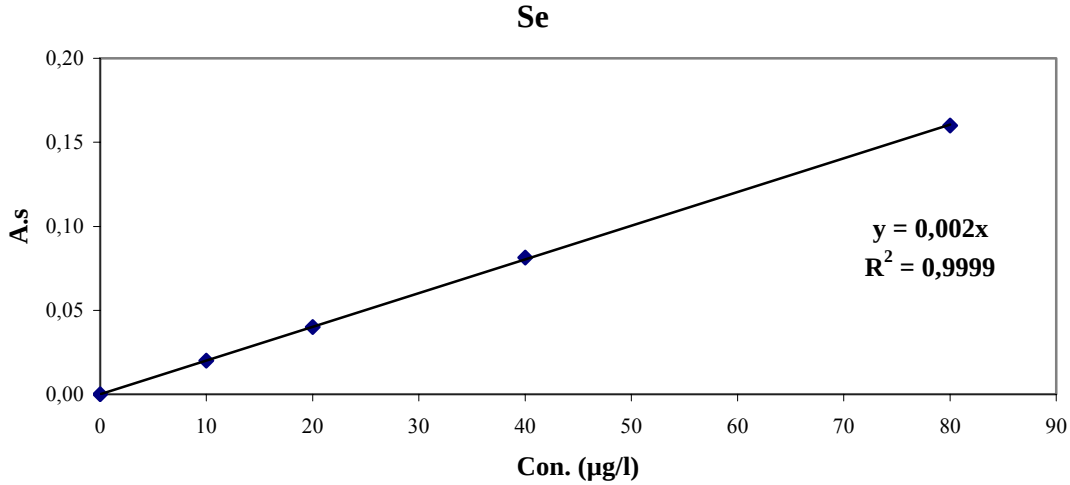

Table 5.6 Comparing the single-element mode with the multi-element mode of Pb and Se using Ir permanent modifier (pyrolysis=1200°C, atomization=2000°C)

Element	Pyrolysis (Single) (°C)	Atomization (Single) (°C)	LOD (ppb)		Characteristic mass (pg)	
			Single	Multi	Single	Multi
Se	1300	2000	0.30	0.45	44.0	44.0
Pb	1200	1900	0.17	0.33	48.9	48.9

5.4.5 Multi-Element Determination of Bi, Sb, and Cd

The multi-element determination of this group has been carried out using 2-operating mode because the Sb lamp is a multi-element lamp (for Sb and Bi). As for the simultaneous determination of Pb and Se, two types of modifiers have been used for the simultaneous determination of Bi, Sb, and Cd. The first one was the mixture of palladium nitrate and magnesium nitrate (5µg Pd + 3µg Mg). The second one was iridium as a permanent modifier.

5.4.5.1 With Pd+Mg Modifier

The dependence of Bi, Sb, and Cd absorbance on the pyrolysis and atomization temperatures was studied and shown in Figure 5.15. The pyrolysis and atomization curves were made using the following concentrations: 100 ppb Bi, 100 ppb Sb and 2 ppb Cd in 0.2% HNO_3 in the presence of 5µg Pd and 3µg Mg as a modifier. In order to determine all three elements simultaneously, 700 and 1900°C were chosen as the optimum pyrolysis and atomization temperatures. The optimized temperature program for the multi-element determination of Bi, Sb, and Cd is shown in Table 4.3. The cleanout temperature was 2400°C and the hold time 3s. This optimized temperature program has been used to determine the

characteristic masses and detection limits for these elements in the multi-element mode .These values are compared with those in the single-element mode and shown in Table 5.7. The detection limits values for multi-element determination of Sb and Bi were higher than those of single-element determination. This was a result of decreased intensity in multi-element mode compared that of single-element mode. For Cd, the detection limits values were similar. This was because of high Cd lamp intensity which does not so affect in multi-element mode. It was a decrease in the sensitivity of Cd (0.0351) and Bi (0.0011) compared with of single-element mode (0.0417 for Cd and 0.0013 for Bi). This was an effect of using a higher atomization temperature comparing with single-element mode. The calibration curves which have used to determine the characteristic masses and detection limits are shown in Figure 5.16.

Figure 5.15 Pyrolysis and atomization curves for multi-element mode in aqueous solution of Bi, Sb, and Cd using Pd+Mg modifier

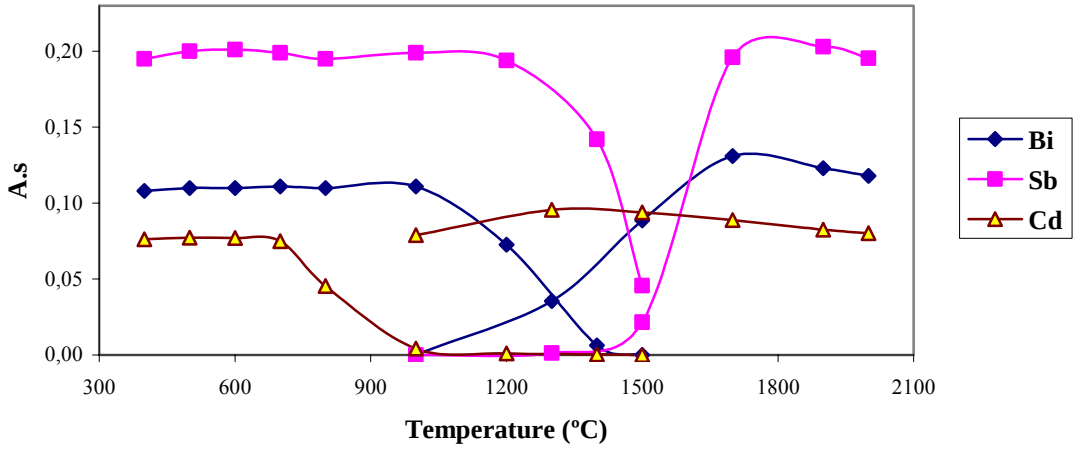

Figure 5.16 Calibration curves of the multi-element mode in aqueous solution of Bi, Sb, and Cd with Pd+Mg modifier

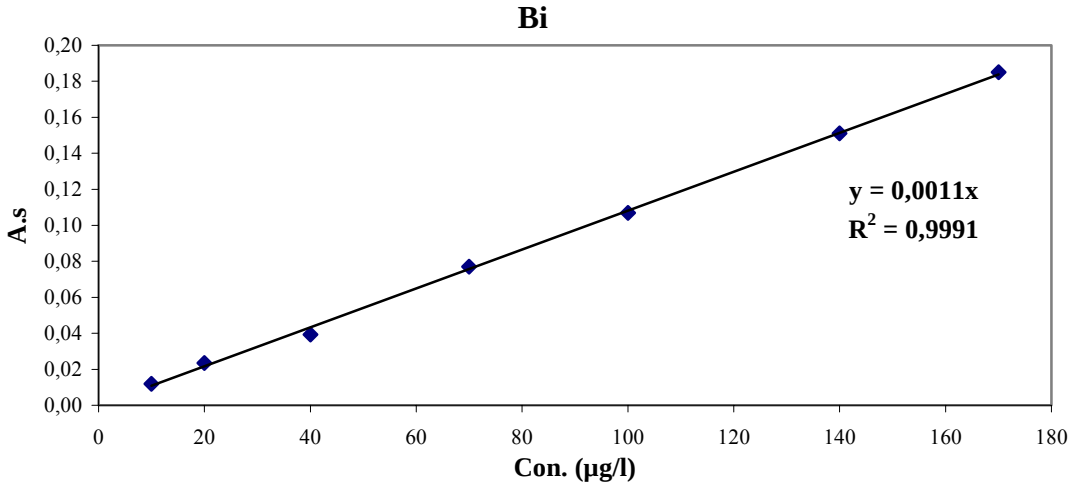

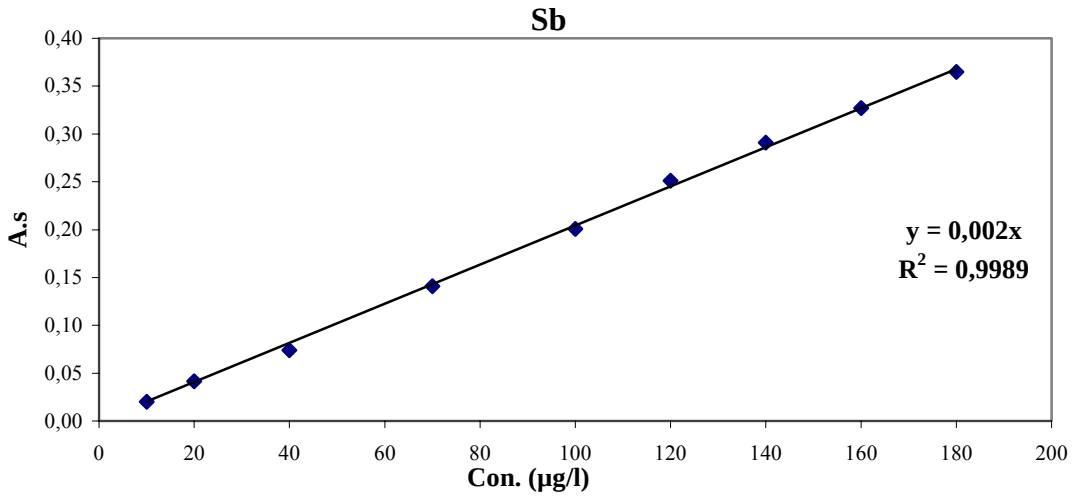

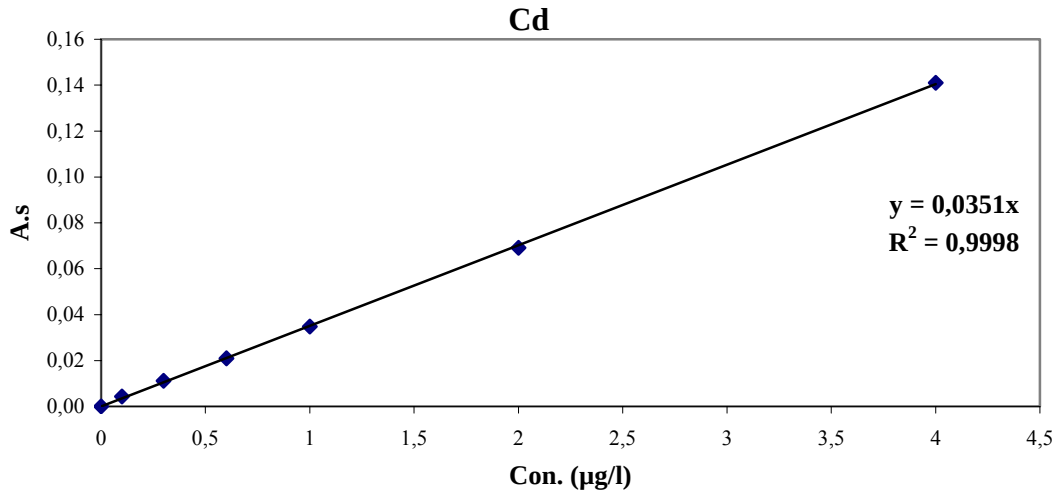

Table 5.7 Comparing the single-element mode with the multi-element mode of Bi, Sb, and Cd using Pd+Mg modifier (pyrolysis=700°C, atomization=1900°C)

Element	Pyrolysis (Single) (°C)	Atomization (Single) (°C)	LOD (ppb)		Characteristic mass (pg)	
			Single	Multi	Single	Multi
Bi	1100	1800	0.46	0.82	67.7	80
Cd	700	1500	0.007	0.0085	2.1	2.5
Sb	1300	1900	0.29	0.75	41.9	44

5.4.5.2 With Ir Permanent Modifier

The thermal behaviour of the elements was evaluated using pyrolysis and atomization curves of 100 ppb Bi, 100 ppb Sb, and 2 ppb Cd obtained in the presence of 500µg iridium which is thermally deposited on the graphite tube platform. The pyrolysis and atomization curves obtained for each element are presented in Figure 5.17. A pyrolysis of 700°C and an atomization of 2100°C were chosen as the optimum for the simultaneous determination of

these elements. The optimum temperature program for the simultaneous determination of Bi, Sb, and Cd with Ir permanent modifier in 0.2% HNO_3 is shown in Table 4.3. The cleanout temperature was 2400°C and the hold time 3s. This temperature program was used to evaluate the characteristic mass and detection limits for these elements. The calibration curves are shown in Figure 5.18. The values of characteristic mass and detection limits in the multi-element mode compared with single-element mode are presented in Table 5.8. The higher detection limits values of Sb (about 1.5 times) and Bi (about 2 times) can be explained as a result of decreased Sb lamp intensity in the case of multi-operating mode. This effect can be understood by comparing the two absorbance peaks. For Cd, the detection limits value was similar with that of single-element mode. The characteristic mass values were comparable with those of single-element mode. The use of Ir as a modifier increases the stabilization of the elements that at high atomization temperatures there are no such change in the characteristic mass values.

Figure 5.17 Pyrolysis and atomization curves for multi-element mode in aqueous solution of Bi, Sb, and Cd using Ir modifier

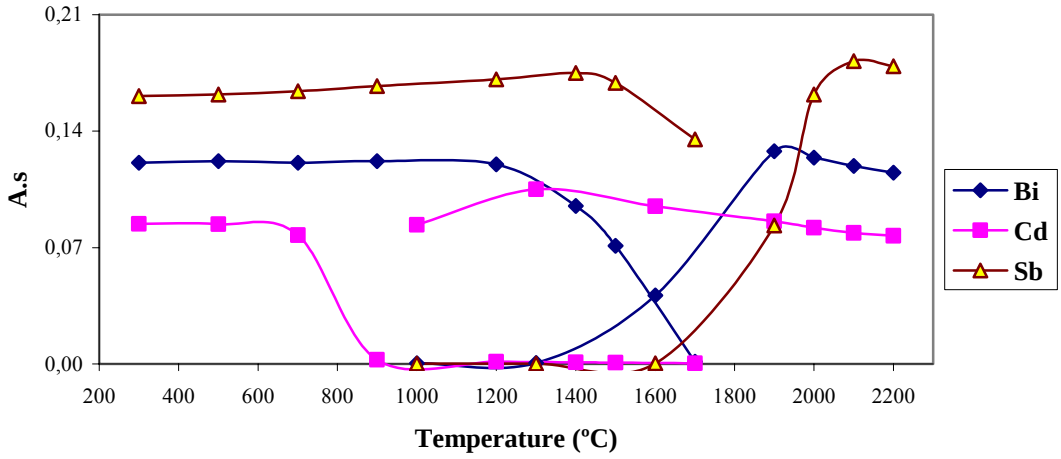

Figure 5.18 Calibration curves of the multi-element mode in aqueous solution of Bi, Sb, and Cd with Ir modifier

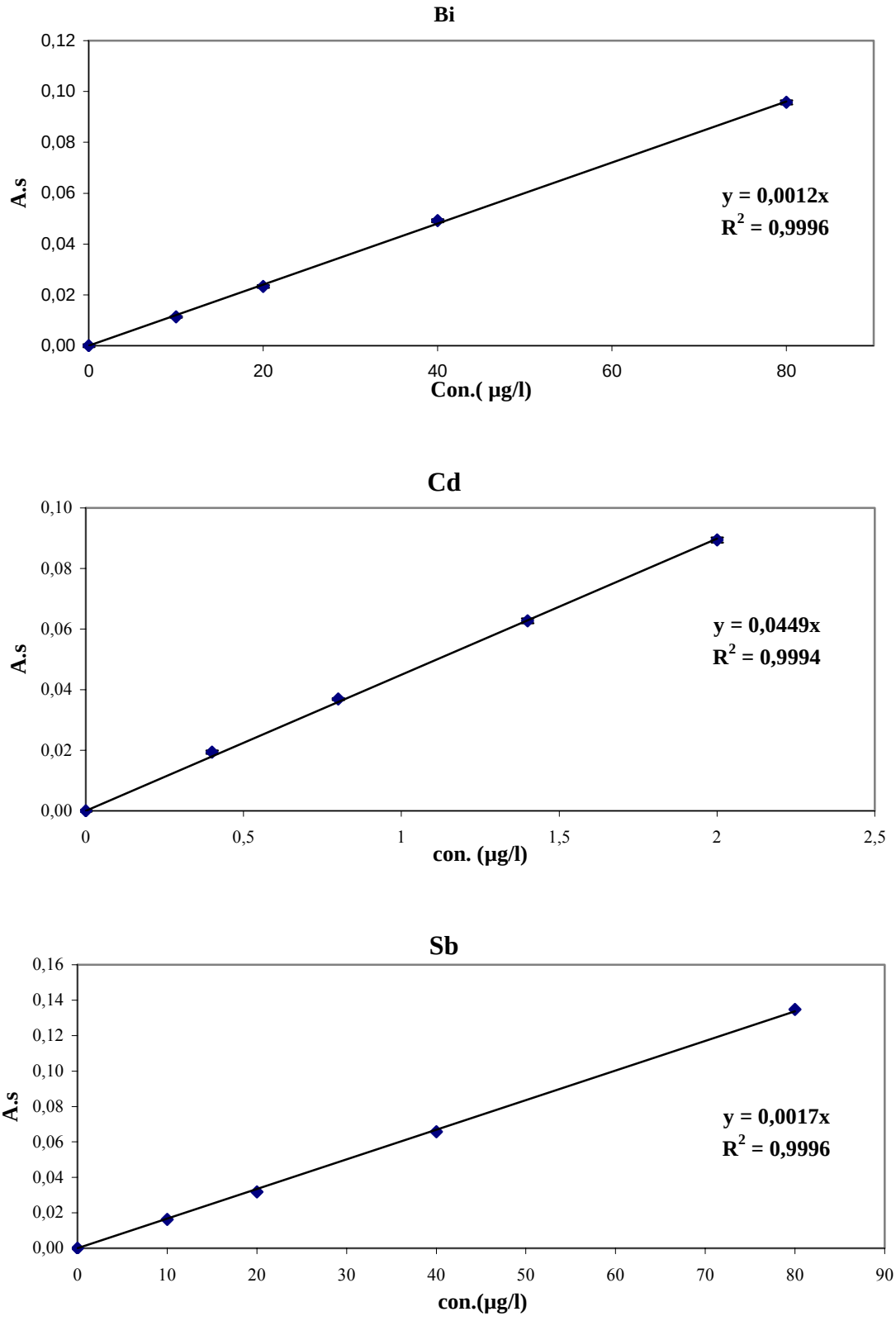

Table 5.8 Comparing the single-element mode with the multi-element determination of Bi, Sb, and Cd using Ir modifier (pyrolysis=700°C, atomization=2100°C)

Element	Pyrolysis (Single) (°C)	Atomization (Single) (°C)	LOD (ppb)		Characteristic mass (pg)	
			Single	Multi	Single	Multi
Bi	1200	1900	0.50	1.00	73.3	73.3
Cd	700	1500	0.0058	0.0067	1.7	1.96
Sb	1500	2100	0.63	1.06	46.3	51.8

5.5 Multi-Element Determinations with 4-Operating Mode

In the previous section, the multi-element mode using 2-operating mode has been studied. In this section we are going to study 4-operating mode to see whether the sensitivity of the determination will be affected or not. In 4-operating mode, four elements can be used but simultaneously only six elements could be determined. The advantage of 4-operating mode is that we can determine more element (up to six) comparing to 2-operating mode. But this will cause the sensitivity of the determination in terms of detection limits or/and characteristic mass to be affected. We are going to increase the number the elements in some previous groups but without changing the other conditions like pyrolysis and atomization temperatures.

5.5.1 Multi-Element determination of Al, Be, Cr, and V

As we have mentioned before, in section 5.3.2, the multi-element determination of this group of elements have been carried out using end-capped tubes and in the presence of 5 µg $Mg(NO_3)_2$ as a modifier. These elements have approximately the same thermal stabilization in the presence of this modifier; therefore, we have decided to determine them simultaneously. From the pyrolysis curves, Figure 5.19, the best pyrolysis and atomization temperatures for the multi-element determinations are 1500 and 2500°C, simultaneously. Generally, atomization temperature more than 2600°C can not be used with SIMAA 6000 and with that temperature the lifetime of the tube will be decreased, for that reason we have decided to choose 2500°C as the optimum atomization temperature for the simultaneous determination of this group. The pyrolysis and atomization curves were made using the following concentrations: 30 ppb Al, 4 ppb Be, 10 ppb Cr, and 100 ppb V in 0.2% HNO_3. The optimum temperature program for the multi-element determination is shown in Table 4.3 except the hold time for cleanout step was 4s and cleanout temperature 2550°C. Higher clean-out temperature (2550°C) and more time (4s) have been used because of the memory effects problems which have been observed for these elements especially Cr and V. The

compromised temperature program has been used to determine the characteristic masses and detection limits for theses elements in the multi-element mode and these are compared with the single-element mode values. The results are shown in Table 5.9. The detection limits and values in multi-element mode are higher than those of single-element mode which can be attributed to the compromised conditions used and the operating mode (4-mode lamp). For V, the main reason will be the operating mode because the atomization temperature is same as in single-element mode. For the other elements; Al, Be, Cr, the higher atomization temperature and 4-operating mode that have been used caused the higher values. The characteristic mass values were similar to those of the single-element mode especially for Cr and Be. The calibration curves which have been used to determine the characteristic masses and detection limits are shown in Figure 5.20.

Figure 5.19 Pyrolysis and atomization curves for multi-element mode in aqueous solutions of Al, Be, Cr, and V using $Mg(NO_3)_2$ as a modifier

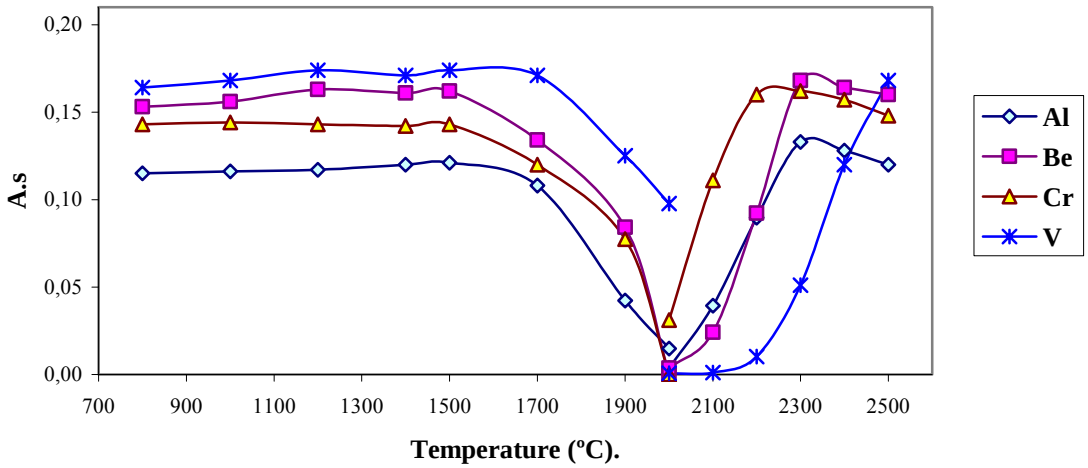

Table 5.9 Comparing the single-element mode with the multi-element mode of Al, Be, Cr, and V (pyrolysis=1500°C, atomization=2500°C)

Element	Pyrolysis (Single) (°C)	Atomization (Single) (°C)	LOD (ppb)		Characteristic mass (pg)	
			Single	Multi	Single	Multi
Al	1700	2300	0.18	0.62	25.9	30.4
Be	1600	2300	0.013	0.021	1.9	2.0
Cr	1500	2300	0.032	0.081	4.7	4.7
V	1700	2500	0.47	0.83	46.3	48.9

Figure 5.20 Calibration curves of the multi-element mode in aqueous solution of Al, Be, Cr, and V with Mg modifier

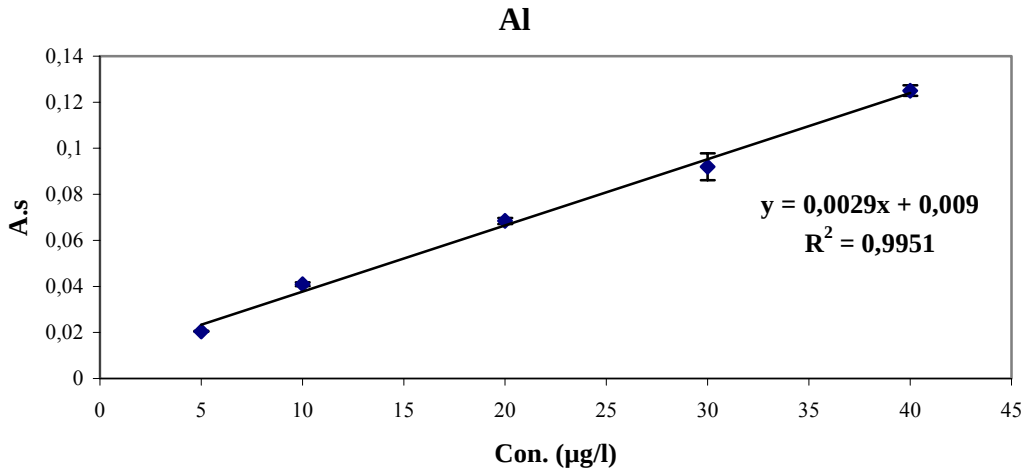

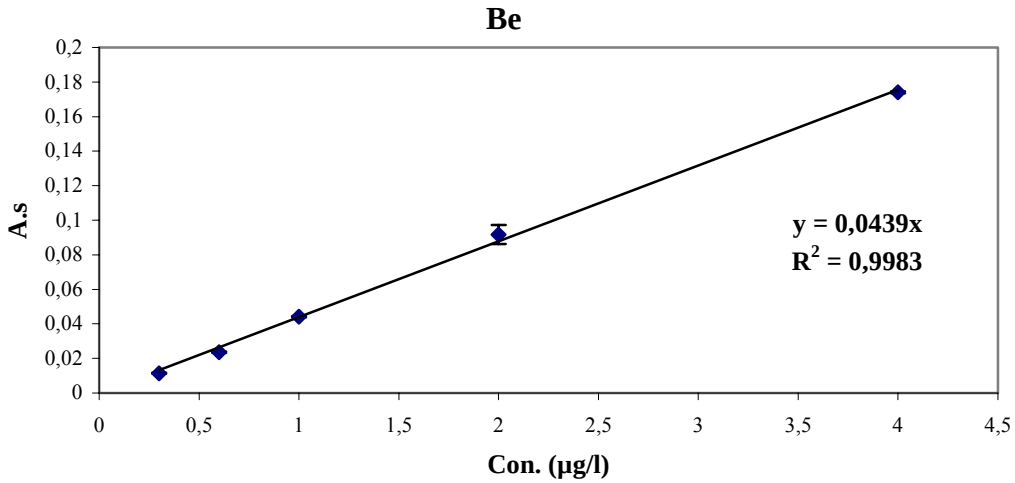

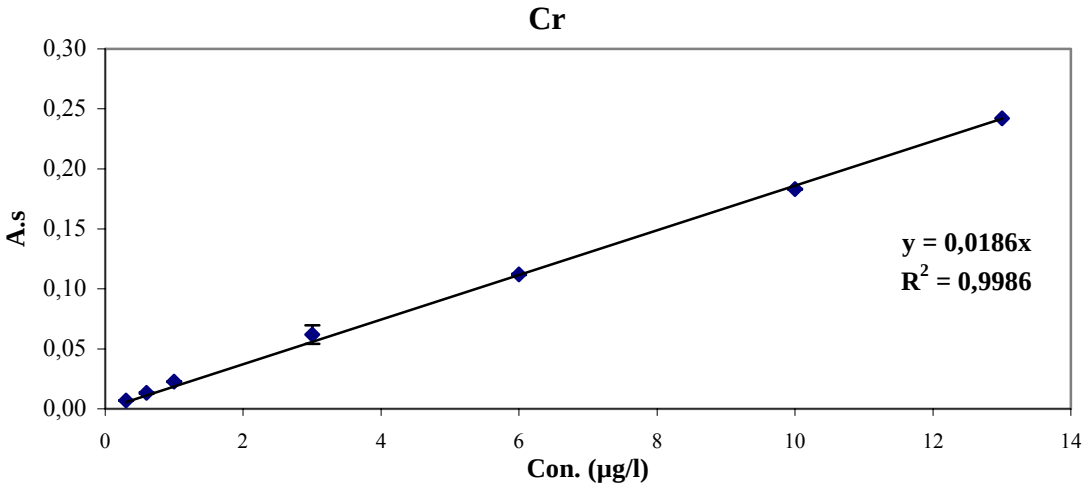

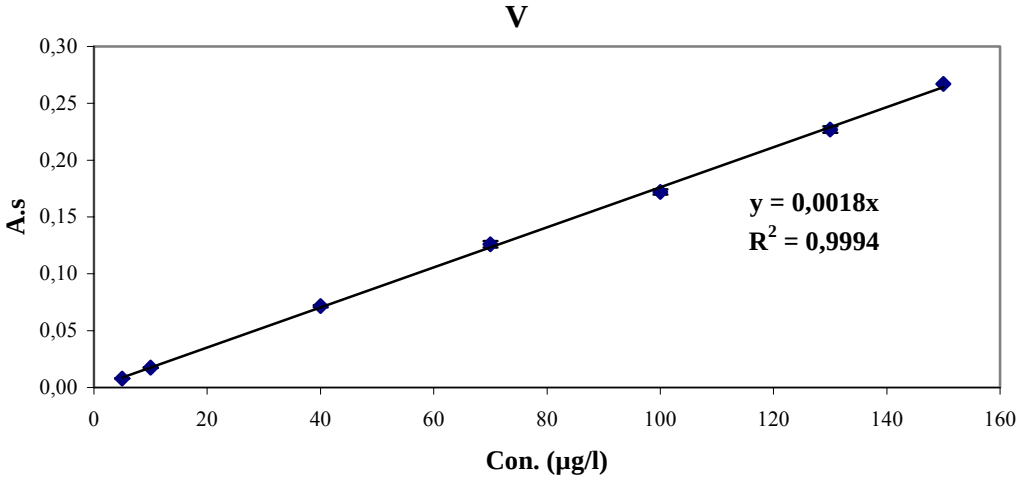

5.5.2 Multi-Element Determination of Be, Cr, Cu, and Mn

The dependence of Be, Cr, Cu, and Mn absorbance on the pyrolysis and atomization temperatures was not studied because we have used the same conditions as the multi-element determination of Be, Cr, and Cu (1200 and 2300^{o} as an optimum pyrolysis and atomization temperatures, respectively). The solutions were prepared in 0.2% HNO_3 in the presence of 5µg Pd and 3µg Mg as a modifier. This optimized temperature program has been used to determine the characteristic masses and detection limits for these elements in the multi-element mode. These values are compared with those in the single-element mode and shown in Table 5.10. The calibration curves are shown in Figure 5.21. The increasing in the detection limits values is higher comparing with 2-operating mode. By comparing the values with those of single-element mode, the values were higher by 3.5 and 2.5 times for Cu and (Be, Cr, and Mn). The values of the characteristic mass were also higher comparing with those of 2-operating mode. The increasing in characteristic mass values comparing with single-element mode was by 32%, 23%, 18%, and 30% for Be, Cr, Cu, and Mn, respectively. The decreasing in lamps intensity can cause the increase in detection limits and characteristic values. In the case of Cu and Mn, there is another effect, which is the atomization temperature.

Table 5.10 Comparing the single-element mode with the multi-element determination of Be, Cr, Cu, and Mn using Pd+Mg modifier (pyrolysis=1200°C, atomization=2300°C)

Element	Pyrolysis (Single) (°C)	Atomization (Single) (°C)	LOD (ppb)		Characteristic mass (pg)	
			Single	Multi	Single	Multi
Be	1600	2300	0.026	0.066	3.9	4.9
Cr	1500	2300	0.049	0.121	7.2	8.9
Cu	1200	2000	0.130	0.474	19.6	23.2
Mn	1400	2000	0.051	0.133	5.0	6.5

Figure 5.21 Calibration curves of the multi-element mode in aqueous solution of Be, Cr, Cu, and Mn with Pd+Mg modifier

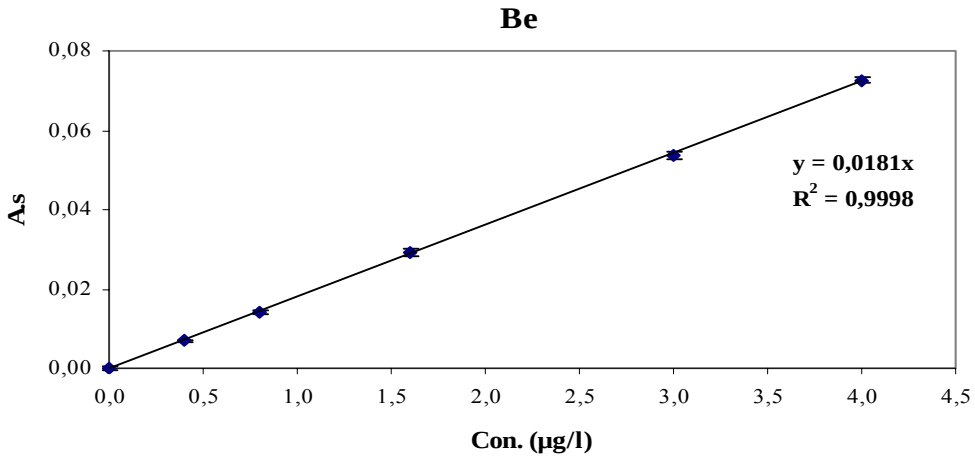

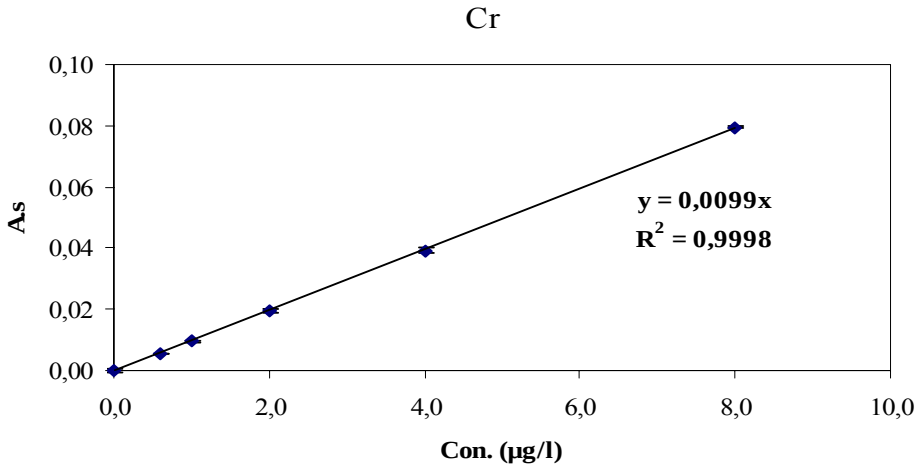

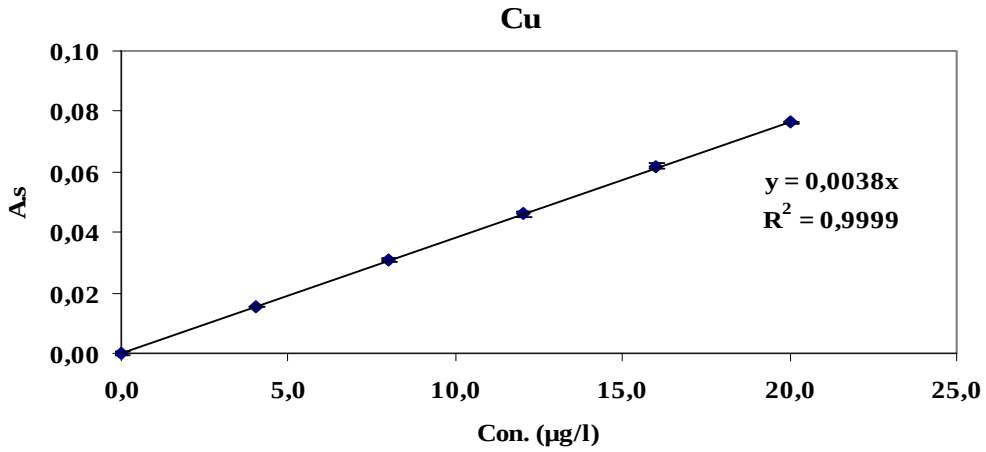

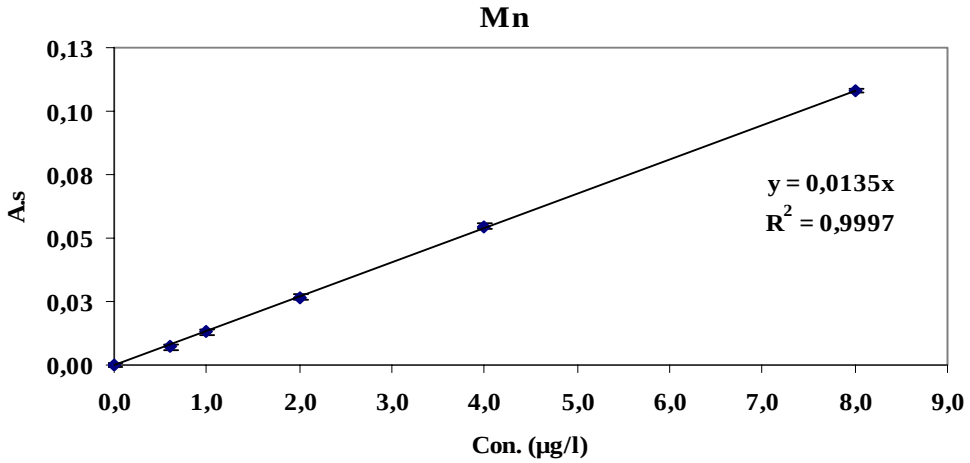

5.5.3 Multi-Element Determination of Bi, Sb, Cu, Mn, and Se

The dependence of Bi, Sb, Cu, Mn, and Se absorbance on the pyrolysis and atomization temperatures was not studied because we have used the same conditions as the multi-element determination of Bi, Sb, Mn, Se, and Cu (1100 and 2000^{o} as an optimum pyrolysis and atomization temperatures, respectively). The solutions were prepared in 0.2% HNO_3 in the presence of 5µg Pd and 3µg Mg as a modifier. This optimized temperature program has been used to determine the characteristic masses and detection limits for these elements in the multi-element mode. These values are compared with those in the single-element mode and shown in Table 5.11. The calibration curves are shown in Figure 5.22. From the values of detection limits, there were high increases comparing with single-element mode. The increases were in the range from about 4 times (Bi) to 12 times (for Mn) which are higher than those of 2-operating mode. However, the increasing in the characteristic mass values was not as in detection limits. By comparing with single-element values, the increasing in

characteristic mass values was by 18%, 5%, 32%, 11%, and 25% for Bi, Cu, Mn, Sb, and Se, respectively.

Table 5.11 Comparing the single-element mode with the multi-element determination of Bi, Cu, Mn, Sb, and Se using Pd+Mg modifier (pyrolysis=1100°C, atomization=2000°C)

Element	Pyrolysis (Single) (°C)	Atomization (Single) (°C)	LOD (ppb)		Characteristic mass (pg)	
			Single	Multi	Single	Multi
Bi	1100	1800	0.46	1.91	67.7	80.0
Cu	1200	2000	0.13	0.56	19.6	20.5
Mn	1400	2000	0.051	0.61	5.0	6.6
Sb	1300	1900	0.29	1.30	41.9	46.3
Se	1200	1900	0.40	1.75	58.7	73.3

Figure 5.22 Calibration curves of the multi-element mode in aqueous solution of Bi, Cu, Mn, Sb, and Se with Pd+Mg modifier

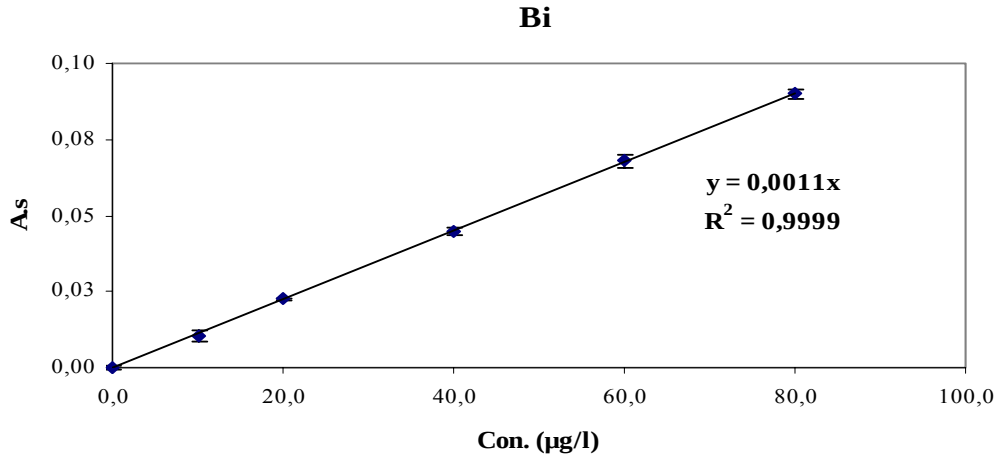

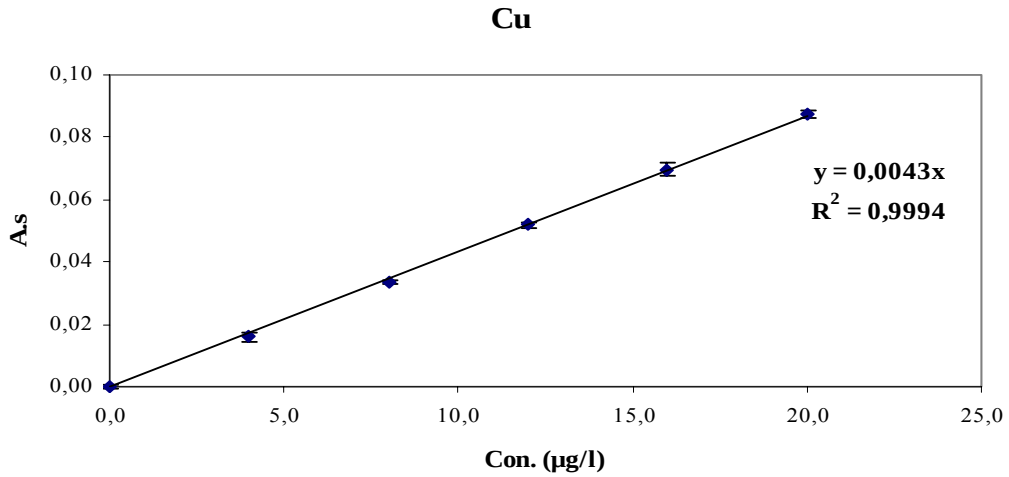

Mn

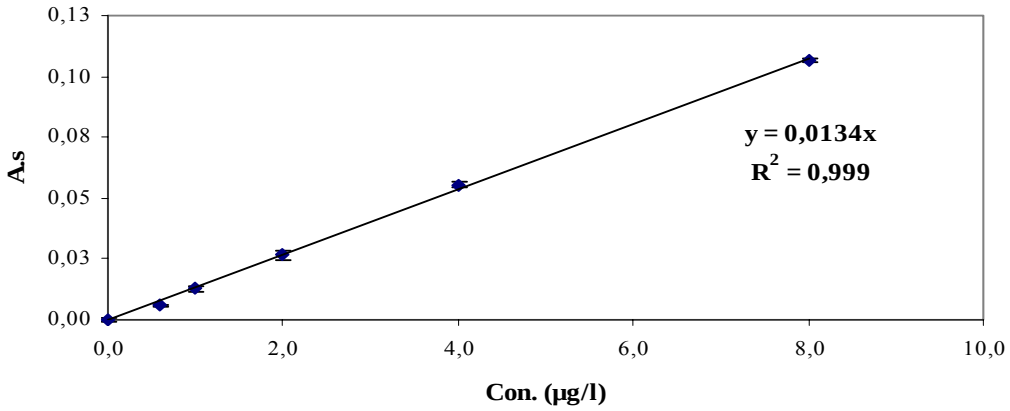
0,13
0,10
0,08
0,05
0,03
0,00
A.s
y = 0,0134x
R2 = 0,999
0,0
2,0
4,0
6,0
8,0
10,0
Con. (µg/l)

Sb

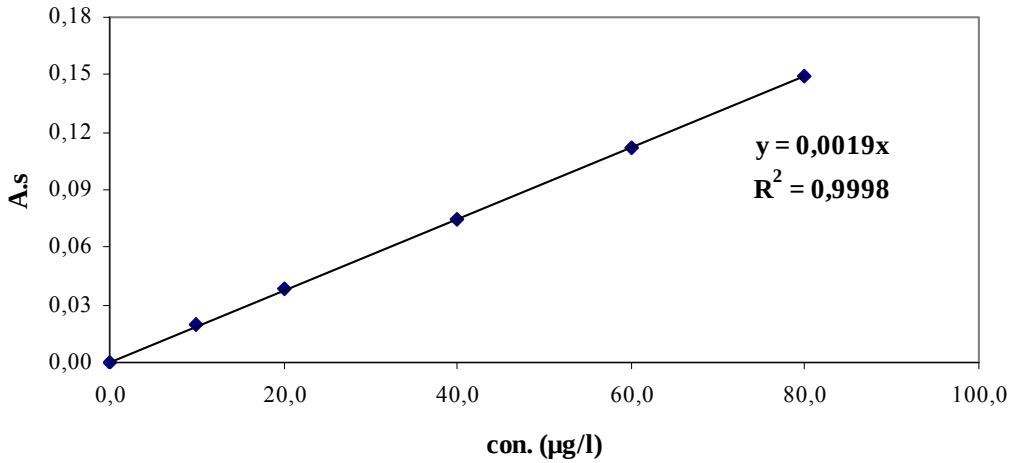
0,18
0,15
0,12
0,09
0,06
0,03
0,00
A.s
y = 0,0019x
R2 = 0,9998
0,0
20,0
40,0
60,0
80,0
100,0
con. (µg/l)

Se

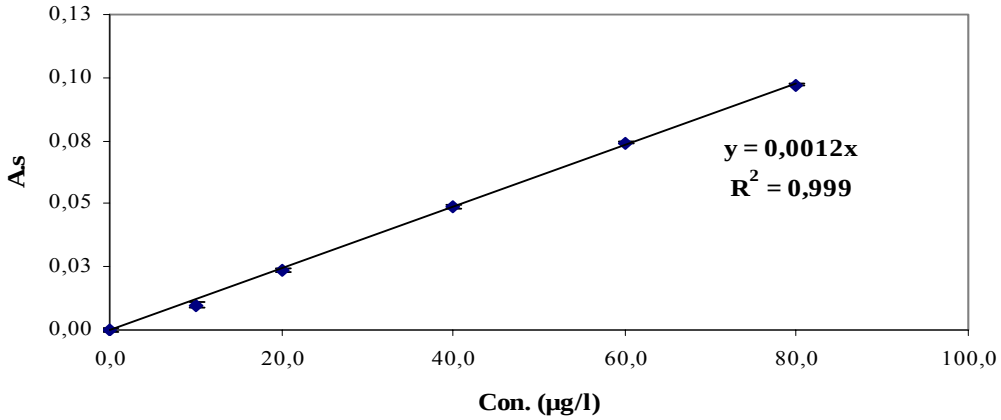
0,13
0,10
0,08
0,05
0,03
0,00
A.s
y = 0,0012x
R2 = 0,999
0,0
20,0
40,0
60,0
80,0
100,0
Con. (µg/l)

5.5.4 Multi-Element Determination of Bi, Pb, Sb, and Se

The dependence of Bi, Sb, Pb, and Se absorbance on the pyrolysis and atomization temperatures was not studied because we have used the same conditions as the multi-element determination of Pb and Se (1000 and 1900^{o} as an optimum pyrolysis and atomization temperatures, respectively). The solutions were prepared in 0.2% HNO_3 in the presence of 5µg Pd and 3µg Mg as a modifier. This optimized temperature program has been used to determine the characteristic masses and detection limits for these elements in the multi-element mode. These values are compared with those in the single-element mode and shown in Table 5.12. The calibration curves are shown in Figure 5.23. The values of detection limits are obviously higher than those of single-element mode. The increasing of detection limits values is in the range between 3-4 times which is a result of decreasing the lamp intensities. This effect can be seen by comparing the absorbance peaks. However, the characteristic values are comparable with those of single-element values, except Pb, and they were in the range 5-90%. For Pb, the sensitivity has been too affected by using the multi-element mode (0.0019→0.0016→0.0010). This is an indication of the effect of operating mode not only on detection limits but also on characteristic mass.

Table 5.12 Comparing the single-element mode with the multi-element determination of Bi, Pb, Sb, and Se using Pd+Mg modifier (pyrolysis=1000^{o}C, atomization=1900^{o}C)

Element	Pyrolysis (Single) (^{o}C)	Atomization (Single) (^{o}C)	LOD (ppb)		Characteristic mass (pg)	
			Single	Multi	Single	Multi
Bi	1100	1800	0.46	1.50	67.7	73.3
Pb	1000	1900	0.32	0.90	46.3	88.0
Sb	1300	1900	0.29	1.20	41.9	44.0
Se	1200	1900	0.40	1.38	58.7	67.7

Figure 5.23 Calibration curves of the multi-element mode in aqueous solution of Bi, Cu, Mn, Sb, and Se with Pd+Mg modifier

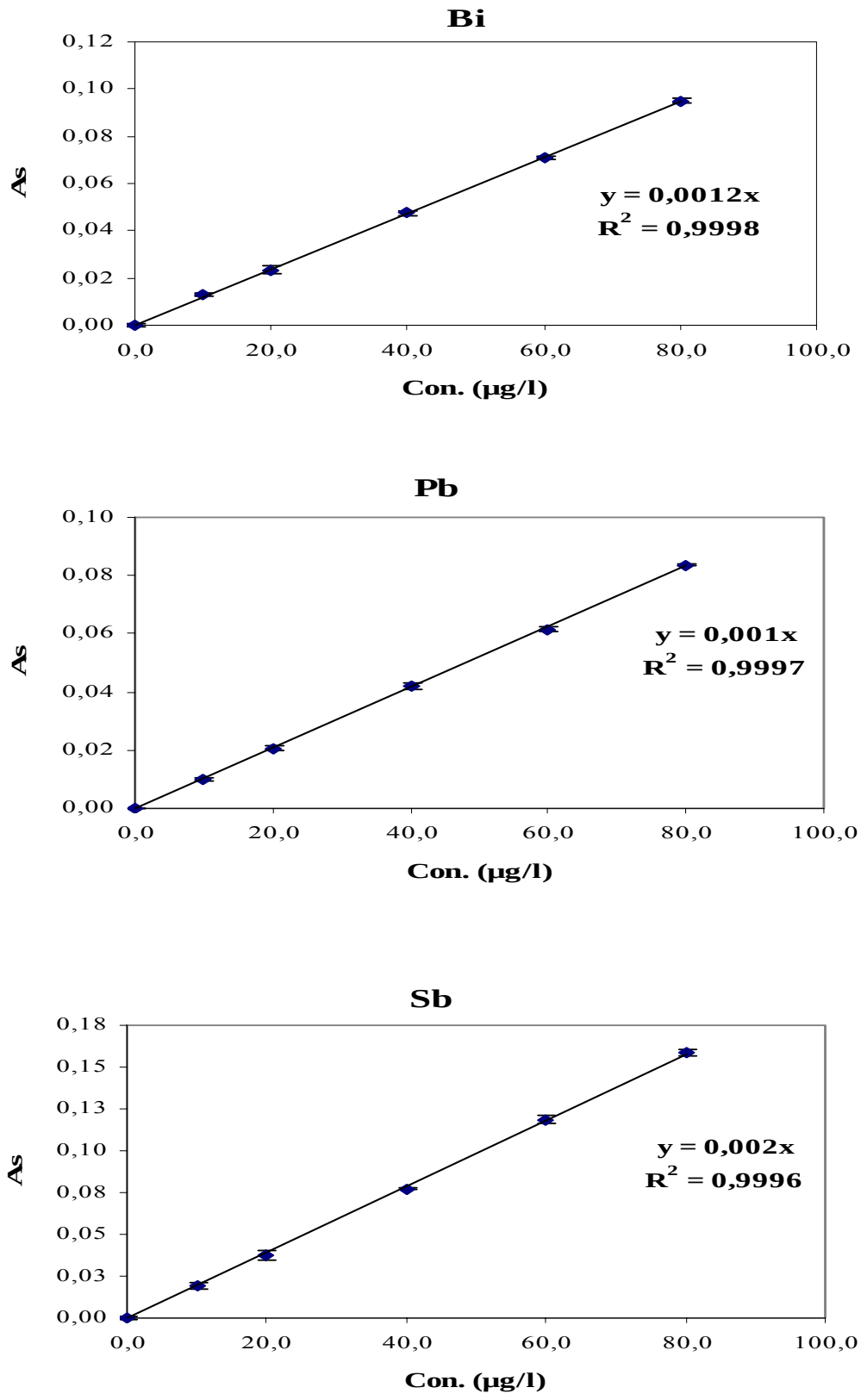

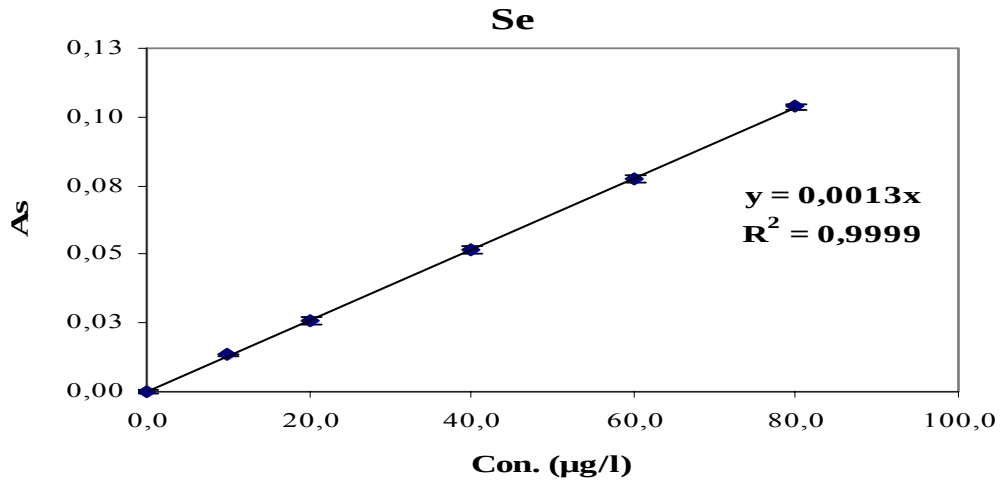

5.6 The Effect of the Operating mode and the Use of Modifier on Absorption Signals and Sensitivity

In this section, the effects of the operating mode and the modifiers on the absorption signal and sensitivity have been studied. The absorption signals for each element have been compared for different situations in terms of appearing time, peak height, and band width. The sensitivity values have been also compared.

5.6.1 Aluminium (Al)

The absorption signals of Al in different modes and with and without modifier are shown in Figure 5.24.

Figure 5.24 Absorption signals of aluminium

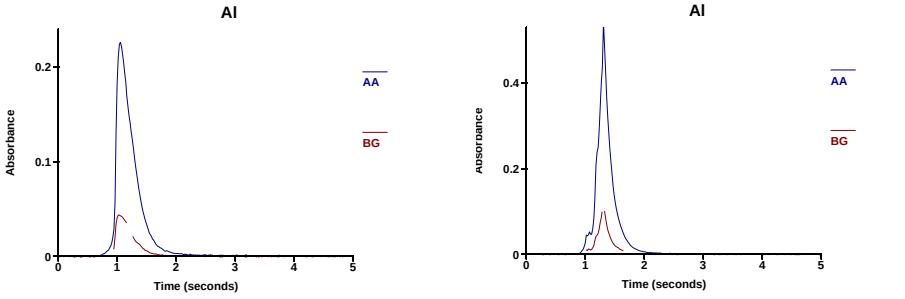

a. Single-element, without modifier, 1500°C, 2300°C

b. Single-element, with Mg, 1700°C, 2300°C, slope=0.0034

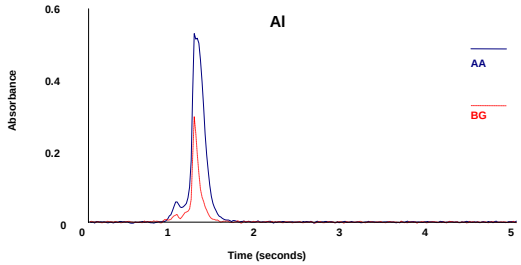

c. Multi-element (4), with Mg, 1500°C, 2500°C, slope=0.0029

As be seen, the absorption signals are different depending on experimental conditions. By comparing a (single, without modifier) with b (single, with Mg modifier), the signal becomes sharper (smaller bandwidth) which indicates the ease of Al atoms atomization in presence of Mg modifier. The modifier may prevent the formation of refractory compounds (e.g. carbides). The peak height also increases (from about 0.22 to about 0.5).

By comparing b with c (multi, in presence of Be, Cr, and V), however, the slight increase in peak height of multi-element determination (to about 0.60) comparing to that of single-element (about 0.50) is due to higher atomization temperature (2500^{o}C) which needed in the multi-element mode. The higher atomization causes analyte atoms to be faster atomized. The sensitivity decreases with increasing the number of elements to be determined in the multi-element determination [0.0034(1-element) → 0.0029(4-element)].

5.6.2 Beryllium (Be)

The absorption signals of Be in different modes and with and without modifier are shown in Figure 5.25.

Figure 5.25 Absorption signals of beryllium

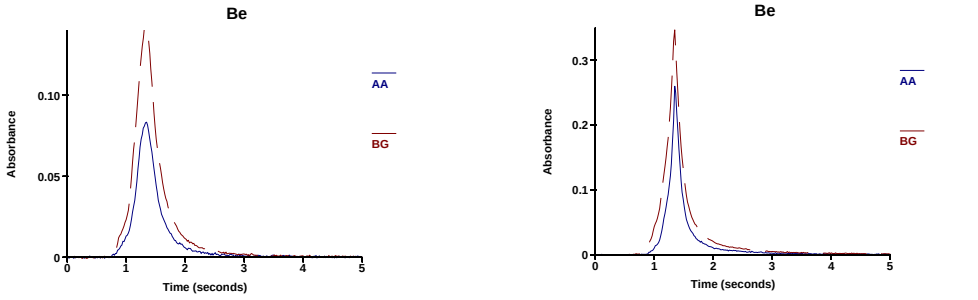

a. Single-element, without modifier, 1000°C, 2300°C

b. Single-element, with Mg, 1600°C, 2300°C, slope=0.0455

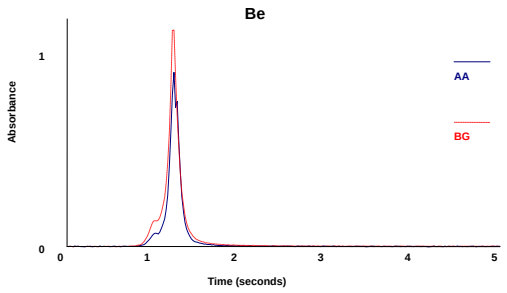

c. Multi-element (4), with Mg, 1500°C, 2500°C, slope=0.0439

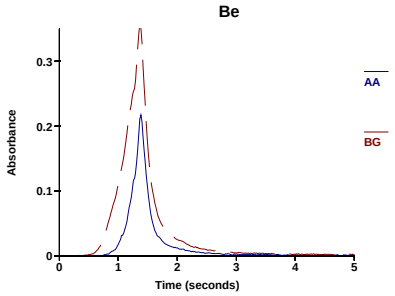

d. Single-element, with Mg+Pd, 1600°C, 2300°C, slope=0.0227

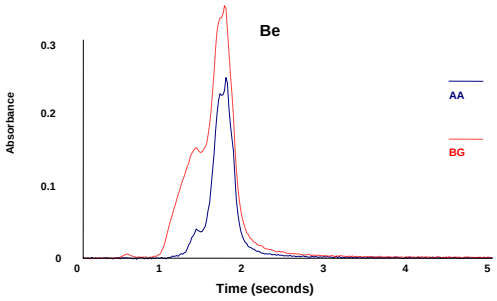

e. Multi-element (3), with Pd+Mg, 1200°C, 2300°C, slope=0.0198

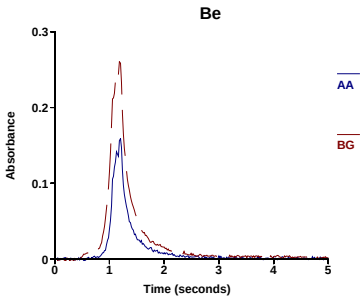

f. Multi-element (4), with Pd+Mg, 1200°C, 2300°C, slope=0.0181

As be seen for figures, the absorption signals depend on the operational conditions. From a (single, without modifier), b (single, with Mg modifier, end-capped tube), and d (single, with Pd+Mg modifier, normal tube), the signal becomes sharper (smaller band width) which indicates the ease of releasing Be atoms (faster atomization). The presence of the modifier may prevent the formation of refractory compounds (e.g. carbides). The peak height increases [from about 0.07 to about 0.3 (with Mg and using end capped tubes) and to about 0.21 (with Pd+Mg)]. However, the sensitivity is higher using the end capped tubes than with normal tubes [0.0455 → 0.0227]. This is due to the diffusional losses of the atomic vapour out of the tube are lowered and consequently the sensitivity improved.

By comparing b with c [multi, Mg modifier, in presence of (Al, Cr, V)], the peak height increases (to about 0.90) because of the use of higher atomization temperature (from 2300°C to 2500°C) which is needed in multi-element determination. With increasing the atomization temperature, the evaporation process increases. The sensitivity also decreases with increasing the number of element to be determined (0.0455 → 0.0439). This is due to the decrease of lamp intensity in multi-element mode.

By comparing d with e (in presence of Cr and Cu) and f (in presence of Cr, Cu, and Mn), however, the peak height slightly decreases with increasing the number of element to be determined. The sensitivity decreases with increasing the number of elements to be determined [0.0227(1) → 0.0198(3) → 0.0181(4)].

5.6.3 Bismuth (Bi)

The absorption signals of Bi in different modes and with and without modifier are shown in Figure 5.26.

Figure 5.26 Absorption signals of bismuth

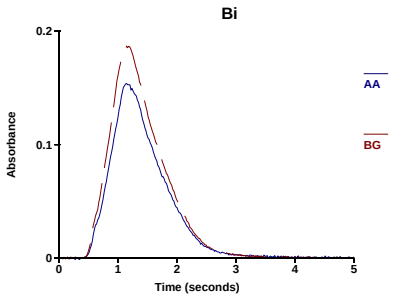

a. Single-element, without modifier, 450°C, 1300°C

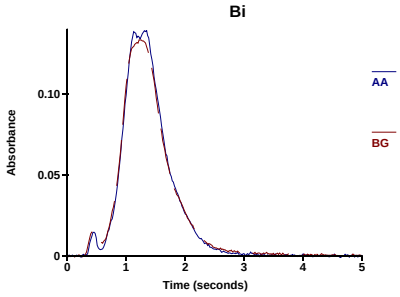

b. Single-element, with Pd+Mg, 1100°C, 1800°C, slope=0.0013

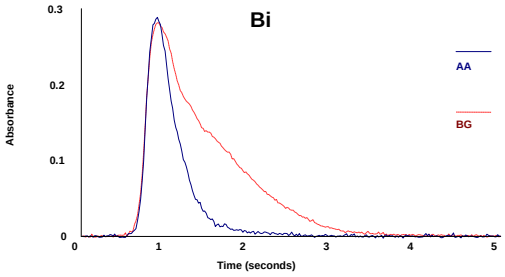

c. Multi-element (4), with Pd+Mg, 1100°C, 2000°C, slope=0.0011

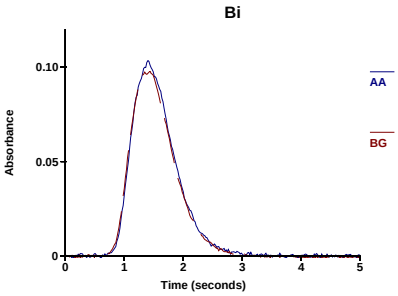

d. Single-element, with Ir, 1200°C, 1900°C, slope=0.0012

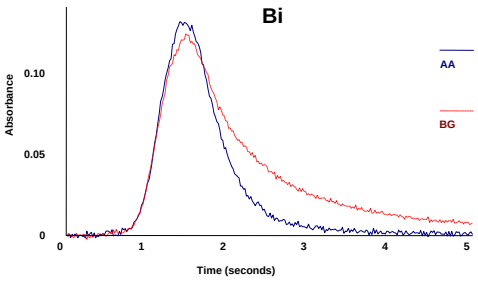

e. Multi-element (3), with Pd+Mg, 700°C, 1900°C, slope=0.0011

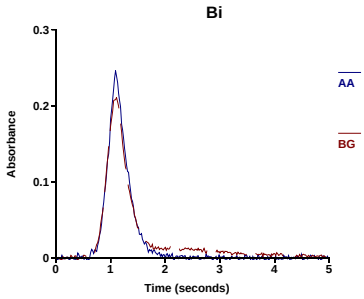

f. Multi-element (5), with Pd+Mg, 1100°C, 2000°C, slope=0.0011

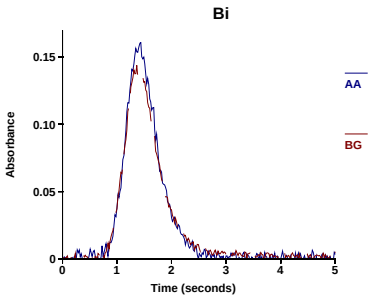

g. Multi-element (4), with Pd+Mg, 1000°C, 1900°C, slope=0.0012

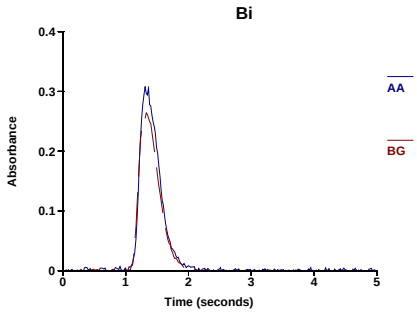

h. Multi-element (3), with Ir, 700°C, 2100°C, slope=0.0012

From the absorption signals a (single, without modifier) with b (single, with Pd+Mg modifier) and d (single, with Ir modifier), the signal becomes slightly sharper (smaller bandwidth) and the appearing time increases also (from 0.5s to 0.9s). This is due formation of stable compounds between Bi atoms and the modifiers. The peak height, however, decreases slightly [from about 0.16 to about 0.1 (Ir modifier)] which causes the sensitivity to decrease [0.0012 with Pd+Mg modifier to 0.0011 with Ir modifier].

By comparing b with c (presence of Cu, Mn, and Sb), e (presence of Cd and Sb), f (presence of Cu, Mn, Sb, and Se), and g (presence of Pb, Sb, and Se), the signal becomes sharper (smaller bandwidth) and the peak height increases with the atomization temperature [e.g. about 0.14 (single, 1800°C) and about 0.30 (multi, 2000°C] which is due to faster atomization of analyte atoms at higher atomization temperatures. However, the peak height decreases with increasing the number of element to be determined which can be related to lamp intensity [about 0.30 (4-element) and about 0.24 (5-element)]. No significant change in sensitivity values with increasing the number of elements to be determined and the atomization temperature (e.g. 0.0011 for 4- and 5-element determination at 2000°C).

By comparing d with h [multi (presence of Cd and Sb), with Ir modifier], the signal becomes sharper (smaller bandwidth) and the peak height increases (0.10 → 0.30) which is due to the increase of atomization temperature (1900°C → 2100°C). However, the sensitivity does not affect.

5.6.4 Cadmium (Cd)

The absorption signals of Cd in different modes and with and without modifier are shown in Figure 5.27.

Figure 5.27 Absorption signals of cadmium

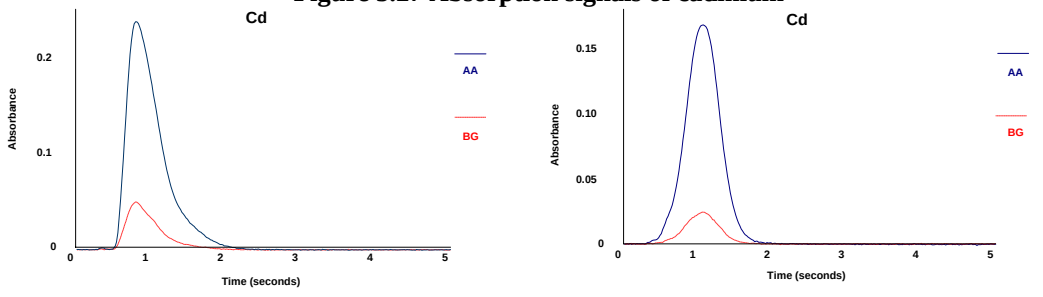

a. Single-element, without modifier, 300°C, 1200°C

b. Single-element, with Pd+Mg, 0.0417, 700°C, 1500°C, slope=0.0417

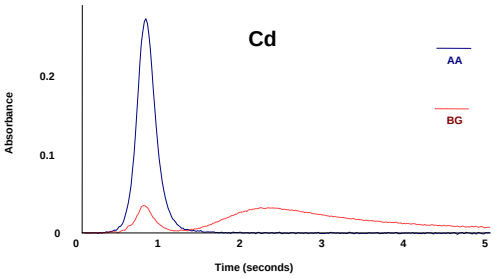

c. Multi-element (3), with Pd+Mg, 700°C, 1900°C, slope=0.0351

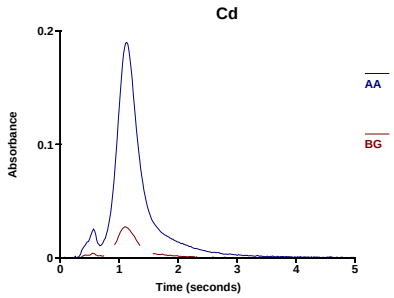

d. Single-element, with Ir, 700°C, 1500°C, slope=0.0513

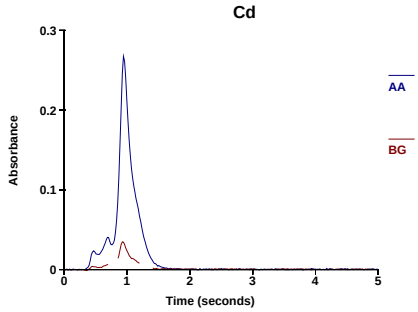

e. Multi-element, with Ir, 700°C, 2100°C, slope=0.0449

As be seen from absorption signals a (single, without modifier) and b (single, with Pd+Mg modifier), the presence of the modifiers does not change the appearance time and the peak width. However, the peak height decreases (from about 0.25 to about 0.17) in presence of the modifiers which leads to lower sensitivities values. This could be to the formation of stable compound with the modifier which needs higher atomization temperature to completely atomize (1200°C → 1500°C). However, by comparing signals a with d (single, with Ir modifier), the signal becomes sharper and the peak height slightly decreases. The sensitivity with Ir modifier is higher than with Pd+Mg modifier (0.0417 → 0.0513) but no stability difference in terms of pyrolysis and atomization temperatures and appearing time. The Cd atoms are more volatilized in presence of Ir modifier than in presence of Pd+Mg modifier.

By comparing the signals b with c [multi (with Sb and Bi), Pd+Mg modifier] and d with e [multi (Sb and Bi), with Ir modifier], the signals become sharper and the peak height increases [0.17 → 0.25 and 0.20 → 0.28] which is due to higher atomization temperature used in multi-element determination [1500°C → 1900°C and 2100°C]. This is due to faster atomization of analyte atoms at higher atomization temperatures. The sensitivity decreases with increases the element to be determined [0.0417 (1) → 0.0351 (3) using Pd+Mg modifier and 0.0513 (1) → 0.0449 (3) using Ir modifier].

5.6.5 Chromium (Cr)

The absorption signals of Cr in different modes and with and without modifier are shown in Figure 5.28.

Figure 5.28 Absorption signals of chromium

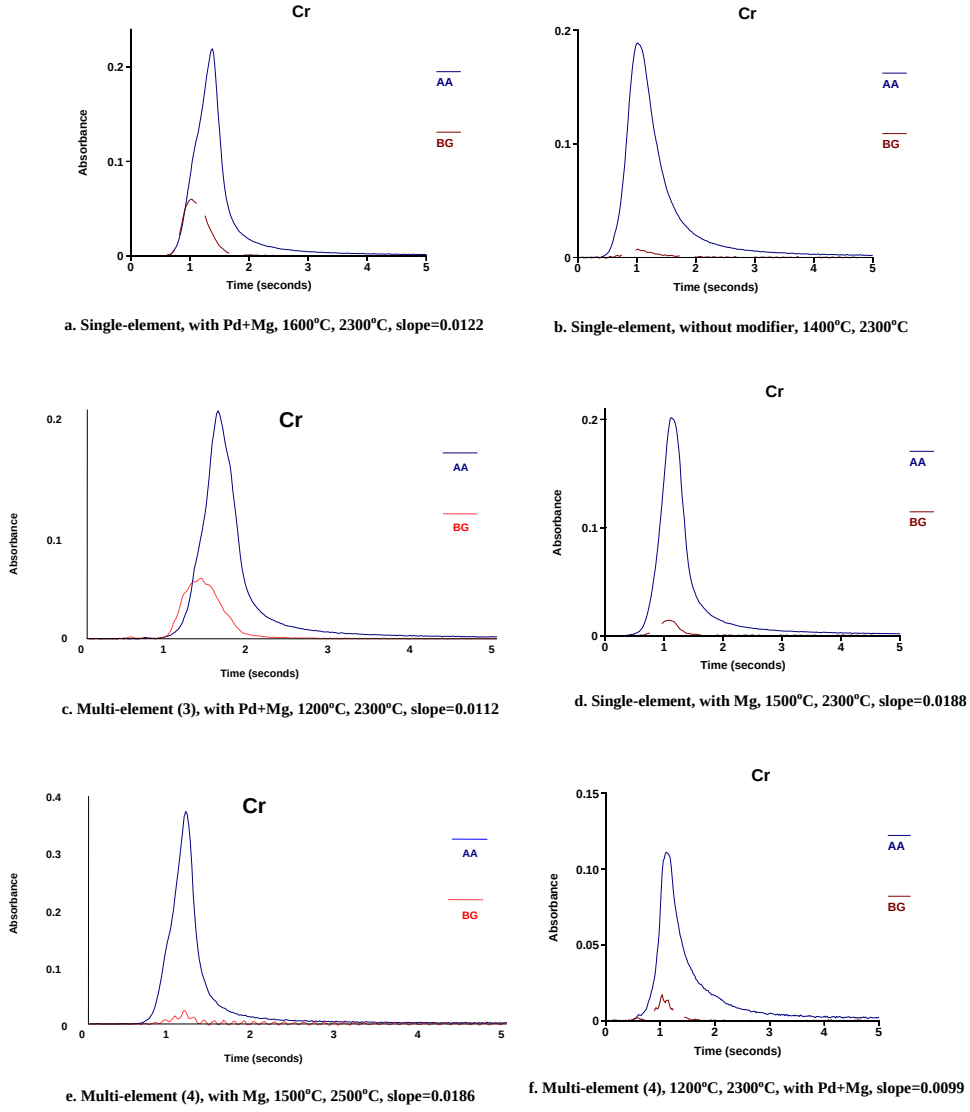

a. Single-element, with Pd+Mg, 1600°C, 2300°C, slope=0.0122

b. Single-element, without modifier, 1400°C, 2300°C

c. Multi-element (3), with Pd+Mg, 1200°C, 2300°C, slope=0.0112

d. Single-element, with Mg, 1500°C, 2300°C, slope=0.0188

e. Multi-element (4), with Mg, 1500°C, 2500°C, slope=0.0186

f. Multi-element (4), 1200°C, 2300°C, with Pd+Mg, slope=0.0099

By comparing the signals b (without modifier) with a (with Pd+Mg modifier) and d (with Mg modifier and end-capped tube), no change in appearing time and peak height [with Pd+Mg is slightly higher (0.22)] can be observed. The peak width, however, is slightly decreased using the modifier. The sensitivity in d (0.0188) is higher than in a (0.0122) which is due to using end-capped tube in d. The use of the modifier increases the atomization process of Cr atoms.

By comparing the signals a with c [multi (presence of Be and Cu)] and f [multi (presence of Be, Cu, and Mn)], the peak height and sensitivity decrease with increasing the number of element to be determined [peak height: 0.22 → 0.12 and sensitivity: 0.0122 → 0.0099] which is due to the decreasing of lamp intensity in multi-element determination.

From the signals d and e [multi (Al, Be, and V)], the peak height is higher in multi-element mode than in single-element mode because higher atomization temperature is used (2300°C → 2500°C). However, the sensitivity decreases with increasing the number of element to be determined [0.0188 (1-element) → 0.0186 (4-element)].

5.6.6 Copper (Cu)

The absorption signals of Cu in different modes and with and without modifier are shown in Figure 5.29.

Figure 5.29 Absorption signals of copper

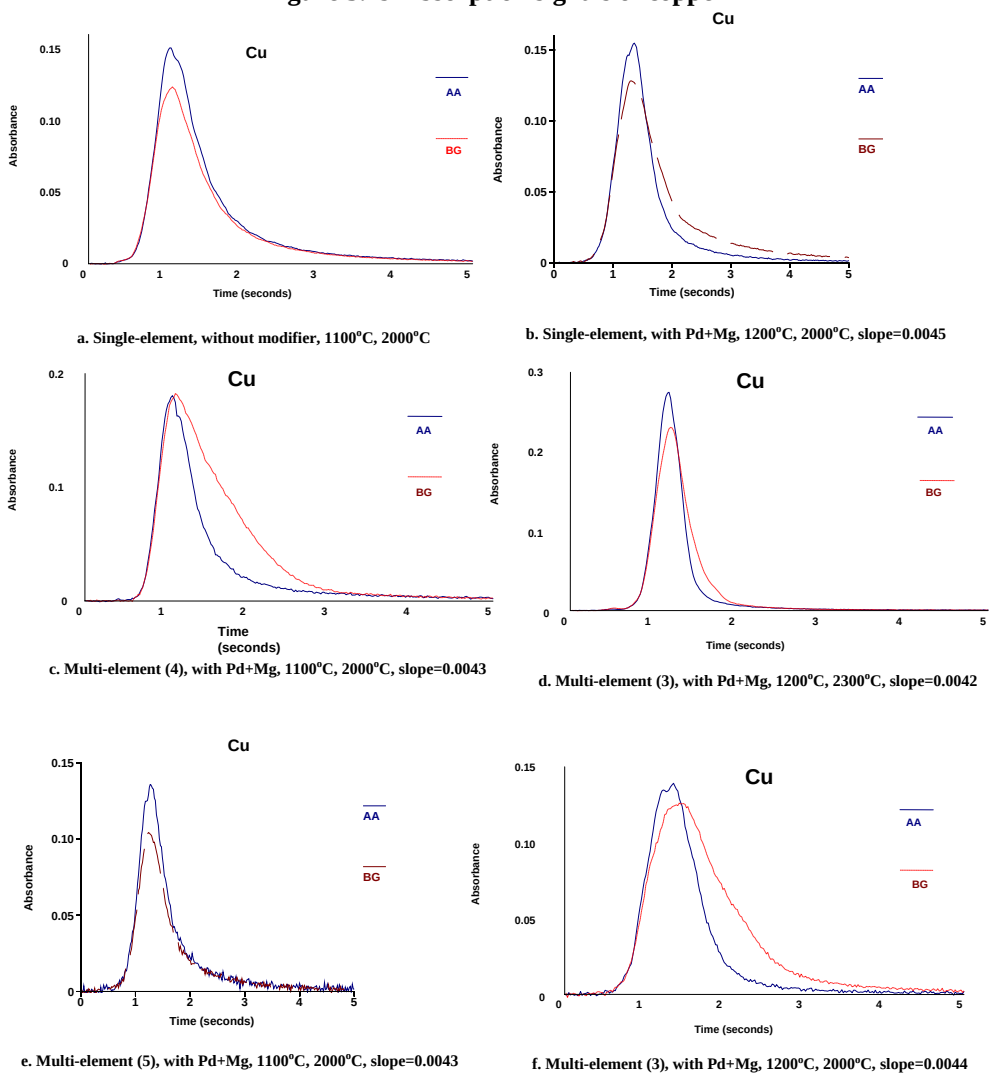

a. Single-element, without modifier, 1100°C, 2000°C

b. Single-element, with Pd+Mg, 1200°C, 2000°C, slope=0.0045

c. Multi-element (4), with Pd+Mg, 1100°C, 2000°C, slope=0.0043

d. Multi-element (3), with Pd+Mg, 1200°C, 2300°C, slope=0.0042

e. Multi-element (5), with Pd+Mg, 1100°C, 2000°C, slope=0.0043

f. Multi-element (3), with Pd+Mg, 1200°C, 2000°C, slope=0.0044

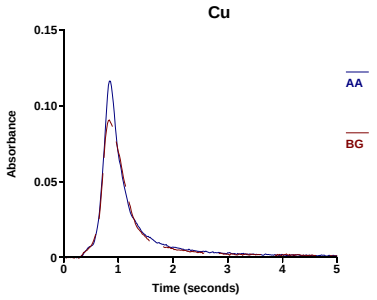

g. Multi-element (4), with Pd+Mg, 1200°C, 2300°C, slope=0.0038

By comparing the absorption signals a (without modifier) and b (with Pd+Mg modifier), slight decrease in peak width and no change in peak height can be seen. This could cause the sensitivity to be decreased. The sharpness of the peak indicates increasing the volatilization process of Cu atoms in presence of the modifier.

By comparing the signal b with the signals c (multi with Bi, Mn, and Sb), d (multi with Be and Cr), e (multi with Bi, Mn, Sb, and Se), f (multi with Mn and Se), and g (Be, Cr, and Mn), the signal becomes sharper (smaller bandwidth) and the peak height increases with increasing the atomization temperature [e.g. about 0.15 (1-element) at 2000°C to about 0.30 (3-element) at 2300°C] which is due to increase atomization process at higher atomization temperature. However, the peak height and the sensitivity decreases with increasing the number of elements to be determined [peak height: 0.30 (3-element) → 0.12 (4-element)], sensitivity: 0.0042 (3-element) → 0.0038 (4-element)] which could be attributed to the decrease in lamp intensity. Slight decrease in sensitivity with increasing the atomization temperature has been observed [e.g. 0.0044 (at 2000°C) → 0.0042 (at 2300°C)].

5.6.7 Manganese (Mn)

The absorption signals of Mn in different modes and with and without modifier are shown in Figure 5.30.

Figure 5.30 Absorption signals of manganese

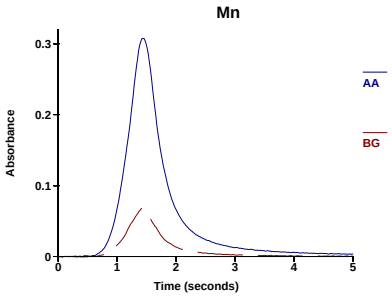

a. Single-element, without modifier, 1200°C, 1600°C

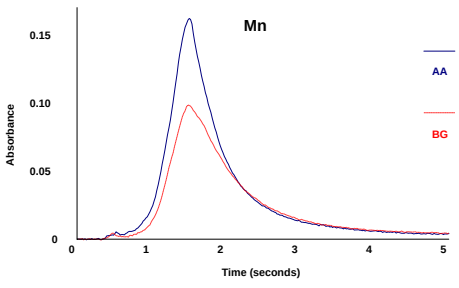

b. Single-element, with Pd+Mg, 1400°C, 2000°C, slope=0.0177

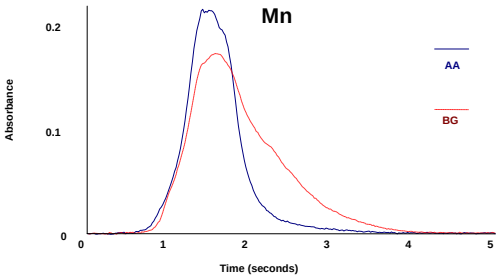

c. Multi-element (3), with Pd+Mg, 1200°C, 2000°C, slope=0.0170

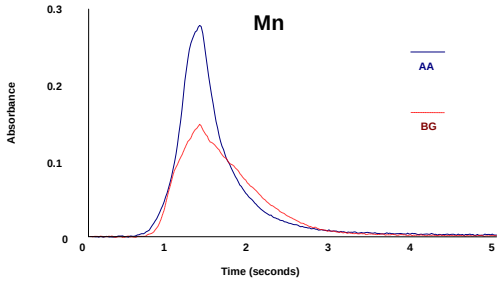

d. Multi-element (4), with Pd+Mg, 1100°C, 2000°C, slope=0.0172

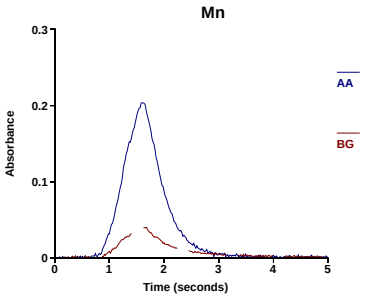

e. Multi-element (5), with Pd+Mg, 1100°C, 2000°C, slope=0.0134

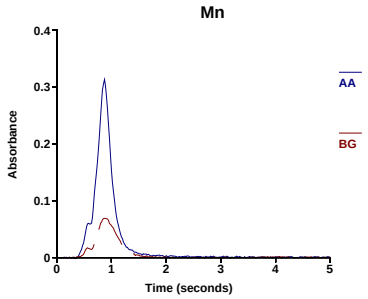

f. Multi-element (4), with Pd+Mg, 1200°C, 2300°C, slope=0.0135

As be seen from the absorption signals, the signals depend on the operational conditions. By comparing the signal a (single without modifier) with b (single with Pd+Mg modifier), the signal becomes broader (larger bandwidth) which indicates the formation of stabilized compound between Mn and the modifier delays the atomization of Mn atoms. The peak height decreases (from about 0.30 to about 0.17) in presence of Pd+Mg modifier which results in decreased sensitivity.

By comparing the signal b with the signals c (multi with Cu and Se), d (Cu, Bi, and Sb), e (Cu, Bi, Sb, and Se), and f (multi with Be, Cr, and Cu), the peak height and sensitivity decrease with increasing the number of element to be determined [peak height: 0.28 (4-element) → 0.20 (5-element), sensitivity: 0.0172 (4-element) → 0.0134 (5-element)] which a result of decrease the lamp intensity. The signal becomes sharper and the peak height increases with increasing the atomization temperature [0.028 (2000°C) → 0.32 (2300°C)]. With increasing atomization temperature, the signal becomes sharper because the fast atomization of atoms at higher atomization temperature. The sensitivity decreases with increasing the atomization temperature [0.0172 (2000°C) → 0.0135 (2300°C)]. There is also an increase in peak height with increasing the pyrolysis temperature [0.17 (1400°C) → 0.21 (1200°C) → 0.28 (1100°C)]. This can be attributed to the decrease of modifier action at lower pyrolysis temperature.

5.6.8 Lead (Pb)

The absorption signals of Pb in different modes and with and without modifier are shown in Figure 5.31.

Figure 5.31 Absorption signals of lead

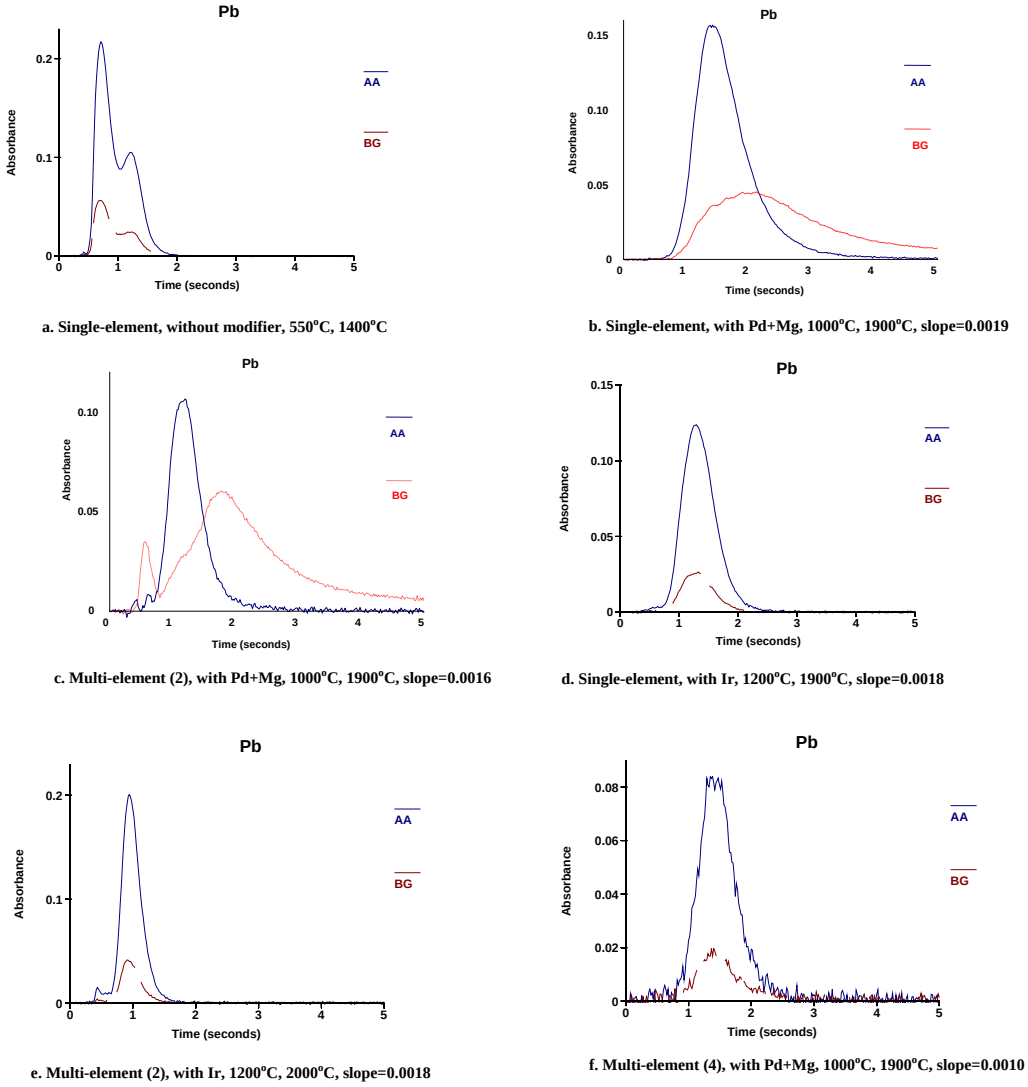

a. Single-element, without modifier, 550°C, 1400°C

b. Single-element, with Pd+Mg, 1000°C, 1900°C, slope=0.0019

c. Multi-element (2), with Pd+Mg, 1000°C, 1900°C, slope=0.0016

d. Single-element, with Ir, 1200°C, 1900°C, slope=0.0018

e. Multi-element (2), with Ir, 1200°C, 2000°C, slope=0.0018

f. Multi-element (4), with Pd+Mg, 1000°C, 1900°C, slope=0.0010

From the absorption signals, it can be seen the effect of the operational conditions. By comparing the signal a (single without modifier) with the signals b (single with Pd+Mg modifier) and d (single with Ir modifier), the signal becomes broader (especially with Pd+Mg modifier) and the appearing time increases [from 0.5s to 1s] which indicates the stabilization effect of the modifier as a result of formation a stabilized compound between Pb atoms and the modifier. The peak height decreases [from about 0.22 to about 0.16 (with Pd+Mg) and to about 0.13 (with Ir)]. In presence of Ir modifier, the signal becomes sharper than with Pd+Mg modifier but the sensitivity becomes slightly lower (0.0018 → 0.0019).

By comparing the signal b with the signals c (multi with Se) and f (multi with Bi, Sb, and Se), the sensitivity and the peak height decrease with increasing the number of elements to be determined [sensitivity: 0.0019 (1-element) → 0.0016 (2-element) → 0.0010 (4-element), peak height: 0.16 (1-element) → 0.12 (2-element) → 0.08 (4-element)]. This can be attributed to decreased lamp intensity in multi-element determination.

By comparing the signal d with the signal e (multi with Se in presence of Ir modifier), the peak height increases (0.13 → 0.20) and the signal becomes sharper (smaller bandwidth) as a result of increasing the atomization temperature. no change in sensitivity value can be seen (0.0018).

5.6.9 Antimony (Sb)

The absorption signals of Sb in different modes and with and without modifier are shown in Figure 5.32.

Figure 5.32 Absorption signals of antimony

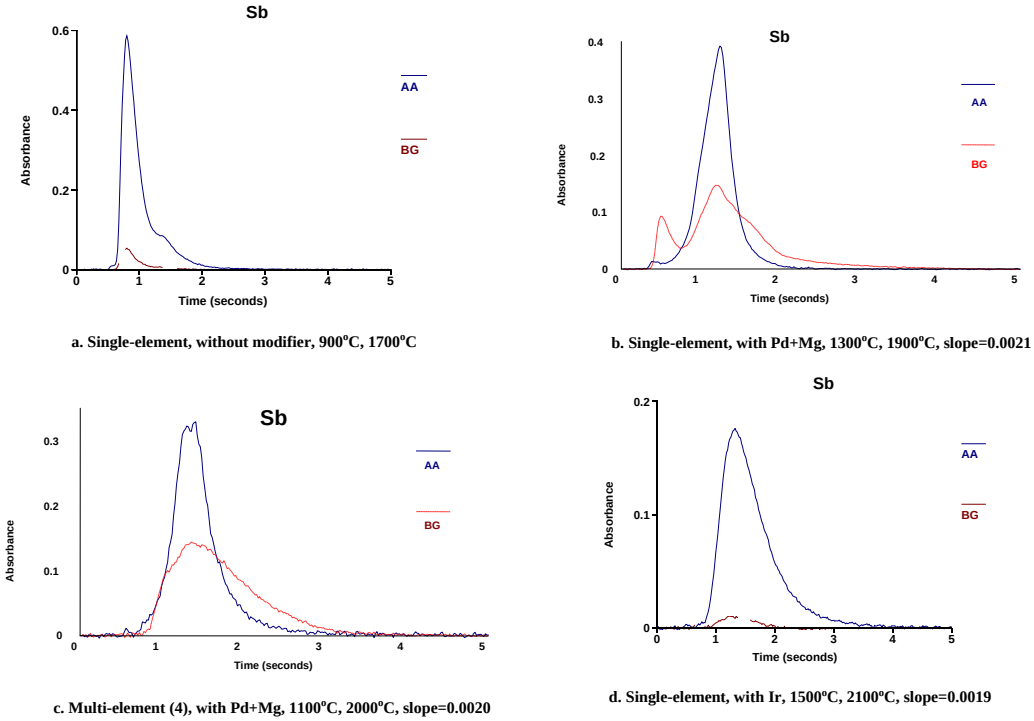

a. Single-element, without modifier, 900°C, 1700°C

b. Single-element, with Pd+Mg, 1300°C, 1900°C, slope=0.0021

c. Multi-element (4), with Pd+Mg, 1100°C, 2000°C, slope=0.0020

d. Single-element, with Ir, 1500°C, 2100°C, slope=0.0019

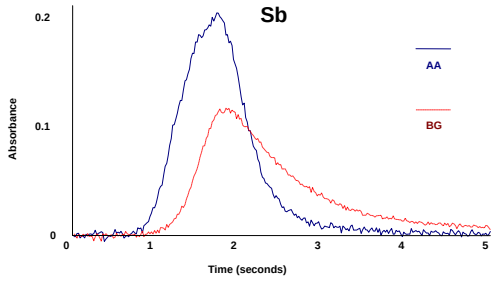

e. Multi-element (3), with Pd+Mg, 700°C, 1900°C, slope=0.0020

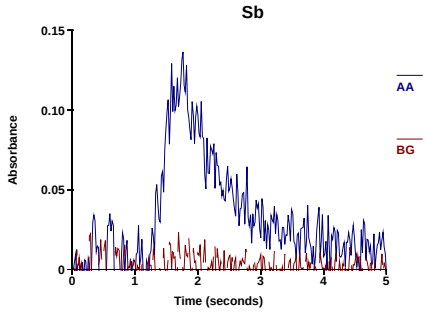

f. Multi-element (3), with Ir, 700°C, 2100°C, slope=0.0017

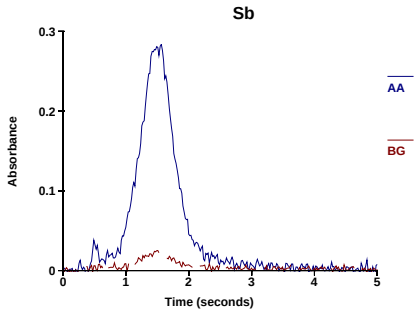

g. Multi-element (5), with Pd+Mg, 1100°C, 2000°C, slope=0.0019

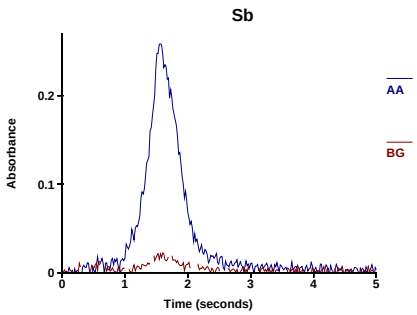

h. Multi-element (4), 1000°C, 1900°C, with Pd+Mg, slope=0.0020

By comparing the signal a (single without modifier) with the signals b (single with Pd+Mg modifier) and d (single with Ir modifier), the signal becomes broader and the appearing time increases (from about 0.5s to about 1s) in presence of the two modifiers which is a result of the stabilization effect of these modifier. However, the peak height decreases (from about 0.80 to about 0.40 with Pd+Mg and to about 0.20 with Ir) in presence of the modifiers. The signal is sharper and the peak height is larger in the presence Pd+Mg compared to Ir modifier. This could be due to the formation of more stable compound in presence of Ir. The higher atomization [2100°C (Ir) → 1900°C (Pd+Mg)] and pyrolysis [1500°C (Ir) → 1300°C (Pd+Mg)] temperatures in presence of Ir modifier can explain this stability.

By comparing the signal b with the signals c (multi with Cu, Mn, and Bi), e (multi with Bi and Cd), g (multi with Cu, Mn, Bi, and Se), and h (multi with Bi, Pb, and Se), the peak height decreases with increasing the number of element to be determined [0.33 (4-element) → 0.29 (5-element)] which as a result of decreasing the lamp intensity. Also, the peak height decreases with decreasing pyrolysis temperature and the signal becomes broader [0.20 (700°C, 3-element) → 0.25 (1000°C, 4-element) → 0.40 (1300, single-element)]. The Sb atoms become more volatile at pyrolysis temperatures near to 1300°C. The sensitivity decreases slightly with increasing the number of elements to be determined [0.0021 (single-element) → 0.0020 (3-element) and 0.20 (4-element) → 0.0019 (5-element)].

By comparing the signals d and f, the peak height [0.18 (single, 1500°C) → 0.13 (multi, 700°C)] and the sensitivity [0.0019 (single, 1500°C) → 0.0017 (multi, 700°C)] decrease with increasing the number of elements to be determined. The decreasing in pyrolysis temperature has a strong effect on the absorption signal. The Sb atoms atomize more easily at pyrolysis temperature near to 1500°C.

5.6.10 Selenium (Se)

The absorption signals of Se in different modes and with and without modifier are shown in Figure 5.33.

Figure 5.33 Absorption signals of selenium

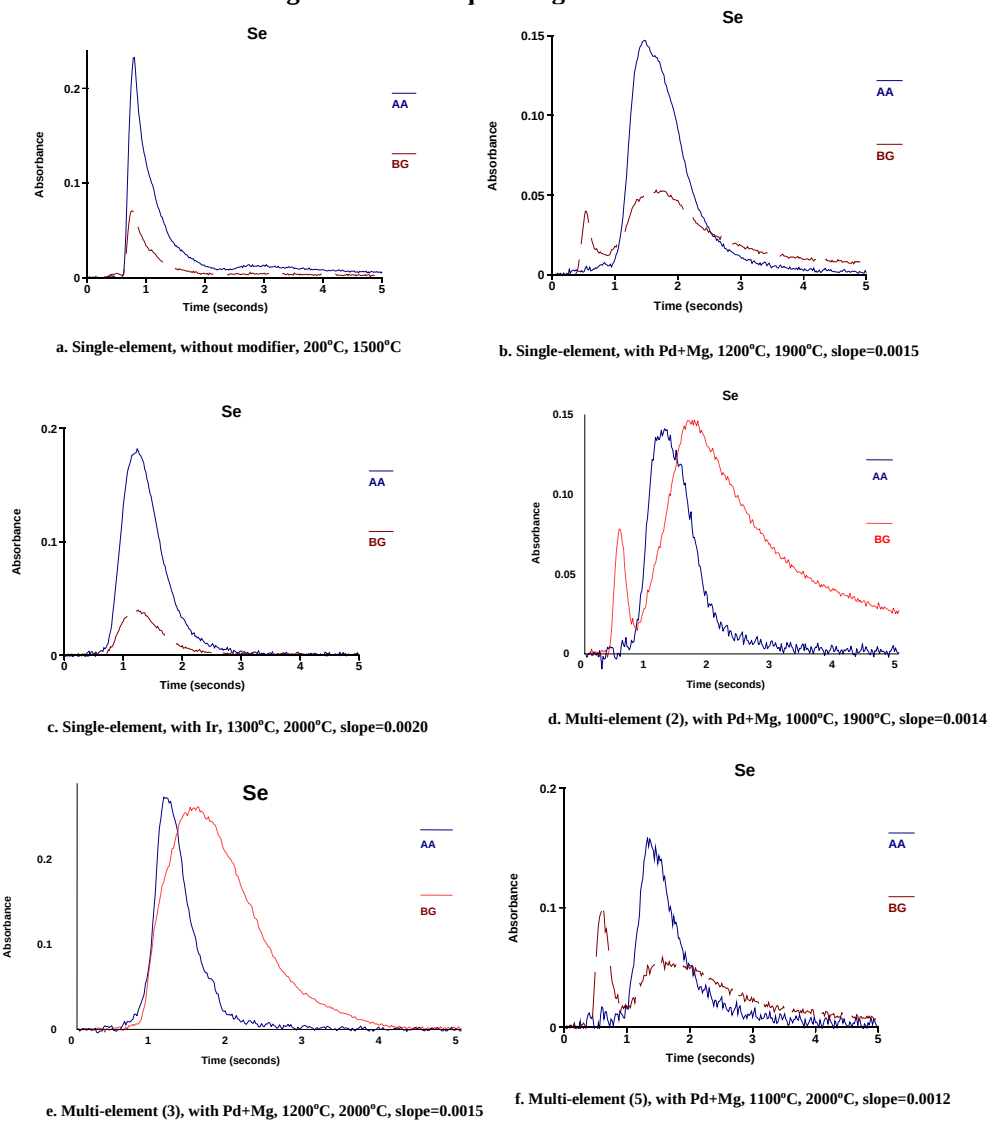

a. Single-element, without modifier, 200°C, 1500°C

b. Single-element, with Pd+Mg, 1200°C, 1900°C, slope=0.0015

c. Single-element, with Ir, 1300°C, 2000°C, slope=0.0020

d. Multi-element (2), with Pd+Mg, 1000°C, 1900°C, slope=0.0014

e. Multi-element (3), with Pd+Mg, 1200°C, 2000°C, slope=0.0015

f. Multi-element (5), with Pd+Mg, 1100°C, 2000°C, slope=0.0012

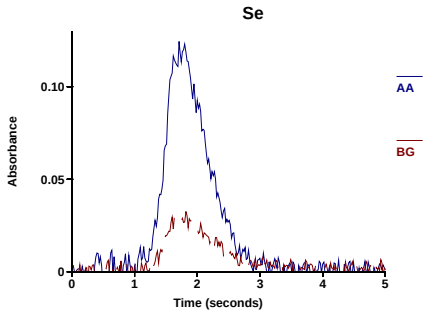

g. Multi-element (4), with Pd+Mg, 1000°C, 1900°C, slope=0.0013

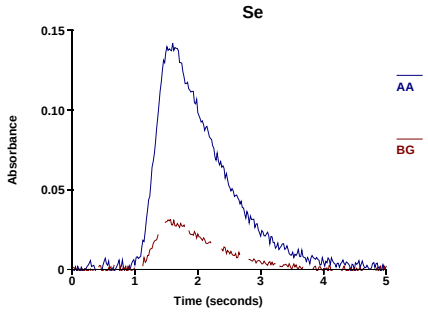

h. Multi-element (2), with Ir, 1200°C, 2000°C, slope=0.0020

As be seen, the absorption signals are different at different operational conditions. By comparing the signal a (single without modifier) with the signals b (single with Pd+Mg modifier) and c (single with Ir modifier), the signal becomes broader and the appearing time increases (from 0.5s to 1s) in presence of two the modifiers which indicates the stabilization effect of the modifiers. The Se atoms need higher temperature to be atomized and they are stable to higher pyrolysis temperature (1200°C with Pd+Mg and 1300°C with Ir). The peak height also decreases in presence of the modifiers [0.22 (without modifier) → 0.15 (Pd+Mg) and 0.18 (Ir). The sensitivity is higher using Ir as a modifier than with Pd+Mg modifier (0.0020 and 0.0015).

By comparing the signal b with the signals d (multi with Pb), e (multi with Cu and Mn), f (multi with Cu, Mn, Sb, and Bi), and g (Bi, Sb, and Pb), the peak height increases [from about 0.15 (single, 1900°C) to about 0.28 (multi, 2000°C)] with increasing the atomization temperature which due to faster atomization of analyte atoms at higher atomization temperatures. However, the peak height decreases with increasing the number of element to be determined [0.28 (3-element) → 0.17 (5-element)] due to the decreasing in lamp intensity. The sensitivity decreases with increasing the number of elements to be determined [0.0015 (single) → 0.0014 (2-element) → 0.0013 (3-element)].

By comparing the signals c and h (multi with Pb), the peak height decreases [from 0.18 to 0.14] and the peak width slightly increases. In the multi-element determination, lower pyrolysis temperature has been used [1300°C → 1200°C]. The Se atoms atomize more easily at pyrolysis temperature of 1300°C. No change in the sensitivity has been observed (0.0020).

5.6.11 Vanadium (V)

The absorption signals of Se in different modes and with and without modifier are shown in Figure 5.34.

Figure 5.34 Absorption signals of vanadium

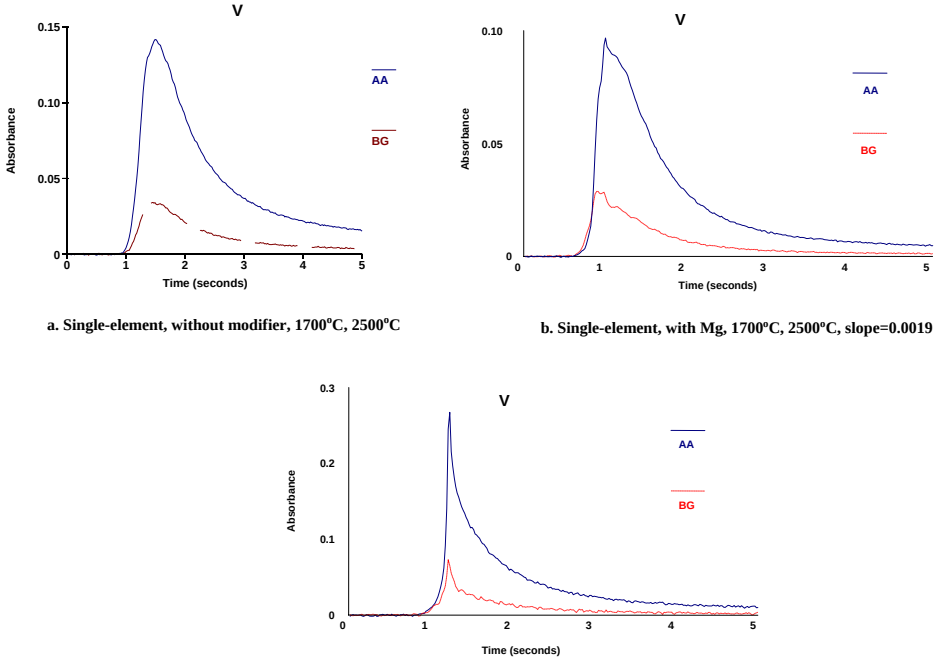

a. Single-element, without modifier, 1700°C, 2500°C

b. Single-element, with Mg, 1700°C, 2500°C, slope=0.0019

c. Multi-element (4), with Mg, 1500°C, 2500°C, slope=0.0018

By comparing the signals a and b, the signal becomes sharper in presence of the modifier. The addition of modifier prevents the formation of refractory compounds like carbides. However, the peak height decreases (from about 0.15 to about 0.10) in presence of the modifier which results in decreased sensitivity.

By comparing the multi-element determination signal (c), the signal sharpness and peak height are increased which indicates increasing the atomization process. The sensitivity decreases with increasing the number of elements to be determined [0.0019 (single) → 0.0018 (4-element)].

5.7 Summary of Multi-Element Determination

From the results of the previous sections:

- By using the multi-operating mode, more than one element (up to six) can be determined in one run. The multi-element capability of the system can be used by applying multi-element lamps since four lamps only can be inserted. This will decrease the measurement time and sample and standard volume. The cost of analysis will be finally improved using multi-element mode.

- The use of multi-element mode requires an optimization of instrumental and experimental parameters. These conditions include the pyrolysis and atomization temperatures, the use of modifier, and the operating mode.
- The use of multi-operating mode and compromised conditions cause loss of sensitivity and increase of detection limits. The degradation of sensitivity and detection limits depends on group of elements to be determined simultaneously. However, the multi-operating mode will affect mainly the detection limits and this effect will increase by increase the number of elements and/or use higher operating mode. For some elements, e.g. Pb, this will affect also the sensitivity. The reason of this effect is the reduction of lamp intensities. Table 5.13 shows the effect of operating mode on detection limits and characteristic mass. The atomization temperatures in all modes (2- and 4-mode) are same as in single-element mode. From Table 5.13, the detection limits values have increased in multi-operating mode compared to single-element mode and the amount of increasing depends on the element. However, the characteristic mass values can increase in multi-element mode but this increasing is less than as with detection limits.
- The atomization temperature will affect mainly the sensitivity of determination. By using higher atomization temperature, the volatile elements will volatilize before the final furnace temperature is reached and this will lead to loss of sensitivity of volatile elements. The detection limits can also be affected. The increase in characteristic mass values as a result of increasing atomization temperatures were not as high as with detection limits values (Table 5.13).
- For further study, 2-operating mode will be used which give more sensitive results than 4-operating mode (except multi-element determination of Al, Be, Cr, and V). The 2-operating mode is still having the advantages of multi-element determination over single-element like the analysis time and costs.
- The use of modifier affects the absorption signals of elements in terms of peak width, appearing time, and peak height. However, this effect depends on element. Generally, the peaks become sharper for the less volatile because the modifier prevents the formation refractory compounds during the pyrolysis step resulting in increasing the atomization process. No change or broader signals for mid- and high volatile elements. The broader signals are a result of formation of stable compounds between the elements and the modifier. Higher pyrolysis and atomization temperatures for high

volatile elements can be applied in the presence of the modifier. The use of modifier, also, causes the peak height to decrease for volatile elements and to increase for less volatile (except V).

- By increasing the number of element to be determined, the peak height decreases as a result of decreasing the lamp intensities in the multi-element mode.
- By changing the pyrolysis temperature in the multi-element mode compared to the single-element mode, the peak height and peak width could be affected which is related to the interaction between the analyte atoms and the modifier.

Table 5.13 The effect of operating mode on detection limits and characteristic mass values

Element	1-lamp mode		2-lamp mode		4-lamp mode	
	D.L. (µg/l)	C.M. (pg)	D.L. (µg/l)	C.M. (pg)	D.L. (µg/l)	C.M. (pg)
Be	0.026	3.9	0.030	4.4	0.066	4.9
Cr	0.049	7.2	0.054	7.9	0.121	8.9
Cu	0.13	19.6	0.20*/0.28**	20*/20.5**	0.56	20.5
Mn	0.051	5.0	0.070*/0.087**	5.2*/5.1**	0.61	6.6
Pb	0.32	46.3	0.38	55.0	0.90	88.0
Sb	0.29	41.9	0.75	44.0	1.20	44.0
Se	0.40	58.7	0.64	62.9	1.38	67.7

*Three elements have been determined
**Four elements have been determined

5.8 The Effect of the Urine Matrix on the Multi-Element Determination

Urine is actually a highly complex matrix, consisting of high levels of both organic and inorganic substances. The majority of the constituents are either waste products of cellular metabolism or products derived directly from certain foods that are eaten. The most important organic substances are urea, uric acid, and creatinine. Urea is a product formed by the liver from ammonia and carbon dioxide. Uric acid is an end-product of the oxidation of purines in the body. Creatinine is a hydrated form of creatine. The principle inorganic constituents of urine are chlorides, phosphate, sulphates, and ammonia. Sodium chloride is the predominant chloride and makes up about half of the inorganic substances. Since ammonia is toxic to the body and lacking in plasma, there is very little of it normally present in fresh urine. Urine is also one of the main routes of excretion and can be used for toxicological and therapeutic investigations[172-174]. However, the large salt peptide content of urine with its low trace element concentrations leads to considerable difficulties in the analysis. The constituents of the urine may affect the peak shape, absorbance time, and peak area. The use of the matrix

modification improved the precisions of the determination but it could not possible to eliminate all of the background; however, it can be reduced.

In our work, we have used standard reference urine sample from Seronorm (LOT 0511545) to study the effect of the matrix on the pyrolysis and atomization curves of the simultaneous multi-element determination of our elements. Since the concentrations of most elements in the reference material were high, we have diluted it (1:4), which has also reduced the concentration of the interferences. The resulting temperature program has been used to evaluate the concentrations of the elements in different types of reference materials (including the urine reference material). The concentration of all components in Seronorm urine sample is listed in Table 5.14.

Table 5.14 The analytical values of Seronorm Trace Elements Urine

Component	Analytical value	Component	Analytical value
Aluminium (Al)	100 µg/l	Potassium (K)	1775 mg/l
Antimony (Sb)	99.9 µg/l	Selenium (Se)	58.6 µg/l
Arsenic (As)	142 µg/l	Silicon (Si)	5.5 µg/l
Beryllium (Be)	4.9 µg/l	Silver (Ag)	26 ng/l
Bismuth (Bi)	20.1 µg/l	Sodium (Na)	2303 mg/l
Bromine (Br)	2.0 mg/l	Strontium (Sr)	106 µg/l
Cadmium (Cd)	4.6 µg/l	Sulphur (S)	548 mg/l
Chloride (Cl)	127 mmol/l	Tellurium (Te)	25.3 µg/l
Chromium (Cr)	19.7 µg/l	Thallium (Tl)	9.26 µg/l
Cobalt (Co)	10.0 µg/l	Tin (Sn)	54.6 µg/l
Copper (Cu)	72 µg/l	Titanium (Ti)	21.0 µg/l
Fluorine (F)	4.0 mg/l	Vanadium (V)	25.2 µg/l
Iodine (I)	304 µg/l	Zinc (Zn)	1141 µg/l
Iron (Fe)	12.3 µg/l	Creatinine	97.9 mg/dl
Lead (Pb)	40.3 µg/l	1-Hydroxypyrene	55 µg/l
Lithium (Li)	10.2 µg/l	Formic acid	10.8 mg/l
Magnesium (Mg)	70.1 mg/l	Phenol	300 mg/l
Manganese (Mn)	12.3 µg/l	Mandelic acid	490 µg/l
Mercury (Hg)	40.7 µg/l	Tetracloroethylene	1000 µg/l
Molybdenum (Mo)	49.3 µg/l	Trichloroacetic acid (TCA)	350 µmol/l

5.8.1 Multi-Element Determination of Al, Be, Cr, and V

The diluted reference material (1:4) has been spiked with 10 ppb Al, 2 ppb Be, 6 ppb Cr, and 80 ppb V. 20 µl diluted spiked reference material has been injected with 5 µg $Mg(NO_3)_2$ as a modifier into the atomizer each time during this study. The effect of the matrix on the pyrolysis and atomization curves has been studied and the results are shown in Figure 5.35. For the first part, the pyrolysis curves, the absorption signals were studied at an atomization temperature of 2500^{o}C. The atomic absorption signals remained approximately constant as the pyrolysis varied from 800-1500^{o}C for Be and Cr, from 800-1600^{o}C for Al, and from 800-

1700°C for V. When the temperature increased above 1500°C, the absorption signal randomly decreased for Be and Cr due to the volatilization of these elements. In order to determine all these elements simultaneously, 1500°C was chosen as an optimum pyrolysis temperature. The effects of atomization temperature were studied at a pyrolysis temperature of 1500°C and shown in Figure 5.35. For Al, Be, and Cr, the atomic absorption signal increased with increasing atomization temperature and has its maximum and best precision at 2300°C. However, for V, the absorption signal increased with increasing atomization temperature until 2500°C. Because the lifetime of the tube will decrease above 2500°C and with SIMAA 6000 we can not use atomization temperature more than 2600°C, we have decided to use 2500°C as an optimum atomization temperature for the multi-element determination of this group. The absorption peaks at the optimum pyrolysis and atomization temperatures are shown in Figure 5.36, which are similar (peak shapes and absorption time) to those obtained in the case without matrix (aqueous solutions). This is because the high pyrolysis temperature (1500°C) that can be used with these elements which resulted in minimizing the effect of the urine matrix. Another effect is the dilution of the urine sample that resulted also in the dilution of the matrix and also to the effect of the modifier which facilitates the formation of stable compounds and prevents the volatilization of the elements during the pyrolysis stage.

Figure 5.35 Pyrolysis and atomization curves for multi-element determinations of Al, Be, Cr, and V using 5µg Mg modifier in diluted (1:4) urine sample spiked with 10, 2, 6, 80 ppb Al, Be, Cr, and V, respectively

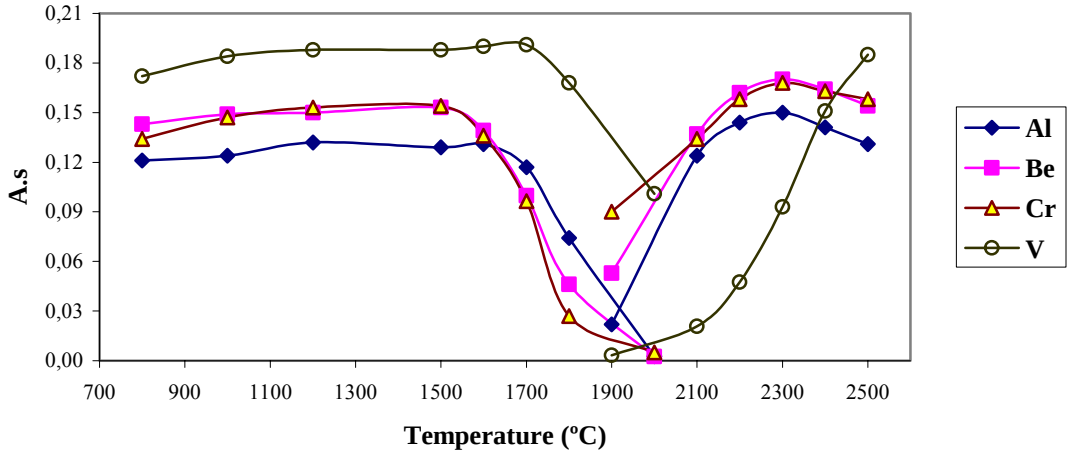

Figure 5.36 Absorbance signals of diluted (1:4) spiked urine sample at 1500°C pyrolysis and 2500°C atomization with 5µg Mg modifier in the multi-element determinations of Al, Be, Cr, and V

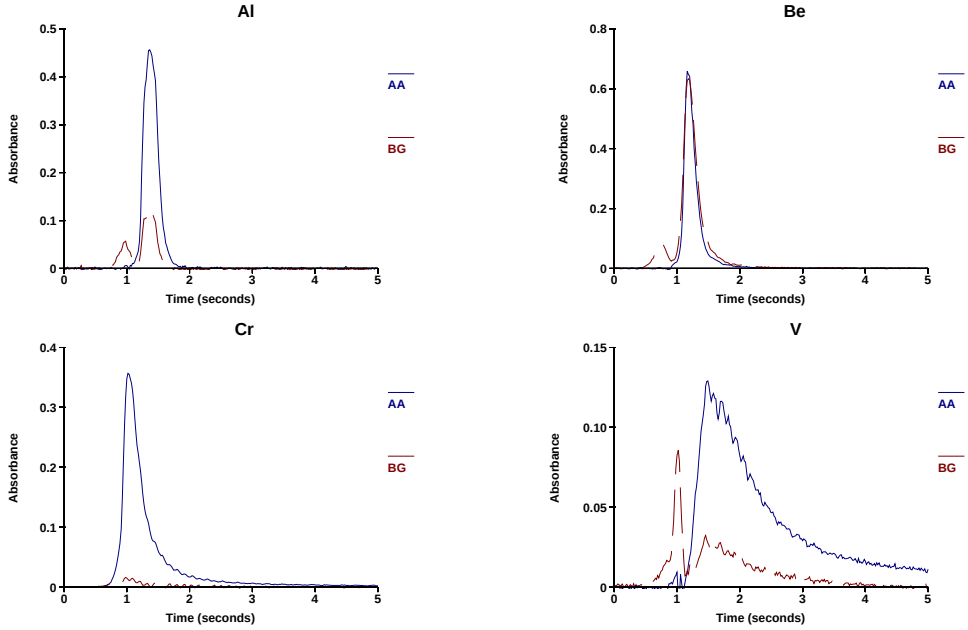

5.8.2 Multi-Element Determination of Be, Cr, Cu

The diluted reference material (1:4) has been spiked with 2 ppb Be, 6 ppb Cr, and 10 ppb Cu. 20 µl diluted spiked reference material has been injected with 5µg Pd + 3µg $Mg(NO_3)_2$ as a modifier into the atomizer each time during this study. The effect of the matrix on the pyrolysis and atomization curves has been studied and the results are shown in Figure 5.37. For pyrolysis curves, the absorption signals were studied at an atomization temperature of 2300°C and for atomization curves, the absorption signals were studied at a pyrolysis temperature of 1200°C. The atomic signal for Cu remained approximately constant till the pyrolysis temperature reached 1200°C and then started to decrease gradually. For Be and Cr, the atomic signal was almost constant till 1400°C and then started gradually to decrease. In order to determine all three elements simultaneously, 1200°C was chosen as an optimum pyrolysis temperature. Similarly, the effects of atomization temperature on the atomic absorbance are studied and shown in Figure 5.37. For Cu, the atomic absorption signal increased with increasing atomization temperature till 2000°C at which it had its maximum value. For Cr and Be, they had their maximum at atomization of 2200 and 2300°C, respectively. Hence we decided to choose 2300°C as an optimum atomization temperature for the simultaneous determination of these elements. The absorption peaks at the optimum pyrolysis and atomization temperatures are shown in Figure 5.38. From the comparing between the pyrolysis and atomization curves and the absorption peaks in the case of aqueous solutions and diluted urine sample; in terms of absorption time and peak shape, there was no

matrix effect on the multi-element determination of these elements which can be attributed to the high pyrolysis temperature (1200°C) that minimize the matrix interferences and the effect of the modifier which prevented the loss of the elements as volatile compounds.

Figure 5.37 Pyrolysis and atomization curves for multi-element determinations of Be, Cr, and Cu using 5µg Pd + 3µg Mg modifier in diluted (1:4) urine sample spiked with 2, 6, 10 ppb Be, Cr, and Cu, respectively

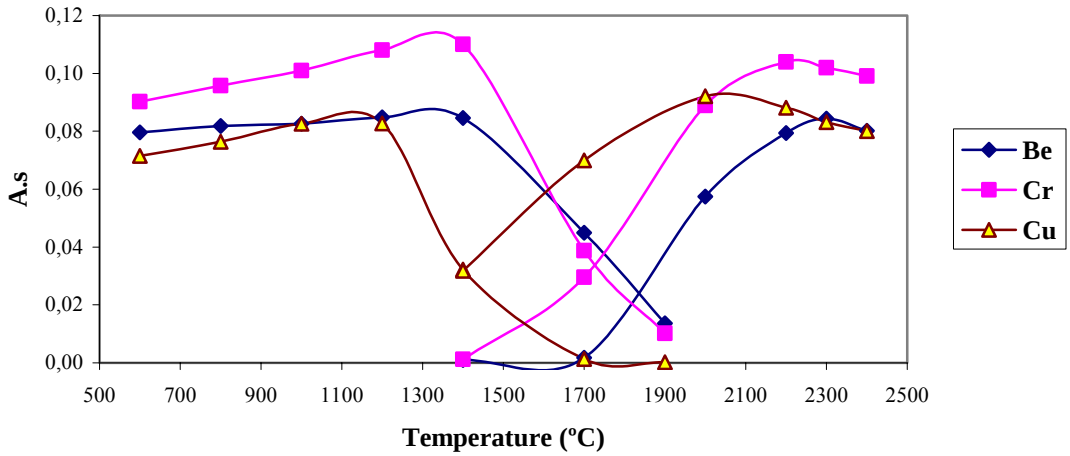

Figure 5.38 Absorbance signals of diluted (1:4) spiked urine sample at 1200°C pyrolysis and 2300°C atomization with 5µg Pd + 3µg Mg modifier in the multi-element determinations of Be, Cr, and Cu

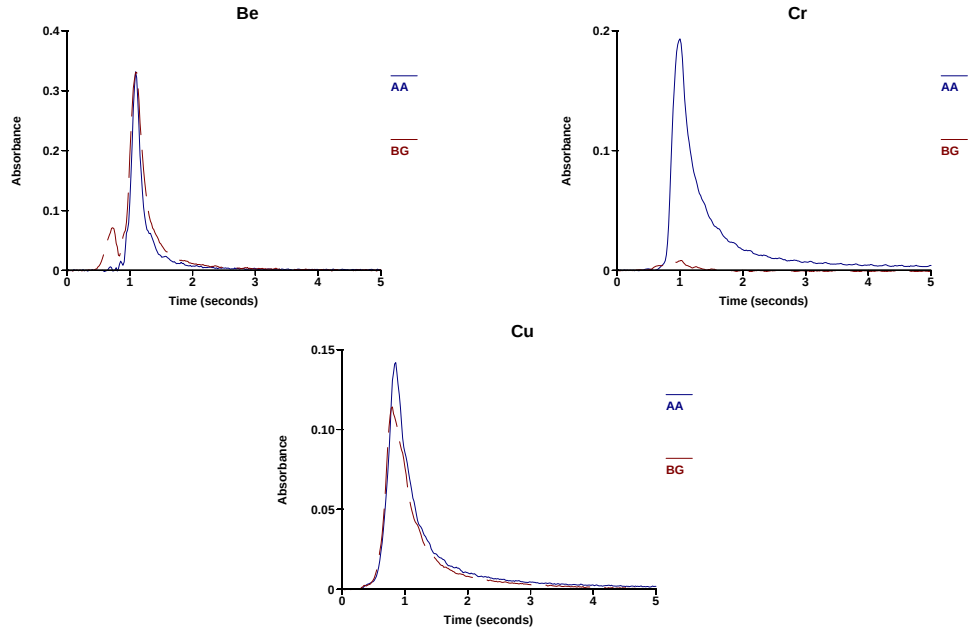

5.8.3 Multi-Element Determination of Bi, Sb, Cu, and Mn

The diluted reference material (1:4) has been spiked with 80 ppb Bi, 10 ppb Cu, 6 ppb Mn, and 80 ppb Sb. 20 µl diluted spiked reference material has been injected with 5µg Pd +

3µg $Mg(NO_3)_2$ as a modifier into the atomizer each time during this study. Pyrolysis and atomization curves were carried out in order to define the compromise conditions for the simultaneous determination of these elements in the presence of the matrix, since in simultaneous detection the heating program of the atomizer is the same for all analytes. Shown in Figure 5.39 are the pyrolysis and atomization curves for diluted spiked urine sample in the presence of Pd+Mg modifier. The dependence of the atomic absorption of Bi, Sb, Cu, and Mn with varying pyrolysis temperatures were evaluated at 2000^{o}C atomization temperature. The atomic absorption values for Bi remained approximately constant between 600 and 1000^{o}C and started to decrease gradually above 1000^{o}C. For Cu, the absorption signal remained approximately constant till 1200^{o}C and decreased gradually. For Sb and Mn, the atomic absorption remained almost constant until 1300^{o}C and then gradually decreased. In order to determine all four elements simultaneously, 1000^{o}C was chosen as an optimum pyrolysis temperature. The effects of atomization temperature on the atomic absorption of the elements were studied at 1000^{o}C pyrolysis temperature. The atomic absorption for Bi increased with increasing temperature until 1600^{o}C and then remained approximately constant when varying atomization temperature from 1600 to 1800^{o}C. For Sb, it increased until 1800^{o}C and then remained constant until 2000^{o}C. The atomic absorption for Cu and Mn reached its maximum at 2000^{o}C. For the simultaneous determination of these elements, we have decided to choose 2000^{o}C as an optimum atomization temperature. The atomic absorption peaks at the optimum pyrolysis and atomization temperatures are shown in Figure 5.40. From the absorption peaks, Bi and Sb were more affected by the urine matrix because the appearances of their signals were more closely to the background signal. Welz et al.[100] reported that the integrated absorbance signal of bismuth is decreased by about 20% by NaCl concentrations higher than 1g.l^{-1}. For Sb, they[100] found that the peak shape for Sb was broadened and the peak height suppressed by 40% in the presence of 30 g.l^{-1} NaCl while the integrated absorbance changed by less than 5% at the same NaCl concentration (30g.l^{-1}). However, only about 20mg.l^{-1} sulphate decreased the integrated absorbance by 10%. This is probably due to gas phase interference[100]. The signals of Cu and Mn were similar to those without matrix (in aqueous solutions).

Figure 5.39 Pyrolysis and atomization curves for multi-element determinations of Bi, Cu, Mn, and Sb using 5µg Pd + 3µg Mg modifier in diluted (1:4) urine sample spiked with 80, 10, 6, 80 ppb Bi, Cu, Mn, and Sb, respectively

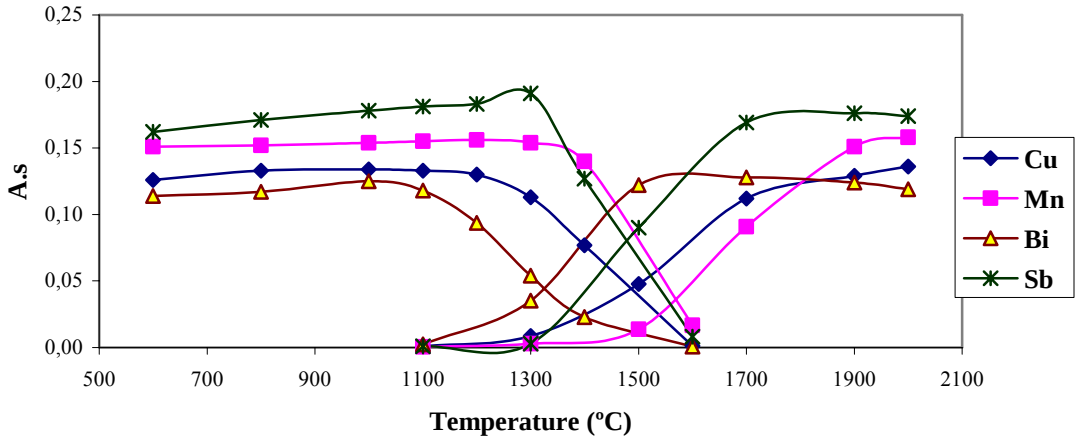

Figure 5.40 Absorbance signals of diluted (1:4) spiked urine sample at 1000°C pyrolysis and 2000°C atomization with 5µg Pd + 3µg Mg modifier in the multi-element determinations of Bi, Cu, Mn, and Sb

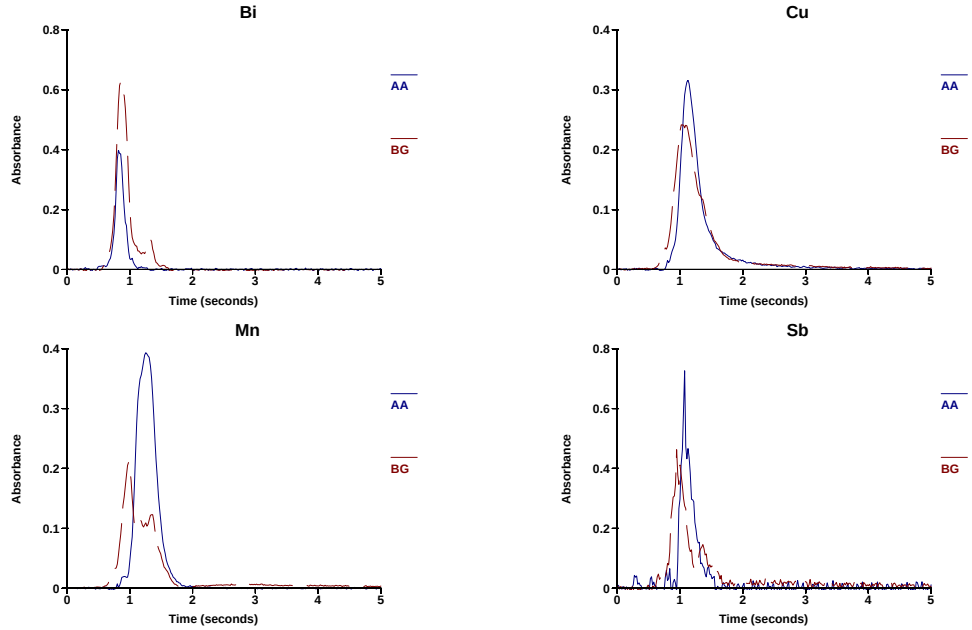

5.8.4 Multi-Element Determination of Cu, Mn, and Se

The diluted reference material (1:4) has been spiked with 10 ppb Cu, 6 ppb Mn, and 80 ppb Se. 20 µl diluted spiked reference material has been injected with 5µg Pd + 3µg $Mg(NO_3)_2$ as a modifier into the atomizer each time during this study. Pyrolysis and atomization curves were carried out in order to define the compromise conditions for the simultaneous determination of these elements in the presence of the matrix, since in simultaneous detection the heating program of the atomizer is the same for all analytes. The

dependence of the atomic absorption of Cu, Mn, and Se with varying pyrolysis temperatures were evaluated at 2000^{o}C atomization temperature and shown in Figure 5.41. From the pyrolysis curves, the absorption signal obtained for Se remained constant as the pyrolysis temperature increased until 900^{o}C and then gradually decreased with increasing the temperature. For Cu and Mn, the absorption signals remained approximately constant until 1200 and 1300^{o}C, respectively. For the simultaneous determination of the elements, 900^{o}C was chosen as an optimum pyrolysis temperature. A decreased in pyrolysis temperature found for selenium in diluted urine sample (900^{o}C) compared to that in aqueous solution (1200^{o}C) which has been also reported by G. Schlemmer and B. Welz[99]. They found that slight selenium losses were observed in biological materials if pyrolysis temperature above 900^{o}C were used. J. L. Fischer[175] reported that an increase of the amount of phosphate in the sample was accompanied with increasing losses of selenium. This phosphate interference observed when selenium is determined with palladium modifiers, can be explained by decreasing the number of active palladium sites necessary to stabilize selenium in the presence of phosphate[175]. The dependence of the atomic absorption of Cu, Mn, and Se with varying atomization temperatures were evaluated at 900^{o}C pyrolysis temperature and shown in Figure 5.41. From the atomization curves, the atomic signals of Se, Cu, and Mn increased with increasing atomization temperature and reached their maximum at atomization temperature of 2000^{o}C. For the simultaneous determination, 2000^{o}C was chosen as the optimum atomization temperature. The absorption peaks of the elements at the optimum pyrolysis and atomization temperatures are shown in Figure 5.42. From the absorption peaks, a decrease in the integrated absorbance signal of selenium has been observed. B. Welz et al.[100] reported that potassium sulphate had very pronounced influence on selenium when a pyrolysis temperature of 1000^{o}C was used. 0.1 μg of SO_4^{-2} reduced the integrated absorbance signal by more than 10% and the influence increased to 25% suppression in the presence of 3g.l^{-1} and finally the selenium signal disappeared entirely if the concentration of SO_4^{-2} was increased further[100]. Lowered integrated absorbance observed for Se can be explained by molecular interference, which occurs due to the vaporization of SO_4^{-2} decomposition products, such as SO_3, SO_2, and SO[40]. High concentrations of NaCl can cause increasing suppression of the integrated absorbance signal[100]. For Cu and Mn, a small decrease in the integrated absorbance signal have been observed compared to those obtained in the simultaneous determination of Bi, Sb, Cu, and Mn. This can be attributed to a less pyrolysis temperature (900^{o}C) that has been used. If low pyrolysis temperatures are applied, expulsion and gas phase reaction between the

elements (Mn and Cu) in the atomization step are very likely[176]. NaCl depressive interference on Mn was reported at pyrolysis temperature between 800-900°C.

Figure 5.41 Pyrolysis and atomization curves for multi-element determinations of Cu, Mn, and Se using 5µg Pd + 3µg Mg modifier in diluted (1:4) urine sample spiked with 10, 6, 80 ppb Cu, Mn, and Se, respectively

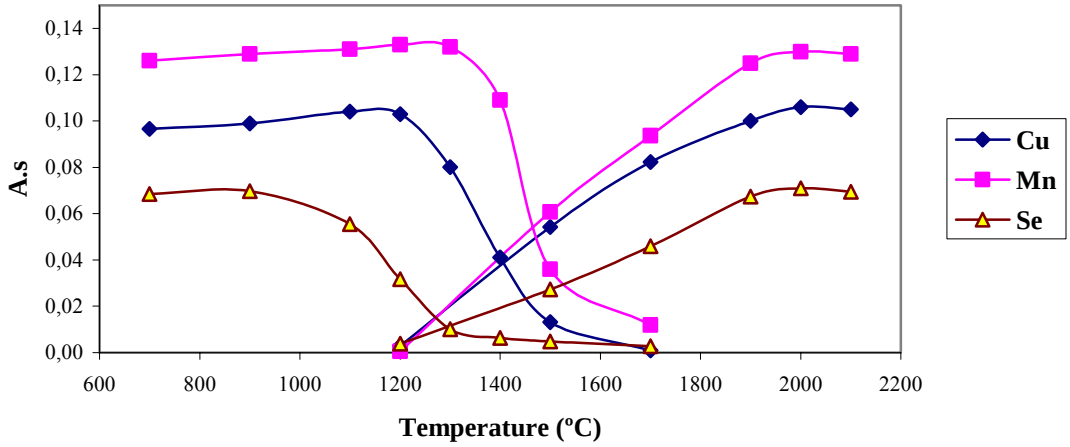

Figure 5.42 Absorbance signals of diluted (1:4) spiked urine sample at 900°C pyrolysis and 2000°C atomization with 5µg Pd + 3µg Mg modifier in the multi-element determinations of Cu, Mn, and Se

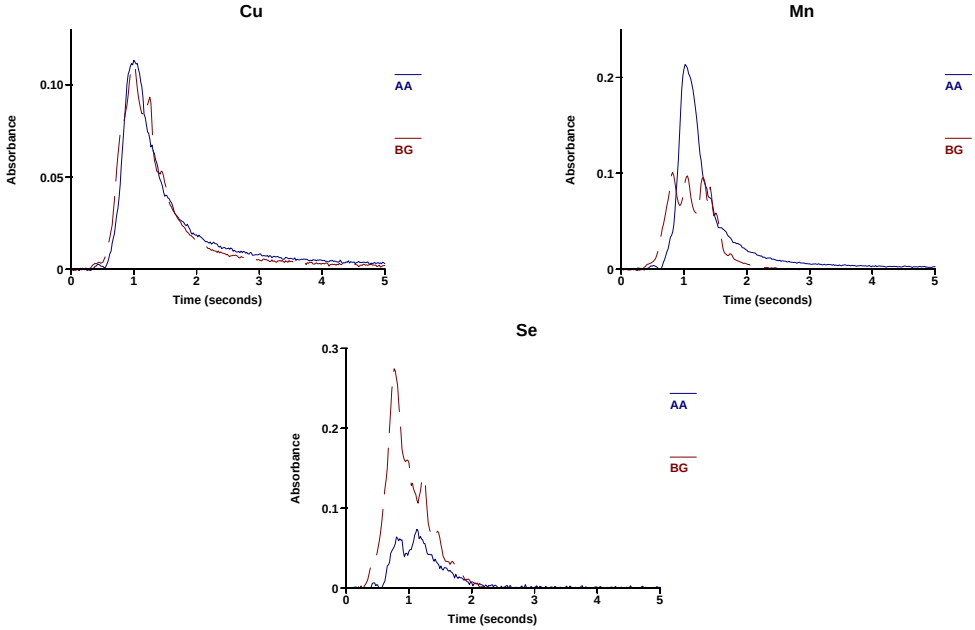

5.8.5 Multi-Element Determination of Pb and Se

Two types of modifiers have been used to simultaneous determination of Pb and Se in urine reference material.

5.8.5.1 With 5µg Pd + 3µg Mg Modifier

The diluted reference material (1:4) has been spiked with 40 ppb Pb and 80 ppb Se. 20 µl diluted spiked reference material has been injected with 5µg Pd + 3µg $Mg(NO_3)_2$ as a modifier into the atomizer each time during this study. Pyrolysis and atomization curves were carried out in order to define the compromise conditions for the simultaneous determination of the two elements in the presence of the urine matrix, since in simultaneous detection the heating program of the atomizer is the same for all analytes. The dependence of the atomic absorption of Pb and Se with varying pyrolysis temperatures were evaluated at 1900^{o}C atomization temperature and shown in Figure 5.43. The absorption signals was approximately constant as the pyrolysis temperature varied from 600-1000^{o}C for Pb and Se. The atomic absorption values decreased correspondingly above 1000^{o}C. In order to determine the elements simultaneously, 1000^{o}C was chosen as an optimum pyrolysis temperature. For Se, the absorption signal was affected by the urine matrix (compared with the determination of Se in aqueous solutions) for the same reasons that we have discussed before. For Pb, sharper absorbance peak compared to the aqueous solution and decreased appearance time have been observed. However, the integrated absorption values are approximately similar indicating effective removing of the interferences in the presence of the modifier. The effects of the atomization temperature are studied at pyrolysis temperature of 1000^{o}C (shown in Figure 5.43). The absorption signals for Pb and Se increased with increasing temperature below 1900^{o}C. Above this temperature, the absorption signals remained approximately constant. Therefore, we have decided to use 1900^{o}C as an optimum atomization temperature for the simultaneous determination of Pb and Se. The absorption peaks of the elements at the optimum pyrolysis and atomization temperatures are shown in Figure 5.44.

Figure 5.43 Pyrolysis and atomization curves for multi-element determinations of Pb and Se using 5µg Pd + 3µg Mg modifier in diluted (1:4) urine sample spiked with 40, 80 ppb Pb and Se, respectively

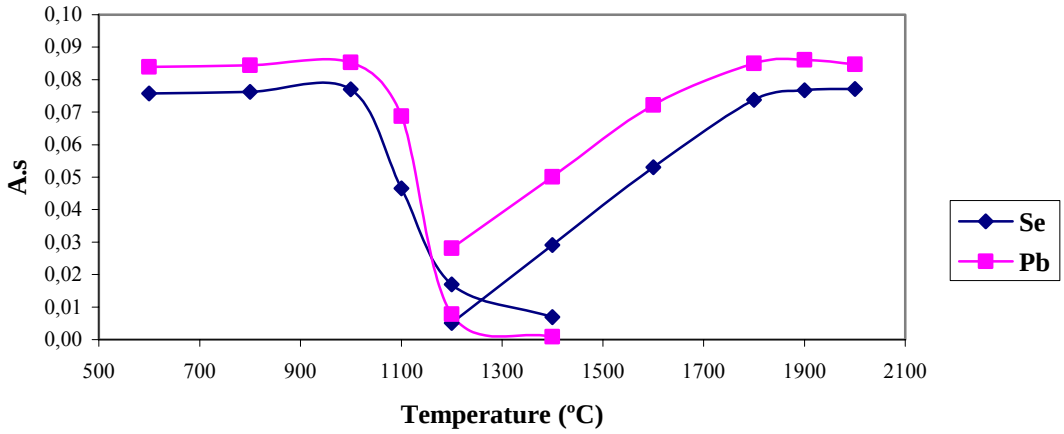

Figure 5.44 Absorbance signals of diluted (1:4) spiked urine sample at 1000°C pyrolysis and 1900°C atomization with 5µg Pd + 3µg Mg modifier in the multi-element determinations of Pb and Se

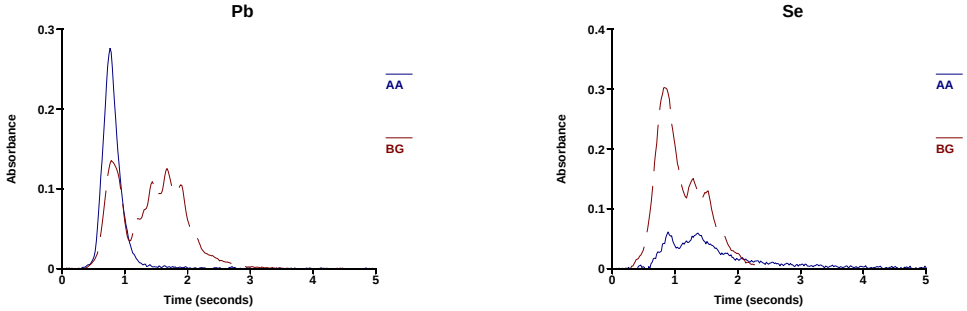

5.8.5.2 With Ir Permanent Modifier

The 500µg iridium was thermally deposited on the graphite tube platform and used as permanent modifier. The diluted reference material (1:4) has been spiked with 40 ppb Pb and 80 ppb Se. 20 µl diluted spiked reference material has been injected into the atomizer each time during this study. Pyrolysis and atomization curves were carried out in order to define the compromise conditions for the simultaneous determination of the two elements in the presence of the urine matrix, since in simultaneous detection the heating program of the atomizer is the same for all analytes. From the pyrolysis curves; Figure 5.45, the atomic absorption signals remained approximately constant as the pyrolysis temperature varied from 400-800°C and from 400-1000°C for Pb and Se, respectively. Above these temperatures, the absorption signals decreased with increasing the pyrolysis temperature. A pyrolysis temperature of 800°C was chosen as the optimum. A decreased in the pyrolysis temperature comparing with the determination of these elements in the aqueous solution (1200 and 1300°C for Pb and Se, respectively) can be seen. We can also see that the sensitivity for the

simultaneous determination of Pb and Se in the presence of this modifier is decreased comparing with that in the presence of Pd+Mg modifier. M. Hoenig et al.[118] reported that for masses of Ir > 300µg, a decrease of approximately 10% in sensitivity was observed for Pb, Cd, Cr, and Ni. This depressive effect with increasing amounts of such chemical modifiers has also been observed by other authors[161]. From the atomization curves; Figure 5.45, the atomic absorption signals increased with increasing the temperature as the atomization temperature varied from 1200-1700°C and from 1200-2000°C for Pb and Se, respectively. Above 1800°C, the absorption signal of Pb remained approximately constant. For the simultaneous determination, we have decided to choose 2000°C as an optimum atomization temperature. The absorption peaks of the elements at the optimum pyrolysis and atomization temperatures are shown in Figure 5.46.

Figure 5.45 Pyrolysis and atomization curves for multi-element determinations of Pb and Se using 500µg Ir permanent modifier in diluted (1:4) urine sample spiked with 40, 80 ppb Pb and Se, respectively

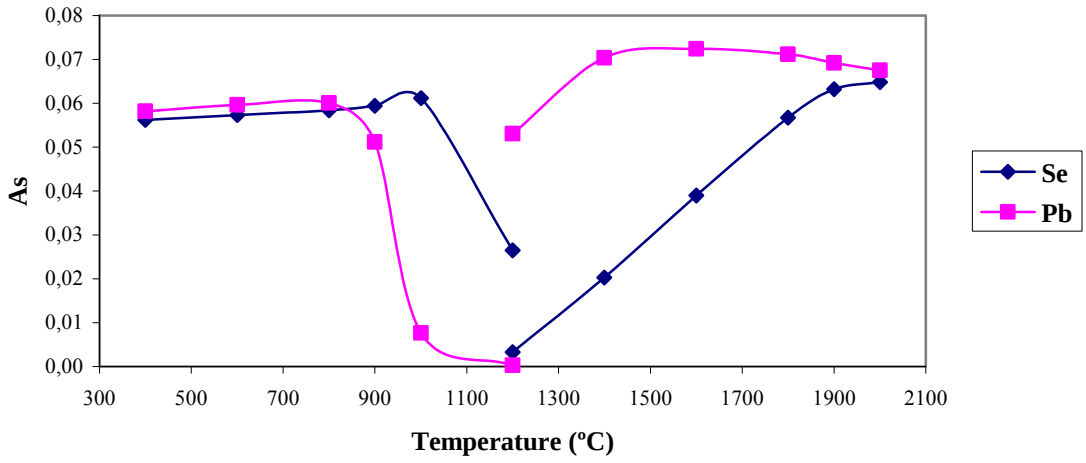

Figure 5.46 Absorbance signals of diluted (1:4) spiked urine sample at 800°C pyrolysis and 2000°C atomization with 500µg Ir permanent modifier in the multi-element determinations of Pb and Se

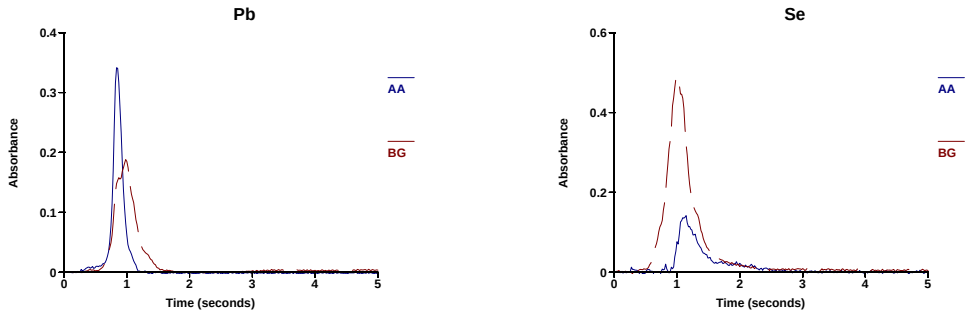

5.8.6 Multi-Element Determination of Bi, Sb, and Cd

As for the simultaneous determination of Pb and Se, two types of modifiers have been used for the simultaneous determination of Bi, Sb, and Cd in urine reference material.

5.8.6.1 With 5µg Pd + 3µg Mg modifier

The diluted reference material (1:4) has been spiked with 80 ppb Bi, 80 ppb Sb, and 2 ppb Cd. 20 µl diluted spiked reference material has been injected with 5µg Pd + 3µg $Mg(NO_3)_2$ as a modifier into the atomizer each time during this study. The dependence of Bi, Sb, and Cd absorbance on the pyrolysis temperature at 1900^oC atomization temperature was studied and shown in Figure 5.47. The atomic signal for Cd remained approximately constant till the pyrolysis temperature reached 600^oC and then started to decrease. Oliveira et al.[177] found that 550^oC was the best pyrolysis temperature obtained for the determination of cadmium in urine in the presence of Pd+Mg modifier. This can be attributed to the volatilization of Cd as chloride. The formation and volatilization of $CdCl_2$ occurred before the interaction between Cd and Pd on the graphite tube surface. Oliveira et al.[40] found that Cl^- ions in low amounts damaged the thermal stabilization obtained for Cd in presence of the W+Rh as permanent chemical modifier. For Bi and Sb, the atomic signal was almost constant till 1000^oC and 1300^oC, respectively, then started gradually to decrease. In order to determine all three elements simultaneously, 600^oC was chosen as an optimum pyrolysis temperature. Similarly, the effects of atomization temperature on the atomic absorbance are studied and shown in Figure 5.47. The effect of the atomization temperature was studied at the pyrolysis of 600^oC. For Cd, the atomic absorption signal increased with increasing the temperature as the atomization temperature varied from 1000-1400^oC and then started to decrease gradually due to increased diffusional losses of analyte atoms under high atomization temperatures. For Bi, the atomic absorption signal increased with increasing atomization temperature and had its maximum at atomization temperature between 1600-1700^oC and then started to decrease. Sb atomic absorption signal had its maximum at approximately 1800^oC atomization temperature. By taking into account the atomic signal, 1900^oC was chosen as an optimum atomization temperature for the simultaneous determination of the elements. The absorption peaks of the elements at the optimum pyrolysis and atomization temperatures are shown in Figure 5.48.

Figure 5.47 Pyrolysis and atomization curves for multi-element determinations of Bi, Sb, and Cd using 5µg Pd + 3µg Mg modifier in diluted (1:4) urine sample spiked with 80, 80, and 2 ppb Bi, Sb, and Cd, respectively

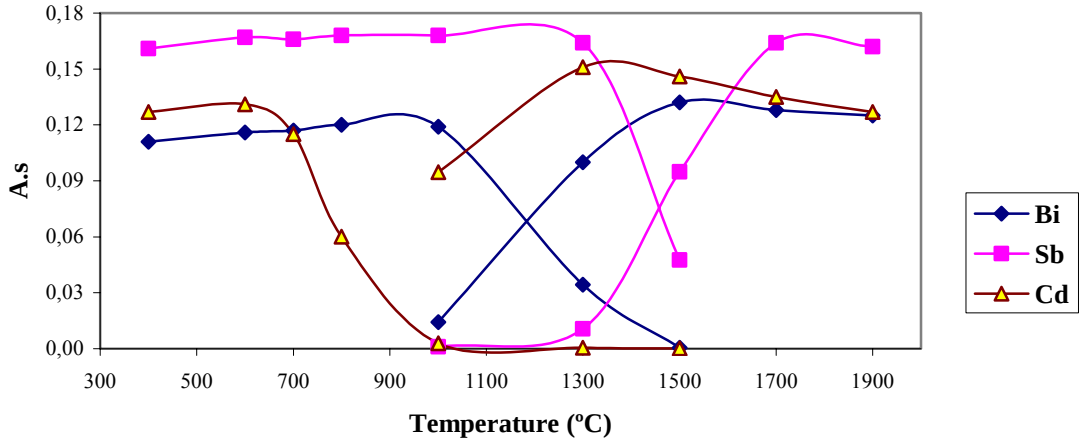

Figure 5.48 Absorbance signals of diluted (1:4) spiked urine sample at 600°C pyrolysis and 1900°C atomization with 5µg Pd + 3µg Mg modifier in the multi-element determinations of Bi, Sb, and Cd

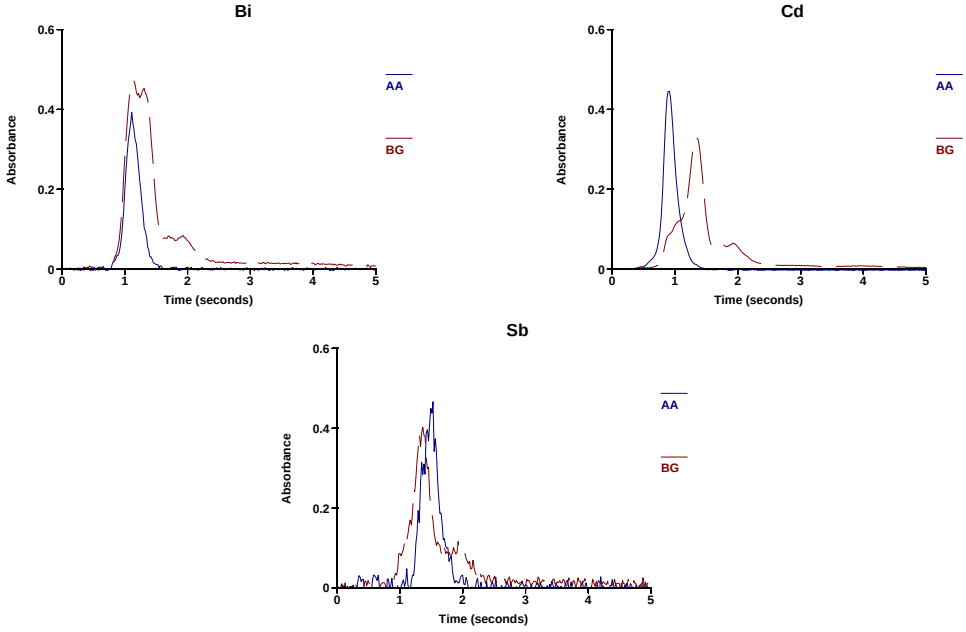

5.8.6.2 With Ir Permanent Modifier

The 500µg iridium was thermally deposited on the graphite tube platform and used as permanent modifier. The diluted reference material (1:4) has been spiked with 80 ppb Bi, 80 ppb Sb, and 2 ppb Cd. 20 µl diluted spiked reference material has been injected into the atomizer each time during this study. The dependence of Bi, Sb, and Cd absorbance on the pyrolysis temperature at 1900°C atomization temperature was studied and shown in Figure 5.49. The atomic signal for Cd remained approximately constant till the pyrolysis temperature

reached 600^{o}C and then decreased rapidly. For Bi and Sb, the atomic signal was almost constant till 900^{o}C and 1200^{o}C, respectively, then started gradually to decrease. A decreased in the pyrolysis temperature comparing with the determination of these elements in the aqueous solution (700, 1200 and 1500^{o}C for Cd, Bi, and Sb, respectively) can be seen. C. G. Magalhães et al.[178] found that with iridium applied in solution together with the urine sample, the best pyrolysis temperature was 900^{o}C but the sensitivity was analogous with that obtained using Pd+Mg modifier. They[178] found also with Ir+Rh permanent modifier that the best pyrolysis temperature was 900^{o}C. Using W+Rh permanent modifier, Oliveira et al.[177] reported 400^{o}C as the best pyrolysis temperature for the determination of Cd in urine sample. E. Bulska et al.[179] determined Sb in biological samples using different types of modifiers and fond that iridium stabilized antimony to higher temperature when compared with palladium, but significant decrease in absorbance value of 23% was observed. In order to determine all three elements simultaneously, 5500^{o}C was chosen as an optimum pyrolysis temperature. The effect of the atomization temperature was studied at the pyrolysis of 550^{o}C. For Cd, the analytical atomic absorption was high at 1000^{o}C (the less atomization temperature can be used) and the signal peak was too broad. Above 1000^{o}C the signal peak start to become sharper and the integrated absorbance value to decrease gradually. For Bi, the atomic absorption signal increased with increasing atomization temperature and had its maximum at atomization temperature between 1400-1500^{o}C and then started to decrease. Sb atomic absorption signal had its maximum at approximately 1800^{o}C atomization temperature. For the simultaneous determination of the elements, 1900^{o}C was chosen as an optimum atomization temperature. The signal absorption peaks at the optimum pyrolysis and atomization temperatures are shown in Figure 5.50.

Figure 5.49 Pyrolysis and atomization curves for multi-element determinations of Bi, Sb, and Cd using 500µg Ir permanent modifier in diluted (1:4) urine sample spiked with 80, 80, and 2 ppb Bi, Sb, and Cd, respectively

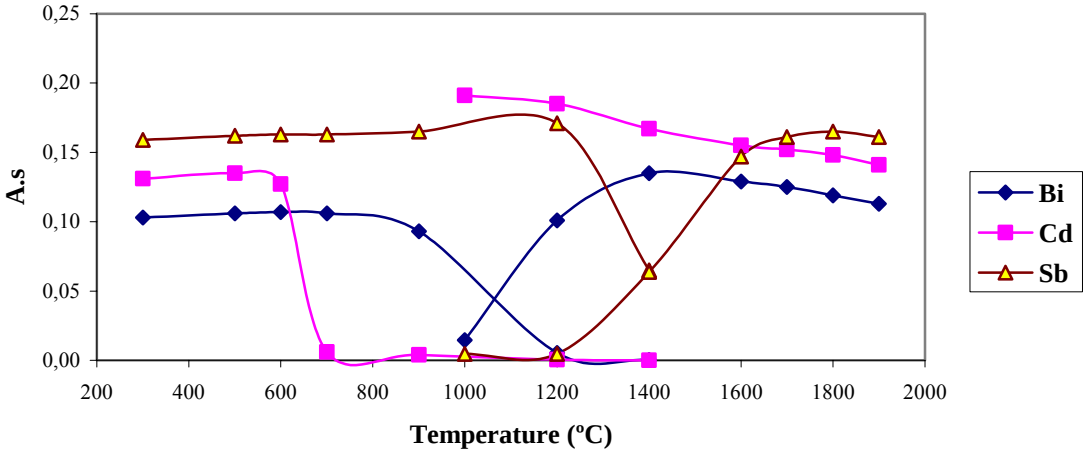

Figure 5.50 Absorbance signals of diluted (1:4) spiked urine sample at 550°C pyrolysis and 1900°C atomization with 500µg Ir permanent modifier in the multi-element determinations of Bi, Sb, and Cd

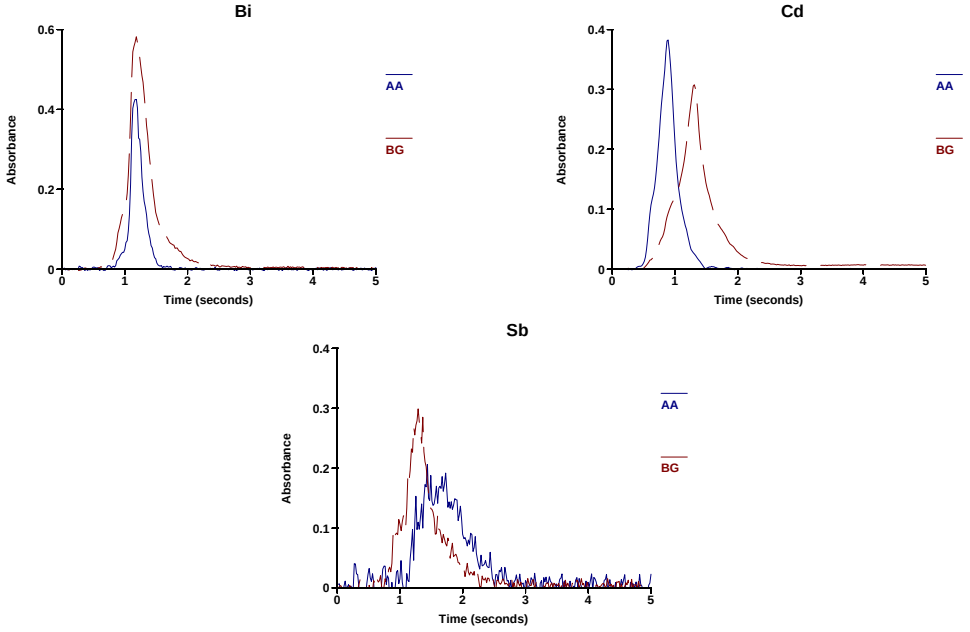

5.9 Analysis of Certified Reference Materials

Number of certified reference materials was used to test the simultaneous determination methodologies that we have developed. The optimum pyrolysis and atomization temperatures that have been developed using urine matrix were used to analyze the reference materials. In all measurements, 20 µl of sample which contains spiked concentrations from each element was injected into the graphite tube. The modifier was injected in a separate step into the tube. The standard addition curves were used to analyze the reference materials. In each

measurement, except the first one, the sample was spiked with different concentrations of the elements in order to get the standard addition curve for each element. The peak area of the atomic absorption signal was used for the determination and each experimental value is the average of five determinations. Generally, the analyzed values for all elements in all reference materials were within the range of certified values.

5.9.1 Multi-Element Determination of Al, Be, Cr, and V

The accuracy of the multi-element determination of this group was confirmed by the analysis of the following certified reference materials: Trace Element Urine Sample from Seronorm, Lyphocheck Urine Metals Control- Level 1 from BIO-RAD, Bovine Liver from National Institute of Standards and Technology, and Pork Liver from National Research Centre for Certified Reference Materials. Each sample has been diluted according to the concentration of the elements in the sample.

5.9.1.1 Trace Element Urine Sample from Seronorm (0511545)

The sample was diluted (1:4, v/v) with 0.2% HNO_3. For each measurement, 20 µl of the diluted sample and 5 µl of 1.00 $g.l^{-1}$ $Mg(NO_2)_3$ modifier solution were injected into the graphite tube at 20^oC. The temperature program is summarized in Table 5.15.

Table 5.15 Optimum Temperature Program for Simultaneous Determination of Al, Be, Cr, and V in Urine reference sample from Seronorm

Step	Temperature (^oC)	Ramp Time (s)	Hold Time (s)	Gas Flow ($ml.min^{-1}$)
Dry 1	110	1	30	250
Dry 2	130	15	30	250
Pyrolysis	1500	10	20	250
Atomization	2500	0	5	0
Clean-out	2550	1	4	250

The standard addition curves for each element are shown in Figure 5.51. The standard addition curves with good linearity (R^2 = 0.9991, 0.999, 0.9994, and 0.9994 for Al, Be, Cr, and V, respectively) were used to determine the concentration of the elements in the sample. The results are summarized and compared with the certified concentrations in Table 5.16. The experimentally determined concentrations were in good agreement with the certified values. The analyzed values were in the range of 96.3, 98.0, 101.0, and 96.8% for Al, Be, Cr, and V, respectively. The relative standard deviations (RSD) of the non spiked sample measurements

were in the range: 2.5-4.8% for Al, 0.8-2.6% for Be, 1.0-1.6% for Cr, and 1.4-7.4% for V. Detection limits were calculated as three times the standard deviation of ten replicate measurements of the blank. The detection limits (LOD) and the characteristic mass were determined and given in Table 5.17.

Figure 5.51 The standard addition curves in the multi-element determination of Al, Be, Cr, and V in urine reference sample from Seronorm

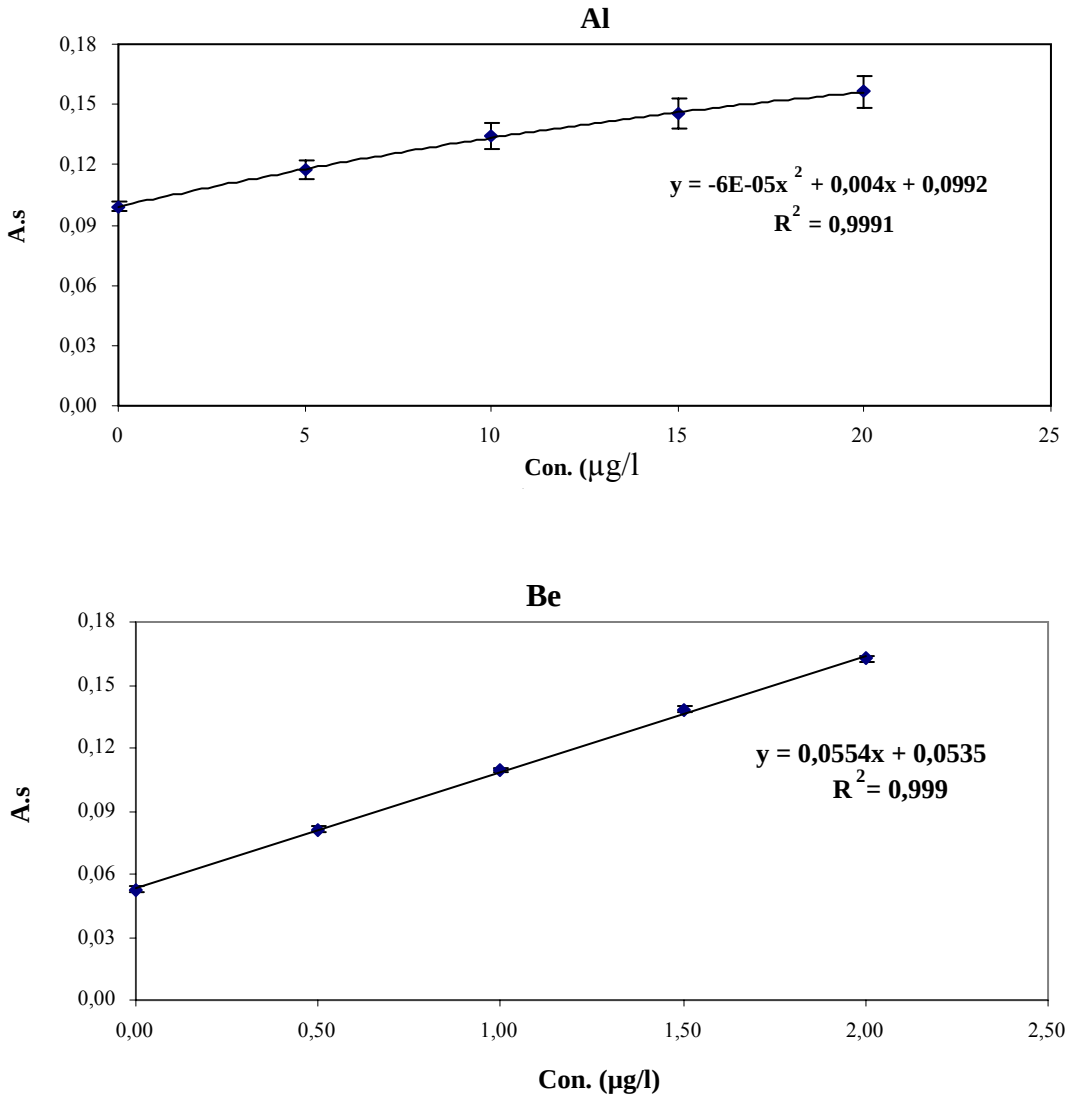

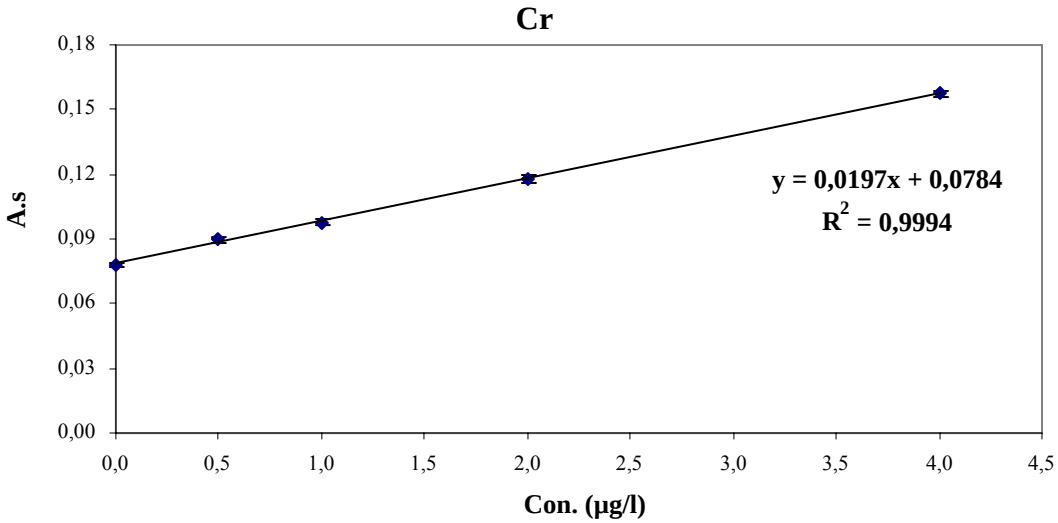

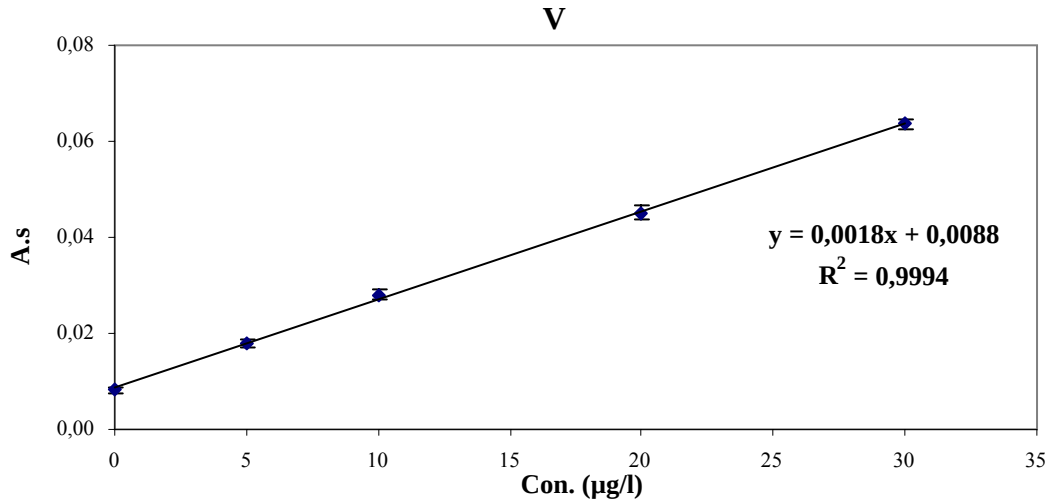

Table 5.16 The results of simultaneous determination of Al, Be, Cr, and V in urine reference sample from Seronorm

Element	Con. Found (ppb)	Certified		
		Con. (ppb)	Uncertainty	Acceptable range
Al	96.3	100	94-106	88-112
Be	4.8	4.9	4.7-5.1	4.5-5.3
Cr	19.9	19.7	18.4-21.0	17.1-22.3
V	24.4	25.2	23.8-26.6	22.4-28.0

Table 5.17 Detection limits, characteristic mass, and relative standard deviations for simultaneous determination of Al, Be, Cr, and V in urine reference material from Seronorm

Element	LOD (µg.l^{-1})	CM (pg)	RSD* (%)
Al	0.96	31.4	2.5
Be	0.022	1.6	2.6
Cr	0.11	4.5	1.4
V	0.83	48.9	7.4

*For five sample measurements.

5.9.1.2 Lyphochek Urine Metals Control Level 1 from BIO-RAD (69061)

The sample was diluted (1:1, v/v) with 0.2% HNO_3. For each measurement, 20 µl of the diluted sample and 5 µl of 1.00 $g.l^{-1}$ $Mg(NO_2)_3$ modifier solution were injected into the graphite tube at 20°C. There were no certified values for beryllium and vanadium, there fore, the sample has been spiked with them before the dilution. The optimum temperature program was as in Table 5.15.

The standard addition curves for each element are shown in Figure 5.52. The standard addition curves with good linearity (R^2 = 0.9996, 0.9998, 0.9999, and 0.9997 for Al, Be, Cr, and V, respectively) were used to evaluate the concentration of the elements in the sample. The results are summarized and compared with the certified concentrations in Table 5.18. The experimentally determined concentrations were in good agreement with the certified values. The analyzed values were in the range of 111.3, 91.7, 95.0, and 100.0% for Al, Be, Cr, and V, respectively. The relative standard deviations (RSD) of the non spiked sample measurements were in the range: 1.3-1.8% for Al, 0.8-2.6% for Be, 0.7-1.3% for Cr, and 0.8-2.3% for V. Detection limits were calculated as three times the standard deviation of ten replicate measurements of the blank. The detection limits (LOD) and the characteristic mass were determined and given in Table 5.19.

Figure 5.52 The standard addition curves in the multi-element determination of Al, Be, Cr, and V in urine reference sample from BIO-RAD

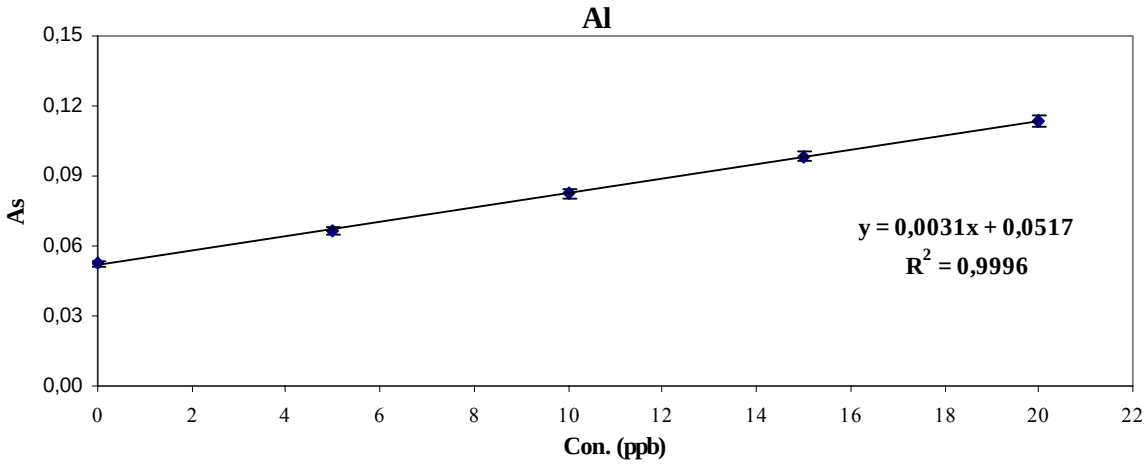

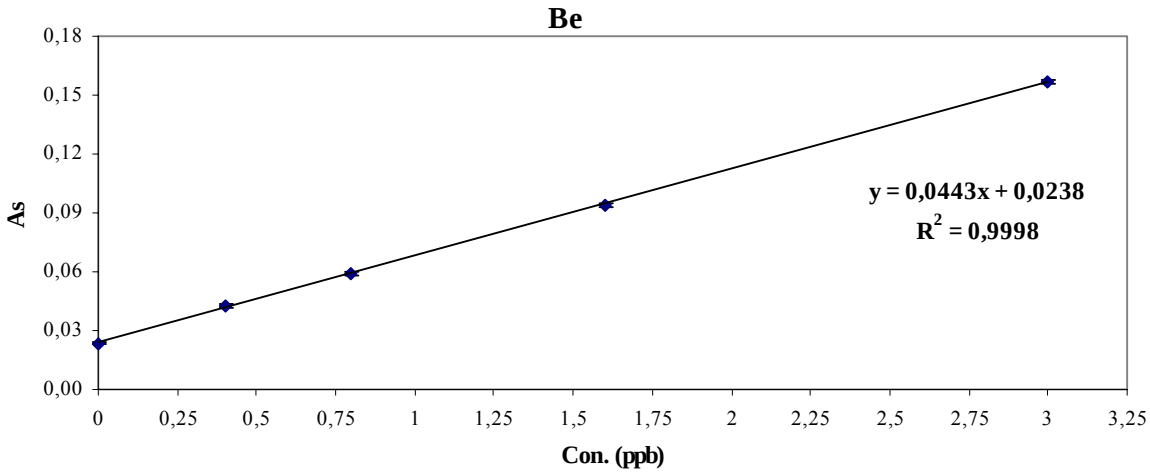
Be
0,18
0,15
0,12
0,09
0,06
0,03
0,00
As
y = 0,0443x + 0,0238
R2 = 0,9998
0
0,25
0,5
0,75
1
1,25
1,5
1,75
2
2,25
2,5
2,75
3
3,25
Con. (ppb)

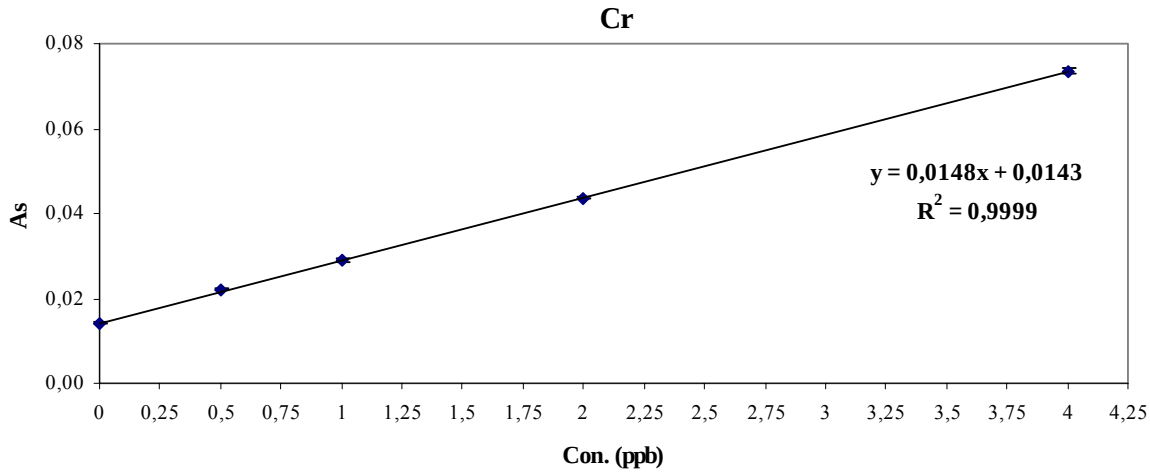
Cr
0,08
0,06
0,04
0,02
0,00
As
y = 0,0148x + 0,0143
R2 = 0,9999
0
0,25
0,5
0,75
1
1,25
1,5
1,75
2
2,25
2,5
2,75
3
3,25
3,5
3,75
4
4,25
Con. (ppb)

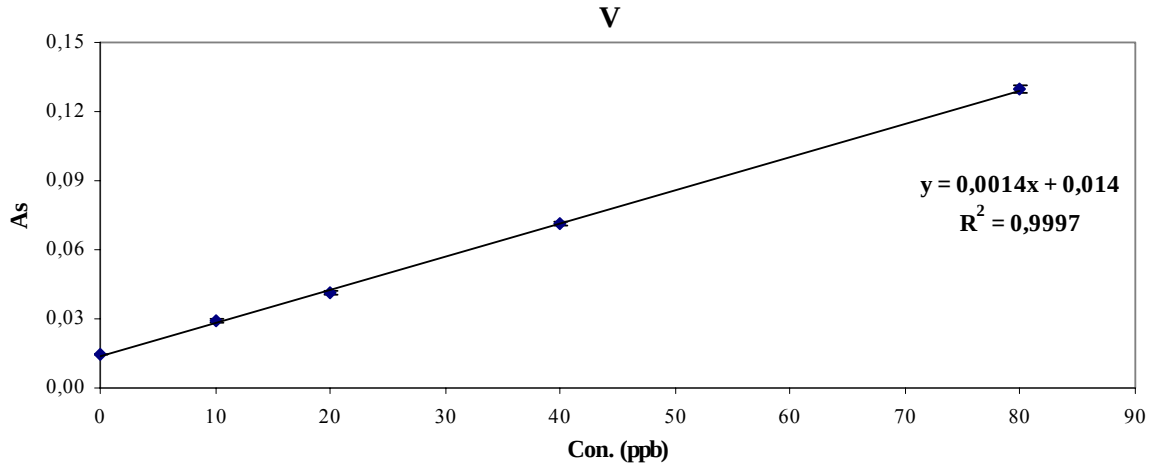
V
0,15
0,12
0,09
0,06
0,03
0,00
As
y = 0,0014x + 0,014
R2 = 0,9997
0
10
20
30
40
50
60
70
80
90
Con. (ppb)

Table 5.18 The results of simultaneous determination of Al, Be, Cr, and V in urine reference sample from BIO-RAD

Element	Con. Found (ppb)	Certified	
		Con. (ppb)	Acceptable range
Al	33.4	30	24-36
Be	1.1	1.2*	-
Cr	1.9	2.0	1.5-2.5
V	20	20*	-

*They have been added.

Table 5.19 Detection limits, characteristic mass, and relative standard deviations for simultaneous determination of Al, Be, Cr, and V in urine reference material from BIO-RAD

Element	LOD ($\mu g.l^{-1}$)	CM (pg)	RSD* (%)
Al	0.68	28.4	1.3
Be	0.027	2.0	2.1
Cr	0.081	5.9	1.3
V	0.86	62.9	0.8

*For five sample measurements.

5.9.1.3 Bovine Liver from National Institute of Standards and Technology (NIST-SRM 1577b)

After the digestion with HNO_3, the sample was transferred into 50 ml volumetric flask and made up to the mark with de-ionized water. Since there were no certified values for beryllium and chromium and the concentration of vanadium is too low for the determination, the sample has been spiked with the elements before the addition of de-ionized water. Before the simultaneous determination of Al, Be, Cr, and V, the sample was diluted (1:9, v/v) with 0.2% HNO_3. The optimum temperature program for the simultaneous determination was as in Table 5.15.

The standard addition curves for each element are shown in Figure 5.53. The standard addition curves with good linearity (R^2 = 0.9999, 0.9998, 0.9999, and 0.9999 for Al, Be, Cr, and V, respectively) were used to determine the concentration of the elements in the sample. The results are summarized and compared with the certified concentrations in Table 5.20. The experimentally determined concentrations were in good agreement with the certified values. The analyzed values were in the range of 99.4, 102.0, 96.5, and 100.0% for Al, Be, Cr, and V, respectively. The relative standard deviations (RSD) of the non spiked sample measurements were in the range: 0.4-2.8% for Al, 0.8-2.0% for Be, 0.3-5.1% for Cr, and 1.6-4.2% for V. Detection limits were calculated as three times the standard deviation of ten replicate measurements of the blank. The detection limits (LOD) and the characteristic mass were determined and given in Table 5.21.

Figure 5.53 The standard addition curves in the multi-element determination of Al, Be, Cr, and V in Bovine Liver sample

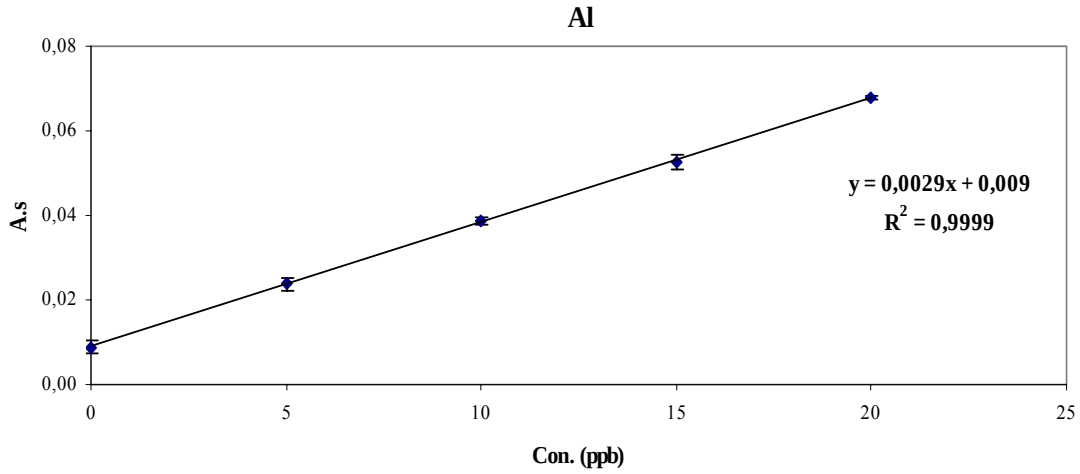

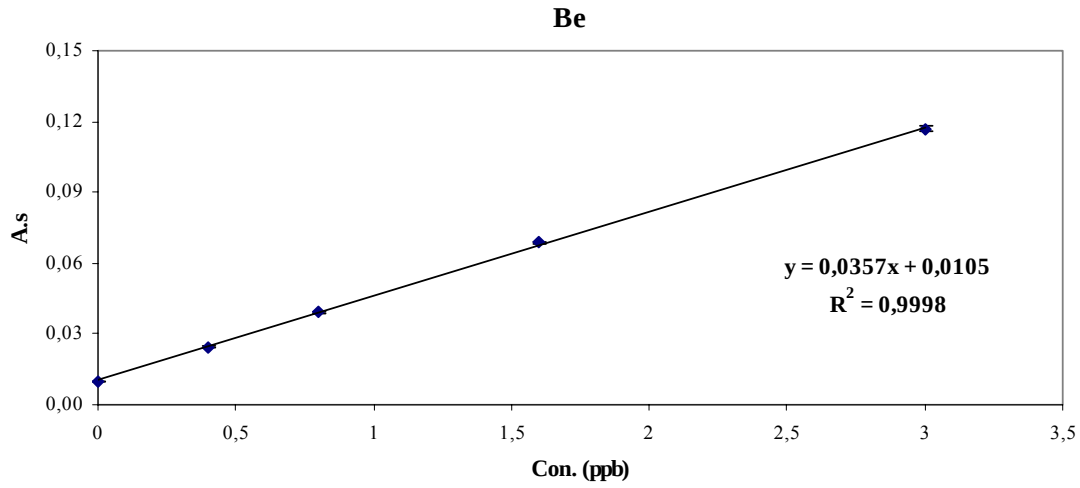

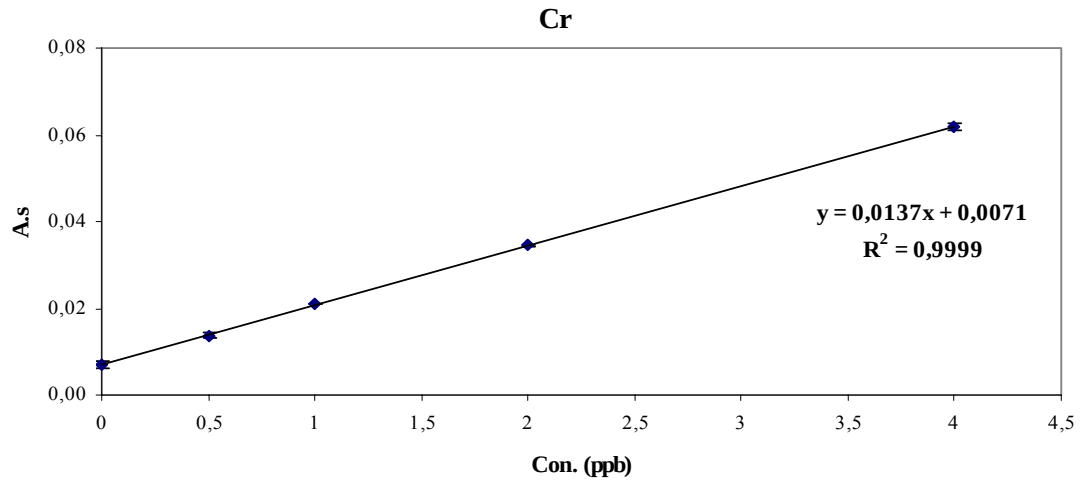

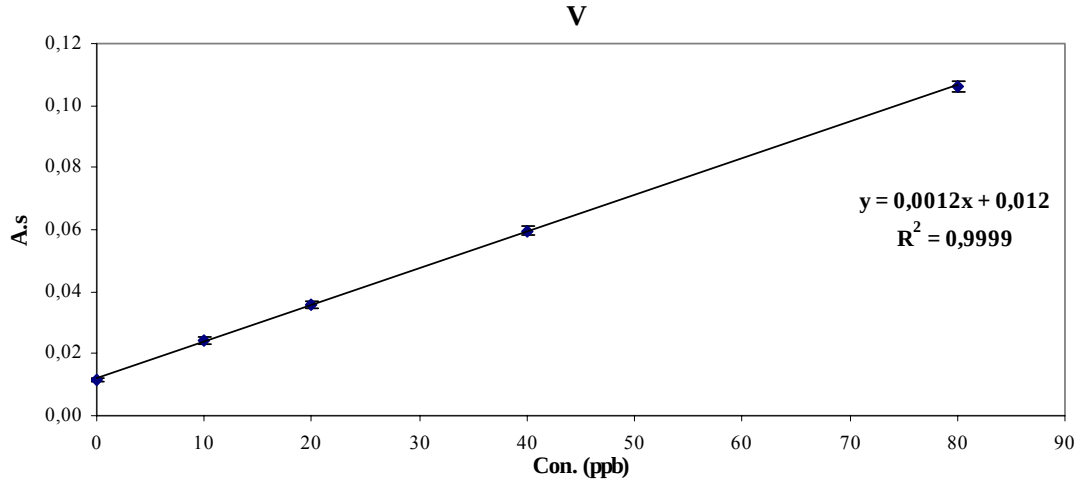

Table 5.20 The results of simultaneous determination of Al, Be, Cr, and V in Bovine Liver sample

Element	Con. Found (µg)	Con. certified (µg)
Al	1.54	1.55
Be	0.150	0.147*
Cr	0.250	0.259*
V	5.00	5.00*

*They have been added.

Table 5.21 Detection limits, characteristic mass, and relative standard deviations for simultaneous determination of Al, Be, Cr, and V in Bovine Liver sample

Element	LOD (µg.l^{-1})	CM (pg)	RSD* (%)
Al	0.62	30.3	2.8
Be	0.034	2.5	1.0
Cr	0.088	6.4	5.1
V	1.5	73.3	2.7

*From five replicates

5.9.1.4 Pork Liver from National Research Centre for Certified Reference Materials (GBW 08551)

After the digestion with HNO_3, the sample was transferred into 50 ml volumetric flask and made up to the mark with de-ionized water. Since there were no certified values for aluminium, beryllium, and vanadium, the sample has been spiked with the elements before the addition of de-ionized water. Before the simultaneous determination of Al, Be, Cr, and V, the sample was diluted (1:3, v/v) with 0.2% HNO_3. The optimum temperature program for the simultaneous determination was as in Table 5.15.

The standard addition curves for each element are shown in Figure 5.54. The standard addition curves with good linearity (R^2 = 0.9995, 0.9999, 0.9998, and 0.9999 for Al, Be, Cr, and V, respectively) were used to determine the concentration of the elements in the sample. The results are summarized and compared with the certified concentrations in Table 5.22. The experimentally determined concentrations were in good agreement with the certified values.

The analyzed values were in the range of 117.0, 96.0, 100.0, and 100.0% for Al, Be, Cr, and V, respectively. The relative standard deviations (RSD) of the non spiked sample measurements were in the range: 1.3-2.1% for Al, 0.3-3.9% for Be, 0.5-1.6% for Cr, and 1.4-4.1% for V. Detection limits were calculated as three times the standard deviation of ten replicate measurements of the blank. The detection limits (LOD) and the characteristic mass were determined and given in Table 5.23.

Figure 5.54 The standard addition curves in the multi-element determination of Al, Be, Cr, and V in Pork Liver sample

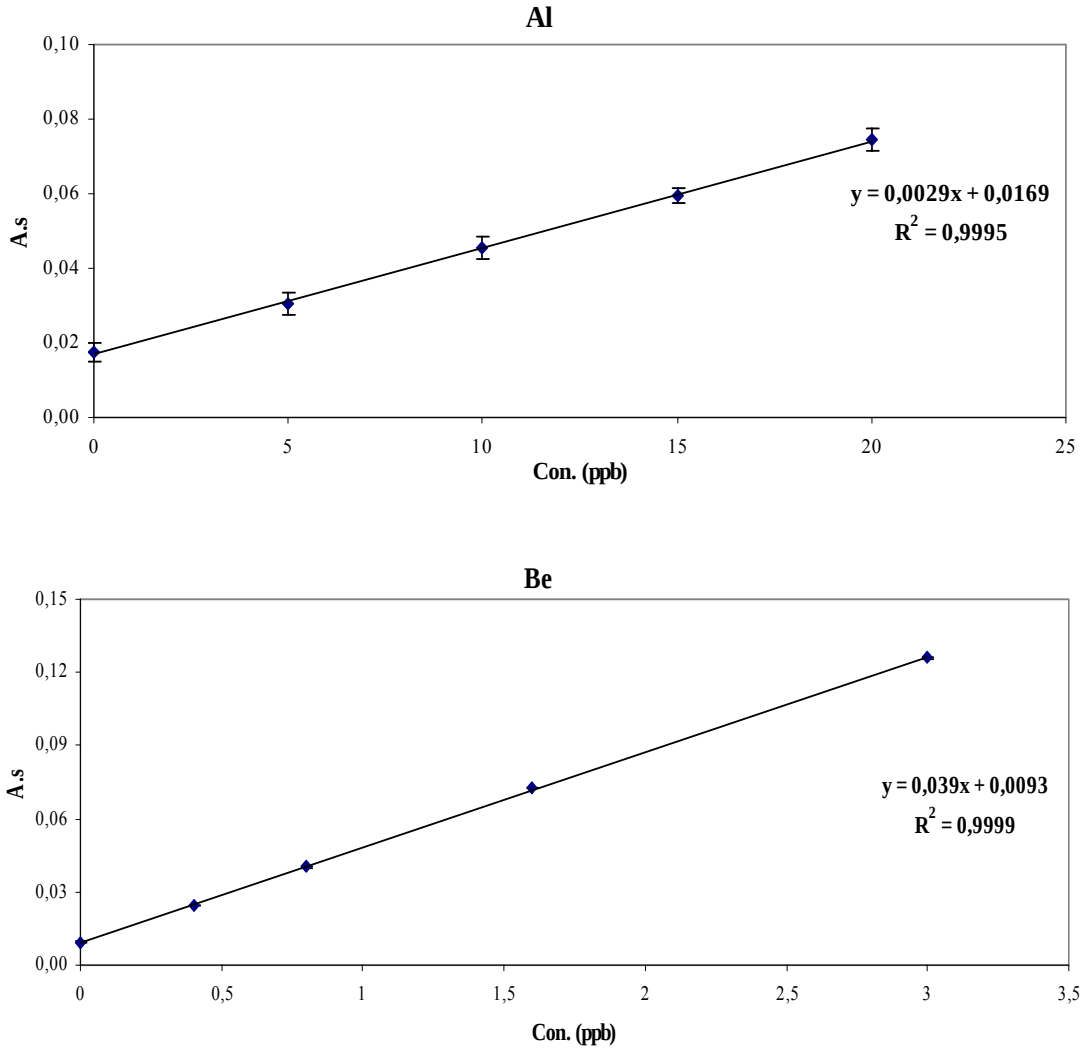

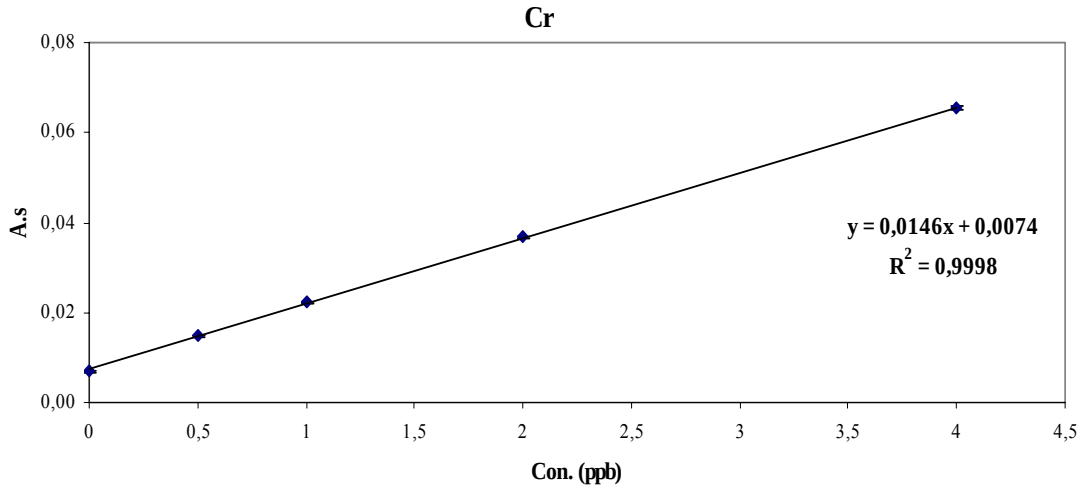

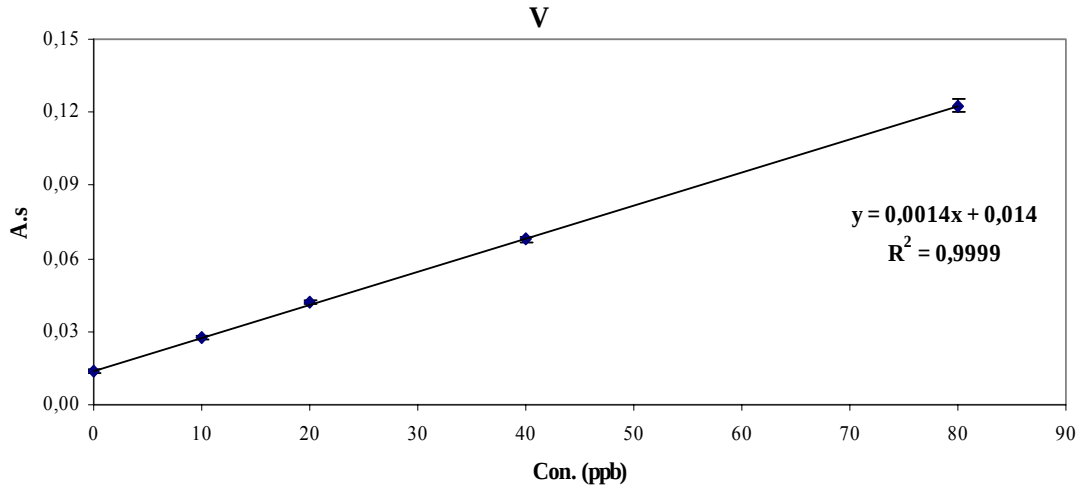

Table 5.22 The results of simultaneous determination of Al, Be, Cr, and V in Pork Liver sample

Element	Con. Found (µg)	Con. certified (µg)
Al	1.17	1.00*
Be	0.048	0.050*
Cr	0.101	0.101
V	2.00	2.00*

*They have been added

Table 5.23 Detection limits, characteristic mass, and relative standard deviations for simultaneous determination of Al, Be, Cr, and V in Pork Liver sample

Element	LOD (µg.l^{-1})	CM (pg)	RSD* (%)
Al	0.62	30.3	2.0
Be	0.031	2.3	3.9
Cr	0.082	6.0	1.6
V	0.86	62.9	4.1

*From five replicates

5.9.1.5 Comparison of the results of Different Samples

By comparing the results of the samples, the same experimental conditions; pyrolysis (1500^{o}C) and atomization (2500^{o}C) temperatures, have been used for the simultaneous

determinations in different types of samples with different dilutions. From the detection limits values, the results were similar to those of aqueous solution. The highest increased in the values compared to aqueous solution were as follows: 1.5 times in Seronorm urine for Al, 1.6 times in bovine liver for Be, 1.4 times in Seronorm urine for Cr, and 2.2 times in bovine liver for V. The most increased in detection limits values were in the case of Seronorm urine and bovine liver samples which have the highest dilution factor (1:4 and 1:9, respectively). The results of characteristic mass, however, were comparable to those of aqueous solution and the increasing percentages were in the range of: - 6.6% to + 3.3% for Al, - 20% to + 25% for Be, - 4.3% to + 36.2% for Cr, and 0% to +49.9% for V. The lowest sensitivity values were obtained with bovine liver sample and the highest sensitivities with Seronorm.

5.9.2 Multi-Element Determination of Be, Cr, and Cu

The accuracy of the multi-element determination of this group was confirmed by the analysis of the following certified reference materials: Trace Element Urine Sample from Seronorm, Lyphocheck Urine Metals Control- Level 1 from BIO-RAD, Bovine Liver from National Institute of Standards and Technology, Bovine Liver from National Institute of Standards and Technology, and Tea sample from National Research Centre for Certified Reference Materials. Each sample has been diluted according to the concentration of the elements in the sample.

5.9.2.1 Trace Element Urine Sample from Seronorm (0511545)

The sample was diluted (1:4, v/v) with 0.2% HNO_3. For each measurement, 20 µl of the diluted sample, 5 µl of 1.00 $g.l^{-1}$ $Pd(NO_2)_3$ and 3 µl 1.00 $g.l^{-1}$ $Mg(NO_2)_3$ modifier solution were injected into the graphite tube at 20^oC. The temperature program is summarized in Table 5.24.

Table 5.24 Optimum Temperature Program for Simultaneous Determination of Be, Cr, and Cu in Urine reference sample from Seronorm

Step	Temperature (^oC)	Ramp Time (s)	Hold Time (s)	Gas Flow ($ml.min^{-1}$)
Dry 1	110	1	30	250
Dry 2	130	15	30	250
Pyrolysis	1200	10	20	250
Atomization	2300	0	5	0
Clean-out	2500	1	4	250

The standard addition curves for each element are shown in Figure 5.55. The standard addition curves with good linearity (R^2 = 0.9992, 0.9968, and 0.9981 for Be, Cr, and Cu, respectively) were used to determine the concentration of the elements in the sample. The results are summarized and compared with the certified concentrations in Table 5.25. The experimentally determined concentrations were in good agreement with the certified values. The analyzed values were in the range of 95.9, 102.0, and 101.1% for Be, Cr, and Cu, respectively. The relative standard deviations (RSD) of the non spiked sample measurements were in the range: 2.1-5.6% for Be, 0.4-2.0% for Cr, and 0.6-1.8% for Cu. Detection limits were calculated as three times the standard deviation of ten replicate measurements of the blank. The detection limits (LOD) and the characteristic mass were determined and given in Table 5.26.

Figure 5.55 The standard addition curves in the multi-element determination of Be, Cr, and Cu in urine reference sample from Seronorm

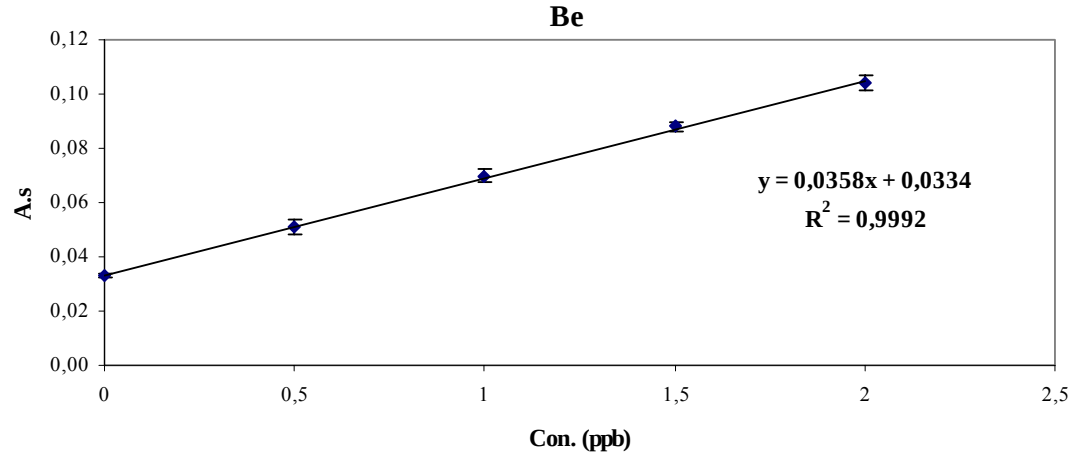

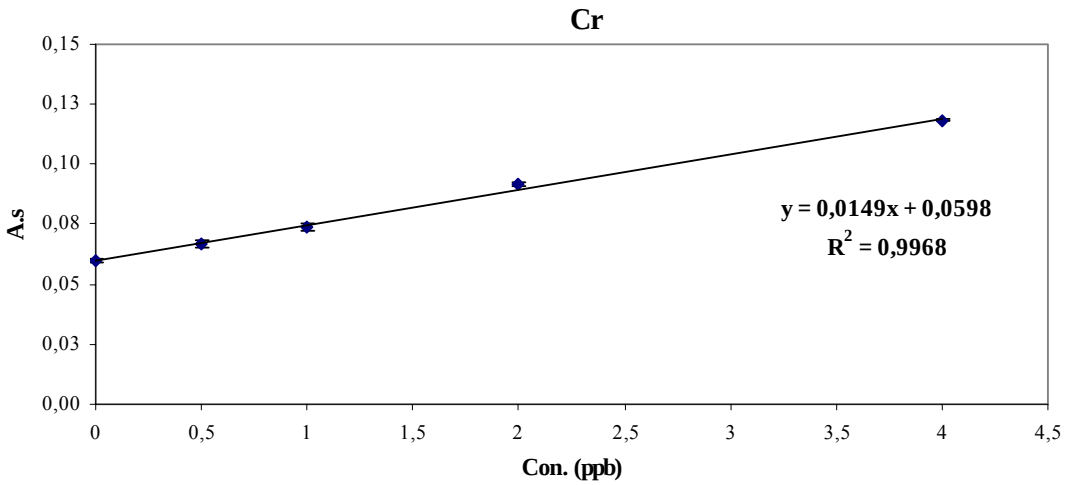

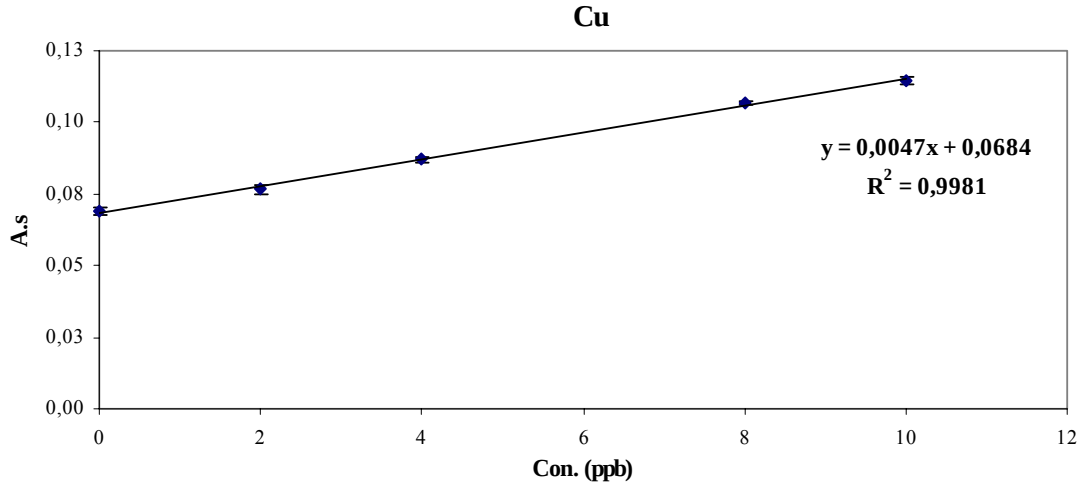

Table 5.25 The results of simultaneous determination of Be, Cr, and Cu in urine reference sample from Seronorm

Element	Con. Found (ppb)	Certified		
		Con. (ppb)	Uncertainty	Acceptable range
Be	4.7	4.9	4.7-5.1	4.5-5.3
Cr	20.1	19.7	18.4-21.0	17.1-22.3
Cu	72.8	72	±3	-

Table 5.26 Detection limits, characteristic mass, and relative standard deviations for simultaneous determination of Be, Cr, and Cu in urine reference material from Seronorm

Element	LOD ($\mu g.l^{-1}$)	CM (pg)	RSD* (%)
Be	0.042	2.5	2.1
Cr	0.081	5.9	1.2
Cu	0.26	18.7	1.6

*Five replicate measurements

5.9.2.2 Lyphochek Urine Metals Control–Level 1 from BIO-RAD (69061)

The sample was diluted (1:1, v/v) with 0.2% HNO_3. For each measurement, 20 µl of the diluted sample, 5 µl of 1.00 $g.l^{-1}$ $Pd(NO_3)_2$ and 3 µl of 1.00 $g.l^{-1}$ $Mg(NO_2)_3$ modifier solution were injected into the graphite tube at 20°C. There was no certified value for beryllium; therefore, the sample has been spiked with beryllium before the dilution. The optimum temperature program was as in Table 5.24.

The standard addition curves for each element are shown in Figure 5.56. The standard addition curves with good linearity (R^2 = 0.9998, 0.9999, and 0.9998 for Be, Cr, and Cu, respectively) were used to determine the concentration of the elements in the sample. The results are summarized and compared with the certified concentrations in Table 5.27. The experimentally determined concentrations were in good agreement with the certified values. The analyzed values were in the range of 91.7, 90.0, and 100.0% for Be, Cr, and Cu, respectively. The relative standard deviations (RSD) of the non spiked sample measurements

were in the range: 1.7-4.8% for Be, 1.1-3.0% for Cr, and 1.4-2.7% for Cu. Detection limits were calculated as three times the standard deviation of ten replicate measurements of the blank. The detection limits (LOD) and the characteristic mass were determined and given in Table 5.28.

Figure 5.56 The standard addition curves in the multi-element determination of Be, Cr, and Cu in urine reference sample from BIO-RAD

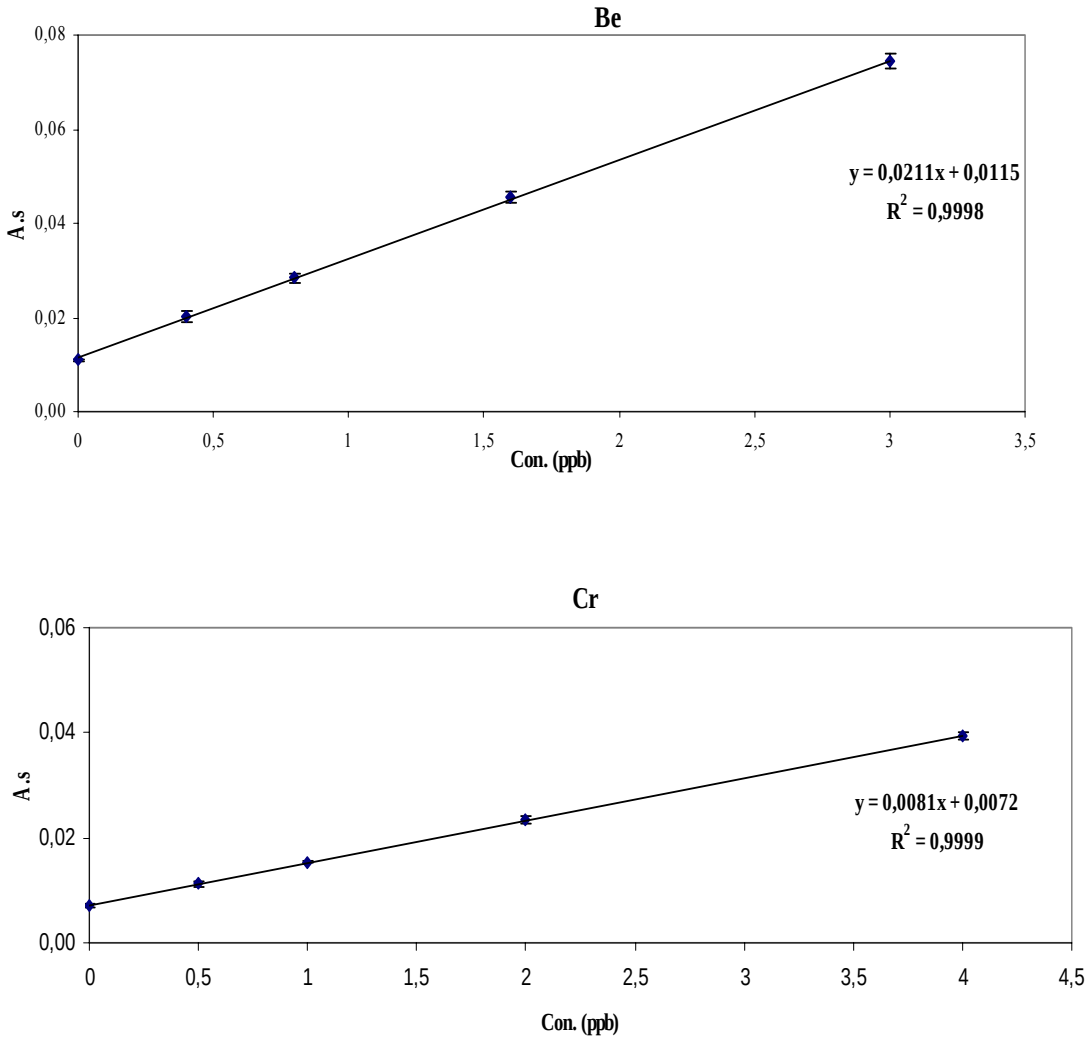

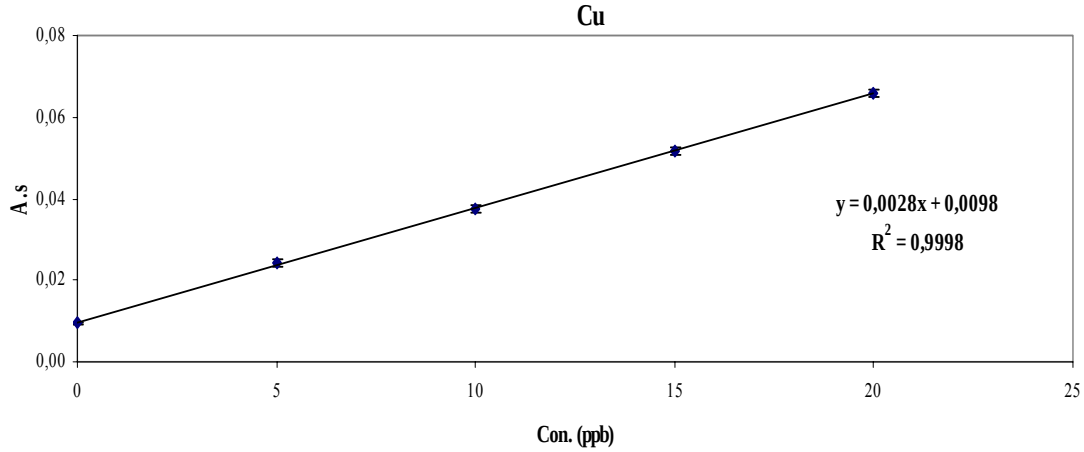

Table 5.27 The results of simultaneous determination of Be, Cr, and Cu in urine reference sample from BIO-RAD

Element	Con. Found (ppb)	Certified	
		Con. (ppb)	Acceptable range
Be	1.1	1.2*	-
Cr	1.8	2	1.5-2.5
Cu	7	7	5.3-8.8

*added

Table 5.28 Detection limits, characteristic mass, and relative standard deviations for simultaneous determination of Be, Cr, and Cu in urine reference material from BIO-RAD

Element	LOD ($\mu g.l^{-1}$)	CM (pg)	RSD* (%)
Be	0.057	4.2	1.7
Cr	0.074	10.9	2.8
Cu	0.21	31.4	2.1

*Five replicate measurements

5.9.2.3 Tea sample from National Research Centre for Certified Reference Materials (GBW 08505)

The sample was diluted (1:39, v/v) with 0.2% HNO_3. For each measurement, 20 µl of the diluted sample, 5 µl of 1.00 $g.l^{-1}$ $Pd(NO_3)_2$ and 3 µl of 1.00 $g.l^{-1}$ $Mg(NO_2)_3$ modifier solution were injected into the graphite tube at 20°C. There was no certified value for beryllium; therefore, the sample has been spiked with beryllium before the dilution. The optimum temperature program was as in Table 5.24.

The standard addition curves for each element are shown in Figure 5.57. The standard addition curves with good linearity (R^2 = 1.0, 0.9999, and 0.9998 for Be, Cr, and Cu, respectively) were used to evaluate the concentration of the elements in the sample. The results are summarized and compared with the certified values in Table 5.29. The experimentally determined concentrations were in good agreement with the certified

concentrations. The analyzed values were in the range of 98.0, 98.8, and 99.4% for Be, Cr, and Cu, respectively. The relative standard deviations (RSD) of the non spiked sample measurements were in the range: 1.1-6.3% for Be, 0.5-2.4% for Cr, and 0.2-1.0% for Cu. Detection limits were calculated as three times the standard deviation of ten replicate measurements of the blank. The detection limits (LOD) and the characteristic mass were determined and given in Table 5.30.

Figure 5.57 The standard addition curves in the multi-element determination of Be, Cr, and Cu in Tea sample

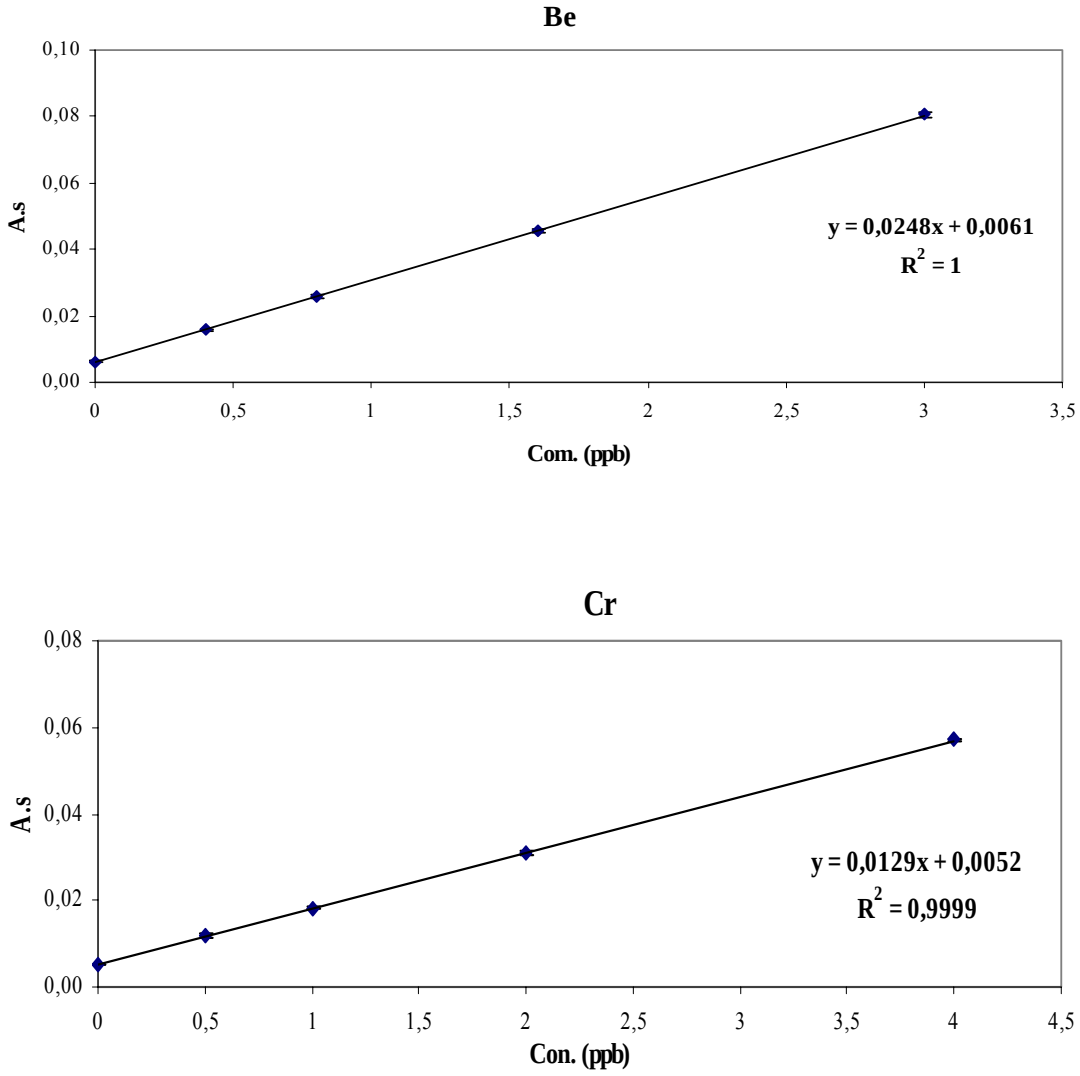

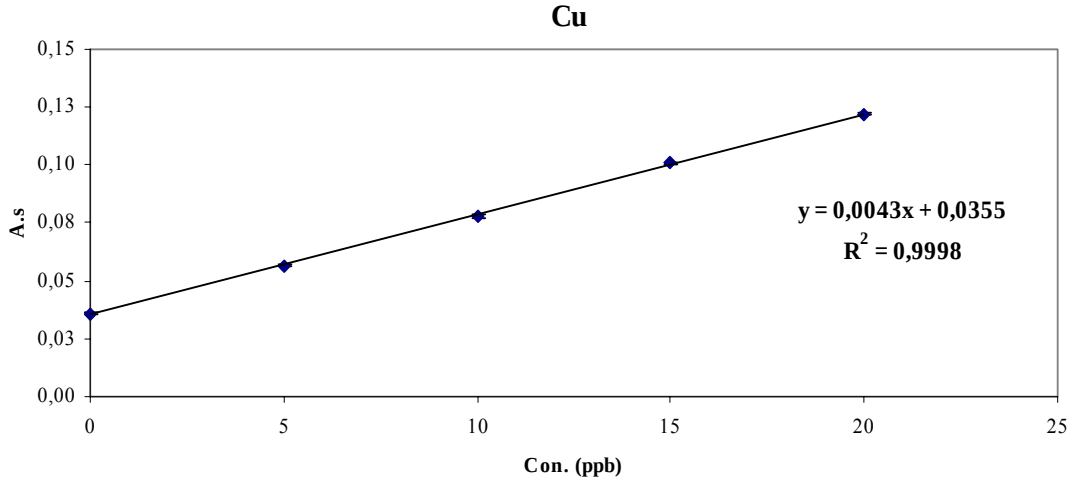

Table 5.29 The results of simultaneous determination of Be, Cr, and Cu in Tea sample

Element	Con. Found (µg)	Con. certified (µg)
Be	0.49	0.50*
Cr	0.81	0.82
Cu	16.5	16.6

*added

Table 5.30 Detection limits, characteristic mass, and relative standard deviations for simultaneous determination of Be, Cr, and Cu in Tea sample

Element	LOD (µg.l^{-1})	CM (pg)	RSD* (%)
Be	0.036	3.5	6.3
Cr	0.070	6.8	2.0
Cu	0.28	20.5	0.2

*Five replicate measurements

5.9.2.4 Bovine Liver from National Institute of Standards and Technology (NIST-SRM 1577b)

The sample was diluted (1:99, v/v) with 0.2% HNO_3. For each measurement, 20 µl of the diluted sample, 5 µl of 1.00 g.l^{-1} $Pd(NO_3)_2$ and 3 µl of 1.00 g.l^{-1} $Mg(NO_2)_3$ modifier solution were injected into the graphite tube at 20^{o}C. There were no certified values for beryllium and chromium; therefore, the sample has been spiked with them before the dilution. The optimum temperature program was as in Table 5.24.

The standard addition curves for each element are shown in Figure 5.58. The standard addition curves with good linearity (R^2 = 0.9999, 0.9997, and 0.9995 for Be, Cr, and Cu, respectively) were used to determine the concentration of the elements in the sample. The results are summarized and compared with the certified concentrations in Table 5.31. The experimentally determined concentrations were in good agreement with the certified values. The analyzed values were in the range of 103.2, 96.0, and 86.0% for Be, Cr, and Cu, respectively. The relative standard deviations (RSD) of the non spiked sample measurements

were in the range: 2.8-9.1% for Be, 3.2-4.9% for Cr, and 1.8-3.3% for Cu. Detection limits were calculated as three times the standard deviation of ten replicate measurements of the blank. The detection limits (LOD) and the characteristic mass were determined and given in Table 5.32.

Figure 5.58 The standard addition curves in the multi-element determination of Be, Cr, and Cu in Bovine Liver sample

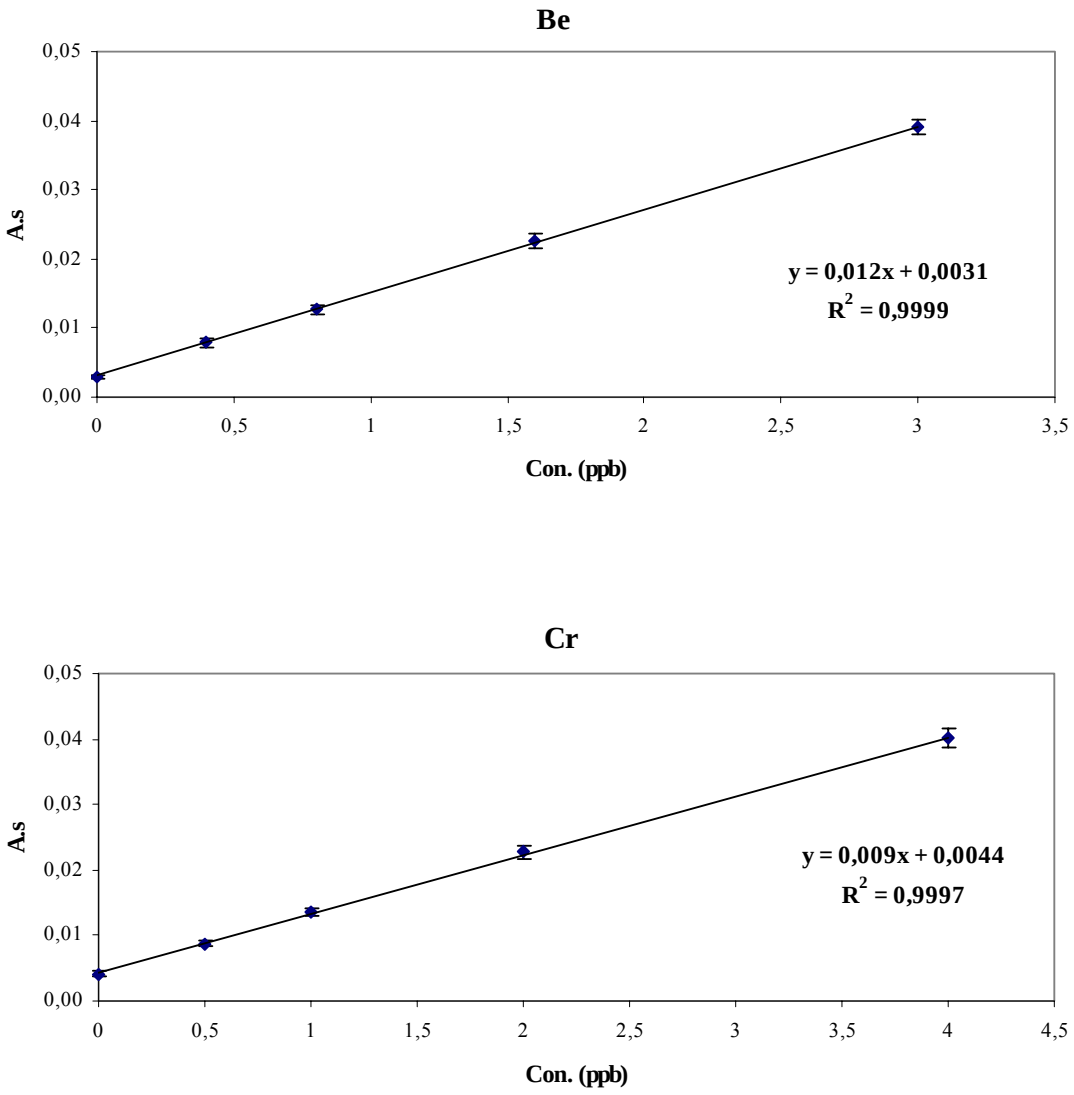

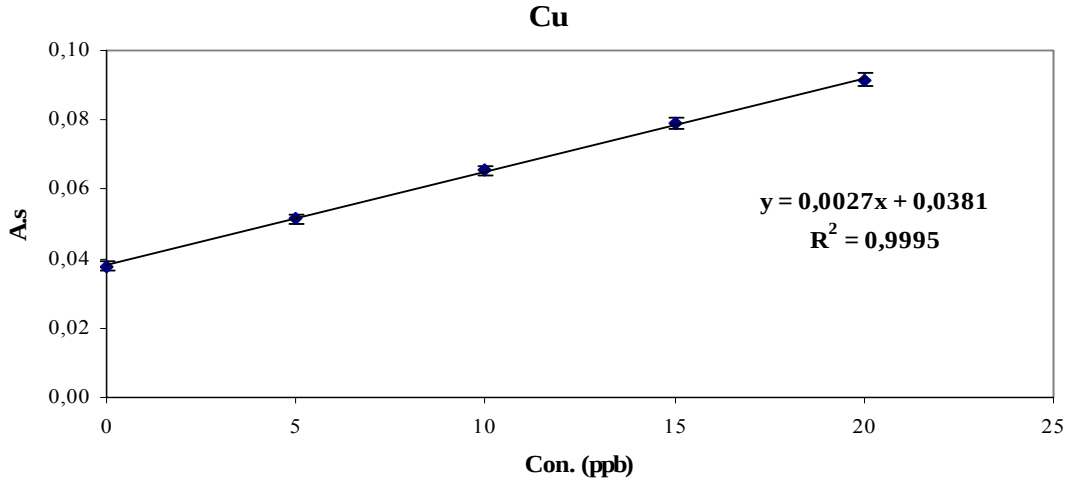

Table 5.31 The results of simultaneous determination of Be, Cr, and Cu in Bovine Liver

Element	Con. Found (µg)	Con. certified (µg)
Be	1.29	1.25*
Cr	2.4	2.5*
Cu	70.6	82.1

*added

Table 5.32 Detection limits, characteristic mass, and relative standard deviations for simultaneous determination of Be, Cr, and Cu in Bovine Liver

Element	LOD (µg.l^{-1})	CM (pg)	RSD* (%)
Be	0.05	7.3	9.1
Cr	0.070	9.8	4.9
Cu	0.44	32.6	3.3

5.9.2.5 Comparison of the Results of Different Samples

The experimental conditions; pyrolysis (1200^{o}C) and atomization (2300^{o}C) temperatures, were as same as for the simultaneous determinations in different types of samples with different dilutions. The detection limits values of sample results were comparable to those of aqueous solution. The highest increasings in the values compared to aqueous solution were as follows: 1.9 times in Bio-Rad urine for Be, 1.5 times in Seronorm urine for Cr, and 3 times in bovine liver for Cu. The most increasing in detection limits values was in the determination of Cu in bovine liver which has a highest dilution factor (1:99). The results of characteristic mass, however, were comparable to those of aqueous solution and the increased percentages were in the range of: - 43% to + 66% for Be, - 25% to + 38% for Cr, and - 11% to +55% for Cu. The lowest sensitivity values, as in multi-element determination of Al, Be, Cr, and V, were obtained with bovine liver sample and the highest sensitivities with Seronorm urine sample.

5.9.3 Multi-Element Determination of Bi, Cu, Mn, and Sb

The accuracy of the multi-element determination of this group was confirmed by the analysis of the following certified reference materials: Trace Element Urine Sample from Seronorm, Lyphocheck Urine Metals Control- Level 1 from BIO-RAD, Bovine Liver from National Institute of Standards and Technology, and Pig Kidney from Institute for Reference Materials and Measurements Each sample has been diluted according to the concentration of the elements in the sample.

5.9.3.1 Trace Element Urine Sample from Seronorm (0511545)

The sample was diluted (1:4, v/v) with 0.2% HNO_3. For each measurement, 20 µl of the diluted sample, 5 µl of 1.00 $g.l^{-1}$ $Pd(NO_2)_3$ and 3 µl 1.00 $g.l^{-1}$ $Mg(NO_2)_3$ modifier solution were injected into the graphite tube at 20^oC. The temperature program is summarized in Table 5.33.

Table 5.33 Optimum Temperature Program for Simultaneous Determination of Bi, Sb, Cu, and Mn in Urine reference sample from Seronorm

Step	Temperature (^oC)	Ramp Time (s)	Hold Time (s)	Gas Flow ($ml.min^{-1}$)
Dry 1	110	1	30	250
Dry 2	130	15	30	250
Pyrolysis	1000	10	20	250
Atomization	2000	0	5	0
Clean-out	2500	1	4	250

The standard addition curves for each element are shown in Figure 5.59. The standard addition curves with good linearity (R^2 = 0.9999, 0.9979, 0.9997, and 0.9992 for Bi, Cu, Mn, and Sb, respectively) were used to determine the concentration of the elements in the sample. The results are summarized and compared with the certified concentrations in Table 5.34. The experimentally determined concentrations were in good agreement with the certified values. The analyzed values were in the range of 97.5, 104.6, 111.4, and 105.9% for Bi, Cu, Mn, and Sb, respectively. The relative standard deviations (RSD) of the non spiked sample measurements were in the range: 0.9-2.8% for Cu, 0.7-2.3% for Mn, 1.2-2.7% for Bi, and 1.2-4.3% for Sb. Detection limits were calculated as three times the standard deviation of ten replicate measurements of the blank. The detection limits (LOD) and the characteristic mass were determined and given in Table 5.35.

Figure 5.59 The standard addition curves in the multi-element determination of Bi, Cu, Mn, and Sb in urine reference sample from Seronorm

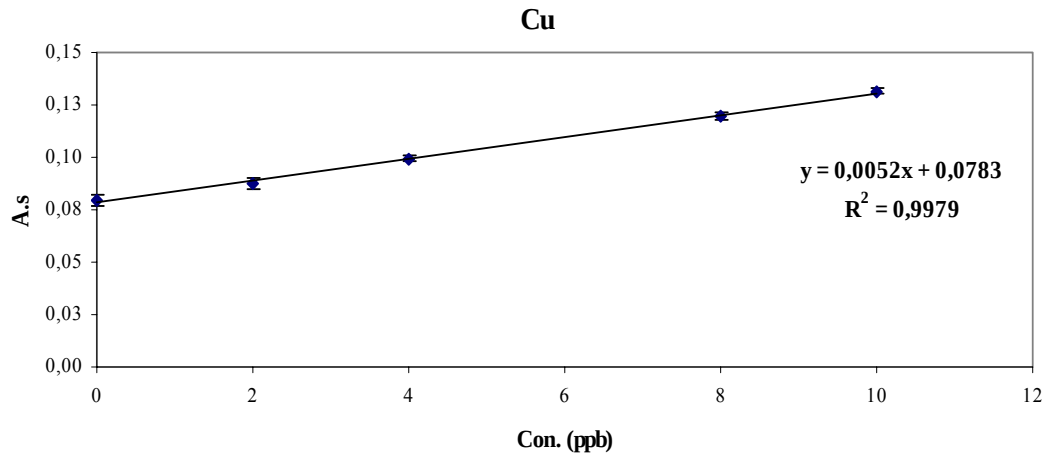

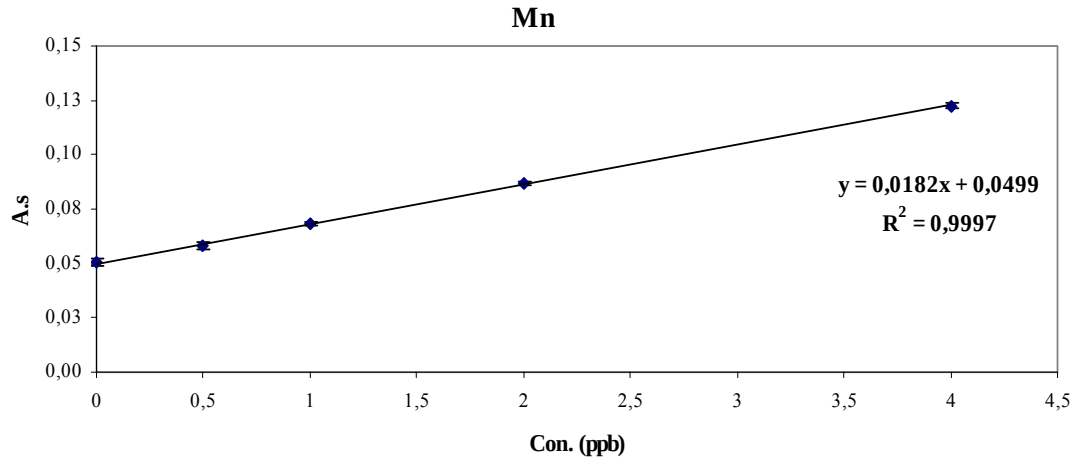

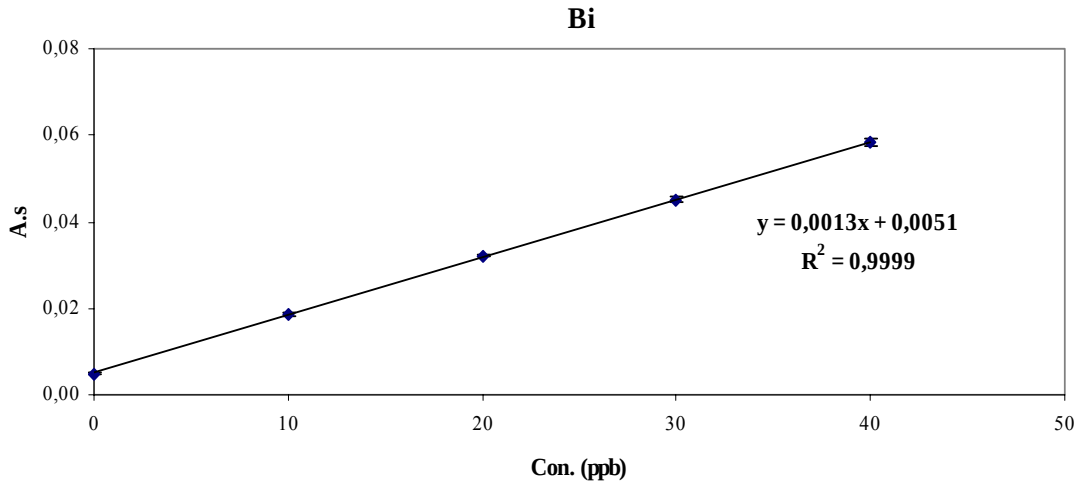

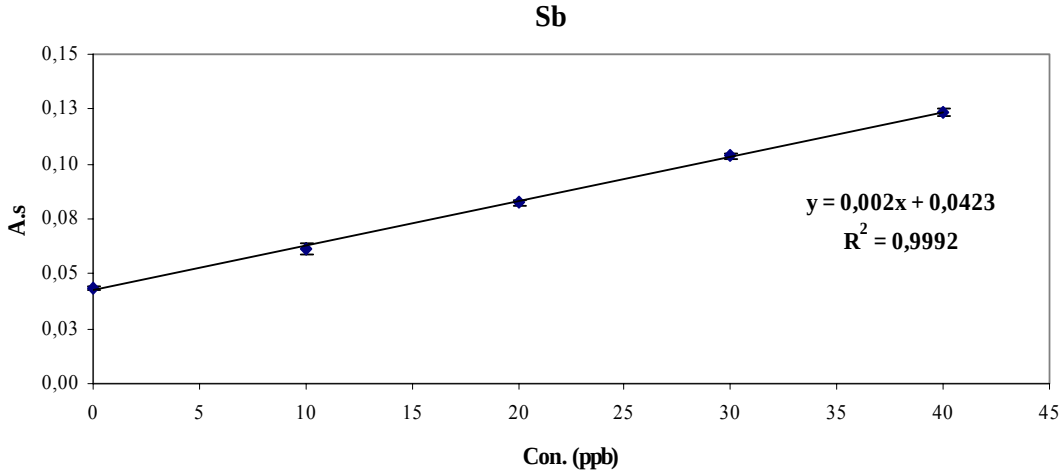

Table 5.34 The results of simultaneous determination of Bi, Cu, Mn, and Sb in urine reference sample from Seronorm

Element	Con. Found (ppb)	Certified		
		Con. (ppb)	Uncertainty	Acceptable range
Cu	75.3	72	±3	-
Mn	13.7	12.3	10.9-13.7	9.5-15.1
Bi	19.6	20.1	19.0-21.2	17.9-22.3
Sb	105.8	99.9	94.2-106	88.5-111

Table 5.35 Detection limits, characteristic mass, and relative standard deviations for simultaneous determination of Bi, Cu, Mn, and Sb in urine reference material from Seronorm

Element	LOD ($\mu g.l^{-1}$)	CM (pg)	RSD* (%)
Cu	0.29	16.9	2.8
Mn	0.12	4.8	2.3
Bi	1.4	67.7	2.7
Sb	0.90	44	2.1

*For five replicates

5.9.3.2 Lyphochek Urine Metals Control–Level 1 from BIO-RAD (69061)

The sample was diluted (1:1, v/v) with 0.2% HNO_3. For each measurement, 20 µl of the diluted sample, 5 µl of 1.00 $g.l^{-1}$ $Pd(NO_3)_2$ and 3 µl of 1.00 $g.l^{-1}$ $Mg(NO_2)_3$ modifier solution were injected into the graphite tube at 20°C. There was no certified value for bismuth; therefore, the sample has been spiked with bismuth before the dilution. The optimum temperature program was as in Table 5.33.

The standard addition curves for each element are shown in Figure 5.60. The standard addition curves with good linearity (R^2 = 0.9998, 0.9999, 0.9997, and 0.9999 for Bi, Cu, Mn, and Sb, respectively) were used to determine the concentration of the elements in the sample. The results are summarized and compared with the certified concentrations in Table 5.36. The experimentally determined concentrations were in good agreement with the certified values. The analyzed values were in the range of 101.7, 105.7, and 99.9% for Bi, Cu, and Sb,

respectively. The relative standard deviations (RSD) of the non spiked sample measurements were in the range: 0.5-1.5% for Cu, 1.2-3.1% for Mn, 0.6-5.8% for Bi, and 0.9-4.6% for Sb. Detection limits were calculated as three times the standard deviation of ten replicate measurements of the blank. The detection limits (LOD) and the characteristic mass were determined and given in Table 5.37.

Figure 5.60 The standard addition curves in the multi-element determination of Bi, Cu, Mn and Sb in urine reference sample from BIO-RAD

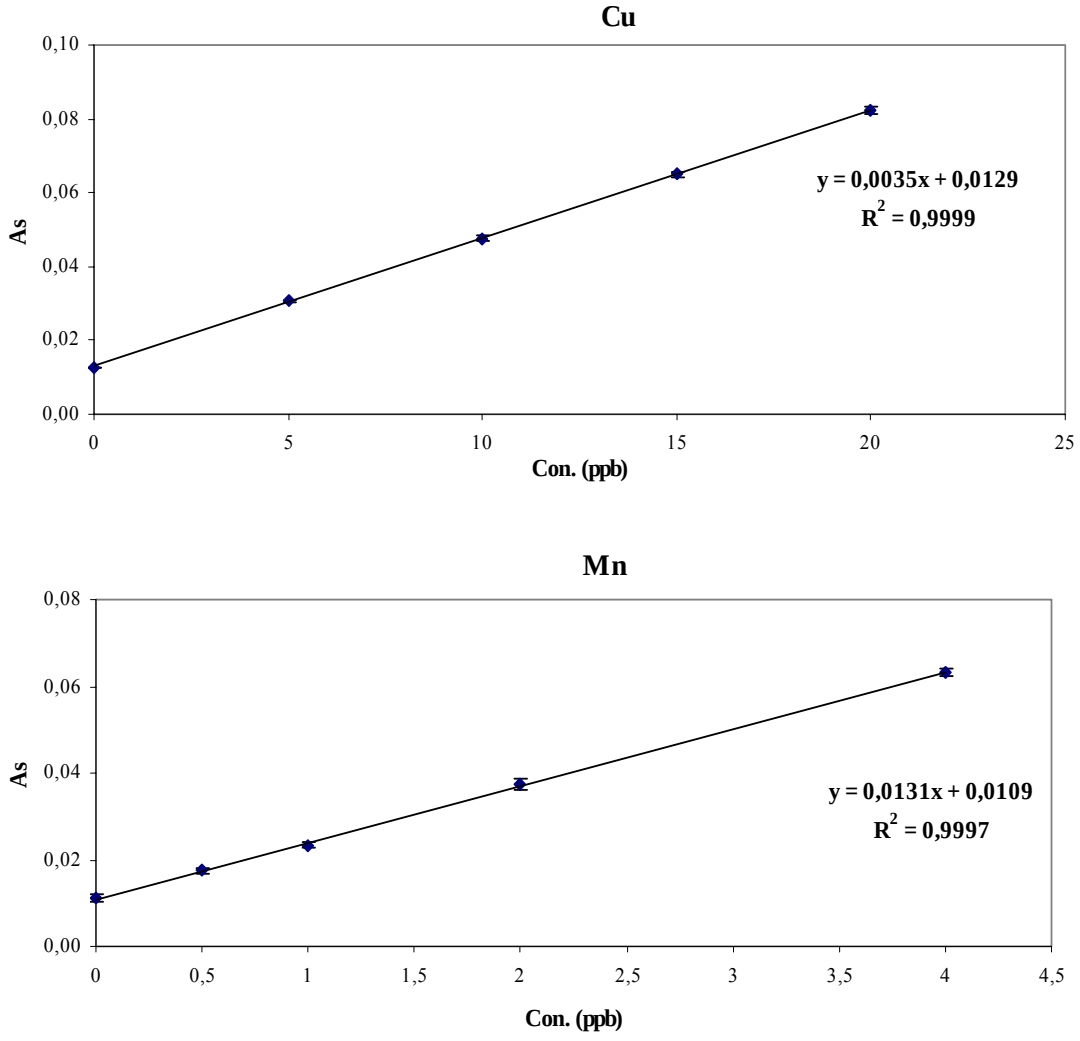

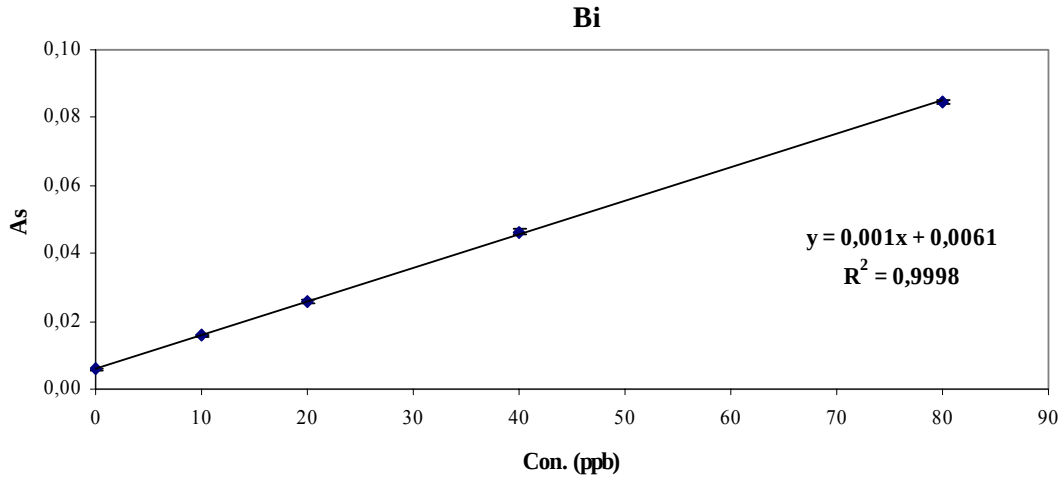

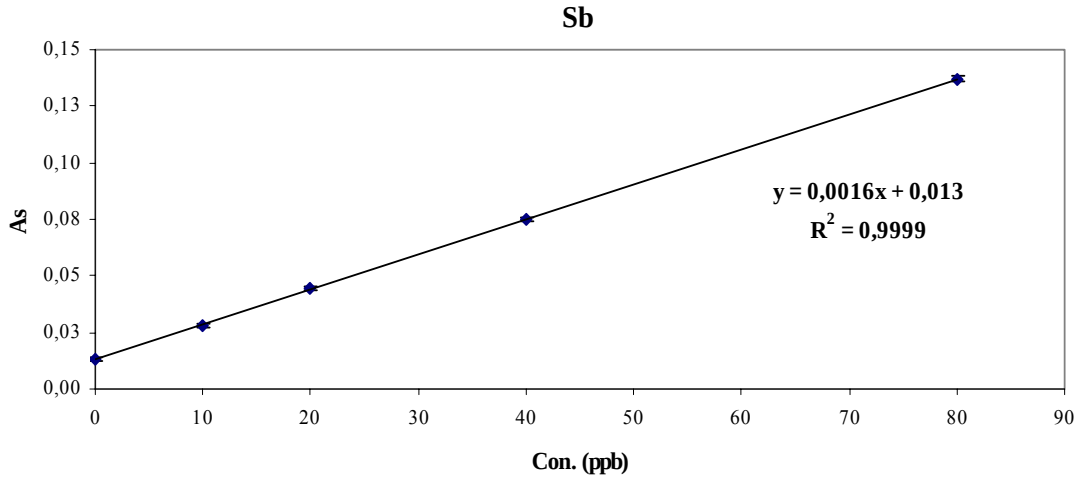

Table 5.36 The results of simultaneous determination of Bi, Cu, Mn, and Sb in urine reference sample from BIO-RAD

Element	Con. Found (ppb)	Certified	
		Con. (ppb)	Acceptable range
Cu	7.4	7	5.3-8.8
Mn	1.7	<3.5	-
Bi	12.2	12*	-
Sb	16.3	16.4	13.1-19.6

*added

Table 5.37 Detection limits, characteristic mass, and relative standard deviations for simultaneous determination of Bi, Cu, Mn, and Sb in urine reference material from BIO-RAD

Element	LOD ($\mu g.l^{-1}$)	CM (pg)	RSD* (%)
Cu	0.34	25.1	0.5
Mn	0.11	6.7	3.1
Bi	1.5	88	5.8
Sb	1.1	55	4.6

*Five replicates

5.9.3.3 Pig Kidney from Institute for Reference Materials and Measurements (BCR-CRM 186)

The sample was diluted (about 1:28.5, v/v) with 0.2% HNO_3. For each measurement, 20 µl of the diluted sample, 5 µl of 1.00 $g.l^{-1}$ $Pd(NO_3)_2$ and 3 µl of 1.00 $g.l^{-1}$ $Mg(NO_2)_3$ modifier solution were injected into the graphite tube at 20°C. There were no certified values for bismuth and antimony; therefore, the sample has been spiked with them before the dilution. The optimum temperature program was as in Table 5.33, except that the pyrolysis temperature could be increased to 1100°C.

The standard addition curves for each element are shown in Figure 5.61. The standard addition curves with good linearity (R^2 = 0.9999, 0.9998, 0.9998, and 0.9997 for Bi, Cu, Mn, and Sb, respectively) were used to determine the concentration of the elements in the sample. The results are summarized and compared with the certified concentrations in Table 5.38. The experimentally determined concentrations were in good agreement with the certified values. The analyzed values were in the range of 100.0, 95.8, 98.6, and 100.7% for Bi, Cu, Mn, and Sb, respectively. The relative standard deviations (RSD) of the non spiked sample measurements were in the range: 0.4-2.2% for Cu, 1.2-2.3% for Mn, 1.5-3.5% for Bi, and 1.1-3.8% for Sb. Detection limits were calculated as three times the standard deviation of ten replicate measurements of the blank. The detection limits (LOD) and the characteristic mass were determined and given in Table 5.39.

Figure 5.61 The standard addition curves in the multi-element determination of Bi, Cu, Mn and Sb in Pig Kidney sample

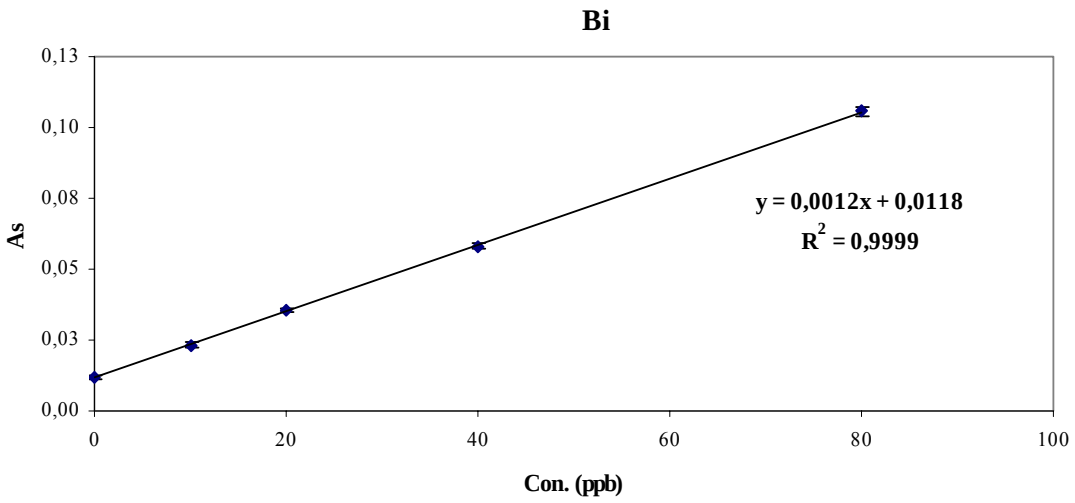

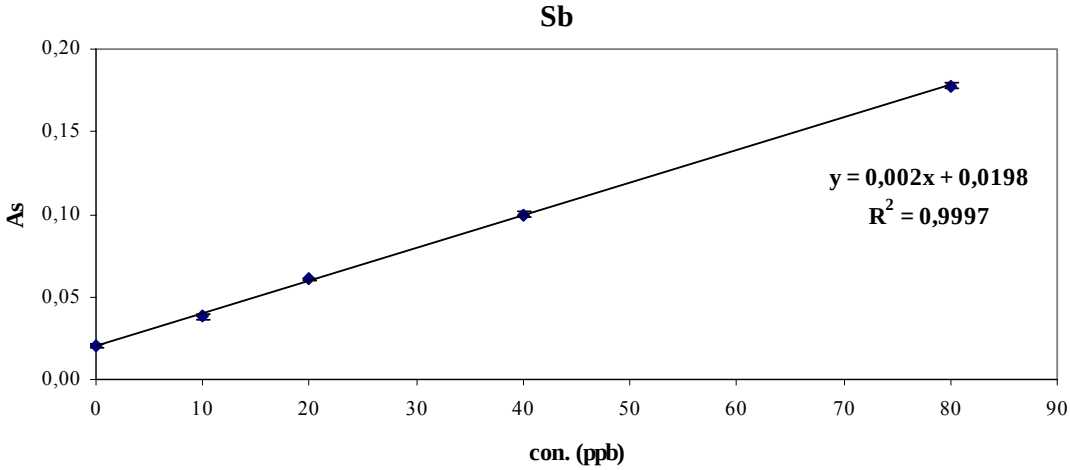

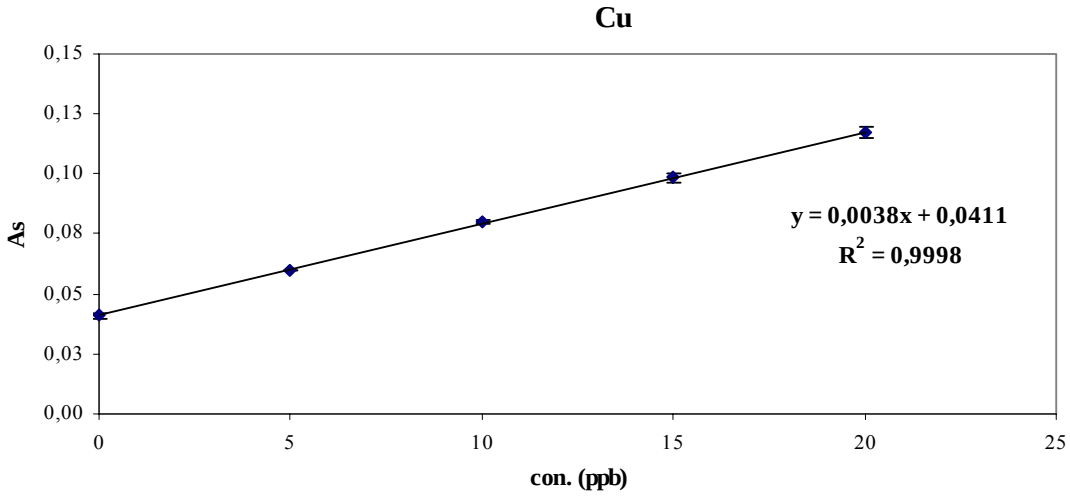

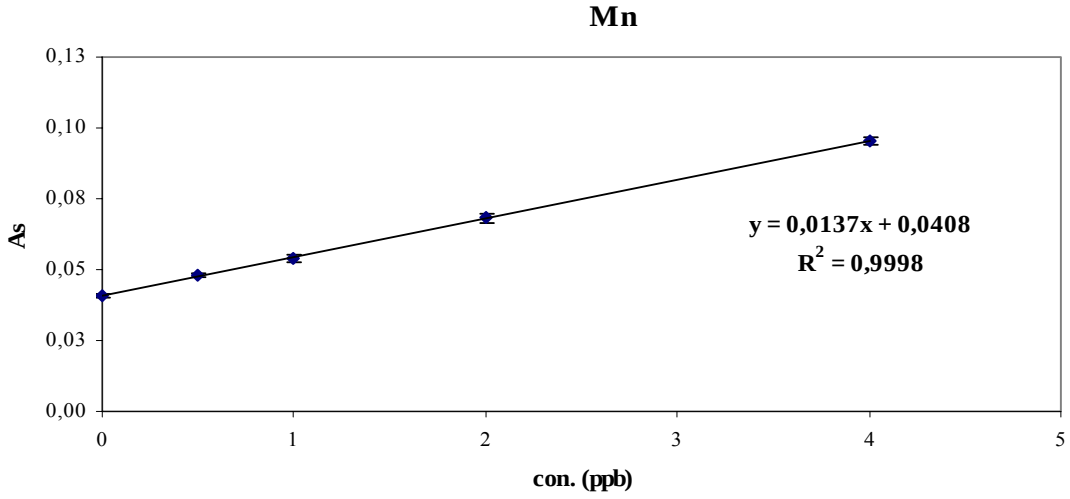

Table 5.38 The results of simultaneous determination of Bi, Cu, Mn, and Sb in Pig Kidney sample

Element	Con. Found (µg)	Con. certified (µg)
Bi	14.5	14.5*
Sb	14.6	14.5*
Cu	15.9	16.6
Mn	4.38	4.44

*added

Table 5.39 Detection limits, characteristic mass, and relative standard deviations for simultaneous determination of Bi, Cu, Mn, and Sb in Pig Kidney

Element	LOD (µg.l^{-1})	CM (pg)	RSD* (%)
Cu	0.32	23.2	2.2
Mn	0.13	6.4	1.6
Bi	1.5	73.3	3.5
Sb	1.1	44	3.8

*Five replicates

5.9.3.4 Bovine Liver from National Institute of Standards and Technology (NIST-SRM 1577b)

The sample was diluted (1:99, v/v) with 0.2% HNO_3. For each measurement, 20 µl of the diluted sample, 5 µl of 1.00 g.l^{-1} $Pd(NO_3)_2$ and 3 µl of 1.00 g.l^{-1} $Mg(NO_2)_3$ modifier solution were injected into the graphite tube at 20^{o}C. There were no certified values for bismuth and antimony; therefore, the sample has been spiked with them before the dilution. The optimum temperature program was as in Table 5.33, except that the pyrolysis temperature could be increased to 1100^{o}C.

The standard addition curves for each element are shown in Figure 5.62. The standard addition curves with good linearity (R^2 = 0.9998, 0.9997, 0.9997, and 0.9996 for Bi, Cu, Mn, and Sb, respectively) were used to determine the concentration of the elements in the sample. The results are summarized and compared with the certified concentrations in Table 5.40. The experimentally determined concentrations were in good agreement with the certified values. The analyzed values were in the range of 103.0, 87.2, 98.1, and 100.6% for Bi, Cu, Mn, and Sb, respectively. The relative standard deviations (RSD) of the non spiked sample measurements were in the range: 0.5-1.9% for Cu, 1.1-3.5% for Mn, 1.4-3.4% for Bi, and 1.8-3.6% for Sb. Detection limits were calculated as three times the standard deviation of ten replicate measurements of the blank. The detection limits (LOD) and the characteristic mass were determined and given in Table 5.41.

Figure 5.62 The standard addition curves in the multi-element determination of Bi, Cu, Mn and Sb in Bivine Liver sample

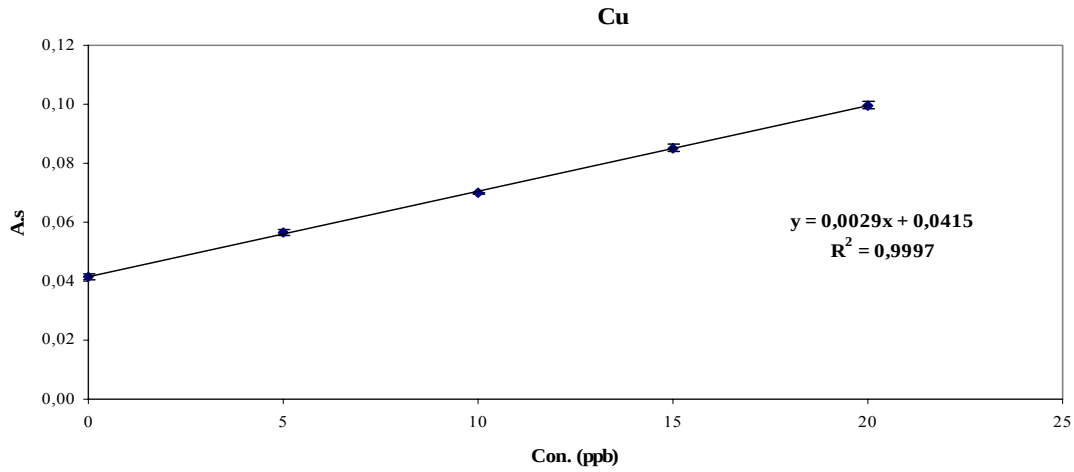

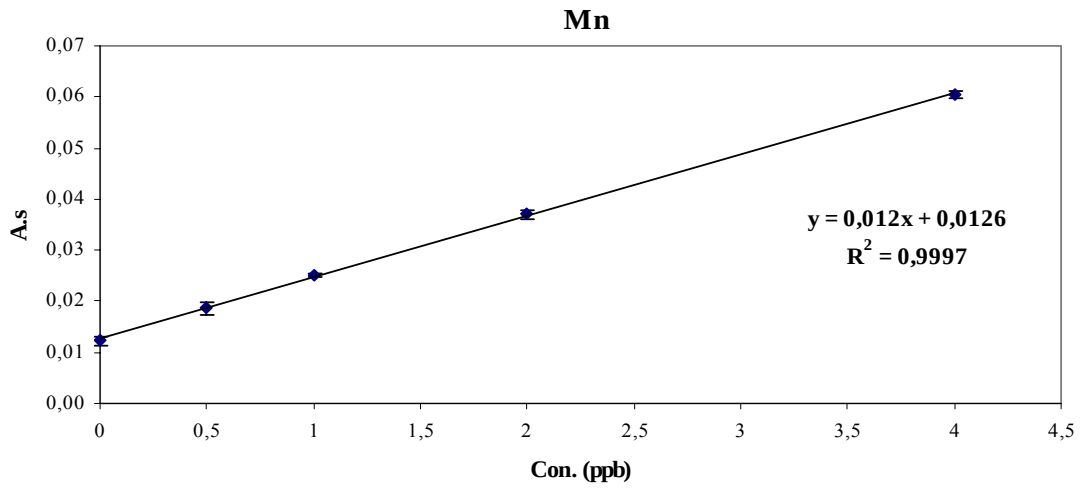

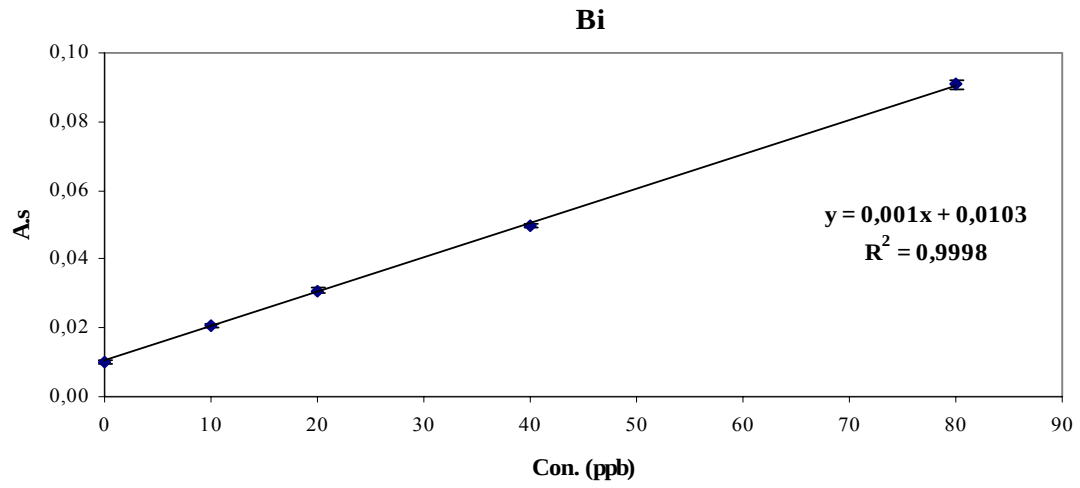

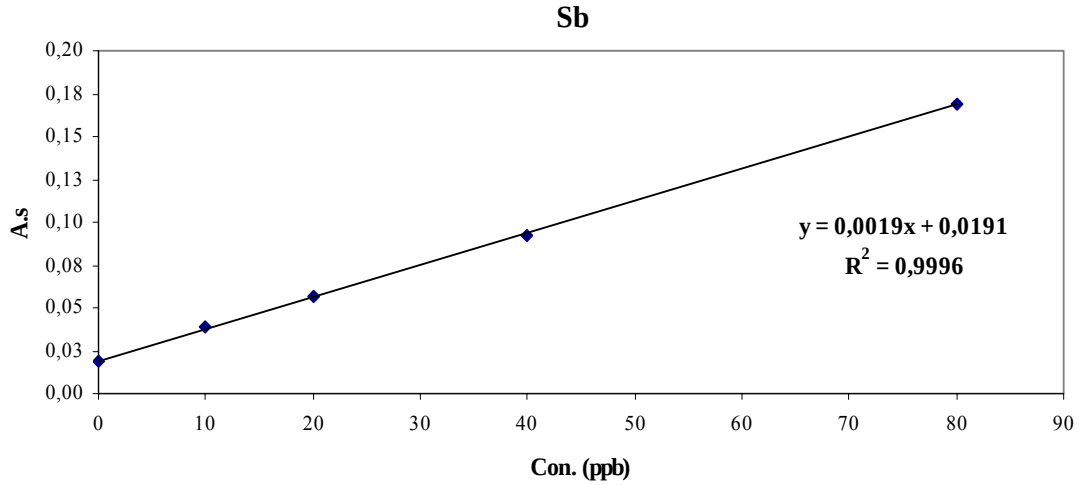

Table 5.40 The results of simultaneous determination of Bi, Cu, Mn, and Sb in Bovine Liver sample

Element	Con. Found (µg)	Con. certified (µg)
Bi	51.5	50.0*
Sb	50.3	50.0*
Cu	71.6	82.1
Mn	5.3	5.4

*added

Table 5.41 Detection limits, characteristic mass, and relative standard deviations for simultaneous determination of Bi, Cu, Mn, and Sb in Bovine Liver

Element	LOD (µg.l^{-1})	CM (pg)	RSD* (%)
Cu	0.41	30.3	1.9
Mn	0.13	7.3	3.2
Bi	1.5	88	3.4
Sb	1.1	46.3	3.6

***For five replicates**

5.9.3.5 Comparison of the results of Different Samples

The pyrolysis temperature was as same as the simultaneous determinations in aqueous solution (1100^{o}C) except the urine samples form Seronorm and Bio-Rad (1000^{o}C). The detection limits values of sample results were comparable to those of aqueous solution. The highest increasings in the values compared to aqueous solution were as follows: 1.5 times in bovine liver and pig kidney for Cu, 1.5 times in bovine liver for Mn, nearly same values in all samples as in aqueous solution for Bi, and 1.2 times in bovine liver for Sb. Generally, the values were similar to those of aqueous solution. However, the highest increases in detection limits values were in bovine liver which has a highest dilution factor (1:99). The results of characteristic mass, however, were comparable to those of aqueous solution and the increased percentages were in the range of: - 18% to + 48% for Cu, - 6% to + 43% for Mn, - 15% to + 10% for Bi, and 0% to +25% for Sb. The lowest sensitivity values, as in multi-element

determination of Al, Be, Cr, and V, were obtained with bovine liver sample, except for Sb which was in Bio-Rad urine sample, and the highest sensitivities with Seronorm urine sample.

5.9.4 Multi-Element Determination of Cu, Mn, and Se

The accuracy of the multi-element determination of this group was confirmed by the analysis of the following certified reference materials: Trace Element Urine Sample from Seronorm, Lyphocheck Urine Metals Control- Level 1 from BIO-RAD, and Pig Kidney from Institute for Reference Materials and Measurements .Each sample has been diluted according to the concentration of the elements in the sample.

5.9.4.1 Trace Element Urine Sample from Seronorm (0511545)

The sample was diluted (1:4, v/v) with 0.2% HNO_3. For each measurement, 20 µl of the diluted sample, 5 µl of 1.00 $g.l^{-1}$ $Pd(NO_2)_3$ and 3 µl 1.00 $g.l^{-1}$ $Mg(NO_2)_3$ modifier solution were injected into the graphite tube at 20°C. The temperature program is summarized in Table 5.42.

Table 5.42 Optimum Temperature Program for Simultaneous Determination of Cu, Mn, and Se in Urine reference sample from Seronorm

Step	Temperature (°C)	Ramp Time (s)	Hold Time (s)	Gas Flow ($ml.min^{-1}$)
Dry 1	110	1	30	250
Dry 2	130	15	30	250
Pyrolysis	900	10	20	250
Atomization	2000	0	5	0
Clean-out	2500	1	4	250

The standard addition curves for each element are shown in Figure 5.63. The standard addition curves with good linearity (R^2 = 0.9965, 0.9993, and 0.9994 for Cu, Mn, and Se, respectively) were used to determine the concentration of the elements in the sample. The results are summarized and compared with the certified concentrations in Table 5.43. The experimentally determined concentrations were in good agreement with the certified values. The analyzed values were in the range of 101.1, 109.8, and 101.2% for Cu, Mn, and Se, respectively. The relative standard deviations (RSD) of the non spiked sample measurements were in the range: 1.3-2.7% for Cu, 1.0-2.6% for Mn, 0.5-8.4% and for Bi. Detection limits were calculated as three times the standard deviation of ten replicate measurements of the blank. The detection limits (LOD) and the characteristic mass were determined and given in Table 5.44.

Figure 5.63 The standard addition curves in the multi-element determination of Cu, Mn, and Se in urine reference sample from Seronorm

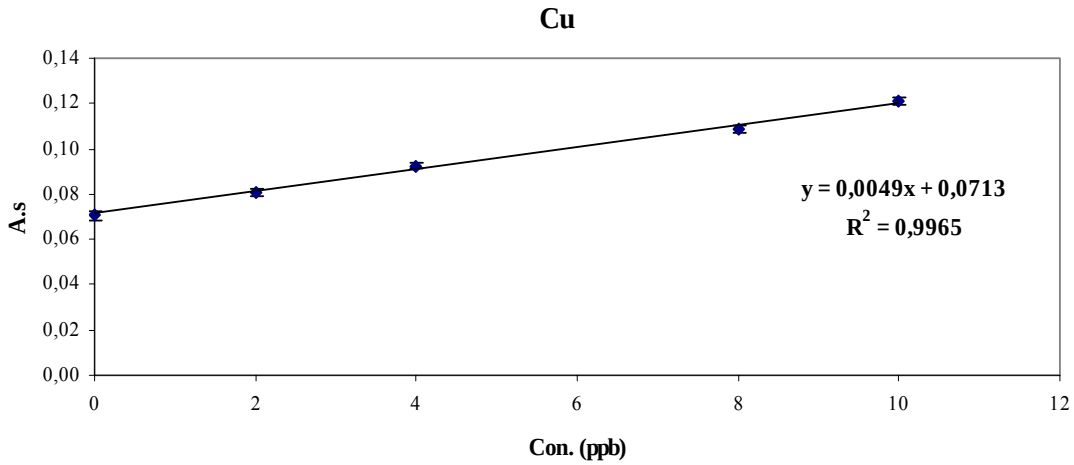

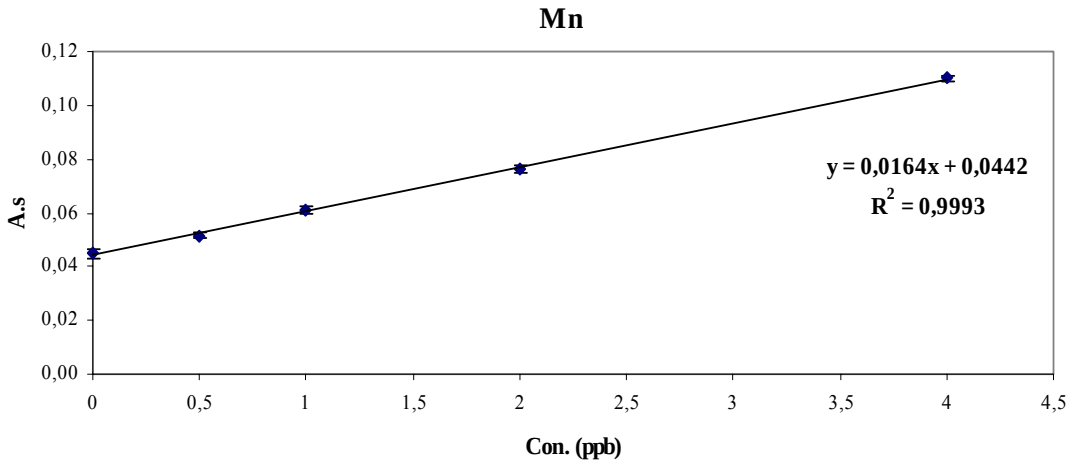

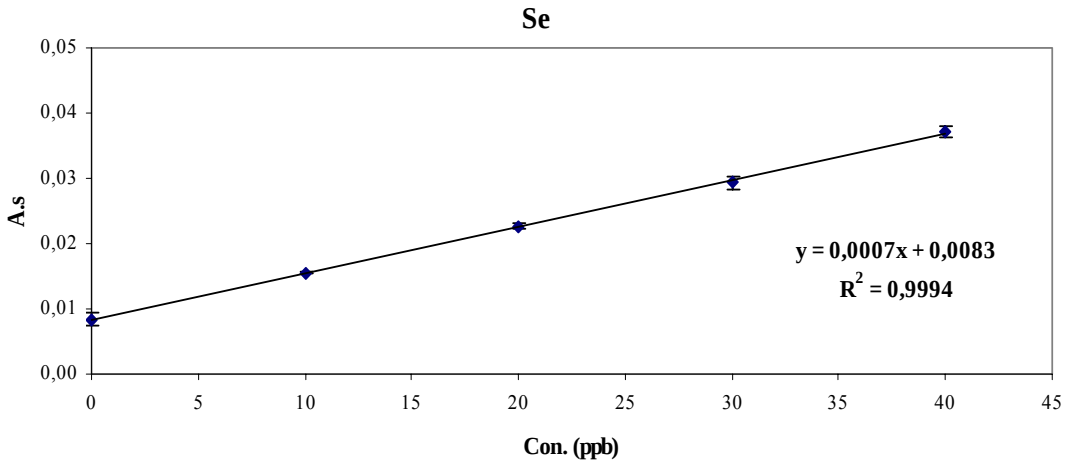

Table 5.43 The results of simultaneous determination of Cu, Mn, and Se in urine reference sample from Seronorm

Element	Con. Found (ppb)	Certified		
		Con. (ppb)	Uncertainty	Acceptable range
Cu	72.8	72	±3	-
Mn	13.5	12.3	10.9-13.7	9.5-15.1
Se	59.3	58.6	55.5-61.7	52.4-64.8

Table 5.44 Detection limits, characteristic mass, and relative standard deviations for simultaneous determination of Cu, Mn, and Se in urine reference material from Seronorm

Element	LOD ($\mu g.l^{-1}$)	CM (pg)	RSD* (%)
Cu	0.24	18.0	2.7
Mn	0.09	5.4	2.6
Se	1.7	125.7	8.4

*For five replicates

5.9.4.2 Lyphocheck Urine Metals Control–Level 1 from BIO-RAD (69061)

The sample was diluted (1:1, v/v) with 0.2% HNO_3. For each measurement, 20 µl of the diluted sample, 5 µl of 1.00 $g.l^{-1}$ $Pd(NO_3)_2$ and 3 µl of 1.00 $g.l^{-1}$ $Mg(NO_2)_3$ modifier solution were injected into the graphite tube at 20°C. The optimum temperature program was as in Table 5.42.

The standard addition curves for each element are shown in Figure 5.64. The standard addition curves with good linearity (R^2 = 0.9995, 0.9999, and 0.9998 for Cu, Mn, and Se, respectively) were used to determine the concentration of the elements in the sample. The results are summarized and compared with the certified concentrations in Table 5.45. The experimentally determined concentrations were in good agreement with the certified values. The analyzed values were in the range of 104.3 and 97.5% for Cu and Se, respectively. The relative standard deviations (RSD) of the non spiked sample measurements were in the range: 0.5-2.2% for Cu, 1.3-2.9% for Mn, and 2.1-4.0% for Se. Detection limits were calculated as three times the standard deviation of ten replicate measurements of the blank. The detection limits (LOD) and the characteristic mass were determined and given in Table 5.46.

Figure 5.64 The standard addition curves in the multi-element determination of Cu, Mn, and Se in urine reference sample from BIO-RAD

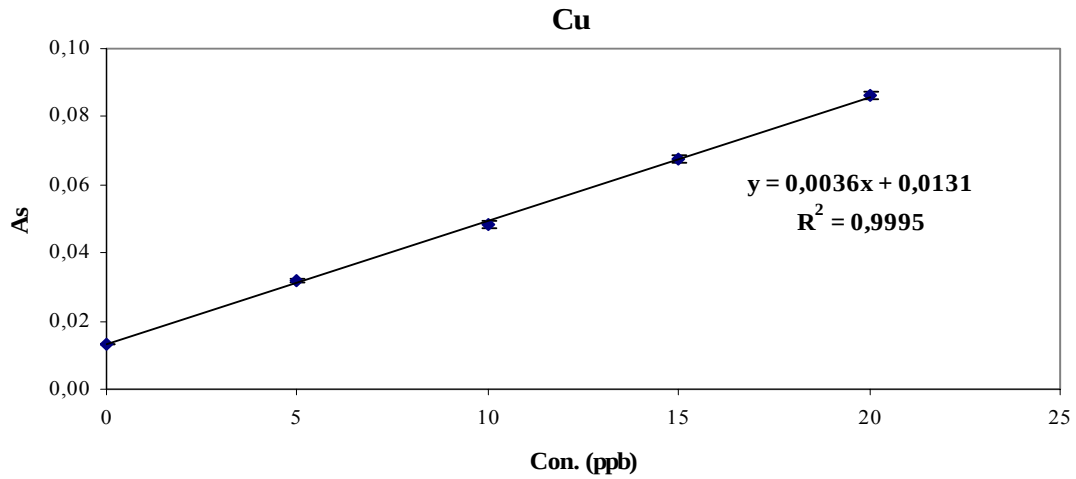

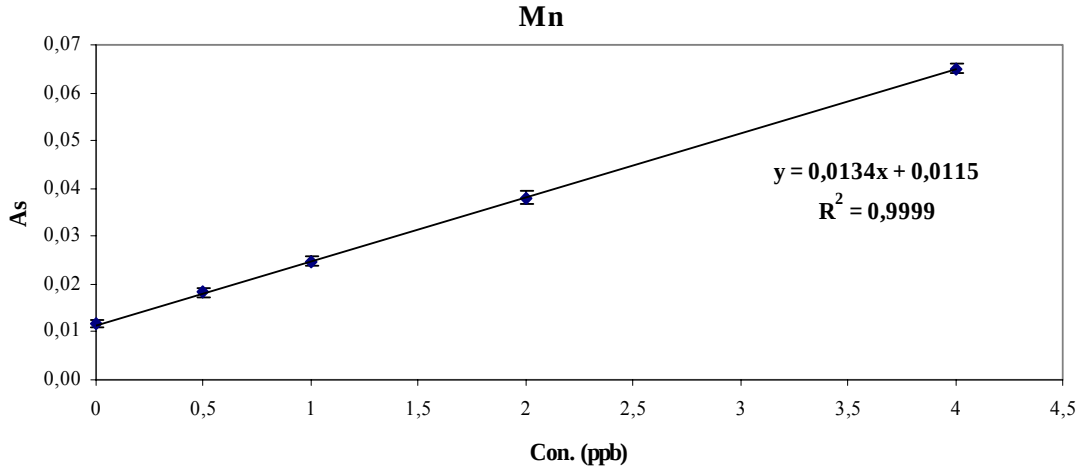

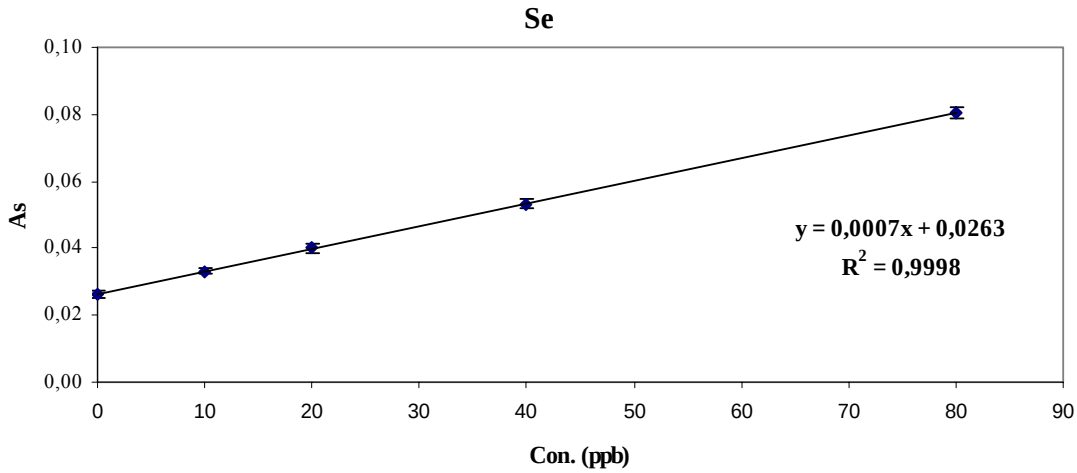

Table 5.45 The results of simultaneous determination of Cu, Mn, and Se in urine reference sample from BIO-RAD

Element	Con. Found (ppb)	Certified	
		Con. (ppb)	Acceptable range
Cu	7.3	7	5.3-8.8
Mn	1.7	<3.5	-
Se	75.1	77	58-96

Table 5.46 Detection limits, characteristic mass, and relative standard deviations for simultaneous determination of Cu, Mn, and Se in urine reference material from BIO-RAD

Element	LOD ($\mu g.l^{-1}$)	CM (pg)	RSD* (%)
Cu	0.17	24.4	0.5
Mn	0.11	6.6	2.7
Se	1.7	125.7	4.0

*For five replicates

5.9.4.3 Pig Kidney from Institute for Reference Materials and Measurements (BCR-CRM 186)

The sample was diluted (about 1:28.5, v/v) with 0.2% HNO_3. For each measurement, 20 µl of the diluted sample, 5 µl of 1.00 $g.l^{-1}$ $Pd(NO_3)_2$ and 3 µl of 1.00 $g.l^{-1}$ $Mg(NO_2)_3$ modifier solution were injected into the graphite tube at 20°C. The optimum temperature program was as in Table 5.42, except that the pyrolysis temperature could be increased to 1000°C.

The standard addition curves for each element are shown in Figure 5.65. The standard addition curves with good linearity (R^2 = 0.9998, 0.9999, and 0.9999 for Cu, Mn, and Se, respectively) were used to evaluate the concentration of the elements in the sample. The results are summarized and compared with the certified concentrations in Table 5.47. The experimentally determined concentrations were in good agreement with the certified values. The analyzed values were in the range of 95.8, 102.4, and 96.3% for Cu, Mn, and Se, respectively. The relative standard deviations (RSD) of the non spiked sample measurements were in the range: 0.4-1.8% for Cu, 0.9-2.5% for Mn, and 1.4-5.0% for Se. Detection limits were calculated as three times the standard deviation of ten replicate measurements of the blank. The detection limits (LOD) and the characteristic mass were determined and given in Table 5.48.

Figure 5.65 The standard addition curves in the multi-element determination of Cu, Mn, and Se in Pig Kidney sample

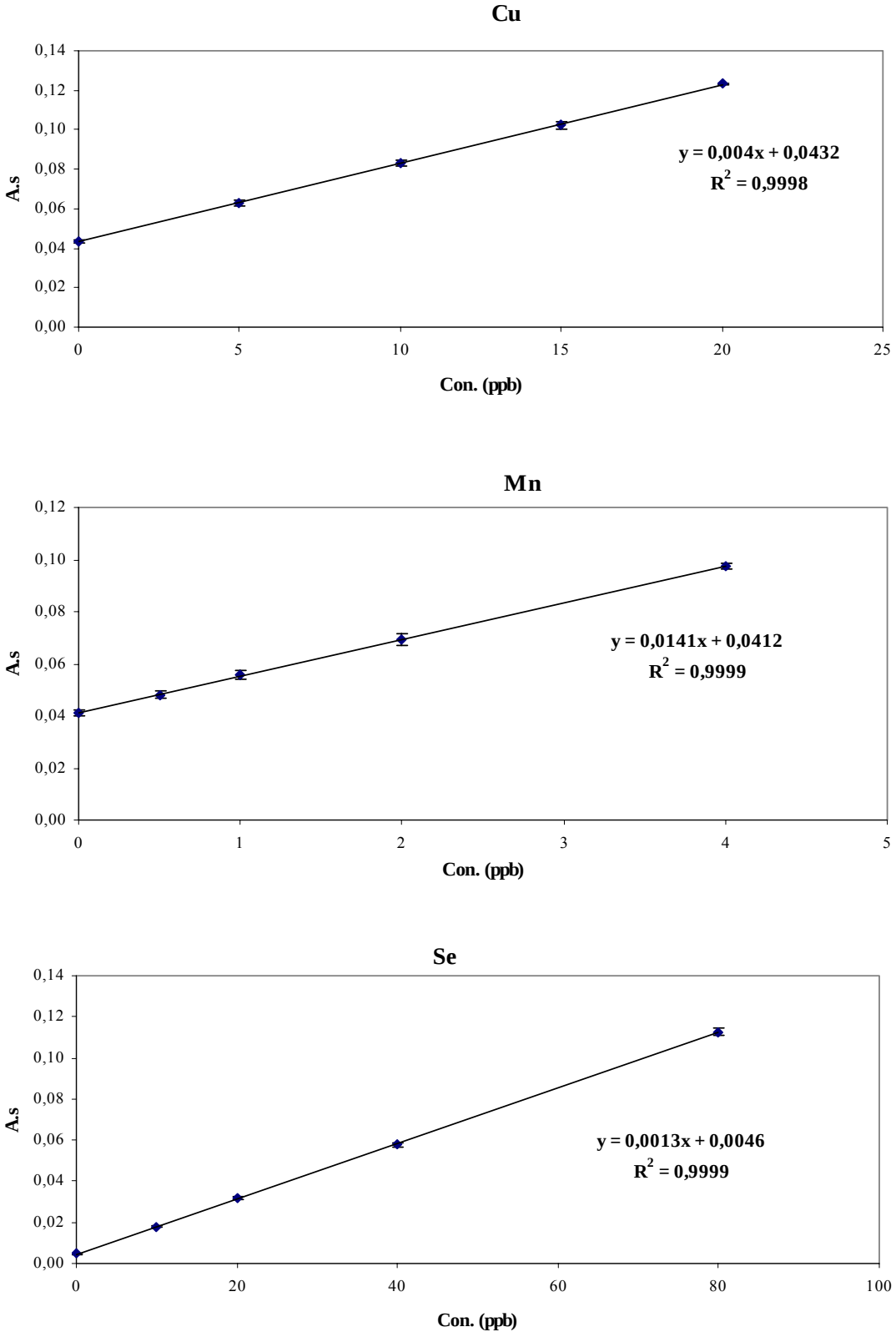

Table 5.47 The results of simultaneous determination of Cu, Mn, and Se in Pig Kidney

Element	Con. Found (µg)	Con. certified (µg)
Cu	15.9	16.6
Mn	4.3	4.2
Se	5.2	5.4

Table 5.48 Detection limits, characteristic mass, and relative standard deviations for simultaneous determination of Cu, Mn, and Se in Pig Kidney

Element	LOD (µg.l^{-1})	CM (pg)	RSD* (%)
Cu	0.23	22	1.8
Mn	0.09	6.2	2.3
Se	1.4	67.7	5.0

*For five replicates

5.9.4.4 Comparison of the results of Different Samples

The pyrolysis temperature was not as the simultaneous determinations in aqueous solution (1200^{o}C). It was 900^{o}C for Seronorm and Bio-Rad urine samples and 1000^{o}C for pig kidney sample. The detection limits values of sample results were similar to those of aqueous solution. The highest increasings in the values compared to aqueous solution were as follows: 1.2 times in Seronorm and Bio-Rad urine samples for Cu, 1.6 times in Bio-Rad urine sample for Mn, and 1.7 times in Seronorm and Bio-Rad urine sample for Se. Generally, the values were similar to those of aqueous solution. The results of characteristic mass, however, were also comparable to those of aqueous solution, except for Se, and the increased percentages were in the range of: - 10% to + 22% for Cu, + 4% to + 27% for Mn, and +15% to +114% for Se. The lowest sensitivity values were in the determination of Se in urine samples comparing to aqueous solution value. This is because of high matrix effect, results from using lower pyrolysis temperature, which lowered the absorbance values of Se.

5.9.5 Multi-Element Determination of Pb and Se

The accuracy of the multi-element determination of this group was confirmed by the analysis of the following certified reference materials: Trace Element Urine Sample from Seronorm, Lyphocheck Urine Metals Control- Level 1 from BIO-RAD, Pork Liver from National Research Centre for Certified Reference Materials, and Tea sample from National Research Centre for Certified Reference Materials. The dilution of the sample was according to the concentration of the elements in the sample.

5.9.5.1 Trace Element Urine Sample from Seronorm (0511545)

We have used two types of modifiers; the mixture of Pd and Mg and Ir as a permanent modifier, in the multi-element determination of lead and selenium in the urine sample from Seronorm. The sample was diluted (1:4, v/v) with 0.2% HNO_3 and 20µl of the sample was injected for each measurement. 5µl of 1.00 g.l^{-1} Pd and 3µl 1.00 g.l^{-1} $Mg(NO_3)_2$ were injected also with the sample into the graphite tube. In the case of the permanent modifier, the Ir was deposited into the graphite tube in a separate step.

5.9.5.1.1 With Pd+Mg modifier

The temperature program is summarized in Table 5.49.

Table 5.49 Optimum Temperature Program for Simultaneous Determination of Pb and Se with Pd+Mg modifier in Urine reference sample from Seronorm

Step	Temperature (°C)	Ramp Time (s)	Hold Time (s)	Gas Flow ($ml.min^{-1}$)
Dry 1	110	1	30	250
Dry 2	130	15	30	250
Pyrolysis	1000	10	20	250
Atomization	1900	0	5	0
Clean-out	2400	1	3	250

The standard addition curves for each element are shown in Figure 5.66. The standard addition curves with good linearity (R^2 = 0.9986 and 0.9974 for Se and Pb, respectively) were used to evaluate the concentration of the elements in the sample. The results are summarized and compared with the certified concentrations in Table 5.50. The experimentally determined concentrations were in good agreement with the certified values. The analyzed values were in the range of 102.5 and 96.1% for Pb and Se, respectively. The relative standard deviations (RSD) of the non spiked sample measurements were in the range: 0.5-4.1% for Pb and 1.4-7.2% for Se. Detection limits were calculated as three times the standard deviation of ten replicate measurements of the blank. The detection limits (LOD) and the characteristic mass were determined and given in Table 5.51.

Figure 5.66 The standard addition curves in the multi-element determination of Pb and Se with Pd+Mg modifier in Urine reference sample from Seronorm

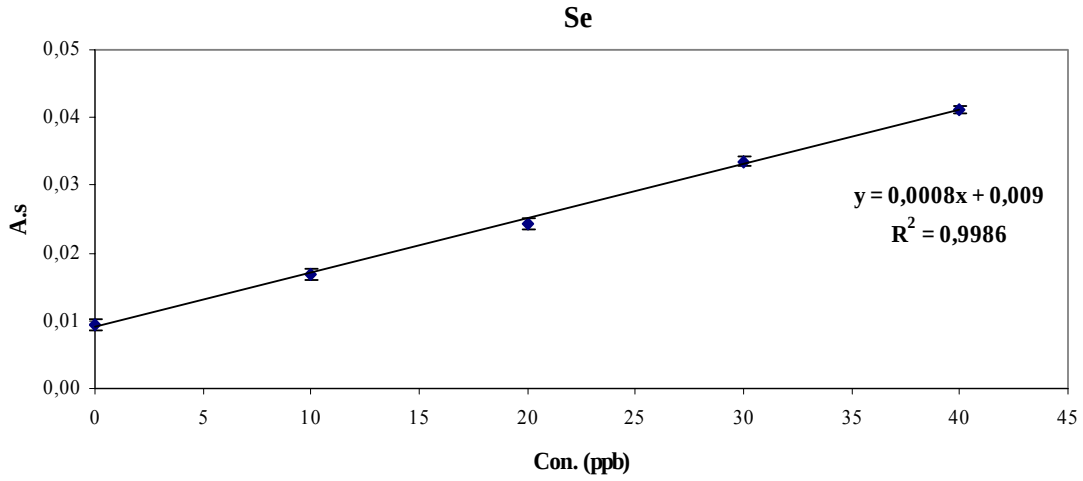

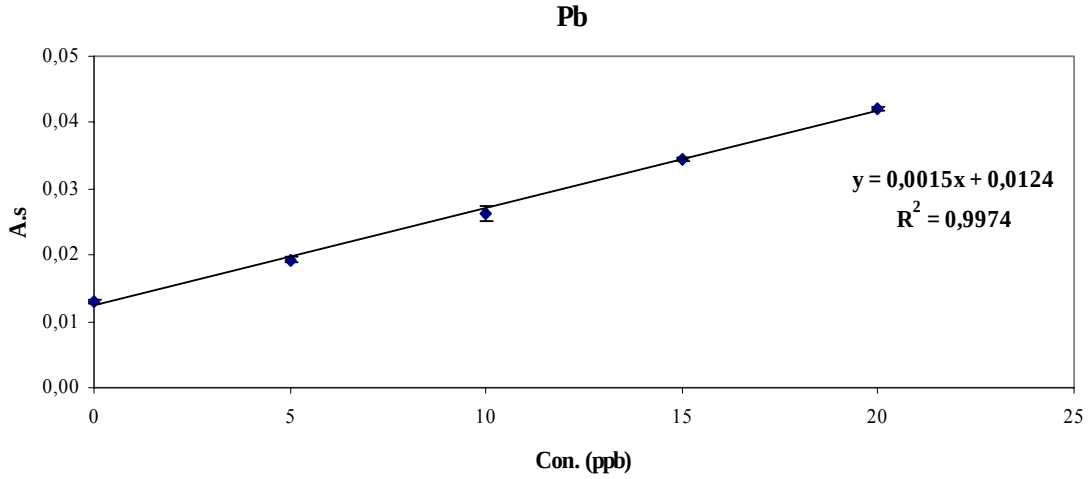

Table 5.50 The results of simultaneous determination of Pb and Se with Pd+Mg modifier in urine reference sample from Seronorm

Element	Con. Found (ppb)	Certified		
		Con. (ppb)	Uncertainty	Acceptable range
Pb	41.3	40.3	37.7-42.9	35.1-45.5
Se	56.3	58.6	55.5-61.7	52.4-64.8

Table 5.51 Detection limits, characteristic mass, and relative standard deviations for simultaneous determination of Pb and Se with Pd+Mg modifier in urine reference material from Seronorm

Element	LOD (µg.l^{-1})	CM (pg)	RSD* (%)
Pb	0.40	58.7	2.2
Se	1.1	110	7.2

*For five replicates

5.9.5.1.2 With Ir permanent Modifier

The temperature program was as in Table 5.49 but the pyrolysis and atomization temperatures were 800 and 2000^{o}C, respectively.

The standard addition curves for each element are shown in Figure 5.67. The standard addition curves with good linearity (R^2 = 0.9989 and 0.9999 for Se and Pb, respectively) were used to determine the concentration of the elements in the sample. The results are summarized and compared with the certified concentrations in Table 5.52. The experimentally determined concentrations were in good agreement with the certified values. The analyzed values were in the range of 100.0 and 100.7% for Pb and Se, respectively. The relative standard deviations (RSD) of the non spiked sample measurements were in the range: 1.8-4.7% for Pb and 1.6-12.4% for Se. Detection limits were calculated as three times the standard deviation of ten replicate measurements of the blank. The detection limits (LOD) and the characteristic mass were determined and given in Table 5.53.

Figure 5.67 The standard addition curves in the multi-element determination of Pb and Se with Ir permanent modifier in Urine reference sample from Seronorm

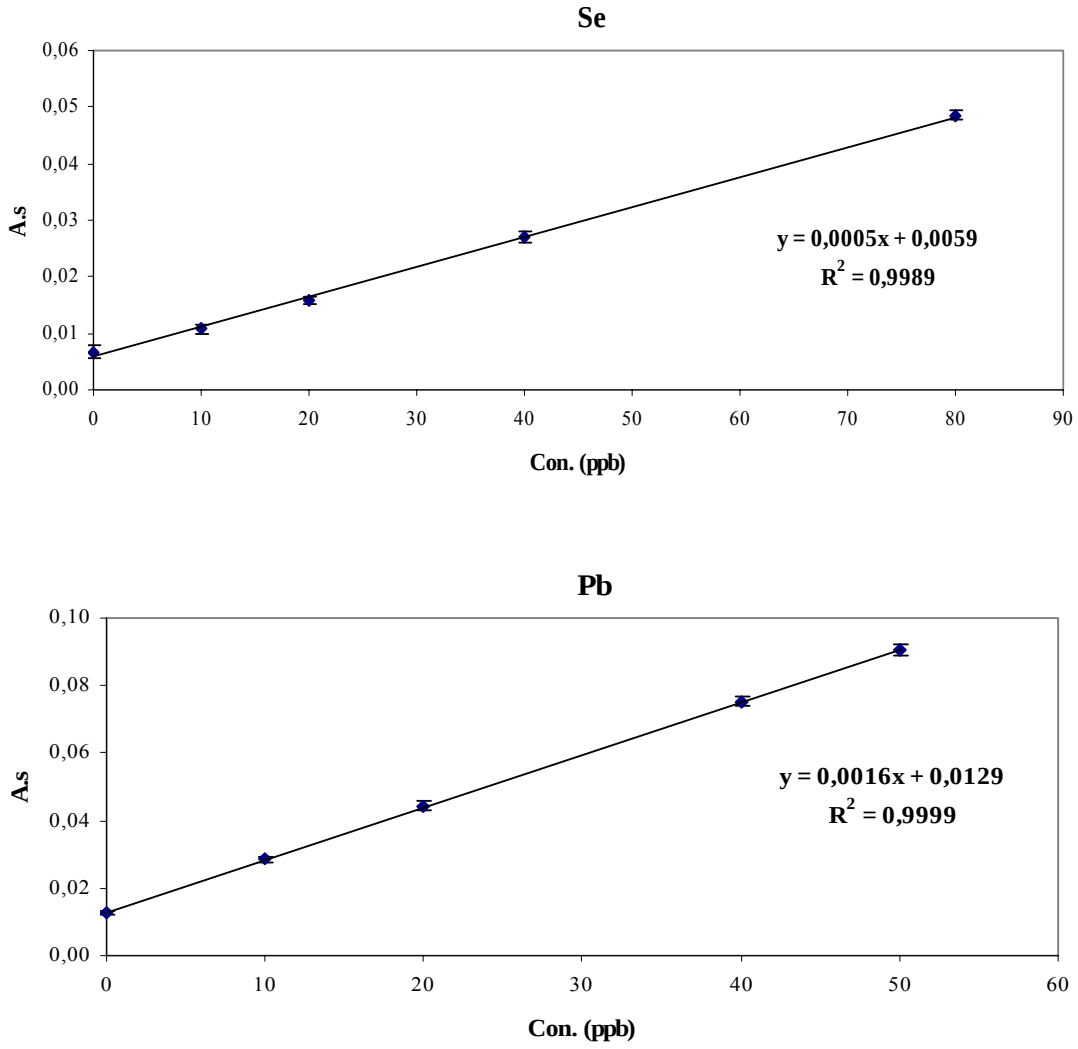

Table 5.52 The results of simultaneous determination of Pb and Se with Ir permanent modifier in urine reference sample from Seronorm

Element	Con. Found (ppb)	Certified		
		Con. (ppb)	Uncertainty	Acceptable range
Pb	40.3	40.3	37.7-42.9	35.1-45.5
Se	59	58.6	55.5-61.7	52.4-64.8

Table 5.53 Detection limits, characteristic mass, and relative standard deviations for simultaneous determination of Pb and Se with Ir permanent modifier in urine reference material from Seronorm

Element	LOD ($\mu g.l^{-1}$)	CM (pg)	RSD* (%)
Pb	0.56	55	4.7
Se	2.4	176	12.4

*For five replicates

5.9.5.2 Lyphocheck Urine Metals Control–Level 1 from BIO-RAD (69061)

The sample was diluted (1:1, v/v) with 0.2% HNO_3. For each measurement, 20 µl of the diluted sample, 5 µl of 1.00 $g.l^{-1}$ $Pd(NO_3)_2$ and 3 µl of 1.00 $g.l^{-1}$ $Mg(NO_2)_3$ modifier solution

were injected into the graphite tube at 20°C. The optimum temperature program was as in Table 5.49.

The standard addition curves for each element are shown in Figure 5.68. The standard addition curves with good linearity (R^2 = 0.9999 and 0.9997 for Se and Pb, respectively) were used to evaluate the concentration of the elements in the sample. The results are summarized and compared with the certified concentrations in Table 5.54. The experimentally determined concentrations were in good agreement with the certified values. The analyzed values were in the range of 102.1 and 101.3% for Pb and Se, respectively. The relative standard deviations (RSD) of the non spiked sample measurements were in the range: 0.6-1.5% for Pb and 1.2-4.4% for Se. Detection limits were calculated as three times the standard deviation of ten replicate measurements of the blank. The detection limits (LOD) and the characteristic mass were determined and given in Table 5.55.

Figure 5.68 The standard addition curves in the multi-element determination of Pb and Se in Urine reference sample from BIO-RAD

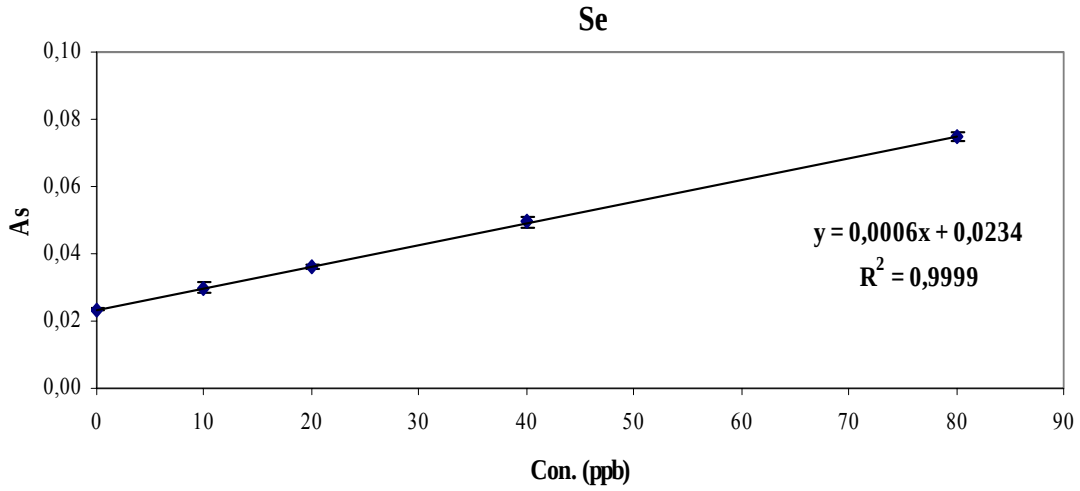

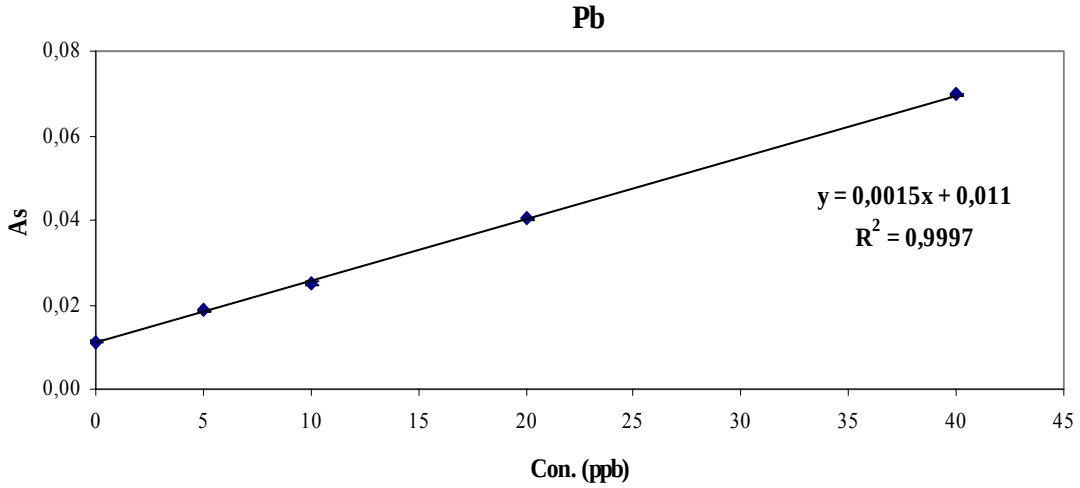

Table 5.54 The results of simultaneous determination of Pb and Se in urine reference sample from BIO-RAD

Element	Con. Found (ppb)	Certified	
		Con. (ppb)	Acceptable range
Pb	14.7	14.4	10.1-18.7
Se	78	77	58-96

Table 5.55 Detection limits, characteristic mass, and relative standard deviations for simultaneous determination of Pb and Se in urine reference material from BIO-RAD

Element	LOD ($\mu g.l^{-1}$)	CM (pg)	RSD* (%)
Pb	0.40	58.7	0.8
Se	1.5	146.7	1.2

*For five replicates

5.9.5.3 Pork Liver from National Research Centre for Certified Reference Materials (GBW 08551)

The sample was diluted (1:3, v/v) with 0.2% HNO_3. For each measurement, 20 µl of the diluted sample, 5 µl of 1.00 $g.l^{-1}$ $Pd(NO_3)_2$ and 3 µl of 1.00 $g.l^{-1}$ $Mg(NO_2)_3$ modifier solution were injected into the graphite tube at 20°C. The optimum temperature program was as in Table 5.49 except that the atomization temperature was 2000°C.

The standard addition curves for each element are shown in Figure 5.69. The standard addition curves with good linearity (R^2 = 0.9995 and 0.9998 for Se and Pb, respectively) were used to evaluate the concentration of the elements in the sample. The results are summarized and compared with the certified concentrations in Table 5.56. The experimentally determined concentrations were in good agreement with the certified values. The analyzed values were in the range of 107.4 and 100.0% for Pb and Se, respectively. The relative standard deviations (RSD) of the non spiked sample measurements were in the range: 1.3-6.8% for Pb and 2.4-8.8% for Se. Detection limits were calculated as three times the standard deviation of ten

replicate measurements of the blank. The detection limits (LOD) and the characteristic mass were determined and given in Table 5.57.

Figure 5.69 The standard addition curves in the multi-element determination of Pb and Se in Pork Liver sample

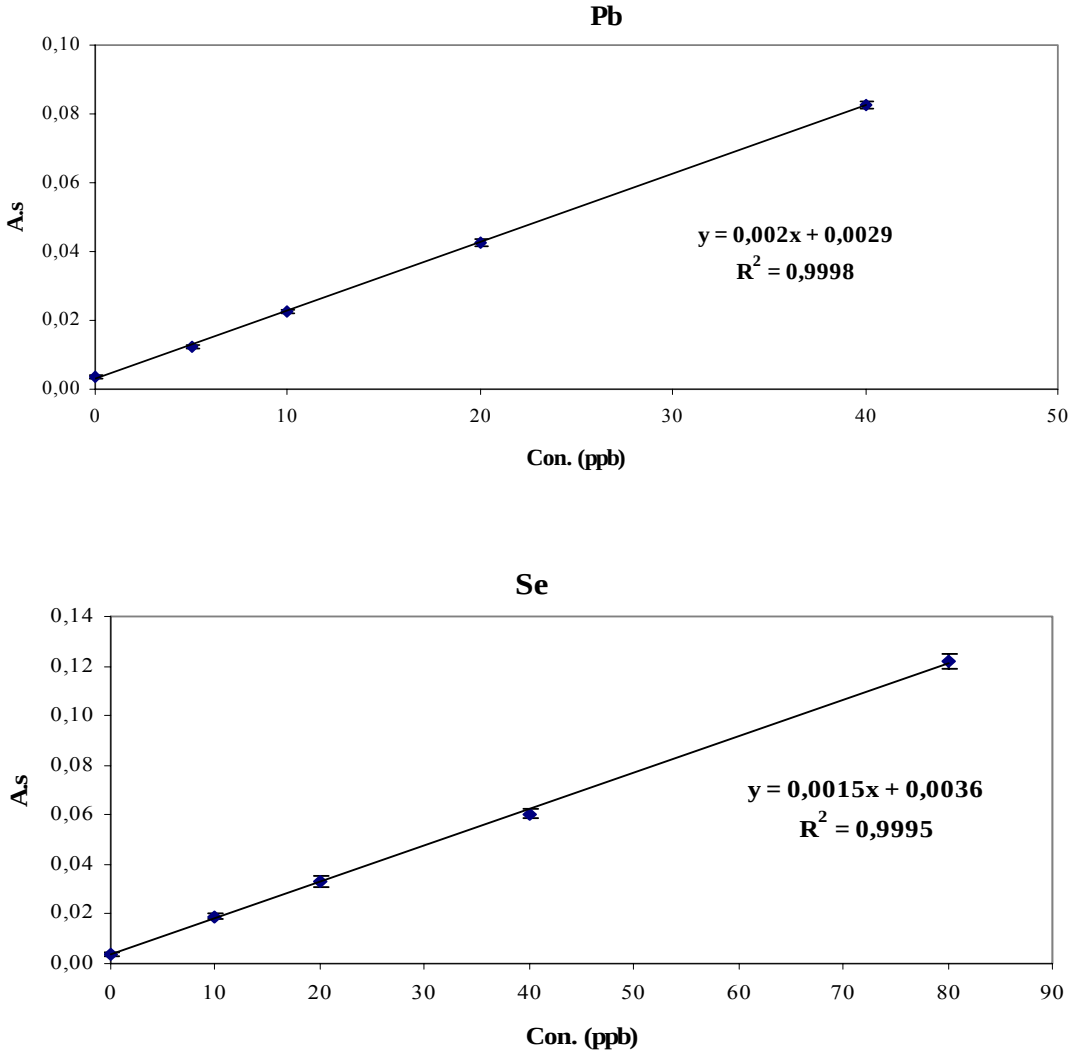

Table 5.56 The results of simultaneous determination of Pb and Se in Pork Liver sample

Element	Con. Found (µg)	Con. certified (µg)
Pb	0.29	0.27
Se	0.48	0.48

Table 5.57 Detection limits, characteristic mass, and relative standard deviations for simultaneous determination of Pb and Se in Pork Liver

Element	LOD (µg.l^{-1})	CM (pg)	RSD* (%)
Pb	0.6	44	6.8
Se	0.8	58.7	8.8

*For five replicates

5.9.5.4 Tea Sample from National Research Centre for Certified Reference Materials (GBW 08505)

The sample was diluted (1:4, v/v) with 0.2% HNO_3. For each measurement, 20 µl of the diluted sample, 5 µl of 1.00 $g.l^{-1}$ $Pd(NO_3)_2$ and 3 µl of 1.00 $g.l^{-1}$ $Mg(NO_2)_3$ modifier solution were injected into the graphite tube at 20°C. The optimum temperature program was as in Table 5.49. The selenium concentration below the detection limits; therefore, the sample has been spiked with it before the dilution.

The standard addition curves for each element are shown in Figure 5.70. The standard addition curves with good linearity (R^2 = 0.9999 and 0.9999 for Se and Pb, respectively) were used to determine the concentration of the elements in the sample. The results are summarized and compared with the certified concentrations in Table 5.58. The experimentally determined concentrations were in good agreement with the certified values. The analyzed values were in the range of 100.0 and 100.0% for Pb and Se, respectively. The relative standard deviations (RSD) of the non spiked sample measurements were in the range: 1.1-3.3% for Pb and 1.1-6.2% for Se. Detection limits were calculated as three times the standard deviation of ten replicate measurements of the blank. The detection limits (LOD) and the characteristic mass were determined and given in Table 5.59.

Figure 5.70 The standard addition curves in the multi-element determination of Pb and Se in Tea sample

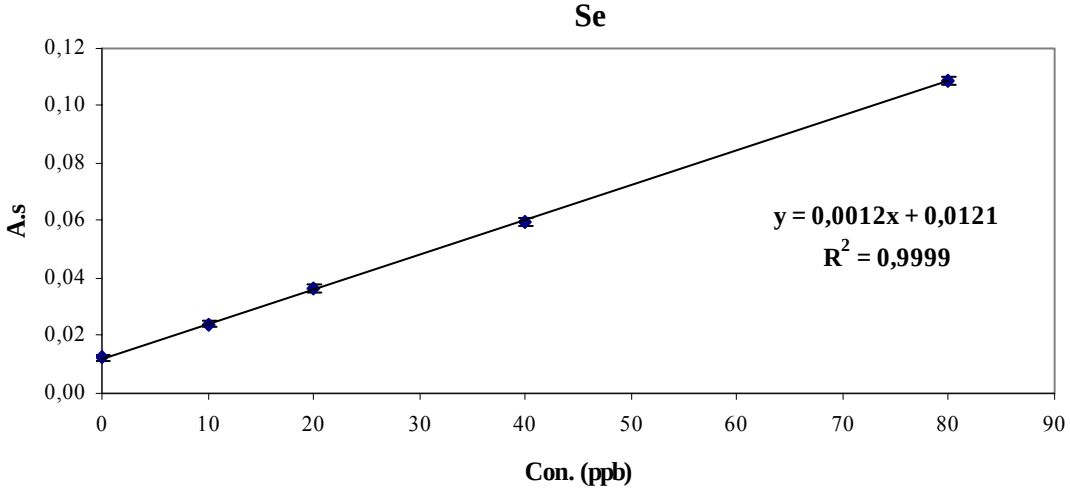

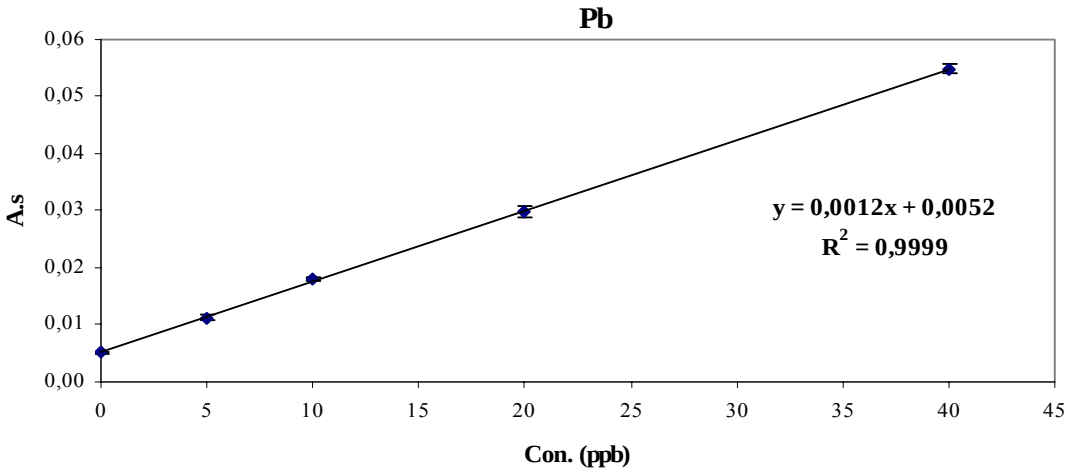

Table 5.58 The results of simultaneous determination of Pb and Se in Tea sample

Element	Con. Found (µg)	Con. certified (µg)
Pb	1.08	1.08
Se	2.5	2.5*

*added

Table 5.59 Detection limits, characteristic mass, and relative standard deviations for simultaneous determination of Pb and Se in Tea sample

Element	LOD (µg.l^{-1})	CM (pg)	RSD* (%)
Pb	0.75	73.3	3.3
Se	1.0	73.3	6.2

***For five replicates**

5.9.5.5 Comparison of the results of Different Samples

With Pd+ Mg as a modifier, the pyrolysis and atomization temperatures were as same as for the simultaneous determinations in aqueous solution (1000 and 1900^{o}C for pyrolysis and atomization, respectively). However, with Ir permanent modifier, it was 800^{o}C for Seronorm urine sample and 1200^{o}C for aqueous solution. By comparing with aqueous solution results, the detection limits values of Pb were more comparable than those of Se. This was also for the characteristic mass values. The highest increasings in detection limits values compared to aqueous solution were as follows: 2 times in Tea sample for Pb and 2.3 times in Bio-Rad urine sample for Se. The results of characteristic mass, however, were also comparable to those of aqueous solution, except for Se, and the increased percentages were in the range of: -20% to + 33% for Pb and - 7% to +133% for Se. The lowest sensitivity values were in the determination of Se in urine samples comparing to aqueous solution value. This was as the simultaneous determination of Cu, Mn, and Se in previous section. The best sensitivities for the two elements were in pork liver sample.

5.9.6 Multi-Element Determination of Bi, Cd, and Sb

The accuracy of the multi-element determination of this group was confirmed by the analysis of the following certified reference materials: Trace Element Urine Sample from Seronorm, Lyphocheck Urine Metals Control- Level 1 from BIO-RAD, Bovine Liver from National Institute of Standards and Technology, Pig Kidney from Institute for Reference Materials and Measurements, Pork Liver from National Research Centre for Certified Reference Materials, and Tea sample from National Research Centre for Certified Reference Materials. The dilution of the sample was according to the concentration of the elements in the sample.

5.9.6.1 Trace Element Urine Sample from Seronorm (0511545)

We have used two types of modifiers; the mixture of Pd and Mg and Ir as a permanent modifier, in the multi-element determination of bismuth, cadmium, and antimony in the urine sample from Seronorm. The sample was diluted (1:4, v/v) with 0.2% HNO_3 and 20µl of the sample was injected for each measurement. 5µl of 1.00 $g.l^{-1}$ Pd and 3µl 1.00 $g.l^{-1}$ $Mg(NO_3)_2$ were injected also with the sample into the graphite tube. In the case of the permanent modifier, the Ir was deposited into the graphite tube in a separate step.

5.9.6.1.1 With Pd+Mg modifier

The temperature program is summarized in Table 5.60.

Table 5.60 Optimum Temperature Program for Simultaneous Determination of Bi, Cd, and Sb in Urine reference sample from Seronorm

Step	Temperature (^oC)	Ramp Time (s)	Hold Time (s)	Gas Flow ($ml.min^{-1}$)
Dry 1	110	1	30	250
Dry 2	130	15	30	250
Pyrolysis	600	10	20	250
Atomization	1900	0	5	0
Clean-out	2400	1	3	250

The standard addition curves for each element are shown in Figure 5.71. The standard addition curves with good linearity (R^2 = 0.9987, 0.9986, and 0.9989 for Bi, Cd, and Sb, respectively) were used to evaluate the concentration of the elements in the sample. The results are summarized and compared with the certified concentrations in Table 5.61. The experimentally determined concentrations were in good agreement with the certified values. The analyzed values were in the range of 97.5, 102.2, and 95.1% for Bi, Cd, and Sb,

respectively. The relative standard deviations (RSD) of the non spiked sample measurements were in the range: 1.5-12.3% for Bi, 0.5-3.3% for Cd, and 0.7-5.6% for Sb. Detection limits were calculated as three times the standard deviation of ten replicate measurements of the blank. The detection limits (LOD) and the characteristic mass were determined and given in Table 5.62.

Figure 5.71 The standard addition curves in the multi-element determination of Bi, Cd, and Sb with Pd+Mg modifier in Urine reference sample from Seronorm

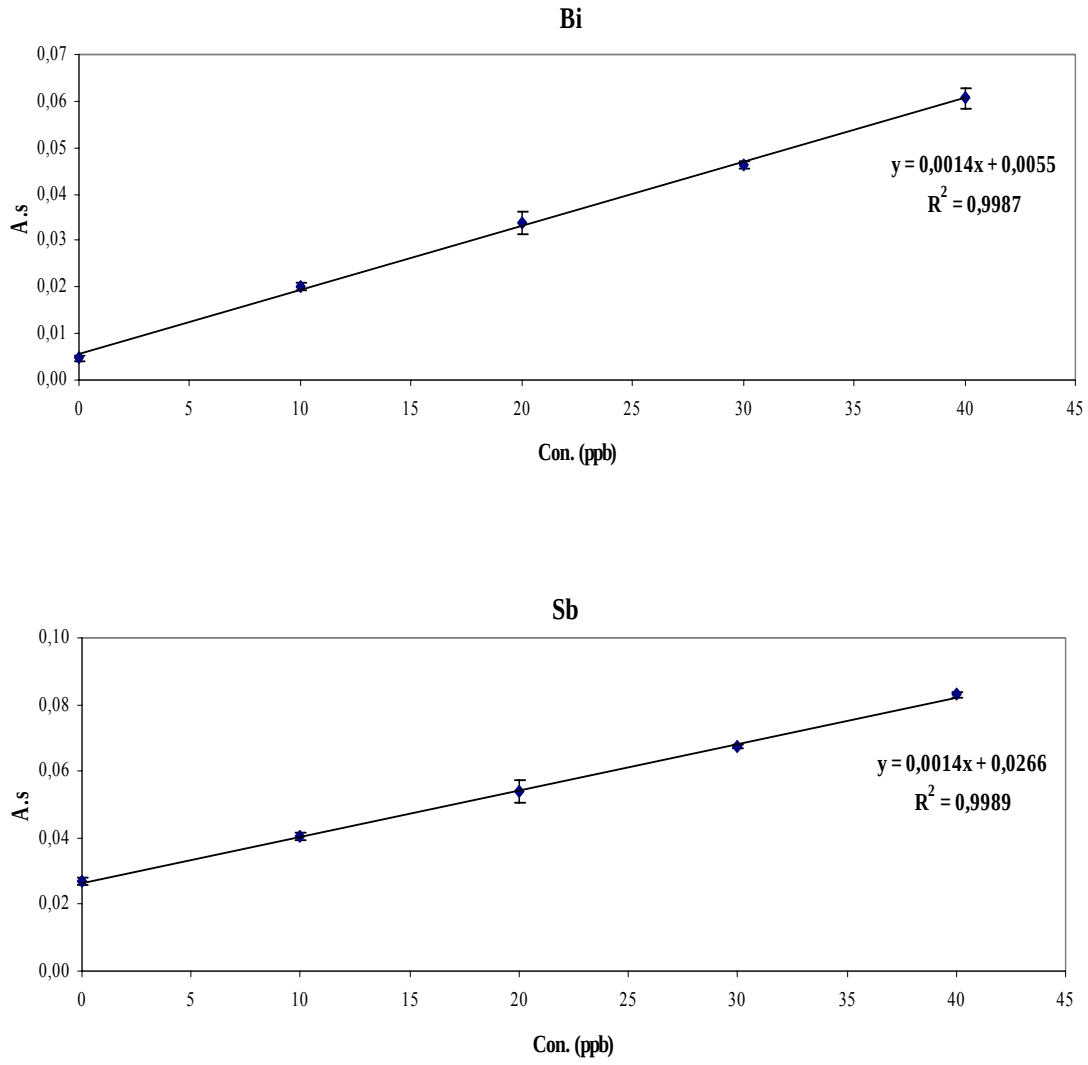

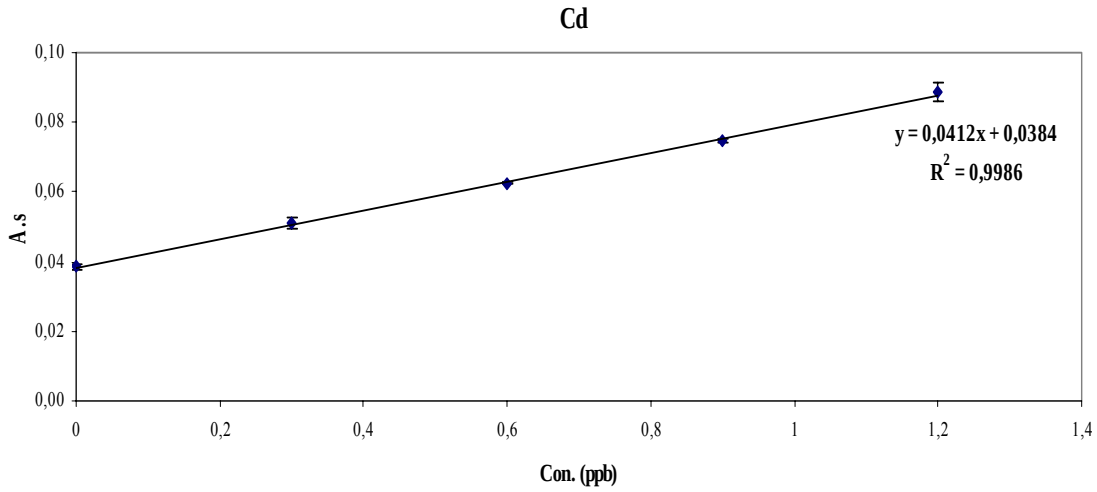

Table 5.61 The results of simultaneous determination of Bi, Cd, and Sb with Pd+Mg modifier in urine reference sample from Seronorm

Element	Con. Found (ppb)	Certified		
		Con. (ppb)	Uncertainty	Acceptable range
Bi	19.6	20.1	19.0-21.2	17.9-22.3
Cd	4.7	4.6	4.2-5.0	3.8-5.4
Sb	95	99.9	94.2-106	88.5-111

Table 5.62 Detection limits, characteristic mass, and relative standard deviations for simultaneous determination of Bi, Cd, and Sb with Pd+Mg modifier in urine reference material from Seronorm

Element	LOD ($\mu g.l^{-1}$)	CM (pg)	RSD* (%)
Bi	0.86	62.9	12.3
Cd	0.015	2.1	2.1
Sb	1.1	62.9	3.7

*For five replicates

5.9.6.1.2 With Ir permanent modifier

The temperature program was as in Table 5.60 but the pyrolysis and atomization temperatures were 500 and 1800^{o}C, respectively.

The standard addition curves for each element are shown in Figure 5.72. The standard addition curves with good linearity (R^2 = 0.9997, 0.9996, and 0.9997 for Bi, Cd, and Sb, respectively) were used to evaluate the concentration of the elements in the sample. The results are summarized and compared with the certified concentrations in Table 5.63. The experimentally determined concentrations were in good agreement with the certified values. The analyzed values were in the range of 109.5, 106.5, and 110.5% for Bi, Cd, and Sb, respectively. The relative standard deviations (RSD) of the non spiked sample measurements were in the range: 0.9-3.6% for Bi, 0.5-2.4% for Cd, and 1.9-5.7% for Se. Detection limits were calculated as three times the standard deviation of ten replicate measurements of the

blank. The detection limits (LOD) and the characteristic mass were determined and given in Table 5.64.

Figure 5.72 The standard addition curves in the multi-element determination of Bi, Cd, and Sb with Ir permanent modifier in Urine reference sample from Seronorm

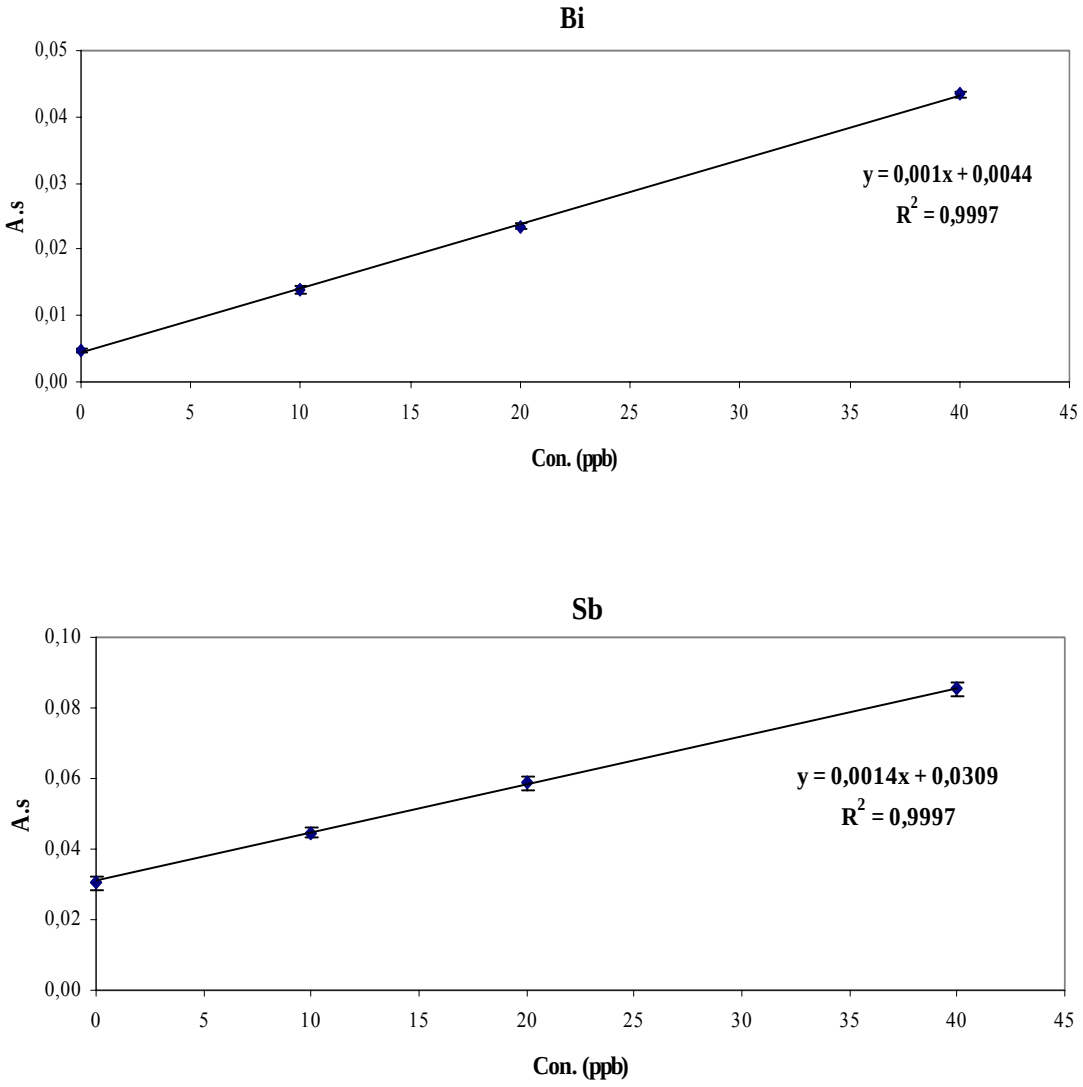

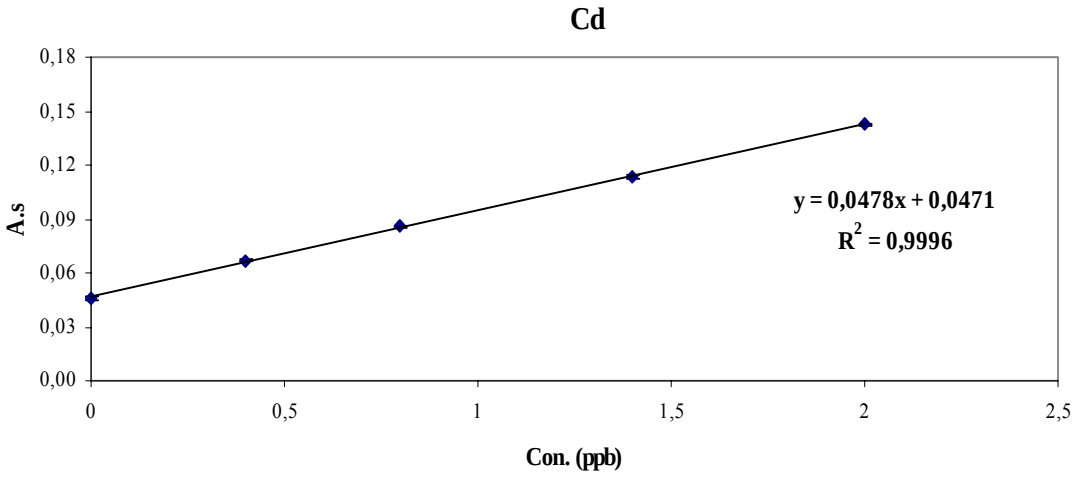

Table 5.63 The results of simultaneous determination of Bi, Cd, and Sb with Ir permanent modifier in urine reference sample from Seronorm

Element	Con. Found (ppb)	Certified		
		Con. (ppb)	Uncertainty	Acceptable range
Bi	22	20.1	19.0-21.2	17.9-22.3
Cd	4.9	4.6	4.2-5.0	3.8-5.4
Sb	110.4	99.9	94.2-106	88.5-111

Table 5.64 Detection limits, characteristic mass, and relative standard deviations for simultaneous determination of Bi, Cd, and Sb with Ir permanent modifier in urine reference material from Seronorm

Element	LOD ($\mu g.l^{-1}$)	CM (pg)	RSD* (%)
Bi	1.5	88	3.6
Cd	0.025	1.8	2.4
Sb	1.3	62.9	5.7

*For five replicates

5.9.6.2 Lyphocheck Urine Metals Control–Level 1 from BIO-RAD (69061)

The sample was diluted (1:1, v/v) with 0.2% HNO_3. For each measurement, 20 µl of the diluted sample, 5 µl of 1.00 $g.l^{-1}$ $Pd(NO_3)_2$ and 3 µl of 1.00 $g.l^{-1}$ $Mg(NO_2)_3$ modifier solution were injected into the graphite tube at 20°C. No certified value for bismuth; therefore, the sample has spiked with bismuth before the dilution. The optimum temperature program was as in Table 5.60.

The standard addition curves for each element are shown in Figure 5.73. The standard addition curves with good linearity (R^2 = 0.9995, 0.9998, and 0.9996 for Bi, Cd, and Sb, respectively) were used to evaluate the concentration of the elements in the sample. The results are summarized and compared with the certified concentrations in Table 5.65. The experimentally determined concentrations were in good agreement with the certified values. The analyzed values were in the range of 102.5, 104.5, and 103.0% for Bi, Cd, and Sb, respectively. The relative standard deviations (RSD) of the non spiked sample measurements

were in the range: 0.9-7.6% for Bi, 0.1-0.5% for Cd, and 1.1-5.9% for Sb. Detection limits were calculated as three times the standard deviation of ten replicate measurements of the blank. The detection limits (LOD) and the characteristic mass were determined and given in Table 5.66.

Figure 5.73 The standard addition curves in the multi-element determination of Bi, Cd, and Sb in Urine reference sample from BIO-RAD

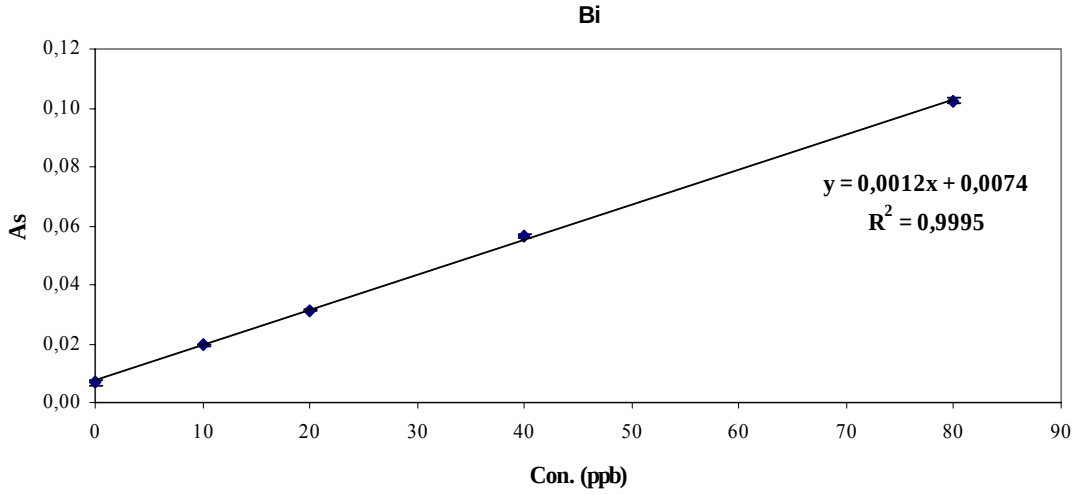

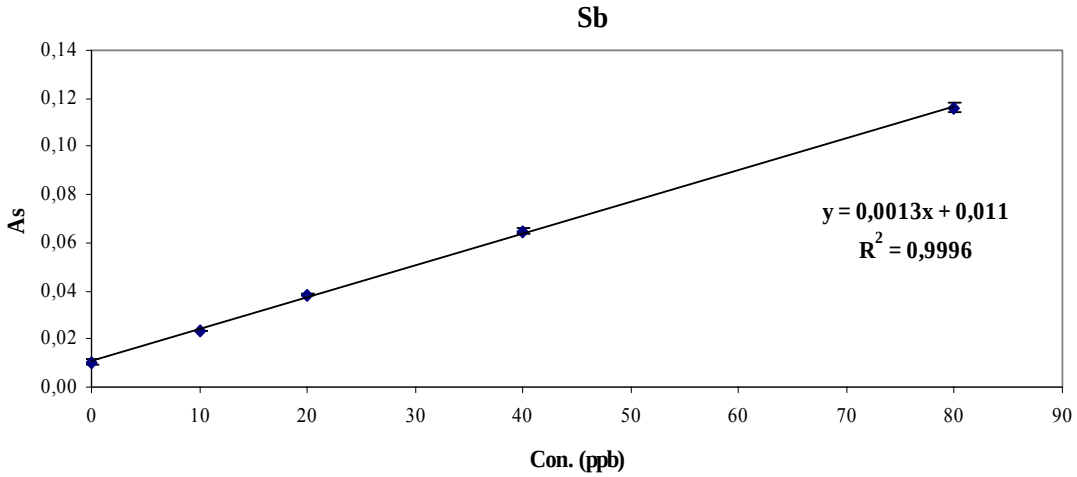

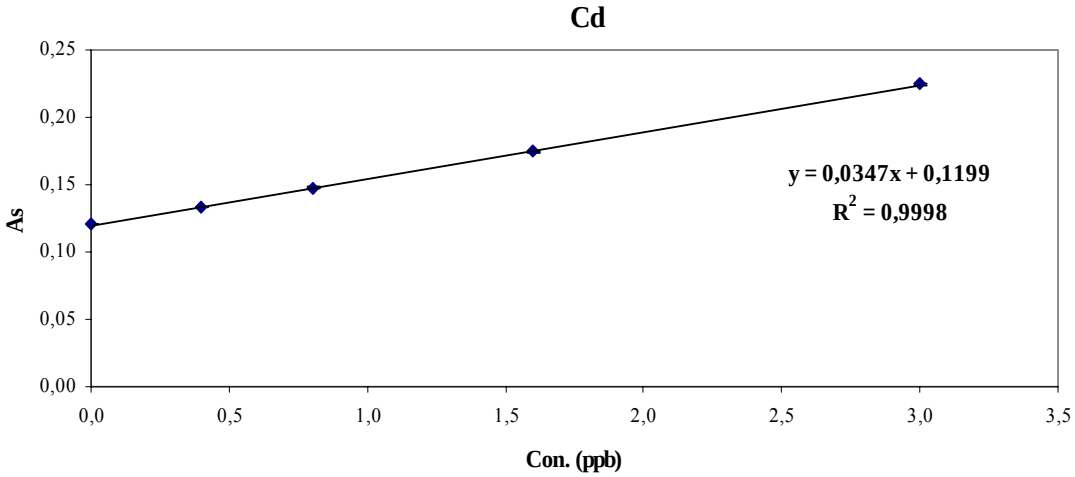

Table 5.65 The results of simultaneous determination of Bi, Cd, and Sb in urine reference sample from BIO-RAD

Element	Con. Found (ppb)	Certified	
		Con. (ppb)	Acceptable range
Bi	12.3	12*	-
Cd	6.9	6.6	5.3-7.9
Sb	16.9	16.4	13.1-19.6

*added

Table 5.66 Detection limits, characteristic mass, and relative standard deviations for simultaneous determination of Bi, Cd, and Sb in urine reference material from BIO-RAD

Element	LOD ($\mu g.l^{-1}$)	CM (pg)	RSD* (%)
Bi	1.0	73.3	7.6
Cd	0.017	2.5	0.2
Sb	0.92	67.7	5.9

*For five replicates

5.9.6.3 Bovine Liver from National Institute of Standards and Technology (NIST-SRM 1577b)

The sample was diluted (1:9, v/v) with 0.2% HNO_3. For each measurement, 20 µl of the diluted sample, 5 µl of 1.00 $g.l^{-1}$ $Pd(NO_3)_2$ and 3 µl of 1.00 $g.l^{-1}$ $Mg(NO_2)_3$ modifier solution were injected into the graphite tube at 20°C. No certified value for bismuth and the amount of antimony was below the detection limits; therefore, the sample has been spiked with them before dilution. The optimum temperature program was as in Table 5.60 except that the atomization temperature was 1950°C.

The standard addition curves for each element are shown in Figure 5.74. The standard addition curves with good linearity (R^2 = 0.9999, 0.9994, and 0.9998 for Bi, Cd, and Sb, respectively) were used to evaluate the concentration of the elements in the sample. The results are summarized and compared with the certified values in Table 5.67. The

experimentally determined concentrations were in good agreement with the certified values. The analyzed values were in the range of 100.0, 96.2, and 98.0% for Bi, Cd, and Sb, respectively. The relative standard deviations (RSD) of the non spiked sample measurements were in the range: 1.4-4.9% for Bi, 1.5-4.7% for Cd, and 1.5-4.4% for Sb. Detection limits were calculated as three times the standard deviation of ten replicate measurements of the blank. The detection limits (LOD) and the characteristic mass were determined and given in Table 5.68.

Figure 5.74 The standard addition curves in the multi-element determination of Bi, Cd, and Sb in Bovine Liver sample

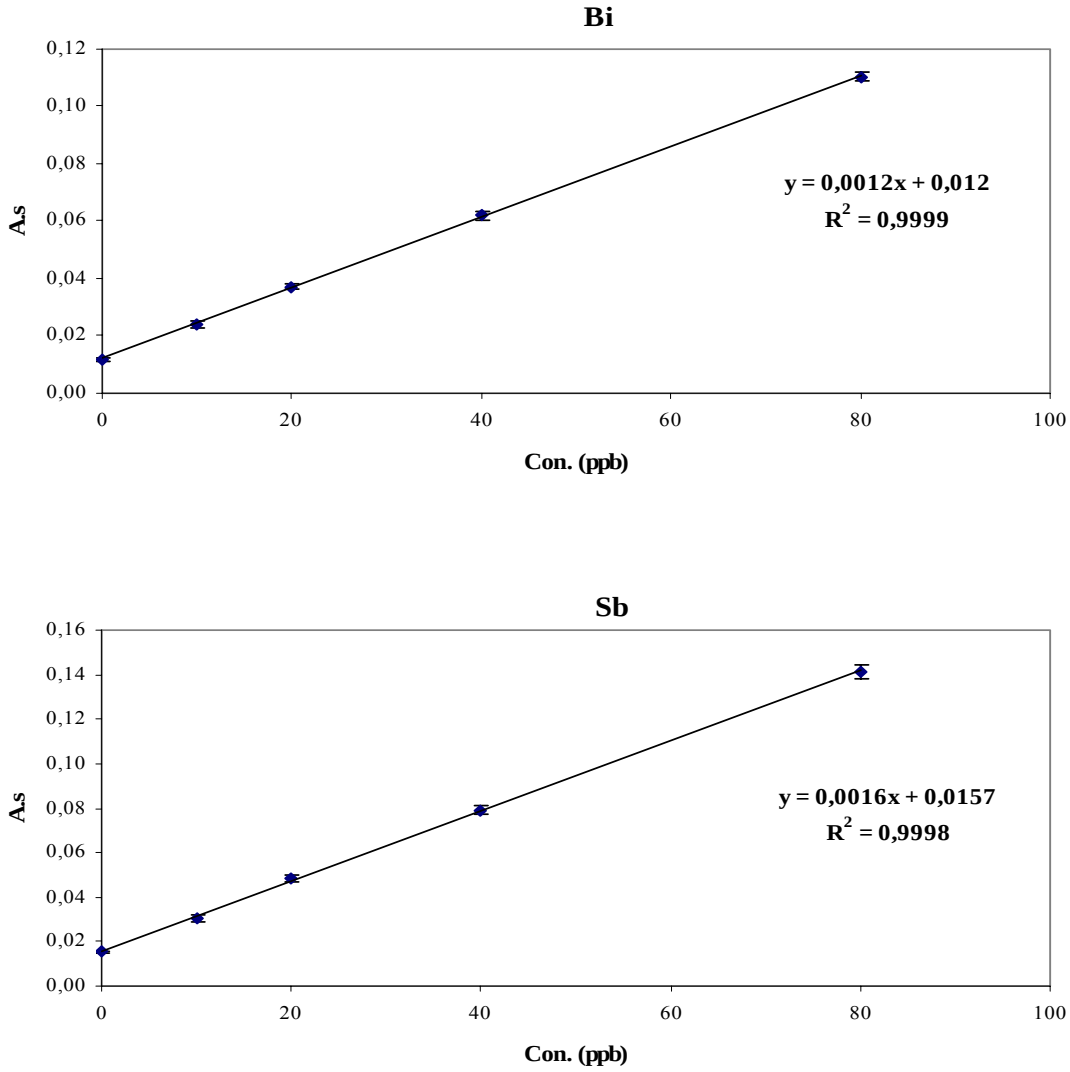

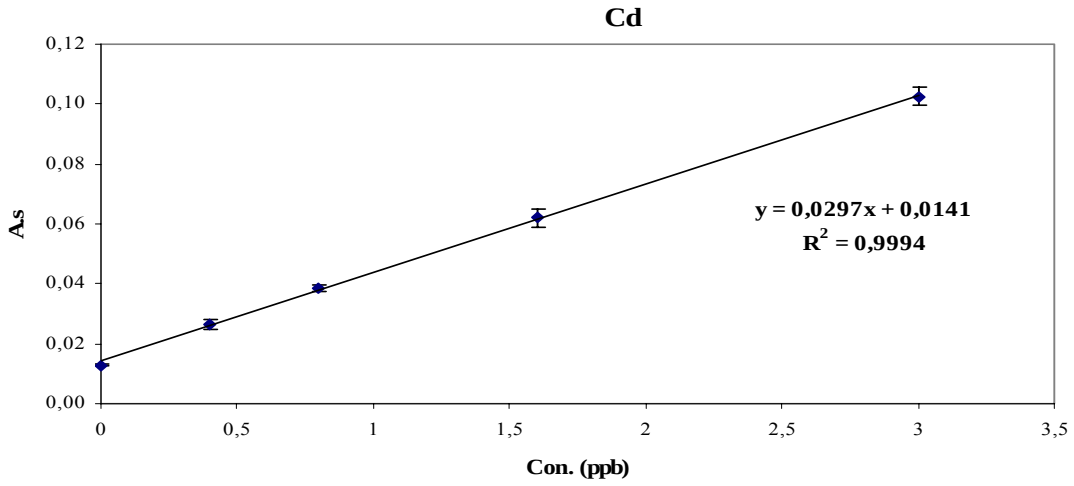

Table 5.67 The results of simultaneous determination of Bi, Cd, and Sb in Bovine Liver sample

Element	Con. Found (µg)	Con. certified (µg)
Bi	5.0	5.0*
Cd	0.25	0.26
Sb	4.9	5.0*

*added

Table 5.68 Detection limits, characteristic mass, and relative standard deviations for simultaneous determination of Bi, Cd, and Sb in Bovine Liver sample

Element	LOD (µg.l^{-1})	CM (pg)	RSD* (%)
Bi	1.0	73.3	4.0
Cd	0.01	3.0	1.5
Sb	0.94	55	1.5

*For five replicates

5.9.6.4 Pig Kidney from Institute for Reference Materials and Measurements (BCR-CRM 186)

The sample was diluted (about 1:28.5, v/v) with 0.2% HNO_3. For each measurement, 20 µl of the diluted sample, 5 µl of 1.00 g.l^{-1} $Pd(NO_3)_2$ and 3 µl of 1.00 g.l^{-1} $Mg(NO_2)_3$ modifier solution were injected into the graphite tube at 20^{o}C. No certified values for bismuth and antimony; therefore, the sample has been spiked with them before dilution. The optimum temperature program was as in Table 5.60 except that the atomization temperature was 2000^{o}C.

The standard addition curves for each element are shown in Figure 5.75. The standard addition curves with good linearity (R^2 = 0.9999, 0.9996, and 0.9996 for Bi, Cd, and Sb, respectively) were used to evaluate the concentration of the elements in the sample. The results are summarized and compared with the certified values in Table 5.69. The experimentally determined concentrations were in good agreement with the certified values. The analyzed values were in the range of 100.7, 92.9, and 100.7% for Bi, Cd, and Sb,

respectively. The relative standard deviations (RSD) of the non spiked sample measurements were in the range: 0.8-5.5% for Bi, 0.3-2.0% for Cd, and 1.3-4.2% for Sb. Detection limits were calculated as three times the standard deviation of ten replicate measurements of the blank. The detection limits (LOD) and the characteristic mass were determined and given in Table 5.70.

Figure 5.75 The standard addition curves in the multi-element determination of Bi, Cd, and Sb in Pig Kidney sample

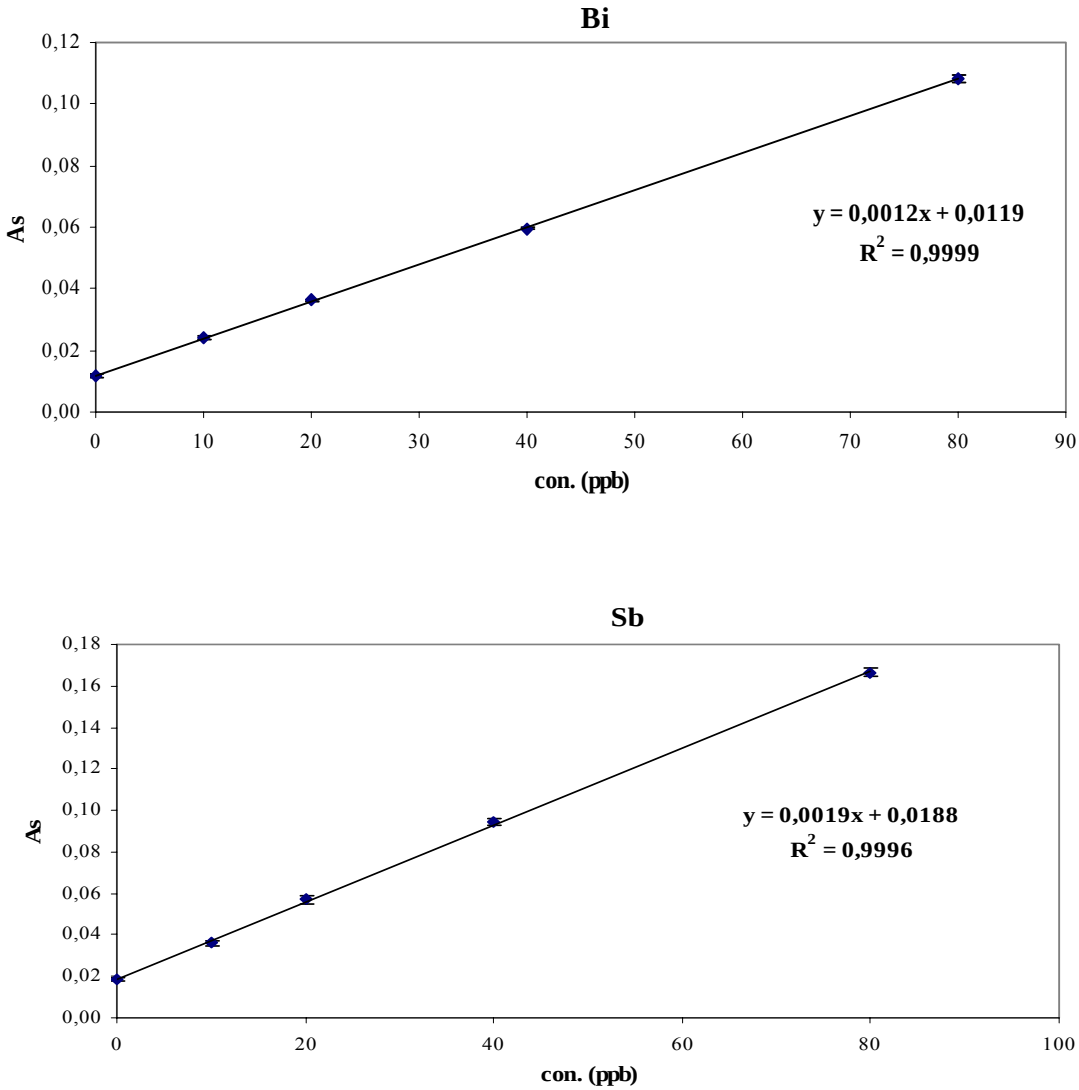

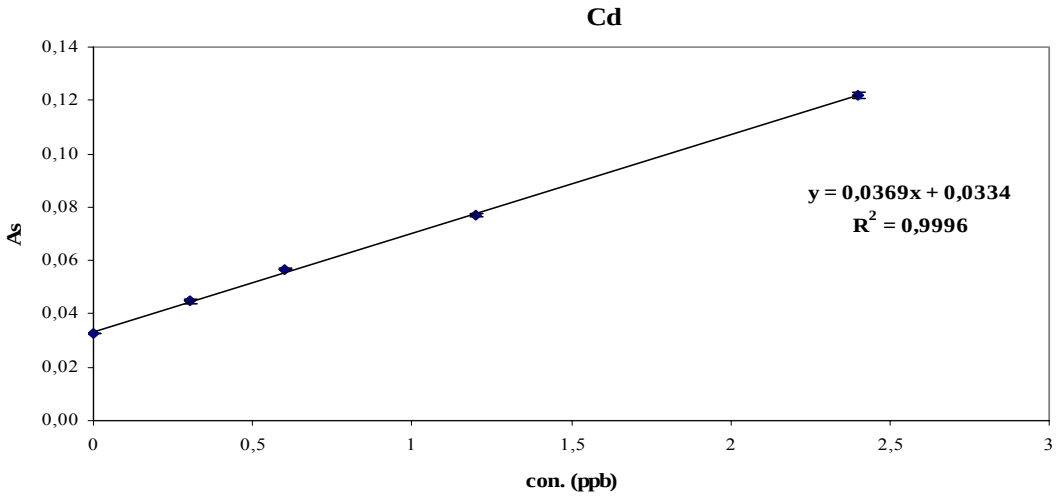

Table 5.69 The results of simultaneous determination of Bi, Cd, and Sb in Pig Kidney sample

Element	Con. Found (µg)	Con. certified (µg)
Bi	14.6	14.5*
Cd	1.3	1.4
Sb	14.6	14.5*

***added**

Table 5.70 Detection limits, characteristic mass, and relative standard deviations for simultaneous determination of Bi, Cd, and Sb in Pig Kidney sample

Element	LOD (µg.l^{-1})	CM (pg)	RSD* (%)
Bi	1.0	73.3	5.5
Cd	0.016	2.4	0.3
Sb	0.79	46.3	4.2

***For five replicates**

5.9.6.5 Pork Liver from National Research Centre for Certified Reference Materials (GBW 08551)

The sample was diluted (about 1:3, v/v) with 0.2% HNO_3. For each measurement, 20 µl of the diluted sample, 5 µl of 1.00 g.l^{-1} $Pd(NO_3)_2$ and 3 µl of 1.00 g.l^{-1} $Mg(NO_2)_3$ modifier solution were injected into the graphite tube at 20^{o}C. No certified values for bismuth and antimony; therefore, the sample has been spiked with them before dilution. The optimum temperature program was as in Table 5.60 except that the atomization temperature was 2000^{o}C.

The standard addition curves for each element are shown in Figure 5.76. The standard addition curves with good linearity (R^2 = 0.9996, 0.9999, and 0.9999 for Bi, Cd, and Sb, respectively) were used to determine the concentration of the elements in the sample. The results are summarized and compared with the certified concentrations in Table 5.71. The experimentally determined concentrations were in good agreement with the certified values. The analyzed values were in the range of 97.5, 100.0, and 98.5% for Bi, Cd, and Sb,

respectively. The relative standard deviations (RSD) of the non spiked sample measurements were in the range: 0.8-4.8% for Bi, 0.8-2.9% for Cd, and 1.3-3.3% for Sb. Detection limits were calculated as three times the standard deviation of ten replicate measurements of the blank. The detection limits (LOD) and the characteristic mass were determined and given in Table 5.72.

Figure 5.76 The standard addition curves in the multi-element determination of Bi, Cd, and Sb in Pork Liver sample

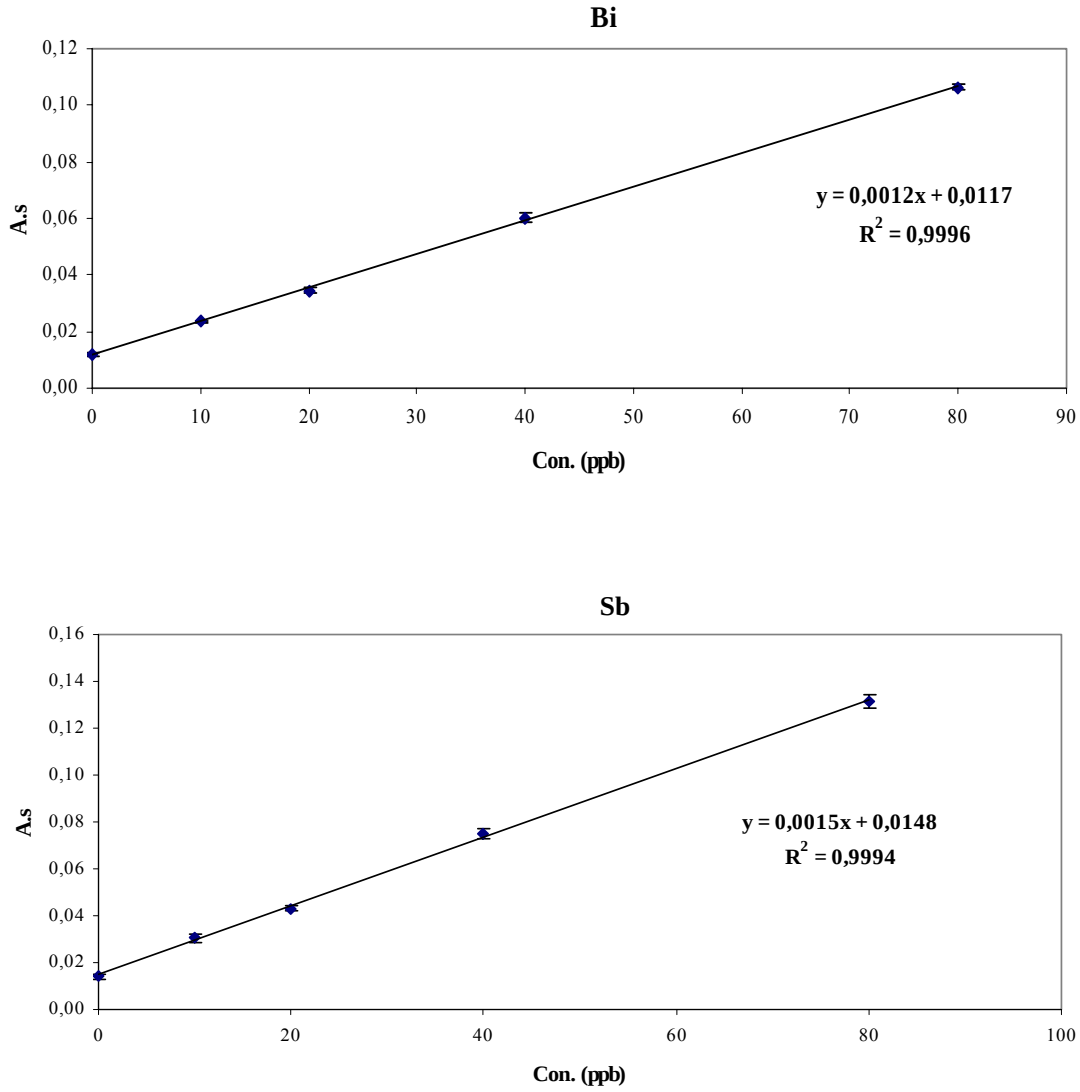

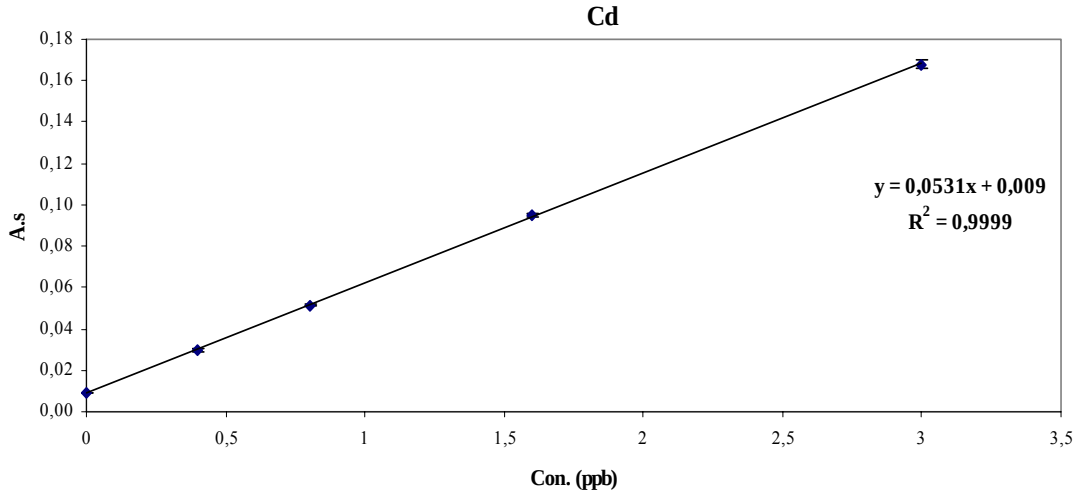

Table 5.71 The results of simultaneous determination of Bi, Cd, and Sb in Pork Liver sample

Element	Con. Found (µg)	Con. certified (µg)
Bi	1.95	2.00*
Cd	0.034	0.034
Sb	1.97	2.00*

*added

Table 5.72 Detection limits, characteristic mass, and relative standard deviations for simultaneous determination of Bi, Cd, and Sb in Pork Liver sample

Element	LOD (µg.l^{-1})	CM (pg)	RSD* (%)
Bi	1.0	73.3	4.8
Cd	0.017	1.7	2.9
Sb	1.0	58.7	2.9

*For five replicates

5.9.6.6 Tea Sample from National Research Centre for Certified Reference Materials (GBW 08505)

The sample was diluted (about 1:4, v/v) with 0.2% HNO_3. For each measurement, 20 µl of the diluted sample, 5 µl of 1.00 g.l^{-1} $Pd(NO_3)_2$ and 3 µl of 1.00 g.l^{-1} $Mg(NO_2)_3$ modifier solution were injected into the graphite tube at 20^{o}C. No certified values for bismuth and antimony; therefore, the sample has been spiked with them before dilution. The optimum temperature program was as in Table 5.60.

The standard addition curves for each element are shown in Figure 5.77. The standard addition curves with good linearity (R^2 = 0.9999, 0.9997, and 0.9999 for Bi, Cd, and Sb, respectively) were used to evaluate the concentration of the elements in the sample. The results are summarized and compared with the certified concentrations in Table 5.73. The experimentally determined concentrations were in good agreement with the certified values. The analyzed values were in the range of 102.2, 103.0, and 96.4% for Bi, Cd, and Sb, respectively. The relative standard deviations (RSD) of the non spiked sample measurements

were in the range: 1.4-7.3% for Bi, 0.3-5.5% for Cd, and 1.7-7.3% for Sb. Detection limits were calculated as three times the standard deviation of ten replicate measurements of the blank. The detection limits (LOD) and the characteristic mass were determined and given in Table 5.74.

Figure 5.77 The standard addition curves in the multi-element determination of Bi, Cd, and Sb in Tea sample

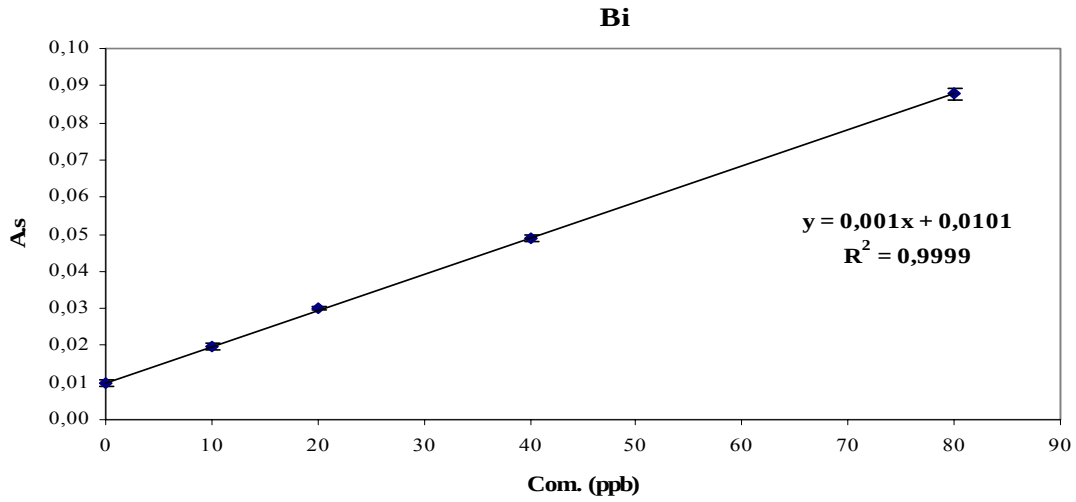

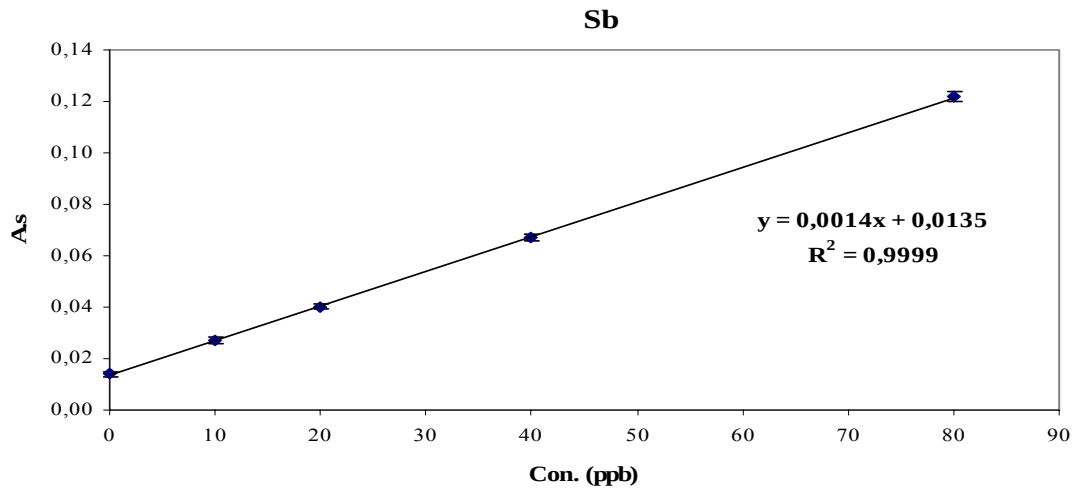

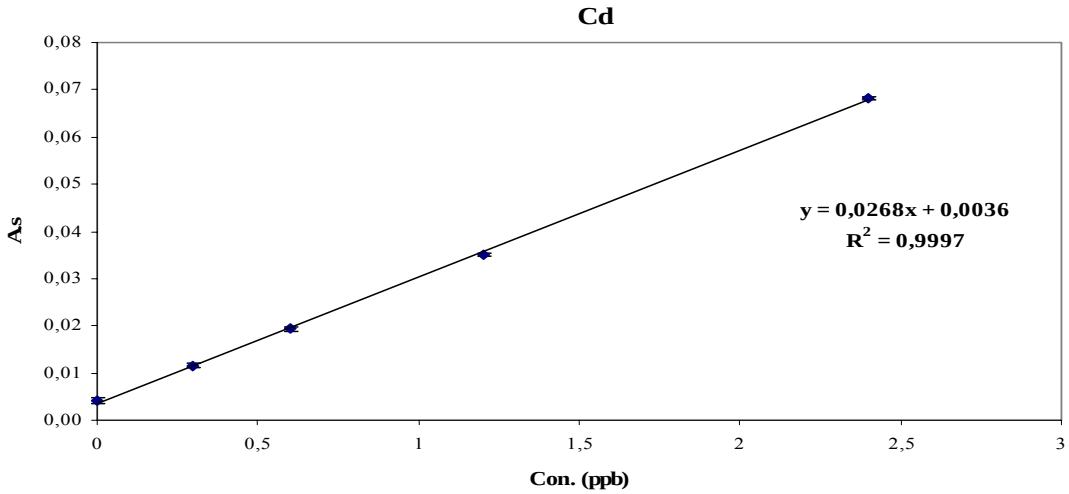

Table 5.73 The results of simultaneous determination of Bi, Cd, and Sb in Tea sample

Element	Con. Found (µg)	Con. certified (µg)
Bi	2.53	2.50*
Cd	0.034	0.033
Sb	2.41	2.50*

***added**

Table 5.74 Detection limits, characteristic mass, and relative standard deviations for simultaneous determination of Bi, Cd, and Sb in Pork Liver sample

Element	LOD (µg.l^{-1})	CM (pg)	RSD* (%)
Bi	0.90	88	7.3
Cd	0.011	3.3	5.5
Sb	1.1	62.9	7.3

***For five replicates**

5.9.6.7 Comparison of the results of Different Samples

With Pd+ Mg as a modifier, the pyrolysis was not as for the simultaneous determinations in aqueous solution (700^{o}C for aqueous solution and 600^{o}C for real samples). However, the pyrolysis was depended on the type of sample. Seronorm and Bio-Rad urine and tea samples was as for aqueous solution (1900^{o}C), bovine liver sample was 1950^{o}C, and pig kidney and pork liver samples was 2000^{o}C. With Ir permanent modifier, they were different from those of aqueous solution (700 and 2100^{o}C for aqueous solution and 500 and 1800^{o}C for urine sample). The detection limits and characteristic mass values were comparable to those of aqueous solution with two modifiers. The highest increasings in detection limits values compared to aqueous solution (with Pd+Mg modifier) were as follows: 1.2 times for Bi, 2 times for Cd, and 1.5 times for Sb. The results of characteristic mass, however, were also comparable to those of aqueous solution and the increased percentages were in the range of: - 21% to + 10% for Bi, - 32% to + 32% for Cd, and + 5% to +54% for Sb.

5.9.7 Summary

All of the results obtained are within the acceptable range indicating the suitability of the optimized methods to determine the elements simultaneously in different types of biological samples. The concentrations obtained were within 90-110% of the certified values (except Cu in the bovine liver 86% and Al in the urine from BIO-RAD 111.3% and in the pork liver 117%). All the samples were diluted according to the concentrations of the elements in the sample. The detection limits and characteristic mass values were matrix and modifier dependent, but generally, they were comparable to those of aqueous solution. The relative standard deviation (RSD) values for all samples, which have been calculated according to five replicates diluted non spiked samples, were less than 10% (except Bi and Se values in the urine sample from Seronorm which were 12.3% and 12.4%, respectively). Good linear correlation coefficients for the elements were obtained except for Al in the urine sample from Seronorm where no acceptable linearity was obtained.

5.10 Conclusion

Simultaneous Multi-Element Atomic Absorption Spectrometer (SIMAA 6000) can be used to determine groups of elements (up to six) simultaneously, by using 2-operating and 4-operating modes, if the temperature program has been carefully optimized taking into account all analytes to be determined. The optimization depends on the elements to be determined simultaneously and the matrix. Also, a universal powerful matrix modifier should be used in order to increase the stability of the elements (especially the volatile elements). This will permit the use of a common temperature program including volatile and less volatile elements. The chemical modifier selection is critical and minimization of interference effects caused by sample matrix must be taken into account as well as the stabilization obtained for the analytes. All tested chemical modifiers increased the thermal stability of the elements. The Pd+Mg mixture modifier stabilizes the high and mid volatile elements. The stabilization effect appears in using higher pyrolysis temperature (up to 1000°C comparison with the situation without modifier) and to some extent the atomization temperature. For less volatile elements, the modifier has no stabilization effect on these elements. But the modifier in this case could prevent the formation of refractory compounds which increase the volatilization process of these elements. Ir coating of the tube or platform extend significantly the tube lifetime. Also, Ir coating is not time-consuming and so the proposed methodology is a useful analytical tool for routine analysis. This work presents a direct, simple, fast, and accurate methodology for the simultaneous multi-element determination of group of elements (up to four) in biological

samples by graphite furnace atomic absorption spectrometry. The accuracy of the methods was tested by analyzing number of certified materials and the concentrations obtained were in good agreement with certified values. The sensitivity values for the multi-element determination were comparable to those of the single-element. The decreasing in sensitivity values is a result of using higher atomization temperature in the multi-element mode and/or decreasing the lamp intensities. The detection limits values of the multi-element determination were higher than those of the single-element which is mainly as a result of decreasing the lamp intensities in the multi-element mode compared to the single-element mode. Another effect which could cause the higher detection limits is the use of higher atomization temperature. The operational conditions (the temperatures, use of modifier, and the operating mode) affect more or slightly the absorption signals of the elements. This effect appears in terms of increasing or decreasing the appearance time, peak height, and bandwidth.

Advantages of simultaneous multi-element analysis over single-element analysis include speed with the overall analysis time (the time reduction being proportional to the number of elements run together), and reduced consumption of reagents per sample. The disadvantage is reflected by the higher detection limits obtained for multi-element analysis when compared with single-element analysis. This can be attributed to reducing the intensities of the lamps as a result of the combining the radiation from them. The sensitivity could be damaged if the compromised parameters were not carefully optimized. For a number of materials, the compromise settings especially the heating program could be developed without any loss of sensitivity. For routine simultaneous multi-element analysis, all analytes should be present at low concentration levels in the sample and must lie within the working range of the instrumentation. This may be the main problem for simultaneous multi-element analyses of real samples where concentrations of analytes may be highly variable.

6 References:

1) H. M. Kuss, R. Maibusch, and B. Bayraktar, Proceedings, Trace Element Determination by means of Simultaneous Multielement Graphite Furnace Atomic Absorption Spectrometry, *XIVth Seminar on Atomic Spectrometry*, High Tatras-Podbanske, September **1998,** 84-90

2) V. de Amorim Filho, K. G. Fernandes, M. de Moraes, and J. A. G. Neto, Evaluation of the Mixtures Phosphate/Magnesium Nitrate and Palladium Nitrate/Magnesium Nitrate as Modifiers for Simultaneous Determination of Cd, Cr, Ni, and Pb in Mineral Water by GFAAS, *Journal of the Brazilian Chemical Society*, 15(**2004**)1, 28-33

3) C. Vandecasteele, C. B. Bkock, *Modern Methods for Trace Element Determination*, John Wiley & Sons, Chichester, **1997**

4) R. H. Williams, *Trace Metals Analysis using Continuum Source Simultaneous Multielement Graphite Furnace Atomic Absorption Spectroscopy*, a Dissertation submitted to the Faculty of the Department of Chemistry, the University of Arizona, **2000**

5) B. Radziuk, G. Rödel, H. Stenz, H. Becker-Ross, and S. Florek, Spectrometer System for Simultaneous Multi-element Electrothermal Atomic Absorption Spectrometry using Line Sources and Zeeman-effect Background Correction, *Journal of Analytical Atomic Spectrometry*, 10(**1995**), 127-136

6) P. J. Parsons and W. Slavin, A rapid Zeeman Graphite Furnace Atomic Absorption Spectrometric Method for the Determination of Lead in Blood, *Spectrochimica Acta*, 48B(**1993**), 925-939

7) S. Hauptkorn and V. Karivan, Determination of Silicon in Boron Nitride by Slurry Sampling Electrothermal Atomic Absorption Spectrometry, *Spectrochimica Acta*, 49B(**1994**), 221-228

8) C. Minoia and S. Caroi, *Applications of Zeeman Graphite Furnace Atomic absorption Spectrometry in the Clinical Laboratory and in Toxicology*, 1st ed., Pergamon Press, New York, **1992**

9) M. Hoenig and A. Cilissen, Performances and Practical Applications of Simultaneous Multi-element Electrothermal Atomic Absorption Spectrometry the Case of the SIMAA 6000, *Spectrochimica Acta*, 52B(**1997**), 1443-1449

10) T. Akagi, K. Fuwa, and H. Harguchi, Simultaneous Multi-element Determination of Trace Metals in Sea Water by Inductively-coupled Plasma Atomic Emission Spectrometry after Coprecipitation with Gallium, *Analytica Chimica Acta*, 177(**1985**), 139-151

11) G. Chapple and J. P. Byrne, Direct Determination of Trace Metals in Sea-water using Electrothermal Vaporization Inductively Coupled Plasma Mass Spectrometry , *Journal of Analytical Atomic Spectrometry*, 11(**1996**), 549-553

12) A. Prange, A. Knöchel, and W. Michaelis, Multi-element Determination of Dissolved Heavy Metal Traces in Sea Water by Total-reflection X-ray Fluorescence Spectrometry, *Analytica Chimica Acta*, 172(**1985**), 79-100

13) C. Colombo and C. M. G. van den Berg, Simultaneous Determination of Several Trace Metals in Seawater using Cathodic Stripping Voltammetry with Mixed Ligands, *Analytica Chimica Acta*, 337(**1997**), 29-40

14) M. Berglund, W. Frech, D. C. Baxter, and B. Radizink, A Critical Evaluation of a Multielement ETAAS System using Line Sources and a Transversely Heated Graphite Atomizer with Zeeman effect Background Correction, *Spectrochimica Acta*, 48B(**1993**), 1381-1392

15) J. G. Sen Gupta and J. L. Bouiver, Direct Determination of Traces of Ag, Cd, Pb, Bi, Cr, Mn, Co, Ni, Li, Be, Cu and Sb in Environmental Waters and Geological Materials by Simultaneous Multi-element Graphite Furnace Atomic Absorption Spectrometry with Zeeman-effect Background Correction, *Talanta*, 42(**1995**), 269-281

16) H. Edel, L. Quick, and K. Cammann, Simultaneous Multielement Determination in Complex Matrices using Frequency-modulated Electrothermal Atomic Absorption Spectrometry, *Analytica Chimica Acta*, 310(**1995**), 181-187

17) B. S. Iversen, A. Panayi, J. P. Camblor, and E. Sabbioni, Simultaneous Determination of Cobalt and Manganese in Urine by Electrothermal Atomic Absorption Spectrometry. Method Development using a Simplex Optimization Approach, *Journal of Analytical Atomic Spectrometry*, 11(**1996**), 591-594

18) Y. I. Lee, M. V. Smith, S. Indurthy, A. Deval, and J. Sneddon, An Improved Impaction-Graphite Furnace System for the Direct and Near Real-time Determination of Cadmium, Chromium, Lead and Manganese in Aerosols and Cigarette Smoke by Simultaneous Multielement Atomic Absorption Spectrometry, *Spectrochimica Acta*, 51B(**1996**), 109-116

19) V. Gottelet, G. Henrion, R. Kalahne, and M. Stoyke, Simultanbestimmungsmethoden für die Elemente Kupfer, Zink, Eisen und Mangan sowie Natrium, Kalium, Calcium und Magnesium mittels Flammen-Atomabsorptionsspektrometrie (F-AAS) , *Nahrung Food*, 40(**1996**), 313-318

20) Pi-guey Su and Shang-da Huang, Direct and Simultaneous Determination of Copper and Manganese in Seawater with a Multielement Graphite Furnace Atomic Absorption Spectrometer, *Spectrochimica Acta*, 53B(**1998**), 699-708

21) J. V. Sullivan and A. Walsh, Application of Resonance Monochromators to Simultaneous Determination of Several Elements, *VI Australian Spectroscopy Conference*, Brisbane, **1967**

22) J. V. Sullivan and A. Walsh, *Proceeding of the XIII Colloquium Spectroscopium Internationale (CSI),* Ottawa, **1967**

23) J. V. Sullivan and A. Walsh, The Isolation and Detection of Atomic Resonance Lines, *Applied Optics*, 7(**1968**), 1271-1280

24) R. Mavrodineanu and R. C. Hughes, A Multichannel Spectrometer for Simultaneous Atomic Absorption and Flame Emission Analysis, *Applied Optics*, 7(**1968**), 1281-1286

25) L. R. P. Butler and A. Strasheim, Multiple Element Atomic Absorption Analysis, *Spectrochimica Acta*, 21B(**1965**), 1207-1216

26) D. G. Mitchell, K. W. Jackson, and K. M. Aldous, Application of a Silicon-target Vidicon Detector to Simultaneous Multielement Flame Spectrometry, *Analytical Chemistry*, 45(**1973**), 1215A-1223A

27) J. F. Alder, D. Alger, A. J. Samuel, and T. S. West, The Design and Development of a Multichannel Atomic Absorption Spectrometer for the Simultaneous Determination of Trace Metals in hair, *Analytica Chimica Acta*, 87(**1976**), 301-311

28) G. R. Dulude, J. J. Sotera, and D. N. Peterson, Practical Utility of Dual-channel Furnace Atomic Absorption Spectrometry for EPA Contract Laboratory Program Samples , *Spectroscopy (Duluth, MN, United States)*, 4(**1989**), 44,46-49

29) T. Kumamaru, Y. Okamoto, S. Matsuo, and M. Kiboku, Simultaneous Determination of Copper and Lead by Graphite-furnace Atomic Absorption Spectrometry after Liquid-liquid Extraction of the Ion-pair with Zephiramine. , *Analytica Chimica Acta*, 218(**1989**), 173-178

30) S. R. Lawson, J. A. Nicholas, P. Viswanadham, and R. Woodriff, Demonstration of Techniques and a Suitable Atomizer for Practical Multielement Atomic Absorption Analysis, *Applied Spectroscopy*, 36(**1982**), 375-378

31) S. Nakamura and M. Kubota, Single-channel Time-divided Simultaneous Multi-element Atomic Absorption Spectrometry using an Electrothermal Atomiser, *Analyst*, 115(**1990**), 283-286

32) J. B. Reust and H. D. Seltner, Trace Determination of Aluminium in Alkaline Earth-containing Pharmaceuticals by Graphite Tube Furnace-atomic Absorption Spectrometry, *5th*

Colloquium Atomspektrometrische Spurenanalytik, Bodenseewerk Perkin-Elmer, Überlingen, (**1989**), 657-665

33) E. Lundberg and G. Johansson, Simultaneous Determination of Manganese, Cobalt, and Copper with a Computer-controlled Flameless Atomic Absorption Spectrophotometer, *Analytical Chemistry*, 48(**1976**), 1922-1926

34) A. T. Zander, T. C. O'Haver, and P. N. Keliher, Continuum Source Atomic Absorption Spectrometry with High Resolution and Wavelength Modulation, *Analytical Chemistry*, 48(**1976**), 1166-1175

35) B. Raziuk, G. Rödel, M. Zeiher, S. Mizuno, and K. Yamamoto, Solid State Detector for Simultaneous Multi-element Electrothermal Atomic Absorption Spectrometry with Zeeman-effect Background Correction, *Journal of Analytical Atomic Spectrometry*, 10(**1995**), 415-422

36) I. L. Shuttler and H. Schulze, Multi-element ETAAS becomes a Reality, *Analysis Europa*, 1(**1994**), 44

37) Chun-Hao Chiu, Yu-Hsiang Sung, and Shang-Da Huang, Simultaneous Determination of Manganese, Iron and Cobalt in Copper with a Multi-element Graphite Furnace Atomic Absorption Spectrometer, *Spectrochimica Acta*, 58B(**2003**), 575-580

38) B. E. Erickson, Graphite Furnace AAS, *Analytical Chemistry*, 72(**2000**)543A

39) W. Slavin, D. C. Manning, and G. R. Garnrick, The Stabilized Temperature Platform Furnace, *Atomic Spectroscopy*, 2(**1981**), 137-145

40) C. S. Nomura, P. R. M. Corriea, P. V. Oliveira, and E. Oliveira, W+Rh as Permanent Chemical Modifier in Simultaneous Atomic Absorption Spectrometry: Interference Studies on As, Cd, Pb and Se Determination, *Journal of the Brazilian Chemical Society*, 15(**2004**)1, 75-82

41) R. D. Ediger, Atomic Absorption Analysis with the Graphite Furnace using Matrix Modification, *Atomic Absorption Newsletter*, 14(**1975**), 127-130

42) M. Y. Shiue, Y. C. Sun, and M. H. Yang, Determination of Tellurium in Indium Antimonide Semiconductor Material by Electrothermal Atomic Absorption Spectrometry, *Analyst*, 126(**2001**), 1449-1452

43) D. A. Skoog and J. J. Leary, *Principles of Instrumental Analysis*, 4th ed., **1992**, Orlando, FL: Harcourt Brace & Company

44) Bernhard Welz, *Atomic Absorption Spectrometry*, 2nd ed., **1985**, VCH Verlagsgesellschaft mbH, D-6940 Weinheim, Germany

45) R. E. Sturgeon, C. L. Chakrabarti and C. H. Langford, Studies on the Mechanism of Atom Formation in Graphite Furnace Atomic Absorption Spectrometry, *Analytical Chemistry*, 48(**1976**), 1792-1807

46) R. E. Sturgeon and C. L. Chakrabarti, Recent Advances in Electrothermal Atomization in Graphite Furnace Atomic Absorption Spectrometry, *Progress in Analytical Atomic Spectroscopy*, 1(**1978**), 5-199

47) C. L. Chakrabarti, H. A. Hamed, C. C. Wan, W. C. Li, P. C. Bertels, D. C. Gregoire, and S. Lee, Capacitive Discharge Heating in Graphite Furnace Atomic Absorption Spectrometry, *Analytical Chemistry*, 52(**1980**), 167-176

48) B. Smets, Atom Formation and Dissipation in Electrothermal Atomization, *Spectrochimica Acta*, 35B(**1980**), 33-42

49) B. V. L'vov, L. A. Pelieva, and A. I. Sharnopolsky, Decrease in the Effect of the Base During the Atomic-absorption Analysis of Solutions in Tube Furnaces by Evaporation of Samples from a Graphite Substrate, *Zhurnal Prikladnoi Spektroskopii*, 27(**1977**), 395-399

50) Leeman Labs, Inc., *Leeman Letter* September (**1994**), p3

51) M. Retzik and D. Bass, Concept and Design of a Simultaneous Multielement GFAAS, *American Laboratory* (Shelton, CT, United States), 20(**1988**), 70, 72-77

52) D. Bass, Considerations in Multielement Graphite Furnace AA Spectroscopy, *American Laboratory* (Shelton, CT, United States), (**1989**), 24, 26-28

53) S. B. Jr. Smith and G. M. Hieftje, A New Background-correction Method for Atomic Absorption Spectrometry, *Applied Spectroscopy*, 37(**1983**), 419-424

54) G. R. Dulude, Thermo Jarrell Ash (personal communication), **1995**

55) J. Sneddon, B. D. Farah, and K. S. Farah, Multielement Atomic Absorption Spectrometry: A Historical Perspective, *Microchemical Journal*, 48(**1993**), 318-325

56) J. M. Harnly, Multielement Atomic Absorption with a Continuum Source, *Analytical Chemistry*, 58(**1986**), 933A-943A

57) K. S. Farah and J. Sneddon, Development and Applications of Multi-element Graphite Furnace Atomic Absorption Spectrometry, Applied Spectroscopy Reviews, 30(**1995**), 351-371

58) C. J. Pickford and G. Rossi, Analysis of High-purity Water by Flameless Atomic-absorption Spectroscopy. Part II. Signal Integration with a Non-resonance Line Correction System for Spurious Absorption Phenomena, *Analyst*, 98(**1973**), 329-334

59) E. D. Salin and J. D. Ingle, Design and Performance of a Time Multiplex Multiple Slit Multielement Flameless Atomic Absorption Spectrometer, *Applied Spectroscopy*, 32(**1978**), 579-584

60) S. L. Tong and K. S. Chin, Simultaneous Multielement Graphite Furnace Atomic Absorption Measurements using a Photodiode Array Detector, *Spectrochimica Acta*, 49B(**1994**), 459-467

61) K. Yasuda, T. Okumoto, A. Yonetani, H. Yamada, and K. Ohishi, Developments in Multichannel Atomic Absorption Spectrometry. Expansion of Dynamic Ranges in Working Curves and Optimization of Atomization for Multielements, *5th Colloquium Atomspektrometrische Spurenanalytik*, **1989**, 133-143

62) J. R. Dulude, Spectroscopist, 1(**1992**), 3-4

63) A. Deval and J. Sneddon, Determination of Cadmium and Lead in Blood Reference Samples by Simultaneous Graphite Furnace Atomic Absorption Spectrometry, *Michrochemical Journal*, 52(**1995**), 96-100

64) J. M. Harnly, Instrumentation for Simultaneous Multielement Atomic Absorption Spectrometry with Graphite Furnace Atomization, *Fresenius' Journal of Analytical Chemistry*, 355(1996), 501-509

65) D. J. Butcher and J. Sneddon, *A Practical Guide to Graphite Furnace Atomic Absorption Spectrometry. Chemical Analysis*, Ed. J. D. Winefordner. Vol. 149, **1998**, New York: John Wiley and Sons, Inc. 250

66) J. M. Harnly, T. C. O'Haver, B. Golden, and W. R. Wolf, Background-corrected Simultaneous Multielement Atomic Absorption Spectrometer, *Analytical Chemistry*, 51(**1979**), 2007-2014

67) P. R. M. Correia, E. Oliveira, a nd P. V. Oliveira, Simultaneous Determination of Manganese and Selenium in Serum by Electrothermal Atomic Absorption Spectrometry, *Talanta*, 57(**2002**), 527-535

68) P. R. M. Correia, E. Oliveira, and P. V. Oliveira, Minimalism Approach for Determination of Cu, Fe and Zn in Serum by Simultaneous Electrothermal Atomic Absorption Spectrometry, *Analytica Chimica Acta*, 458(**2002**), 321-329

69) V. R. A. Filho, K. G. Fernandes, M. De Moraes, and J. A. G. Neto, Simultaneous Determination of As, Cu, Mn, Sb, and Se in Drinking Water by GFAAS with Transversely Heated Graphite Atomizer and Longitudinal Zeeman-effect Background Correction, *Atomic Spectroscopy*, 23(**2002**), 7-11

70) A. P. Oliveira, M. Moraes, J. A. G. Neto, and E. C. Lima, Simultaneous Determination of Al, As, Cu, Fe, Mn, and Ni in Fuel Ethanol by GFAAS, *Atomic Spectroscopy*, 23(**2002**), 39-42

71) K. G. Fernandes, M. Moraes, J. A. G. Neto, J. A. Nóbrega, Evaluation and Application of Bismuth as an Internal Standard for the Determination of Lead in Wines by Simultaneous Electrothermal Atomic Absorption Spectrometry, *Analyst*, 127(**2002**), 157-162

72) C. Chen, K. S. K. Danadurai, and S. Huang, Direct and Simultaneous Determination of Copper, Manganese and Molybdenum in Seawater with a Multi-element Electrothermal Atomic Absorption Spectrometer, *Journal of Analytical Atomic Spectrometry*, 16(**2001**), 404-408

73) A. B. Volynsky and R. Wennrich, Comparative Efficiency of Pd, Rh and Ru Modifiers in Electrothermal Atomic Absorption Spectrometry for the Simultaneous Determination of As, Se and In in a Sodium Sulfate Matrix, *Journal of Analytical Atomic Spectrometry*, 16(**2001**), 179-187

74) P. V. Oliveira and E. Oliveira, Multielement Electrothermal Atomic Absorption Spectrometry: A Study on Direct and Simultaneous Determination of Chromium and Manganese in Urine, *Fresenius' Journal of Analytical Chemistry*, 371(**2001**), 909-914

75) G. P. G. Freschi, C. S. Dakuzaku, M. Moraes, J. A. Nóbrega, and J. A. G. Neto, Simultaneous Determination of Cadmium and Lead in Wine by Electrothermal Atomic Absorption Spectrometry, *Spectrochimica Acta*, 56B(**2001**), 1987-1993

76) N. S. Thomaidis, N. Manalis, L. Viras, T. D. Lekkas, Determination of Lead, Cadmium, Arsenic and Nickel in Atmospheric Particulate Matter by Simultaneous Multi-element Electrothermal Atomic Absorption Spectrometry, *International Journal of Environmental Analytical Chemistry*, 79(**2001**), 121-132

77) T. Lin and S. Huang, Direct and Simultaneous Determination of Copper, Chromium, Aluminum, and Manganese in Urine with a Multielement Graphite Furnace Atomic Absorption Spectrometer, *Analytical Chemistry*, 73(**2001**), 4319-4325

78) L. Bencs, O. Szakács, T. Kántor, I. Varga, and G. Bozsai, Determination of Chromium, Molybdenum and Vanadium Dopants in Bismuth Tellurite Optical Crystals by Multi-element Graphite Furnace Atomic Absorption Spectrometry, *Spectrochimica Acta*, 55B(**2000**), 883-891

79) P. R. M. Correia, E. Oliveira, and P. V. Oliveira, Simultaneous Determination of Cd and Pb in Foodstuffs by Electrothermal Atomic Absorption Spectrometry, *Analytica Chimica Acta*, 405(**2000**), 205-211

80) J. Murphy, G. Schlemmer, I. L. Shutler, P. Jones, and S. J. Hill, Simultaneous Multi-element Determination of Hydride-forming Elements by "In-atomiser Trapping" Electrothermal Atomic Absorption Spectrometry on an Iridium-coated Graphite Tube, *Journal of Analytical Atomic Spectrometry*, 14(**1999**), 1593-1600

81) M. Feuerstein and G. Schlemmer, The Simultaneous Determination of Pb, Cd, Cr, Cu, and Ni in Potable and Surface Waters by GFAAS According to International Regulations, Atomic Spectroscopy, 20(**1999**), 149-154

82) P. Su and S. Huang, Direct and Simultaneous Determination of Molybdenum and Vanadium in Sea-water using a Multielement Electrothermal Atomic Absorption Spectrometer, *Journal of Analytical Atomic Spectrometry*, 13(**1998**), 641-645

83) M. A. White and A. Panati, Simultaneous Multielement AAS Determination of Trace Elements in Human Body Fluids to Establish Reference Values for European Populations, *Atomic Spectroscopy*, 19(**1998**), 89-94

84) A. Viksna and E. S. Lindgren, Determination of Lead and Cadmium in Whole Blood of Mothers and their Babies, *Analytica Chimica Acta*, 353(**1997**), 307-311

85) H. Massmann, Vergleich von Atomabsorption und Atomfluoreszenz in der Graphitküvette, *Spectrochimia Acta*, 23B(**1968**), 215-226

86) M. T. C. de Loos-Vollebreght and L. De Galan, Furnace Design in Electrothermal Atomization-atomic Absorption Spectrometry, *Spectrochimica Acta*, 43B(**1988**), 439-449

87) W. Frech, D. C. Baxter, and B. Hütsch, Spatially Isothermal Graphite Furnace for Atomic Absorption Spectrometry using Side-heated Cuvettes with Integrated Contacts, *Analytical Chemistry*, 58(**1986**), 1973-1977

88) W. Frech and B. V. L'vov, Matrix Vapours and Physical Interference Effects in Graphite Furnace Atomic Absorption Spectrometry—II. Side-heated Tubes, *Spectrochimica Acta*, 48B(**1993**), 1371-1379

89) N. Hadgu and W. Frech, Performance of Side-heated Graphite Atomizers in Atomic Absorption Spectrometry using Tubes with End Caps, *Spectrochimica Acta*, 49B(**1994**), 445-457

90) M. Hoenig and O. Dheere, Fast Programs in Electrothermal Atomic Absorption Spectrometry. Validation of Trace Element Analysis in Plants, *Analusis*, 22(**1994**), 135-140

91) M. Hoenig and O. Dheere, Evaluation of End-capped Tubes for Transverse Heated Graphite Atomizer Electrothermal Atomic Absorption Spectrometry, *Michrochimica Acta*, 119(**1995**), 259-264

92) The THGA Graphite Furnace, Techniques and Recommended Conditions, Technical Documentation, Part No. B050-5538, Publication B3210.10, Bodenseewerk Perkin-Elmer GmbH, **1991**

93) G. Schlemmer and B. Radziuk, Analytical Graphite Furnace Atomic Absorption Spectrometry, A Laboratory Guide, Berlin: Birkhäuser Verlag, **1999**

94) J. M. Harnly and B. Radziuk, Effect of Furnace Atomization Temperatures on Simultaneous Multielement Atomic Absorption Measurement using a Transversely-heated Graphite Atomizer, *Journal of Analytical Atomic Spectrometry*, 10(**1995**), 197-206

95) Perkin-Elmer Corp. (**1994**) Personal communication

96) The Perkin-Elmer Corporation (**1994**) SIMAA 6000 Atomic Absorption Spectrometer, Part No. B050-4270/8.94

97) J. M. Harnly and J. S. Kane, Optimization of Electrothermal Atomization Parameters for Simultaneous Multielement Atomic Absorption Spectrometry, *Analytical Chemistry*, 56(**1984**), 48-54

98) M. Berglund, W. Frech, and D. C. Baxter, Achieving Efficient, Multi-element Atomisation Conditions for Atomic Absorption Spectrometry using a Platform-equipped, Integrated-contact Furnace and a Palladium Modifier, *Spectrochimica Acta*, 46B(**1991**), 1767-1777

99) G. Schlemmer and B. Welz, Palladium and Magnesium Nitrates, a More Universal Modifier for Graphite Furnace Atomic Absorption Spectrometry, *Spectrochimica Acta*, 41B(**1986**), 1157-1165

100) B. Welz, G. Schlemmer, and J. R. Mudakavi, Palladium Nitrate – Magnesium Nitrate Modifier for Electrothermal Atomic Absorption Spectrometry. Part 5. Performance for the Determination of 21 Elements, *Journal of Analytical Atomic Spectrometry*, 7(**1992**), 1257-1271

101) E. L. Henn, Determination of Selenium in Water and Industrial Effluents by Flameless Atomic Absorption, *Analytical Chemistry*, 47(**1975**), 428-432

102) G. Machata and R. Binder, Determination of Lead, Thallium, Zinc, and Cadmium Trace Elements in Biological Material by Flameless Atomic Absorption, *Zeitschrift für Rechtsmedizin*, 73(**1973**), 29-34

103) K. G. Brodie and J. P. Matousek, Determination of Cadmium in Air by Non-flame Atomic Absorption Spectrometry, *Analytica Chimica Acta*, 69(**1974**), 200-202

104) E. J. Czobik and J. P. Matousek, Effect of Anions on Atomization Temperatures in Furnace Atomic-absorption, *Talanta*, 24(**1977**), 573-577

105) W. Slavin, G. R. Carnrick, and D. C. Manning, Magnesium Nitrate as a Matrix modifier in the Stabilized Temperature Platform Furnace, *Analytical Chemistry*, 54(**1982**), 621-624
106) G. F. Kirkbright, S. Hsiao-Chuan, and R. D. Snook, An Evaluation of Some Matrix Modification Procedures for use in the Determination of Mercury and Selenium by Atomic Absorption Spectroscopy with a Graphite Tube Electrothermal Atomizer, *Atomic Spectroscopy*, 1(**1980**), 85-89
107) H. Qiao and K. W. Jackson, Mechanism of Modification by Palladium in Graphite Furnace Atomic Absorption Spectrometry, *Spectrochimica Acta*, 46B(**1991**), 1841-1859
108) M. W. Hinds, M. Katyal, and K. W. Jackson, Effectiveness of Palladium Plus Magnesium as a Matrix Modifier for the Determination of Lead in Solutions and Soil Slurries by Electrothermal Atomisation Atomic Absorption Spectrometry, *Journal of Analytical Atomic Spectrometry*, 3(**1988**), 83-87
109) M. W. Hinds and K. W. Jackson, Lead Atomisation from Soil by Slurry Introduction Electrothermal Atomisation Atomic Absorption Spectrometry. Part 2. Atomisation Characteristics with Various Matrix Modifiers, *Journal of Analytical Atomic Spectrometry*, 3(**1988**), 997-1003
110) X. Q. Shan and M. Z. Ni, Matrix Modification for the Determination of Lead in Urine by Graphite Furnace Atomic Absorption Spectrometry, *Canadian Journal of Spectroscopy*, 27(**1982**), 75-81
111) W. Wendl and G. Müller-Vogt, Chemical Reactions of Lead in Graphite Furnace Atomic Absorption Spectrometry, *Journal of Analytical Atomic Spectrometry*, 3(**1988**), 63-66
112) X-Q Shan and D-X Wang, X-ray Photoelectron Spectroscopic Study of the Mechanism of Palladium Matrix Modification in the Electrothermal Atomic Absorption Spectrometric Determination of Lead and Bismuth, *Analytica Chimica Acta*, 173(**1985**), 315-319
113) J. E. Teague-Nishimura, T. Tominaga, T. Katsura, and K. Matsumoto, Direct Experimental Evidence for in Situ Graphite and Palladium Selenide Formations with Improvement on the Sensitivity of Selenium in Graphite Furnace Atomic Absorption Spectrometry, *Analytical Chemistry*, 59(**1987**), 1647-1651
114) D. L. Styris, L. J. Prell, and D. A. Redfield, Mechanisms of Selenium Vaporization with Palladium Modifiers using Electrothermal Atomization and Mass Spectrometric Detection, *Analytical Chemistry*, 63(**1991**), 508-517
115) T. M. Rettberg and L. M. Beach, Peak Profile Characteristics in the Presence of Palladium for Graphite Furnace Atomic Absorption Spectrometry, *Journal of Analytical Atomic Spectrometry*, 4(**1989**), 427-432

116) J. B. B. da Silva, M. Bertília, O. Giacomelli, I. Gonçalves de Souza, and A. J. Curtius, Iridium and Rhodium as Permanent Chemical Modifiers for the Determination of Ag, As, Bi, Cd, and Sb by Electrothermal Atomic Absorption Spectrometry, *Michrochemical Journal*, 60(**1998**), 249-257

117) D. L. Tsalev, V. I. Slaveykova, L. Lampugnani, A. D'Ulivo, and R. Georgieva, Permanent Modification in Electrothermal Atomic Absorption Spectrometry — Advances, Anticipations and Reality, *Spectrochimica Acta*, 55B(**2000**), 473-490

118) E. Vassileva, H. Baeten, and M. Hoenig, Advantages of the Iridium Permanent Modifier in Fast Programs Applied to Trace-element Analysis of Plant Samples by Electrothermal Atomic Absorption Spectrometry, *Fresenius Journal Analytical Chemistry*, 369(**2001**), 491-495

119) K. W. Jackson and S. Lu, Atomic Absorption, Atomic Emission, and Flame Emission Spectrometry, *Analytical Chemistry*, 70(**1998**), 363R-383R

120) C. J. Rademeyer, B. Radziuk, N. Romanova, N. P. Skaugset, A. Skogstad, and Y. Thomassen, Permanent Iridium Modifier for Electrothermal Atomic Absorption Spectrometry, *Journal of Analytical Atomic Spectrometry*, 10(**1995**), 739-745

121) E. Bulska and W. Jedral, Application of Palladium- and Rhodium-plating of the Graphite Furnace in Electrothermal Atomic Absorption Spectrometry, *Journal of Analytical Atomic Spectrometry*, 10(**1995**), 49-53

122) D. Pozebon, V. L. dressler, and A. J. Curtius, Determination of Arsenic, Selenium and Lead by Electrothermal Vaporization Inductively Coupled Plasma Mass Spectrometry using Iridium-coated Graphite Tubes, *Journal of Analytical Atomic Spectrometry*, 13(**1998**), 7-11

123) H. G. Infante, M. L. F. Sánchez, and A. Sanz-Medel, Ultratrace Determination of Cadmium by Atomic Absorption Spectrometry using Hydride Generation with in Situ Preconcentration in a Palladium-coated Graphite Atomizer, *Journal of Analytical Atomic Spectrometry*, 11(**1996**), 571-575

124) M. Grotti and A. Mazzucotelli, Electrothermal Atomic Absorption Spectrometric Determination of Ultra trace Amounts of Tellurium using a Palladium-coated L'vov Platform after Separation and Concentration by Hydride Generation and Liquid Anion Exchange, *Journal of Analytical Atomic Spectrometry*, 10(**1995**), 325-327

125) D. Tsalev, A. D'Ulivo, A. Lampuganani, M. Di Marco, and R. Zamboni, Thermally Stabilized Iridium on an Integrated, Carbide-coated Platform as a Permanent Modifier for Hydride-forming Elements in Electrothermal Atomic Absorption Spectrometry. Part 1. Optimization Studies, *Journal of Analytical Atomic Spectrometry*, 10(**1995**), 1003-1009

126) H. Th. Uggerud, and W. Lund, Use of Palladium and Iridium as Modifiers in the Determination of Arsenic and Antimony by Electrothermal Vaporization Inductively Coupled Plasma Mass Spectrometry, Following In Situ Trapping of the Hydrides, *Journal of Analytical Atomic Spectrometry*, 12(**1997**), 1169-1174

127) R. G. Treble, T. S. Thompson, and H. R. Lynch, Determination of Copper, Manganese and Zinc in Human Liver, *BioMetals*, 11(**1998**), 49-53

128) Yin Ming and Li Bing, Determination of Rare Earth Elements in Human Hair and Wheat Flour Reference Materials by Inductively Coupled Plasma Mass Spectrometry with Dry Ashing and Microwave Digestion, *Spectrochimica Acta*, 53B(**1998**), 1447-1454

129) B. Welz and M. Sperling, *Atomic Absorption Spectrometry*, 3rd Edition, Wiley, Weinheim, **1999**

130) M-V German, H. Lothar, M. Hans, W. Wolfgang, and J-R Dimitri, Role of Oxygen in the Determination of Oxide Forming Elements by Electrothermal Atomic Absorption Spectrometry Part 2. Effect of Oxygen on the Reactions of Thallium, Bismuth and Lead in Uncoated Furnaces, Pyrilytic Coated Furnaces and on Platforms, *Journal of Analytical Atomic Spectrometry*, 10(**1995**), 777-783

131) R. Chakraborty, A. K. Das, M. L. Cervera, and M. de la Guardia, The Atomization of Cadmium in Graphite Furnace, *Analytical Proceedings Including Analytical Communications*, 32(**1995**), 245-249

132) D. Clark, R. M. Dagnall, and T. S. West, The Atomic Absorption Determination of Zinc with a Graphite Furnace, *Analytica Chimica Acta*, 63(**1973**), 11-18

133) J. P. Matousek and G. K. Brodie, Direct Determination of Lead Airborne Particulates by Nonflame Atomic Absorption, *Analytical Chemistry*, 45(**1973**), 1606-1609

134) J. W. McLaren and R. C. Wheeler, Double Peaks in The Atomic-Absorption Determination of Lead Using Electrothermal Atomisation, *Analyst*, 102(**1977**), 542-546

135) E. Lundbeg, Application of a Versatile Drift-Compensating Digital Peak Reader to the Direct Atomization of Solids in Graphite Furnace Atomic Absorption Spectroscopy, *Applied Spectroscopy*, 32(**1978**), 276-281

136) J. G. T. Regen and J. Warren, The Effect of Graphite Tube Condition and of Ascorbic Acid on Lead Peak Shapes Obtained by Flameless Atomic Absorption Spectroscopy Using Low Temperature Atomization, *Atomic Absorption Newsletters*, 17(**1978**), 89-90

137) W. Slavin and D. C. Manning, Reduction of Matrix Interferences for Lead Determination With The L'vov Platform and The Graphite Furnace, *Analytical Chemistry*, 51(**1979**), 261-265

138) S. Bäckman and W. R. Karlsson, Determination of Lead, Bismuth, Zinc, Silver and Antimony in Steel and Nickel-base Alloys by Atomic-Absorption Spectrometry Using Direct Atomisation of Solid Samples in a Graphite Furnace, *Analyst*, 104(**1979**), 1017-1029

139) S. G. Slamon, R. H. Davis, Jr., and J. A. Holcombe, Time Shifts and Double Peaks of Lead Caused by Chemisorbed Oxygen in Electrothermally heated Graphite Atomizers, *Analytical Chemistry*, 53(**1981**), 324-330

140) C. W. Fuller, The Effect of Graphite Tube Condition on The Determination of Lead in The Presence of Magnesium Chloride by Electrothermal Atomic Absorption Spectrometry, *Atomic Absorption Newsletters*, 16(**1977**), 106-107

141) L. Pszonicki and J. Dudek, Modifier Effects in The Determination of Arsenic, Antimony, and Bismuth by Electrothermal Atomic Absorption Spectrometry, *Journal of Analytical Atomic Spectrometry*, 14(**1999**), 1755-1760

142) W. Frech, E. Lundberg, and A. Cedergren, Investigations of Some Methods Used to Reduce Interference Effects in Graphite Furnace Atomic Absorption Spectrometry, *Progress in Analytical Atomic Spectroscopy*, 8(**1985**), 257-370

143) J. Aggett and A. J. Sprott, Non-flame Atomization in Atomic Absorption Spectrometry, *Analytica Chimica Acta*, 72(**1974**), 49-56

144) S. J. Cathum, Mechanism of Atomization in Massmann-type Graphite Furnace Using The Basic Principles of Thermodynamics, *Canadian Journal Of Chemistry*, 71(**1993**), 21-28

145) W. Wendl and G. Müller-Vogt, Chemical Reactions of Chromium and Vanadium in Graphite Furnace Atomic Absorption Spectrometry, *Spectrochimica Acta*, 40B(**1985**), 527-531

146) E. K. Storms and R. J. McNeal, The Vanadium-Vanadium Carbide System, *Journal of Physical Chemistry*, 66(**1962**), 1401-1408

147) H. Lux and L. Eberle, Chromous Salts and Chromous Oxide. III, *Chemische Berichte*, 94(**1961**), 1562-1571

148) V. Majidi, N. Xu, and R. G. Smith, Electrothermal Vaporization, Part 1: Gas Phase Chemistry, *Spectrochimica Acta*, 55B(**2000**), 3-35

149) L. J. Prell, D. L. Styris, and D. A. Redfield, Comparison of Atomization Mechanisms for Group IIA Elements in Electrothermal Atomic-Absorption Spectrometry, *Journal of Analytical Atomic Spectrometry*, 6(**1991**), 25-32

150) L. Yan-Zhong and N. Zhe-Ming, Atom Release of Mn, Co, Ag, and Tl in a Graphite Furnace Atomizer with and without Palladium Modifier, *Spectrochimica Acta*, 49B(**1994**), 229-241

151) F. Y. Leung and A. R. Henderson, Improved Determination of Aluminium in Serum and Urine with Use of a Stabilized Temperature Platform Furnace, *Clinical Chemistry*, 28(**1982**), 2139-2143

152) M. Bettinelli, U. Baroni, F. Fontana, and P. Poisetti, Evaluation of The L'vov Platform and Matrix Modification for The Determination of Aluminium in Serum, *Analyst*, 110(**1985**), 19-22

153) F. Y. Leung and A. R. Henderson, Determination of Aluminium in Serum and Urine Using Matrix Modification and The L'vov Platform, *Atomic Spectroscopy*, 4(**1983**), 1-4

154) S. Xiao-Quan, L. Shen, and N. Zhe-Ming, Determination of Aluminium in Human Blood and Serum by Graphite Furnace Atomic Absorption Spectrometry Using Potassium Dichromate Matrix Modification, *Journal of Analytical Atomic Spectrometry*, 3(**1988**), 99-103

155) D. C. Manning, W. Slavin, and G. R. Carnrick, Investigation of Aluminum Interferences Using the Stabilized Temperature Platform Furnace, *Spectrochimica Acta*, 37B(**1982**), 331-341

156) W. Slavin, G. R. Carnrick, D. C. Manning, E. Pruszkowska, Recent Experiences with The Stabilized Temperature Platform Furnace and Zeeman Background Correction, *Atomic Spectroscopy*, 4(**1983**), 69-86

157) D. L. Styris and D. A. Redfield, Mechanisms Controlling Graphite Atomization and Stabilization of Beryllium, *Analytical Chemistry*, 59(1987), 2897-2903

158) N. S. Thomaidis, E. A. Piperaki, C. K. Polydorou, and C. E. Efstathiou, Determination of Chromium by Electrothermal Atomic Absorption Spectrometry with Various Chemical Modifiers, *Journal of Analytical Atomic Spectrometry*, 11(**1996**), 31-36

159) J. L. Burguera, M. Burguera, C. Rondon, L. Rodriguez, P. Carrero, Y. Petit de Pena, and E. Burguera, Determination of Chromium in Urine by Electrothermal Atomic Absorption Spectrometry Using Different Chemical Modifiers, *Journal of Analytical Atomic Spectrometry*, 14(**1999**), 821-825

160) S. P. Quinaia and J. A. Nobrega, A Critical Evaluation of The Graphite Furnace Conditions for The Direct Determination of Chromium in Urine, *Fresenius Journal of Analytical Chemistry*, 364(**1999**), 333-337

161) R. E. Sturgeon, S. N. Willie, G. I. Sproule, and S. S. Berman, Sequestration of Volatile Element Hydrides by Platinum Group Elements for Graphite Furnace Atomic Absorption, *Spectrochimica Acta*, 44B(**1989**), 667-682

162) Z. Li, N. Zhe-Ming, S. Xiao-Quan, In Situ Concentration of Metallic Hydrides in a Graphite Furnace Coated with Palladium, *Spectrochimica Acta*, 44B(**1989**), 339-346
163) I. L. Shuttler, M. Feuerstein, and G. Schlemmer, Long-term Stability of Mixed Palladium-Iridium Trapping Reagent for In-situ Hydride Trapping within a Graphite Electrothermal Atomizer, *Journal of Analytical Atomic Spectrometry*, 7(**1992**), 1299-1301
164) H. O. Haung, Study of Stable Coatings for Determination of lead by Flow-injection Hydride Generation and In Situ Concentration in Graphite Furnace Atomic Absorption Spectrometry, *Spectrochimica Acta*, 51B(**1996**), 1425-1433
165) L. Zhang, Z. Ni, X. Shan, In Situ Concentration of Metallic Hydride in a Graphite Furnace Coated with Palladium-determination of Bismuth, Germanium, and Tellurium, *Spectrochimica Acta*, 44B(**1989**), 751-758
166) W. W. Ding and R. E. Sturgeon, Evaluation of Electrochemical Hydride Generation for The Determination of Arsenic and Selenium in Sea Water by Graphite Furnace Atomic Absorption with In Situ Concentration, *Spectrochimica Acta*, 51B(**1996**), 1325-1334
167) H. Matusiewicz and R. E. Sturgeon, Atomic Spectrometric Detection of Hydride Forming Elements Following In Situ Trapping within a Graphite Furnace, *Spectrochimica Acta*, 51B(**1996**), 377-397
168) H. O. Haug and L. Yiping, Automated Determination of Tin Hydride Generation Using In Situ Trapping on Stable Coatings in Graphite Furnace Atomic Absorption Spectrometry, *Spectrochimica Acta*, 50B(**1995**), 1311-1324
169) S. Garbòs, M. Walcez, E. Bulska, and A. Hulanicki, Simultaneous Determination of Se and As by Hydride Generation Atomic Absorption Spectrometry with Analyte Concentration in Graphite Furnace Coated with Zirconium, *Spectrochimica Acta*, 50B(**1995**), 1669-1677
170) D. L. Tsalev, A. D'Ulivo, L. Lampugnani, M. D. Marco, and R. Zamboni, Thermally Stabilized Iridium on an Integrated, Carbide-coated Platform as a Permanent Modifier for Hydride-forming Elements in Electrothermal Atomic Absorption Spectrometry. Part 2. Hydride Generation and Collection and Behaviour of Some Organoelement Species, *Journal of Analytical Atomic Spectrometry*, 11(**1996**), 979-988
171) D. L. Tsalev, A. D'Ulivo, L. Lampugnani, M. D. Marco, and R. Zamboni, Thermally Stabilized Iridium on an Integrated, Carbide-coated Platform as a Permanent Modifier for Hydride-forming Elements in Electrothermal Atomic Absorption Spectrometry. Part 3. Effect of L-cysteine, *Journal of Analytical Atomic Spectrometry*, 11(**1996**), 989-995

172) G. Bozsai and M. Melegh, Application of The Transversely Heated Graphite Atomizer to The Determination of Trace Metals in Environmental and Biomedical Samples, *Michrochemical Journal*, 51(**1995**), 39-45

173) G. Samanta, T. R. Chowdhury, B. K. Mandal, B. K. Biswas, and U. K. Chowdhury, Flow Injection Hydride Generation Atomic Absorption Spectrometry for Determination of Arsenic in Water and Biological Samples from Arsenic-Affected Districts of West Bengal, India, and Bangladesh, *Michrochemical Journal*, 62(**1999**), 174-191

174) E. Hakala and L. Pyy, Assessment of Exposure to Inorganic Arsenic by Determining The Arsenic Species Excreted in Urine, *Toxicology Letters*, 77(**1995**), 249-258

175) J. L. Fishcer, Electrothermal Atomization of Palladium Stabilized Selenium in the Presence of Phosphate, *Spectrochimica Acta*, 57B(**2002**), 525-533

176) H. Ince Tekgül and S. Akman, The Interference Effect of More Than One Salt in Graphite Furnace Absorption Spectrometry Part 1: Effect of Magnesium Chloride – Sodium Chloride Mixture on Manganese, *Spectrochimica Acta*, 52B(**1997**), 621-631

177) P. R. M. Correia, C. S. Nomura, and P. V. Oliveira, Multi-element Determination of Cadmium and Lead in Urine by Simultaneous Electrothermal Atomic Absorption Spectrometry with an End-capped Graphite Tube, *Analytical Sciences*, 19(**2003**), 1519-152

178) C. G. Magalhães, B. R. Nunes, M. B. Oss Giacomelli, and J. B. B. da Selva, Direct Determination of Bismuth in Urine Samples by Electrothermal Atomic Absorption Spectrometry: Study of Chemical Modifier, *Journal of Analytical Atomic Spectrometry*, 18(**2003**), 787-789

179) M. Wojciecchowski, M. Piaścik, and E. Bulska, Nobel Metal Modifiers for Antimony Determination by Graphite Furnace Atomic Absorption Spectrometry in Biological Samples, *Journal of Analytical Atomic Spectrometry*, 16(**2001**), 99-101